ATOH7-INDEPENDENT SPECIFICATION OF RETINAL GANGLION CELL IDENTITY

by
Justin Brodie-Kommit

A dissertation submitted to Johns Hopkins University in conformity with the requirements for

the degree of Doctor of Philosophy

Baltimore, Maryland
August 2020

Abstract

Retinal ganglion cells (RGCs) relay visual information from the eye to the brain. RGCs are the first cell type generated during retinal neurogenesis. Loss of function of the transcription factor *Atoh7*, expressed in multipotent early neurogenic retinal progenitor cells, leads to a selective and essentially complete loss of RGCs. Therefore, *Atoh7* is considered essential for conferring competence on progenitors to generate RGCs. DNA binding sites analysis of Atoh7 using the Cut&Run method demonstrates that Atoh7 directly targets genes controlling RGC specification. Despite the important function of Atoh7 in RGC specification, when apoptosis is inhibited in *Atoh7*-deficient mice by loss of function of *Bax*, only a modest reduction in RGC number is observed. Single-cell RNA-Seq of *Atoh7;Bax*-deficient retinas shows that RGC differentiation is delayed, but that the gene expression profile of RGC precursors is grossly normal. *Atoh7;Bax*-deficient RGCs eventually mature, fire action potentials, and incorporate into retinal circuitry, but exhibit severe axonal guidance defects. This study reveals an essential role for *Atoh7* in RGC survival and demonstrates *Atoh7*-independent mechanisms for RGC specification.

Primary Reader and Advisor: Samer Hattar

Secondary Reader: Haiqing Zhao

Acknowledgements

I am eternally grateful for Samer Hattar, PhD. Samers guidance and training will be with me for the rest of my life. Samer gave me agency to realize who I am by allowing me to take the long and hard path to my eventual success. Samer has made me fall in love with the Retina as a model system for all of neuroscience, as well as the field of Circadian Biology. Samer supported me as I learned from my failures and drove me to take complete ownership of my project and kept me well fed throughout my PhD.

As a member of the Mouse-Tri-Lab at Johns Hopkins university, while Samer was my official mentor, I was lucky to have Haiqing Zhao, PhD and Rejji Kuruvilla, PhD as co-mentors throughout my training. Samer, Haiqing, and Rejji are almost a superhero group, with each providing phenomenal guidance on their own, but together their mentorship and training is second to none. The Mouse-Tri-Lab has also provided me with a close knit group of colleagues with a wide variety of expertise. This style of collaboration and cooperation is something I would suggest to anyone doing research.

There is no amount of thanks I can give to the members of the Hattar lab that guided me through my first few years of graduate school, and who taught me everything I know how to do in lab; Alan Rupp, PhD, Bill Keenan, PhD, Diego Fernandez, PhD, Kylie Chew, PhD, Michael Thompson, PhD, and Tiffany Schmidt, PhD. Tiffany, a Post-doc in the Hattar lab when I joined, was a second mentor to me, and continues to be even after she started her own lab at Northwestern. Tiffany took me under her wing, and together we laid the foundation of what would become my entire thesis project.

Acknowledgements

My thesis work would not have been possible without the help of many labs around the world, who have provided countless guidance, advice, criticism, and expertise in their sub fields, many of which contributed data that was paramount to my thesis including; Brian Clark, PhD, Seth Blackshaw, PhD, Tudor Badea, PhD, Hope Shi, PhD, Tom Glaser, PhD, Joshua Singer, PhD, Thomas Kim, PhD, Michel Fries, Michel Cayouette, PhD, and many more from those who merely listened to my poster presentation to those who I have had lengthy discussions with.

I would also like to thank Joan Miller, the entire Biology office staff, the CMDB program, the mouse facility staff and in particular John Hayes and Ed Baker.

And thanks to Baltimore for becoming for welcoming us in and being kind, generous, genuine, weird, funky, and a whole lot of fun.

Dedication

This thesis is dedicated to Jui-Ko Chang, my partner in life and science, my sister Kayla Kommit, and my parents Kathy Kommit and Michael Brodie for helping me to achieve my dreams in life and providing me with endless love and support.

Contents

List of Tables

List of Figures

List of Figures

Chapter 1 - Introduction

1.1 Light and retina

Light impacts many physiological functions including vision, circadian rhythms and sleep. In mammals, the retina is the only gateway for light information to reach the brain. The retina has been a model system for understanding developmental neurobiology for almost 2 centuries. The retina has six major classes of neurons and one major glia that develop from a common progenitor cell pool, whose multipotency diminishes over time, using a temporally ordered expression of transcription factors. Of the six neuronal classes, retinal ganglion cells (RGCs), the only projection neurons from the retina to the brain, are the first to develop, and are the main focus of this thesis. The RGCs are quickly followed in an overlapping manner by Cones, Horizontal cells and Amacrine cells. A little later Rods start to develop followed by Bipolar cells and lastly Müller glia (Carter-Dawson & LaVail, 1979; Clark et al., 2019; J. W. Hinds & Hinds, 1979; Rapaport, Wong, Wood, Yasumura, & LaVail, 2004; Sidman, 1960; Young, 1985).

1.2 *Transcribing* the Retina

The retina has been a model system for understanding developmental neurobiology for almost 2 centuries. The retina is formed through a process of evagination to form the optic vesicle, invagination to form the optic cup, and proliferation and diversification to form the neural retina. The optic vesicle forms at around e8.25-8.5, though a bilateral evagination of the anterior neural plate. The cells that become the optic vesicle in the anterior neural plate are determined through combinatorial and sequential

expression of the eye field transcription factors (EFTF), specifically the **Lhx2** (LIM homeodomain), **Rax** (Retina and anterior fold homeobox), **Pax6** (Paired box), and **Six3** (Sine oculis homeobox). Lhx2 and Rax are the first of the EFTFs to be expressed in anterior neural plate at e7.5. In the Lhx2 knockout eye, development arrests between the optic vesicle and optic cup stage, the expression of all the other EFTFs is significantly reduced and also delayed, suggesting that Lhx2 controls expression of Rax, Pax6, and Six3 (Furukawa, Kozak, & Cepko, 1997; Tétreault, Champagne, & Bernier, 2009). Rax null mice fail to form an optic vesicle, suggesting that while Rax is downstream of Lhx2 it is instrumental in the evagination of the anterior neural plate into the optic vesicle (Furukawa et al., 1997; Mathers, Grinberg, Mahon, & Jamrich, 1997). Pax6 expression begins at e8.0 and Pax6 null mice have the same phenotype as the Lhx2 null mice with the eye development arresting between the optic vesicle and optic cup stage, however expression of the other EFTFs are unaffected, revealing that Pax6 expression is functionally downstream of Rax, Lhx2, and Six3 (Bernier, Vukovich, Neidhardt, Herrmann, & Gruss, 2001; Grindley, Davidson, & Hill, 1995). Six3 is expressed at e8.5 and in a conditional eye field knockout of Six3 the neural retina fails to form, arresting at optic vesicle stage, but the retinal pigmented epithelium continues to be specified and forms. In this conditional knockout of Six3 the optic vesicle normally expresses Rax, Lhx2, and Pax6 (W. Liu, Lagutin, Swindell, Jamrich, & Oliver, 2010; Oliver et al., 1995).

While all of the EFTF genes are necessary for optic cup formation, most are also sufficient to induce ectopic eye formation. Pax6 is well known to form ectopic eyes on the antennae, wings, and limbs of Drosophila melanogaster (Halder, Callaerts, &

Gehring, 1995). When Rax was overexpressed in both Xenopus and Teleost ectopic retinal tissue was formed (Chuang & Raymond, 2001; Mathers et al., 1997). Ectopic Six3 expression in Drosophila and in Murine models lead to ectopic retinal vesicle formation (Lagutin et al., 2001; Seimiya & Gehring, 2000). This analysis has not been done for Lhx2.

Pax2, a family member of Pax6, is expressed starting at E9 in the optic vesicle and plays an important role in both optic cup formation and axon guidance. Pax2 is expressed in the optic ventricle early, and a little later there is expression in the optic disk, and all along the optic stalk (NORNES, DRESSLER, KNAPIK, DEUTSCH, & Gruss, 1990). Pax2 is required for closure of the optic fissure to form the optic cup and in Pax2 null mice all RGCs project ipsilaterally (Torres, Gómez-Pardo, & Gruss, 1996). When Pax6 family members Pax2 or Pax6 spliceform Pax6(5a) replaced the coding region of Pax6, neither were sufficient to rescue the Pax6 null retinal development deficit. However, when Pax2 replaced the Pax6 coding region, the residual optic vesicle expressed Sox2 and Crx, but not Mitf, suggesting that Pax2 can partially compensate for some Pax6 functions, but not enough to complete optic cup formation or RPE formation (Carbe et al., 2013).

1.2.1 Optic Vesicle to Optic Cup Transition

In the optic vesicle, expression of **Mitf** (bHLH) begins around E9.0 and is throughout the entire optic vesicle and then very shortly thereafter **Vsx2**(Chx10)(Prd-L Homeodomain family) is seen to be expressed in the region of the optic vesicle that will

become the neural retina(distal/ventral optic vesicle), while Mitf expression is then downregulated in what will become the neural retina, while it is maintained in what will become the retinal pigmented epithelium (RPE) (dorsal optic vesicle) (Fuhrmann, 2010; LIU et al., 1994; Nguyen & Arnheiter, 2000). Lhx2 is required for proper regionalization of the optic vesicle by controlling the expression of Mitf and Vsx2 in collaboration with FGF signaling from either the lens ectoderm or the optic vesicle itself (Cai, Feng, & Zhang, 2010; Fuhrmann, 2010; Tétreault et al., 2009; Yun et al., 2009). Lhx2 also controls the expression of **Six6** expression in the neural retina, which is important for regulating the early proliferation of the retinal progenitors into the early born retinal cell types (X. Li, Perissi, Liu, Rose, & Rosenfeld, 2002; Tétreault et al., 2009). The proliferative state of RPCs is controlled by the mouse homolog of **Meis1** and **Meis2** in both Drosophila and Gallus (Bessa et al., 2008; Heine, Dohle, Bumsted-O'Brien, Engelkamp, & Schulte, 2008).

As the optic vesicle matures, it eventually makes contact with the surface ectoderm. Once contact is made, the surface ectoderm begins to form the lens placode and the optic vesicle receives an unknown signal from the lens placode, which includes something more than just FGF, this signal is responsible for inducing the regionalization of the optic vesicle into neural retina. Following the induction of Vsx2 expression in the optic vesicle, both the retinal and lens placodes invaginate. However, both the invagination and the lens placode tissue, post induction, is unnecessary for proper optic cup differentiation (Hyer, Kuhlman, Afif, & Mikawa, 2003; A. N. Smith, Miller, Radice, Ashery-Padan, & Lang, 2009).

1.2.2 Retinal Ganglion Cell Development and Atoh7

The retina consists of six retinal neuronal types and one glial type, which arise from a common progenitor pool, whose multipotency diminishes over time. It is a temporally ordered process starting with Retinal Ganglion Cells (RGCs) and ending with Müller glia and takes almost three weeks to complete in mice (Carter-Dawson & LaVail, 1979; J. W. Hinds & Hinds, 1979; Rapaport et al., 2004; Sidman, 1960; Young, 1985). Pax6 is required for optic cup formation, but it is also required later in retinal development to allow for the retinal progenitor cells (RPCs) to acquire their multi-potency and different retinal fates. This is presumably due to Pax6's direct control over retinogenic bHLH factor expression, like **Atoh7** (atonal homolog 7), also known as Math5 (mammalian atonal homology 5), a basic helix-loop-helix transcription factor (Marquardt et al., 2001).

RGC development in mice has been shown to require **Atoh7** (N. L. Brown, Patel, Brzezinski, & Glaser, 2001; Jarman, Grell, Ackerman, Jan, & Jan, 1994; S. W. Wang et al., 2001). Atoh7 is conserved across many species from Humans (ATOH7) to Zebrafish (Atoh5) and distantly to Drosophila (atonal). Atoh7 mutant mice and zebrafish lack 95% of RGCs (N. L. Brown et al., 2001; Brzezinski, Prasov, & Glaser, 2012; Kay, Finger-Baier, Roeser, Staub, & Baier, 2001; S. W. Wang et al., 2001) and they: (1) have almost no visible optic nerve or functional connections from the retina to the brain (Brzezinski et al., 2005; Wee, Castrucci, Provencio, Gan, & Van Gelder, 2002); (2) lack proper retinal vasculature (Edwards et al., 2012); (3) show an increase in apoptotic cells in the retina

across embryonic development (L. Feng et al., 2010; Prasov & Glaser, 2012b); and (4) show an increase in cones and amacrine cells as well as a small decrease in the numbers of rods, Müller glia, and bipolar cells compared to wildtype (N. L. Brown et al., 2001; Brzezinski et al., 2005; Hufnagel, Le, Riesenberg, & Brown, 2010; S. W. Wang et al., 2001).

In Drosophila atonal is necessary for the first born and organizing photoreceptor, the R8 photoreceptor. Other photoreceptors do not require atonal, but do require the R8 photoreceptor for their local recruitment and development (Jarman et al., 1994). Homozygous or hemizygous mutants for atonal are practically eyeless and what is left contain no photoreceptors. atonal mutants also secondarily have atrophy and apoptosis in the imaginal eye disk due to lack of photoreceptor formation. atonal also acts as the proneural gene for chordotonal organs and thus mutants lack adult and embryonic chordotonal organs (Jarman, Grau, Jan, & Jan, 1995). There are eight atonal-related bHLH genes in the mouse; Atoh7, Math1 (Atoh1), Ngn1, Ngn2, Ngn3, Neurod1, Neurod6, Neurod4, Ascl1. In the mouse Atoh7 is required for the development of RGCs, the first-born cell type in the retina. In Atoh7 mutant mice, not only is there is a 95% reduction in RGC numbers, but no substantial amount of RGCs are seen at any timepoint in development, from E11 until P0 (N. L. Brown et al., 2001; L. Feng et al., 2010; S. W. Wang et al., 2001).

Atoh7 in mouse is only expressed in the developing retina and mature central auditory system (Saul et al., 2008), and in the retina is transiently expressed in neurogenic retinal progenitors cells from embryonic day 11 (E11) through birth (P0) with

a peak of expression at E14 (N. L. Brown et al., 1998; Clark et al., 2019; Kiyama et al., 2011; Prasov & Glaser, 2012a; S. W. Wang et al., 2001) , closely matching the observed birthdates of RGCs (Rapaport et al., 2004; Sidman, 1960; Young, 1985).

In the central auditory system Atoh7 is expressed in the globular and small spherical bushy cell of the VCN (ventral cochlear nucleus), as early as E12. In contrast to the retina, it is solely expressed by post-mitotic cells. This Atoh7 expression is maintained in adulthood in these VCN neurons and in its absence the cells are still present, but their morphology and firing patterns are diminished. Thus Atoh7 in these VCN neurons play a cell-autonomous role in the function of these neurons, which is in contrast to the proposed role and expression pattern of Atoh7 in the retina. The utilization of Atoh7 in these VCN neurons is also in contrast to the use of, closely related, Math1 in the development of these neurons, which is required for the development of all neurons of the caudal rhombic lip that migrate along the cochlear extramural stream (Saul et al., 2008; V. Y. Wang, Rose, & Zoghbi, 2005a).

1.2.2.1 Expression of Atoh7

Atoh7 has complex and temporally regulated expression in retinal development. During the first half of RGC development (E10.5-E14.5), Atoh7 seems to drive cell cycle exit as retinal progenitor cells (RPCs) that express Atoh7 during late S or G2, symmetrically divide into two RGCs (Brzezinski et al., 2012; L. Feng et al., 2010; Kiyama et al., 2011; Pacal & Bremner, 2014; Prasov & Glaser, 2012a; Wu, Sapkota, Li, & Mu, 2012). The expression of Atoh7 it is not always sufficient, however, to drive cell

cycle exit since ectopic expressing of Atoh7 does not always lead to cell cycle exit, depending on the cellular context of this expression (Le, Wroblewski, Patel, Riesenberg, & Brown, 2006; X.-M. Zhang, Hashimoto, Tang, & Yang, 2018). After E14.5, Atoh7 is expressed later in the terminal cell cycle after terminal M phase (Brzezinski et al., 2012; L. Feng et al., 2010; Pacal & Bremner, 2014; Prasov & Glaser, 2012a), but is then turned off shortly after the completion of cell cycle (G0) and the migration to the ganglion cell layer (GCL) (L. Feng et al., 2010; Pacal & Bremner, 2014). In zebrafish, atoh7 is expressed during G2-phase of the terminal division to produce at least one RGC. There is also feedback regulation in zebrafish, as atoh7-expressing RPCs transplanted into a mutant environment lacking RGCs were 4 times more likely to divide symmetrically to give rise to two RGCs (Poggi, Vitorino, Masai, & Harris, 2005). This shows that while determination and development of RGCs is largely cell-intrinsic, extrinsic factors also modulate this process (Mu, Fu, Sun, Liang, et al., 2005b).

PAX6, NGN2, and RBPJ can all directly bind to the conserved primary enhancer of Atoh7 and regulate its expression. PAX6 is a positive regulator of both NGN2 and ATOH7. NGN2 is a positive regulator of Atoh7 expression. RBPJ can bind to Atoh7 at four distinct CSL sites, allowing it to more specifically control expression of Atoh7. The four sites of binding allow RBPJ to prime the Atoh7 locus to allow for its future expression, directly repress the expression of Atoh7, and for canonical Notch pathway suppression. The site of RBPJ-mediated priming of the Atoh7 locus is directly in-between the Pax6 binding site and a NGN2 binding site. In at least chickens (Cath5) and zebrafish (Ath5), ATOH7 also directly regulates its own transcription by binding

approximately 2kb upstream from its coding sequence and enhancing a positive feedback loop, however, this self-regulation might be specific to chicken and Zebrafish Atoh7. All of these factors work together to help drive the very pulsatile expression of Atoh7 (Del Bene et al., 2007; Hufnagel et al., 2010; Le et al., 2006; Miesfeld et al., 2018; A. N. Riesenberg, Le, Willardsen, Blackburn, Vetter, et al., 2009a; A. N. Riesenberg, Liu, Kopan, & Brown, 2009b; Skowronska-Krawczyk, Ballivet, Dynlacht, & Matter, 2004; Souren, Ramon Martinez-Morales, Makri, Wittbrodt, & Wittbrodt, 2009; Willardsen et al., 2009).

1.2.3 Retinal Ganglion Cell Development – Parallel to and downstream of Atoh7

A family of transcription factors downstream of Atoh7 is the Pou-domain family **Brn3a**(Pou4f1), **Brn3b**(Pou4f2), and **Brn3c**(Pou4f3), all three are expressed in development and also through adulthood. Brn3b starts to be expressed at E11.5 in the migrating RGCs in in the neuroblast layer of the retina, and then at E12.5 Brn3a expression was seen only in the ganglion cell layer (Badea, Cahill, Ecker, Hattar, & Nathans, 2009; Mu, Fu, Sun, Beremand, et al., 2005a; L. Pan, Yang, Feng, & Gan, 2005). These are expressed in partially overlapping populations during development and also throughout adulthood. During development they are expressed in 80%, 80%, and ~50% of all RGCs respectively. In the adult 81.6% of RGCs are Brn3a positive and approximately 55% of RGCs are Brn3b positive with even fewer being Brn3c positive. In the adult retina 87% of Brn3a positive RGCs express Brn3b and 78% of Brn3b positive

RGCs express Brn3a. The overlapping expression of Brn3c and the other two Pou-domain family members is approximately 80% as well (Badea et al., 2009; Rodriguez, de Sevilla Müller, & Brecha, 2014; Xiang et al., 1995). Brn3b is required for 70% of RGCs developmental survival, commitment to RGC fate, proper dendritic arbor size, proper inter-retinal axon guidance, and proper brain projections (Badea et al., 2009; Badea & Nathans, 2011; Erkman et al., 1996; Gan, Wang, Huang, & Klein, 1999; Gan et al., 1996). Brn3b is first expressed in late G2/S phase of RPCs in mouse and humans, partially coincident with Atoh7 (L. Feng et al., 2010; Pacal & Bremner, 2014). Interestingly, Brn3a is sufficient to rescue the Brn3b knockout phenotype when placed under control of the Brn3b promoter (L. Pan et al., 2005). Brn3a null mice do have a slightly reduced RGC number, increase in number of bistratified RGCs, and improper dendritic arbor formation (Badea et al., 2009; M. Shi et al., 2013). Brn3c null mice do not have any significant defects, however, Brn3c knockout exacerbates the Brn3b knockouts phenotype with only 13% of wildtype RGC numbers remaining (S. W. Wang et al., 2002). In a Atoh7 null retina, there are only 5% of wildtype RGC numbers, but these remaining RGCs have been seen to express Brn3a, Brn3b, and Islet1, suggesting that while they may be downstream of Atoh7 (Mu, Fu, Sun, Beremand, et al., 2005a; Wu et al., 2015), they can also be activated independently (Hufnagel et al., 2013; Prasov & Glaser, 2012b; S. W. Wang et al., 2001; Wu et al., 2015).

Brn3b has been shown to complex with **Isl1** (Islet1, Lim-homeodomain family), which is also downstream of Atoh7 (R. Li et al., 2014; Mu, Fu, Sun, Beremand, et al., 2005a). Isl1 is expressed at E11.5 in a mostly overlapping population with brn3b in

RGCs, and after E15 it is also expressed in amacrine cells and bipolar cells. In RGCs, from E11 until E13.5 Brn3b and Isl1 have been seen to be co-expressed during late S or G2, however after E15, their expression is seen only in post-mitotic RGCs (Prasov & Glaser, 2012a). A conditional Isl1 knockout leads to defects in bipolar cells, amacrine cells, and RGCs (Elshatory et al., 2007; Rachel et al., 2002). Developmentally, the numbers of RGCs are unchanged in the knockout until E17.5, when RGC specification defects started to arise. By P7 28% of wildtype RGC numbers were seen and by P15 5% of wt RGC numbers were seen, suggesting its role is in the maintenance, differentiation, and survival of RGCs and not their specification (Mu, Fu, Beremand, Thomas, & Klein, 2008). In the adult retina all RGCs, On-bipolar cells, and cholinergic amacrine cells express Isl1. However, a related family member **Isl2** (Islet2) is expressed starting at E13.5 in RGCs and is continued to be expressed in 30-40% of adult RGCs. Isl2 is shown to be expressed only in contralateral projecting RGCs and in Isl2 null mice there is a significant increase in ipsilaterally projecting RGCs, and no decrease in developmental RGC numbers (Elshatory et al., 2007; Pak, Hindges, Lim, Pfaff, & O'Leary, 2004). The effect of Isl2 on survival through development of RGCs is unknown since no conditional mutant exists and Isl2 null mice die at P0.

Brn3b controls the expression of **Tbr2** (Eomes, T-box brain 2) in a subset of Brn3b positive RGCs starting at E14.5. In a retinal specific Tbr2 knockout there is a 30% reduction in RGC numbers (Mao, Kiyama, Pan, Furuta, Hadjantonakis, et al., 2008b). One role of Tbr2 is to specify a unique RGC subtype that express melanopsin making them intrinsically photosensitive RGCs (ipRGCs) as well as a population that have the

ability to express melanopsin. In the retinal specific Tbr2 knockout there are no ipRGCs detectable, and Tbr2 expression allows RGCs to become ipRGCs upon reduction of current ipRGC numbers (Mao et al., 2014). Other rolls for Tbr2 in RGC development are unknown. Another family member **Tbr1** was shown to be directly downstream of Atoh7 (ChIP verified), although its role is unknown (Mao et al., 2013).

Oct1 and **Oct2** (Onecut family) are transcription factors expressed starting at E11.5 in both the neuroblast layer as well as the ganglion cell layer. Oct1&2 are both independent of Atoh7, Brn3b, and Isl1 for expression (Wu et al., 2012). In a retinal specific Oct1 knockout there is an 80% decrease in horizontal cell (HC) numbers, however the rest of the retina seems normal. A similar phenotype is seen for the Oct2 retinal specific knockout which has a 50% decrease in HCs. However, in an Oct1/Oct2 retinal specific double knockout there were no HCs, a 30% reduction in RGC numbers, 30% reduction in cone numbers, 32% reduction in amacrine cell numbers and 16% reduction in bipolar cell numbers. These decreases in cell numbers was not due to an increase in apoptosis suggesting that they are involved in the development of these cells and not their survival (Sapkota et al., 2014; Wu et al., 2013). Thus, Oct1 and Oct2 have compensatory functions in the single knockouts, but combined have a profound role in the development of horizontal cells, cone cells, RGCs, and amacrine cell development. Thus, Oct1 and Oct2 might be involved in a Atoh7-independent RGC developmental program.

Dlx2 (Distal-less homeobox) and **Dlx1** are both expressed in the neural retina during retinogenesis. Dlx2 is expressed beginning at E11.5 and its expression is seen

through adulthood in the GCL, amacrine cells, and horizontal cells, while Dlx1 is expressed at least at E12.5 and it is unknown if it is expressed at E11.5. It is expressed in the GCL and is downregulated after development. Dlx1&2 redundancy is seen elsewhere in the forebrain so was not analyzed in the retina. However, in a Dlx1/Dlx2 null mouse there is a 34% decrease in RGC numbers seen only after E16.5, and no abnormalities were seen in other retinal cell types in the double mutants at least before birth since these animals die at birth. There is also a loss of late born RGCs in the double mutant. The double mutant also showed signs of increased apoptosis of RGCs between E13.5 and E18.5, suggesting Dlx1&2 play a role in the survival or terminal differentiation of these RGCs. The authors suggest Dlx1&2 might play a role in late born RGCs in a Atoh7 independent manner while play a parallel role in early born RGCs, however there is some weak evidence that Dlx1&2 are downstream of Atoh7, and that Dlx1&2 activity is inhibited through direct protein-protein interaction with Brn3b (de Melo et al., 2005; 2007; Eisenstat, Liu, Mione, & Zhong, 1999; L. Feng et al., 2011).

Barhl2 (Bar-class homeodomain) is first expressed at E13.5, however its expression during development is seen only in post-mitotic cells, and in the adult it is expressed in all amacrine cells, all horizontal cells, and 33% of RGCs. Forced overexpression of Barhl2 beginning at P0 leads to increase in amacrine cell numbers and a decrease in bipolar cells and müeler glia cells. A Barhl2 null retina has a 35% decrease in RGC numbers and a 39% decrease in amacrine cell numbers. The reduction in RGC numbers was not observed until after E16.5 correlating with increase in RGC apoptosis in the Barhl2 mutant starting at E16.5. The Barhl2 null retinas had a 95% reduction of

RGCs that lineage label with Barhl2 suggesting it is necessary for the development/survival of the RGCs it is expressed in (Mo, Li, Yang, & Xiang, 2004) (Q. Ding et al., 2009).

Pbx2&4 (Pre-B cell leukemia homeobox family of the Three Amino Acid Loop Extension class) have been studied in Telost retinal formation, but not in mouse. Pbx2&4 expression is seen shortly after optic cup formation and **Pbx1&3b** is expressed in the retina shortly after. Pbx4 null Teleost display a smaller eye phenotype. A Pbx2/Pbx4 null embryo displays normal retinal lamination with axons exiting the retina normally, but the axons stop right before the optic tecturm. This suggests that Pbx2&4 are required for at least the RGC axon targeting in the brain. Interestingly, the authors also saw a massive reduction of Atoh7 in the dorsal retina in the Pbx1/Pbx2 null Teleost suggesting that Atoh7 is downstream of Pbx1&2 or the pathfinding and patterning of the retina leads to loss of Atoh7 expression in this region (French et al., 2007). The role of Pbx1,2,3,&4 is unknown in mouse retinal development.

Vax1 (Ventral-anterior homeobox family) is expressed starting at E8 and at E9-E14 it is expressed in the optic disk, optic stalk, optic chiasm, suprachiasmatic area, and the hypothalamic cell cord (Hallonet et al., 1998). In the Vax1 null mouse the astrocytes of the optic nerve fail to associate with the RGC axons leaving them naked. The RGC axons in the knockout also fail to enter the hypothalamus. Vax1 null optic fissure fails to close (Bertuzzi, Hindges, Mui, O'Leary, & Lemke, 1999).

Vax2 is a family member of Vax1, but it is first expressed at E9.0 in an asymmetric fashion in only the ventral optic vesicle. 70% of Vax2 null mouse have an

incomplete closure of the optic fissure in optic cup development. This is due to the incomplete ventralization in the null retina and also leads to deficits in ventral RGC axon guidance. Specifically, there are no ipsilateral projections and the ventral RGCs terminate where the dorsal RGCs usually terminate in the Superior Colliculus. The targeting deficit can be explained due to reduction in the gradient of EphB2 and EfnB2 expression in RGCs in the Vax2 null retina (Barbieri et al., 2002)(Barbieri et al., 1999).

Tbx2,3,5,&12 (T-box) are expressed beginning at E9.5 in the optic vesicle and are expressed in nested gradients within the dorsal retina. Single knockout of Tbx5 does not have an obvious retina phenotype, suggesting overlapping roles of the family members (Chapman et al., 1996; Schulte & Bumsted-O'Brien, 2008; Sowden, Holt, Meins, Smith, & Bhattacharya, 2001). Interestingly, ectopic ventral overexpression of Tbx5 in the developing chick retina leads to a "dorsalization" of the EphB/ephrinB molecules, but only a minor retinotectal pathfinding deficit was seen in this case (Koshiba-Takeuchi et al., 2000).

1.3 Human Pathologies

Studies have shown that the human homolog of Atoh7, ATOH7, play a similar role in the developing human retina as mutations of this gene have been implicated in genetic retinal diseases. Several single nucleotide polymorphisms (SNPs) in the ATOH7 locus are implicated in susceptibility to glaucoma (Fan, Wang, Pasquale, Haines, & Wiggs, 2011; Ramdas et al., 2011) and smaller optic disc area, as well as the optic cup to optic disk ratio (CDR) (Khor et al., 2011; Macgregor et al., 2010). Glaucoma is the

second leading case of blindness worldwide, projected to effect 79.6 million people worldwide by 2020 (Quigley & Broman, 2006). Glaucoma is defined by RGC injury or malfunction followed by RGC death. Sometimes it is associated with an increase in intraocular pressure (IOP), however this is not always the case (Quigley & Broman, 2006). A smaller optic disk area in addition to a smaller CDR can lead to an increase in inability to diagnose glaucoma. It can also indicate reduced numbers of retinal ganglion cells, however this relationship is debated (Hoffmann, Zangwill, Crowston, & Weinreb, 2007)

Mutations in ATOH7 have been associated with optic nerve hypoplasia (ONH) (reduction in size of the optic nerves) (Khan et al., 2012; Macgregor et al., 2010), optic nerve aplasia (ONA) (absence of optic nerves), and autosomal recessive persistent hyperplasia of the primary vitreous (arPHPV)(persistence of developmental vasculature in the retina), all of which lead to childhood visual impairment or blindness (Prasov, Masud, Khaliq, Mehdi, Abid, et al., 2012a). Severe ONH and ONA have been seen in humans with mutations in OTX2, SOX2, PAX6, HESX1, and ATOH7, however these genes do not explain all cases of ONH or ONA (Azuma et al., 2003; Dattani et al., 1998; Kelberman & Dattani, 2007; McCabe, Alatzoglou, & Dattani, 2011; Ragge et al., 2005). arPHPV occurs when the fetal hyaloid vasculature fails to regress and the retinal vasculature does not form, occurring in some humans patients with Atoh7 mutations and this pathology is also present in mouse Atoh7 mutants (Edwards et al., 2012; Prasov, Masud, Khaliq, Mehdi, Abid, et al., 2012a).

1.4 Development of retinal vasculature

There are two main vascular networks in the retina, the choroid and the retinal vasculature. The choroid is directly below the retinal pigment epithelium (RPE), and supports the photoreceptors. The retinal vasculature is mainly superficial to the retina and provides support for the rest of the retina cells. The retinal vasculature is a beautiful network with three plexi; superficial (NFL), intermediate (IPL), and deep (OPL). However, in mice, this retinal vasculature network only develops after birth and can take up to three weeks to fully develop. To provide support to the lens and retina during embryonic retinal development, and while the retinal vasculature forms postnatally, there is the hyaloid vascular network. This Hyaloid vasculature forms at E10.5 and regresses after birth. The regression is substantial by P8 and is majorly regressed by P16, but traces can be found up until P30 when the retinal vasculature is fully formed (Dorrell, Aguilar, & Friedlander, 2002; Edwards et al., 2011). The mechanism of regression of the hyaloid vasculature is not fully known, but the timing of regression is refined by the retinal clock and Opn4/Opn5 mediated light activity in the retina. In the absence of Opn4, or when dark reared from E16-E17, the hyaloid vasculature regresses a few days later than normal (Rao et al., 2013). In the absence of Opn5 the hyaloid vasculature regresses a few days earlier (Nguyen et al., 2019). If the hyaloid vasculature partly or fully fails to regress there, it can lead to visual deficits later in life and it can prevent the retinal vasculature from properly forming. In mice there are multiple models of persistent hyaloid vasculature, including mutations in Lrp5, Arf, Fzd4, Ang2, Bmp4, and of interest to this study, Atoh7 (Edwards et al., 2012; Prasov, Masud, Khaliq, Mehdi, Abid, et al., 2012a;

Saint-Geniez & D'amore, 2004). In the Atoh7 mutant mice the hyaloid vasculature fails to regress and the retinal vasculature fails to form. The persistent hyaloid vasculature in these mice improperly dove into the retina to provide support that should have been provided by the retinal vasculature. These data lead Edwards et al to propose that RGCs are critical for this hyaloid vasculature regression and ILM development (Edwards et al., 2012; Yoshikawa et al., 2016). In Brn3b mutant mice, which experience early RGC loss, the superficial retinal vasculature also fails to form (Sapieha et al., 2008).

1.5 Retinal Transcription Factor Family Equivalence in the Development of RGCs

Several elegant genetic studies have addressed the mechanism by which Atoh7 regulates RGC specification. In mouse, when Neurod1, a close homolog of Atoh7, was expressed from the Atoh7 locus it rescued only 30% of wildtype RGC numbers and their axons were able to form an optic nerve with a size consistent with the lower number of RGCs (Mao, Wang, Pan, & Klein, 2008a). When NeuroD1 and Atoh7 were both mutated at the same time fewer RGCs were seen compared to the Atoh7 mutant (Kiyama et al., 2011). In addition, ectopic Atoh7 expression from the Neurod1 locus causes an 30% increase over wildtype RGC numbers, and in Atoh7 null animals, this ectopic expression rescued only 28% of RGCs that properly innervated retinorecipient areas in the brain (Mao et al., 2013).However, this was not observed when either of two other close homologues of Atoh7 -- Ascl1 or Neurod4 -- where expressed from the Atoh7 locus (Hufnagel et al., 2013; Mao, Wang, Pan, & Klein, 2008a). Selective rescue of Atoh7

expression during late retinal development in zebrafish, rescued the later born RGCs, but these RGCs were unable to project to the optic tecta. However, early born, Atoh7 expressing, RGCs were sufficient to allow the later born RGCs to properly project to the optic tecta (Pittman, Law, & Chien, 2008). Similar results in mice were observed when Atoh7 was expressed from the Crx locus, which is first expressed at E12.5 in precursor cells, the optic nerve was only weakly rescued and the number of RGCs present were only 12% of wildtype (Prasov & Glaser, 2012b). Remarkably, a full rescue of the Atoh7 null was observed when only two transcription factors known to be required for RGC survival and development, the POU domain, class 4, transcription factor 2 (Pou4f2; also known as Brn3b) and Insulin gene enhancer 1, Islet 1 (Isl1), were ectopically expressed from the endogenous Atoh7 locus (Gan et al., 1999; L. Pan, Deng, Xie, & Gan, 2008; Wu et al., 2015). These studies show that Pou4f2 and Islet1 act downstream of Atoh7, and the regulation of their temporal expression by Atoh7 is sufficient to restore wild-type-like RGCs.

1.6 Not all RGCs are of the Atoh7 Lineage

A complication for the necessity of Atoh7 in RGC specification, however, arises from an observation that only 55% of RGCs in adults are derived from the Atoh7 lineage (Brzezinski et al., 2012; L. Feng et al., 2010; Poggi et al., 2005). Not only are only 55% of RGCs of the Atoh7 lineage, but in the Atoh7^{Cre} mouse line only 11% of all Atoh7 expressing cells become RGCs and that Atoh7 is expressed in 2.9% of all retinal cell types, including some portion of every major cell type in the retina, specifically; 31% of

cones, 29% of amacrine cells, and <0.1% of Müller glia. One explanation for this finding is that the Atoh7^{Cre} mouse line might not reflect endogenous Atoh7 expression, due to leaky Cre activity (Brzezinski et al., 2012). However, the non-RGC cell labeling is consistent across animals and within the same retina, indicating this is unlikely to be "leaky" (Brzezinski et al., 2012; Prasov, 2012). This finding was shocking and quantified previously published reports in an independently made mouse model that showed Atoh7 lineage cells in all major cell types in the retina(L. Feng et al., 2010). These studies went against the current model in the field that suggests that Atoh7 is the master transcriptional regulator of RGC development. If that was the case, then all RGCs should express Atoh7 as they transition from RPCs to RGCs, and the expression of Atoh7 should be instructive of that transition. Also, Atoh7 should be only expressed in RGCs and not in other cell types. The non-RGC-lineage expression of Atoh7 could be explained as asymmetric division of RPCs to RGC and an RPC where the cre-recombinase protein diffuses throughout the dividing cell and thus labels all of its daughter cells. However, the under labeling of RGCs by multiple different Atoh7-driven cre recombinase lineage analysis studies, was never fully accepted. Excuses have been made as to why a certain cre-recombinase line was ineffective, for example a neomycin cassette was left in the locus and that it was a BAC transgenic without the entire regulatory regions. We have seen similar Atoh7 lineage labeling in our hands using different reporters, but the same Atoh7-cre mouse line. The explanation that was proposed by the is that there is a significant population, up to 45% of RGCs, that does not use Atoh7 in its specification. Our work provides substantial evidence that these prior lineage labeling studies are correct. Implicit

in this observation is that 45% of RGCs develop from non-Atoh7-positive precursors, but they are incapable of surviving in the absence of Atoh7, as the Atoh7 mutant lack 95% of RGCs.

1.7 Cell Death during Retinal Development

Cell death is an important part of retinal development, with apoptotic cell death observed in approximately 60-70% of RGCs during normal development (Farah & Easter, 2005; Mosinger Ogilvie, Deckwerth, Knudson, & Korsmeyer, 1998; Strom & Williams, 1998). There are at least three windows of apoptosis that occur during RGC development. The first of these is an early window that lasts from the onset of RGC generation until E13.5, and results in part from intra-retinal signaling of BDNF (Frade, Bovolenta, MartinezMorales, Arribas, & RodriguezTebar, 1997; Péquignot et al., 2003; Rodríguez-Gallardo, Lineros-Domínguez, Francisco-Morcillo, & Martín-Partido, 2005)(reviewed (Valenciano, Boya, & la Rosa, 2009)). The second window of programed cell death, seen from birth until P12, is likely driven mainly by target derived neurotrophic factors (Linden & PINTO, 1985; Péquignot et al., 2003; Pollock et al., 2003; Strom & Williams, 1998; Young, 1984). The third window peaks around eye opening, lasting from P13 to P21, and is driven by refinement of intra-retinal connections (Péquignot et al., 2003; M. A. Williams, Piñon, Linden, & PINTO, 1990).

Apoptosis in all three of these periods is Bax(BCL2 Associated X, Apoptosis Regulator)-mediated, as in its absence there is 226% increase in RGC numbers (Mosinger Ogilvie et al., 1998; Péquignot et al., 2003). Consistent with this requirement for Bax,

loss of function of the programed cell death 1 ligand 1 and ligand 2 (PD-L1/L2) lead to increased numbers of RGCs, although to a much lesser extent than Bax mutants (Braunger et al., 2013; Harada et al., 2006; Pollock et al., 2003; Sham et al., 2012). Surprisingly little is known about how the regulation of these different phases of retinal apoptosis is occurring, with most research focusing only on the P0-P12 phase. Targeted mutants of major neurotrophic receptors such as TrkA, TrkB, BDNF, p75, and TGFbeta all have no effects on adult RGC numbers (Harada et al., 2006; Pollock et al., 2003). The only exception is retinal-specific loss of function of Smad7, a downstream transcription factor that inhibits TGFbeta signaling, which leads to a modest increase of RGCs (17%), compared to Bax mutations. Conversely, TGF-β type II receptor knockouts led to a significant decrease in adult RGC (40%) number (Braunger et al., 2013). To further complicate the story, the developmental overproduction of RGCs is partially dependent on Atoh7 expression levels, as shown in Atoh7$^{+/-}$ mouse, which at birth, has 30% fewer RGCs than wildtype littermates. This lower number of RGCs is corrected after the 2nd and 3rd phases of apoptosis (Prasov, Nagy, Rudolph, & Glaser, 2012b). Even though the earliest RGCs are born at E10.5, starting at E13.5 there is an increase in apoptotic cells in the non-Atoh7 dependent lineage in Atoh7 mutant mice. There is also an increase across retinal development in Atoh7-lineage cells across embryonic retinal development, and an increase in non-Atoh7-lineage cells in the GCL at E16.5 and E17.5 (L. Feng et al., 2010; Prasov & Glaser, 2012b). Interestingly, in zebrafish, there was no signs of apoptosis in the absence of Atoh7 (Kay et al., 2001). These data indicate that Atoh7 may play an underappreciated role in regulating apoptosis at early stages in retinal development.

In Zebrafish mutation of Atoh7 (lakritz), no apoptosis was seen by TUNEL staining (Kay et al., 2001). The differences between mouse and zebrafish could be due to the absence of the Atoh7-dependent survival signal leading to very fast death of developing RGCs, or cross-differentiation since the zebrafish retina is much more plastic. If the cell death is very fast the TUNEL staining might not be sensitive enough to see the apoptosis and the more sensitive "triple death stain" might resolve apoptosis on this timescale (S.-K. Chen et al., 2013). It is also possible that Atoh7 acts differently in zebrafish, who are constantly regenerating their retina throughout their life compared to mice. In the original mouse studies of Atoh7, the increase in apoptosis, now appreciated (L. Feng et al., 2010), was not seen (N. L. Brown et al., 2001), so it could have been missed, or an incorrect timepoint might have been studied, as they only looked at 30 or 48 hpf (Kay et al., 2001).

1.8 Extrinsic Factors in RGC Development

Gdf11, Vegf, Shh, Fgf, and Notch are all the known extrinsic signaling molecules involved in RPC division, RPC exit from cell cycle, and expression of Atoh7. Gdf11 (Growth differentiation factor 11)(TGF-β/BMP superfamily), expressed in neuroblast later (NBL) and GCL, negatively regulates the number of RGCs and is antagonized by Fst (Follistatin-like 3). Fst forms inactive complexes with Gdf11, is expressed in the GCL, and is a positive regulator of RGC development. Gdf11 signaling has a larger effect during the second half of RGC development, as RGC density increases. The increase of RGCs seen in the absence of Gdf11 is at the expense of bipolar and amacrine cells (Kim

et al., 2005). Vegf, secreted by RGCs, acts on RPCs, promoting their proliferation and suppressing RGC development, through the Vegfr2/Flk1 receptor and Hes1 (Hashimoto, Zhang, Chen, & Yang, 2006; Nishiguchi, Nakamura, Kaneko, Kachi, & Terasaki, 2007). Notch3-Rbpj-Hes1 signaling negatively regulates RGC genesis and positively regulates RPC proliferation, however Rbpj and Hes1 can both be activated independently of Notch signaling. Notch1 has also been seen to promote RPC proliferation while inhibiting RPC cell cycle exit, and RGC genesis (Hashimoto et al., 2006; Miesfeld et al., 2018; A. N. Riesenberg, Liu, Kopan, & Brown, 2009b; Yaron, Farhy, Marquardt, Applebury, & Ashery-Padan, 2006). Shh is expressed by RGCs and has been shown to negatively regulate RGC genesis and Atoh7 expression at the point of terminal differentiation as well as Positively regulate Hes1, and RPC cell cycle. Shh signals to the RPCs through Gli1 in a short-range fashion. Shh assists, but is not necessary, for the maintenance of the neurogenic wave front, driven by Neurog2, for RGC genesis (Hufnagel et al., 2010; Sakagami, Gan, & Yang, 2009; Y. P. Wang, Dakubo, Thurig, Mazerolle, & Wallace, 2005b; X. M. Zhang & Yang, 2001). Besides target derived factors in the retino-recipient targets, there are no extrinsic factors are known that regulate RGC survival in the retina.

1.9 Diversity of RGCs

Up until recently there was thought to be 25-32 different types of RGCs many of which transmit different types of information from the retina to the almost 46 retino-recipient areas in the brain (Baden et al., 2016; Masland, 2001; Morin & Studholme, 2014; Sanes & Masland, 2015; Wernet, Huberman, & Desplan, 2014). The classification of an RGC type was done by a combination of morphological, electrophysiological, genetic, and retinal distribution analysis. However, the genetic analysis done up until recently has been low throughput, especially at higher or single cell resolution. Using scRNA-seq of P5 mouse retina, 40 types of RGCs were genetically defined. These data came from the analysis of the transcriptome of 6,225 RGCs. And since this analysis was done at P5, before eye opening, it is possible for the 40 types of RGCs to further diversify into subtypes or more types after eye opening and the completion or eye development. The 40 different types of RGCs were able to be distinguished by a combination of mostly 2 to sometimes 3 genes (Rheaume et al., 2018). The differential regulation of transcription factors that combine to create the diversity in RGC type (dendritic arbor size, electrophysiological properties, brain targets, soma size, etc.) are mostly unknown and a current topic of intense research, a few of the understood mechanisms are mentioned above and the other known factors will not be covered in this thesis (Wernet et al., 2014). However, the current dogma that all 40 of these very diverse and distinct types of RGCs arise from Atoh7 just does not follow common sense. It makes more sense that to generate such a diverse pool of RGCs multiple different and parallel pathways would

be in place, our work, seen in the following chapter, along with others beautiful work vividly suggest this.

1.10 Summary

The necessity but not sufficiency of Atoh7 in the development of RGCs, its expression in only 55% of RGCs, and the increase in RGC cell death seen in the absence of Atoh7, brought us to directly investigate whether Atoh7 indeed acts solely as an RGC specification factor. To differentiate functions of Atoh7 in RGC specification and in regulation of RGC survival, we re-examined the Atoh7 null mouse line on a background that prevents RGC death by knocking out the proapoptotic gene, Bax. If Atoh7 were only responsible for RGC specification and not RGC survival, inhibiting cell death in Atoh7 knockout animals should cause no differences in RGC number relative to animals lacking Atoh7 alone. However, If Atoh7 plays a role in the developmental survival of all RGCs and not their specification, then in the absence of Atoh7 and Bax, RGCs would develop normally. We observed that substantial numbers of retinal progenitor cells differentiate into normal RGCs in the absence of Atoh7 and Bax. These RGCs failed to project to the brain but were able to form functional retinal circuitry. Furthermore, these RGCs showed nearly identical expression of RGC transcripts, with some clear differences that could implicate factors in specification and or survival of RGCs. Our data show conclusively that there are, at least, two populations of RGCs, those that require Atoh7 for specification and those that do not, however nearly all RGCs require Atoh7 for developmental survival in a cell non-autonomous fashion.

Chapter 2 – Atoh7-independent specification of retinal ganglion cell identity

This chapter is based on a manuscript currently in submission:

Justin Brodie-Kommit, Brian S. Clark, Qing Shi, Fion Shiau, Dong Won Kim, Jennifer Langel, Catherine Sheely, Philip A Ruzycki, Michel Fries, Awais Javed, Michel Cayouette, Tiffany Schmidt, Tudor Badea, Thomas Glaser, Haiqing Zhao, Joshua Singer, Seth Blackshaw, Samer Hattar. Atoh7-independent specification of retinal ganglion cell identity. bioRxiv 2020.05.27.116954; doi: https://doi.org/10.1101/2020.05.27.116954

2.1 Abstract

Retinal ganglion cells (RGCs) relay visual information from the eye to the brain. RGCs are the first cell type generated during retinal neurogenesis. Loss of function of the transcription factor *Atoh7*, expressed in multipotent early neurogenic retinal progenitor cells, leads to a selective and essentially complete loss of RGCs. Therefore, *Atoh7* is considered essential for conferring competence on progenitors to generate RGCs. DNA binding sites analysis of Atoh7 using the Cut&Run method demonstrates that Atoh7 directly targets genes controlling RGC specification. Despite the important function of Atoh7 in RGC specification, when apoptosis is inhibited in *Atoh7*-deficient mice by loss of function of *Bax*, only a modest reduction in RGC number is observed. Single-cell RNA-Seq of *Atoh7;Bax*-deficient retinas shows that RGC differentiation is delayed, but that the gene expression profile of RGC precursors is grossly normal. *Atoh7;Bax*-deficient RGCs eventually mature, fire action potentials, and incorporate into retinal circuitry, but exhibit severe axonal guidance defects. This study reveals an essential role for *Atoh7* in RGC survival and demonstrates *Atoh7*-independent mechanisms for RGC specification.

2.2 Introduction

The retina has six major classes of neurons that develop from a common progenitor cell pool during overlapping temporal intervals. Retinal ganglion cells (RGCs), the only projection neurons from the retina to the brain, are the first retinal cell type to be generated. RGC development in zebrafish, mice, and humans has been shown to require the basic helix-loop-helix transcription factor atonal homolog 7 - *Atoh7 (Math5)* (Brown et al., 2001; Ghiasvand et al., 2011; Jarman et al., 1994; Khan et al., 2011; Khor et al., 2011; Macgregor et al., 2010; Prasov et al., 2012; Wang et al., 2001). *Atoh7* is conserved across all vertebrate species, and distantly related to *atonal*, which specifies the earliest-born neurons in *Drosophila* retina (Brown et al., 2001; Jarman et al., 1994; Kanekar et al., 1997; Prasov et al., 2012). *Atoh7*-deficient mice and zebrafish lack upwards of 95% of RGCs (Brown et al., 2001; Brzezinski et al., 2012; Kay et al., 2001; Wang et al., 2001) and likewise lack any visible optic nerve or functional connections from the retina to the brain (Brzezinski et al., 2005; Wee et al., 2002). Human mutations in *ATOH7* or its cis-regulatory regions have been associated with optic nerve agenesis or hypoplasia (Khan et al., 2012; Macgregor et al., 2010) and increased susceptibility to glaucoma (Fan et al., 2011; Ramdas et al., 2011). *Atoh7*-deficiency also disrupts the development of retinal vasculature in both mice and humans, likely as an indirect result of the loss of RGCs (Edwards et al., 2012).

In mice, *Atoh7* is expressed in neurogenic retinal progenitor cells (RPCs) between E12 and P0, corresponding to the interval in which RGCs are generated (Brown et al., 1998; Clark et al., 2019; Feng et al., 2010; Pacal and Bremner, 2014; Prasov and Glaser,

2012; Rapaport et al., 2004; Sidman, 1960; Wang et al., 2001; Young, 1985). Upon cell fate specification, *Atoh7* expression is rapidly down-regulated in mouse RGC precursors (Clark et al., 2019; Miesfeld et al., 2018a) although expression persists in immature human RGCs (Aparicio et al., 2017; Lu et al., 2020). Genetic fate mapping indicates that *Atoh7*-expressing RPCs also give rise to other early-born retinal cells, including cone photoreceptors, horizontal and amacrine cells, and that generation of these cell types is increased in *Atoh7*-deficient mice (Brown et al., 2001; Brzezinski et al., 2005; Hufnagel et al., 2013; Wang et al., 2001). Ectopic expression of *Atoh7* alone, however, typically is not sufficient to drive RGC specification (Gan et al., 1999; Hufnagel et al., 2013; Mao et al., 2013, 2008; Ohnuma et al., 2002; Pan et al., 2008; Pittman et al., 2008; Prasov and Glaser, 2012; Wu et al., 2015), although misexpression of Atoh7 in Crx-expressing photoreceptor precursors was sufficient to rescue the development of a limited number of RGCs (Prasov and Glaser, 2012).

These findings have suggested that *Atoh7* acts in neurogenic RPCs to confer competence to generate RGCs (Brzezinski et al., 2012; Mu et al., 2005; Yang et al., 2003) potentially in combination with as yet unidentified factors. Recent experiments have shown that when *Pou4f2* and *Isl1* are expressed under the control of the endogenous *Atoh7* promoter, these transcription factors are sufficient to fully rescue the defects in RGC development seen in *Atoh7* mutants (Gan et al., 1999; Pan et al., 2008; Wu et al., 2015). This implies that *Atoh7* may act permissively to enable the expression of these two factors in early-stage RPCs.

Other data, however, suggest that a large number of RGCs are specified independent of *Atoh7*. Previous studies indicate that immature RGCs are present in *Atoh7*-deficient mice in embryonic retina, although at reduced numbers relative to controls (Brown et al., 2001; Brzezinski et al., 2012). Genetic fate-mapping studies further raise questions about the necessity of *Atoh7* for all RGC specification. Analysis of *Atoh7-Cre* knock-in mice reveals that only 55% of all RGCs are generated from *Atoh7*-expressing RPCs (Brzezinski et al., 2012; Feng et al., 2010; Poggi et al., 2005). Although this outcome may reflect inefficient activation of Cre-dependent reporter constructs, it may also imply that a subset of RGCs is specified through an *Atoh7*-independent mechanism that requires trophic support from *Atoh7*-expressing RPCs or *Atoh7*-derived RGCs.

To distinguish the role of *Atoh7* in controlling RGC specification and survival, we prevented RGC death in *Atoh7*-deficient mice by simultaneously inactivating the proapoptotic gene *Bax* (Chen et al., 2013; Knudson et al., 1995). The idea being if RGCs can be specified in the absence of Atoh7 but require it for trophic support, we should reveal RGCs that are specified in an Atoh7-independent manner when cell death is prevented. Strikingly, we observed only a 25.2±0.9% reduction in adult RGC numbers in $Atoh7^{-/-}$;$Bax^{-/-}$ retinas relative to $Bax^{-/-}$ controls, implicating an unrecognized Atoh7-independent specification pathway for RGCs. While mutant RGCs showed severe defects in the formation of axonal projections and retinal vasculature, we found that the Atoh7-independent RGCs expressed both *Pou4f2* and *Isl1*, the two transcription factors that are sufficient to fully compensate for Atoh7 function. These RGCs also fired action

potentials in response to light and formed functional synapses with upstream retinal neurons. Single-cell RNA-Sequencing (scRNA-Seq) analysis of *Atoh7;Bax*-deficient retinas shows that *Atoh7*-deficient RGC differentiation is delayed relative to wildtype, implicating Atoh7 as responsible for generating the early born pioneering RGCs. Our results imply a new pathway for specifying RGCs that is independent of Atoh7.

2.3 Results

2.3.1 *Atoh7* promotes RGC survival, but RGC specification is largely *Atoh7*-independent

In the absence of *Atoh7,* there is an increase in apoptosis of both *Atoh7*-derived cells across embryonic retinal development and non-*Atoh7*-derived cells in the GCL at E16.5 and E17.5 (Feng et al., 2010; Prasov and Glaser, 2012). These data suggest that *Atoh7* may promote RGC survival in both a cell-autonomous and cell non-autonomous manner. To better understand the role *Atoh7* plays in RGC development, independent of its role in RGC survival, we disrupted both *Atoh7* and the proapoptotic *Bax* gene, in order to inhibit apoptosis in the retina.

We used $Atoh7^{Cre/Cre}$ mice, in which the *Atoh7* coding sequence is replaced with Cre recombinase via targeted recombination, generating a null allele, to analyze Atoh7 function (Yang et al., 2003). We first examined the expression of RBPMS and Isl1, both of which are broadly expressed in RGCs, in $Atoh7^{Cre/Cre};Bax^{-/-}$ mice (Figure 1A-C) (hereafter referred to as $Atoh7^{-/-};Bax^{-/-}$ mice). *Isl1*, a LIM family homeodomain transcription factor, is necessary for RGC development and maintenance in adulthood

(Mu et al., 2008; Pan et al., 2008), and is expressed in mature RGCs, bipolar, and amacrine cells. Using anti-Rbpms to selectively label all RGCs, we observed an 159±7% (Figure 1A,B) increase in RGC number in *Bax*$^{-/-}$ retinas, in line with previous results indicating that RGCs undergo extensive levels of apoptosis during development. However, we observe only a 25.2±0.9% reduction in RGCs in *Atoh7*$^{-/-}$;*Bax*$^{-/-}$ relative to *Bax*$^{-/-}$ retinas. This contrasts with the 99.54±0.12% reduction in RGCs in the *Atoh7*$^{-/-}$ compared to controls (Figure 1A,B). Similar results were observed for anti-Isl1 cells in the GCL (Figure 1A,C).

Specific RGC markers, Brn3a (Pou4f1) and Brn3b (Pou4f2), were used to quantify RGCs. For wildtype and *Bax*$^{-/-}$ lines, Brn3a and Brn3b numbers were similar to published reports (Figure 1D-F) (Prasov and Glaser, 2012; Rodriguez et al., 2014; Wang et al., 2001; Xiang et al., 1995). In the *Atoh7*$^{-/-}$ line a 99.8±0.2% reduction in Brn3a RGC density was observed. However, in *Atoh7*$^{-/-}$;*Bax*$^{-/-}$ mice, the Brn3a RGCs were substantially rescued in the *Atoh7*$^{-/-}$ background and remained into adulthood. 74.7±0.9% of Brn3a RGCs are rescued in *Atoh7*$^{-/-}$;*Bax*$^{-/-}$ mice relative to *Bax*$^{-/-}$ levels in adult, and RGCs display normal distribution across the entire retina (Figure 1D,E, Supplemental Figure 1A,A'). Interestingly, Brn3b RGCs were also rescued in *Atoh7*$^{-/-}$;*Bax*$^{-/-}$ relative to *Bax*$^{-/-}$ retinas, but to a much lesser extent than the Brn3a (28.8±5.9%; Figure 1D,F, Supplemental Figure 1B,B'). Expression of *Isl1*, *Brn3b*, and, to a lesser extent *Brn3a* have previously reported to require *Atoh7* (Mu et al., 2008, 2004, 2005; Pan et al., 2008; Rodriguez et al., 2014; Wu et al., 2015). However, our data demonstrates that the

expression of *Isl1*, *Brn3a,* and *Brn3b* in RGCs can occur independent of *Atoh7* (Figure 1).

To investigate the extent to which rescued RGCs resembled wildtype neurons, we examined the expression of markers of major classes of mature RGCs. We investigated the prevalence of intrinsically photosensitive RGCs (ipRGCs) within *Atoh7*$^{-/-}$;*Bax*$^{-/-}$ retinas. During the development of ipRGCs, a majority of cells express Brn3b, although in some cases only transiently (Chen and Hattar, 2012). To determine the percentage of rescued ipRGCs in *Atoh7*$^{-/-}$;*Bax*$^{-/-}$ mice, we used a melanopsin antibody that predominantly labels the high melanopsin-expressing M1 and M2 ipRGC populations. We observe that 34.1% of ipRGCs are rescued in *Atoh7*$^{-/-}$;*Bax*$^{-/-}$ mice relative to *Bax*$^{-/-}$, proportions similar to the fraction of Brn3b-positive RGCs in wildtype (Figure 1D,F, Supplemental Figure 1C-F). This indicates that rescued Brn3b-positive ipRGCs can differentiate in the absence of *Atoh7*.

To eliminate the possibility that global loss of function of *Bax* caused a non-specific rescue of RGC development, we tested the effects of retina-specific conditional mutants of *Bax*, using *Chx10-Cre;Atoh7*$^{Cre/Cre}$;*Bax*$^{fl/fl}$ (Figure 1G,H). In this model, *Bax* is selectively disrupted in RPCs beginning at E10-10.5 (Rowan and Cepko, 2004). Removal of *Bax* from all RPCs shows RGC development to the same extent as in *Atoh7*$^{Cre/Cre}$;*Bax*$^{-/-}$ (Figure 1G, H). This indicates that the rescue of RGCs is specific to the retina.

We then reasoned if cell death has to be rescued specifically in Atoh7-independent RGCs, then *Atoh7*$^{Cre/Cre}$;*Bax*$^{fl/fl}$ mice should fail to rescue the deficits of the lack of Atoh7. In fact, we observed that *Atoh7*$^{Cre/Cre}$;*Bax*$^{fl/fl}$ mice did not show any

detectable rescue of RGC development (Figure 1G,H), suggesting that cell death rescue in non-Atoh7 cells is necessary for RGCs to differentiate and form connections with retinal neurons.

In both wildtype and *Atoh7*$^{-/-}$;*Bax*$^{-/-}$ animals, 34±11% and 34±26% of RGCs, respectively, are derived from Atoh7-expressing cells, a finding which independently confirms similar lineage tracings in previous studies (Supplemental Figure 2A-C) (Brzezinski et al., 2012; Feng et al., 2010). This indicates that while RGCs that are normally derived from *Atoh7*-expressing neurogenic RPCs are reduced in the absence of *Atoh7*, *Atoh7* is not required for their specification. Furthermore, RGCs that are derived from non-*Atoh7*-expressing RPCs require *Atoh7* for survival through a non-cell autonomous mechanism.

2.3.2 RGCs specified in the absence of *Atoh7* generate light-driven photic responses transduced from the outer retina

As we determined that loss of Bax in the *Atoh7*$^{-/-}$ background rescues a large percentage of RGC specification, we next sought to investigate the degree to which RGCs differentiated in the absence of *Atoh7*. One hallmark of RGC differentiation is the formation of presynaptic contacts and the generation of light-induced action potentials. We used multi-electrode array (MEA) recordings to test the light responsiveness of the RGCs within the various mutant models. Spatiotemporal noise stimuli were used to activate the retina with a mean excitation of 398 nm ($I_{mean} \approx 5 \times 10^3$ photons/cm^2/s), a wavelength that predominantly activates S-cones (Wang et al., 2011), and does not

activate Opn4-expressing ipRGCs (Berson et al., 2002; Do, 2019; Do and Yau, 2010; Hattar et al., 2002). We observed an identical stimulus-response profile in wildtype and *Bax*$^{-/-}$ RGCs (Figure 2A): an expected result given that *Bax*$^{-/-}$ mice display normal visual responses within the Morris water maze test (Chen et al., 2013). The population of RGCs included cells with similar light-evoked responses as ON sustained, ON transient, ON/OFF transient, OFF transient, or OFF sustained RGCs (Figure 2A, Supplemental Figure 3). The spatial receptive fields of the *Atoh7*$^{-/-}$*;Bax*$^{-/-}$ RGCs were slightly smaller than normal (Atoh7$^{-/-}$;Bax$^{-/-}$ average 191±37.1 μm [n=56 from 8 mice], control average 212±42.3 μm [n=92 from 5 mice] and Bax$^{-/-}$ average 223±42.4 μm [n=96 from 4 mice]) (Figure 2B) and the kinetics of the light-driven responses in the *Atoh7*$^{-/-}$*;Bax*$^{-/-}$ retinas slightly slower than those of control and Bax$^{-/-}$ cells (Figure 2C).

The linear analysis used for the MEA data can only reveal an averaged spike triggered averaging (STA), which could be a compression of multiple receptive fields. Thus those having multiple receptive fields such as ON-OFF cells could potentially be hidden with this method and require more sophisticated analysis strategy (Shi et al., 2019). However, diversity in peristimulus time histogram (PSTH) profiles is clearly observed, suggesting that different cell types coexist in *Atoh7*$^{-/-}$*;Bax*$^{-/-}$ mice. We chose not to perform more complex analysis such as classifying each cell into known cell types due to the relatively small sample size. These will be intriguing questions to address when larger amounts of data are made accessible. The near-normal properties of the *Atoh7*$^{-/-}$*;Bax*$^{-/-}$ RGCs show that RGCs present in the *Atoh7*$^{-/-}$*;Bax*$^{-/-}$ are wired properly to the outer retina, specifically the S-cones, and receive normal circuit input.

2.3.4 RGC axon guidance is *Atoh7*-dependent

While RGCs in *Atoh7*$^{-/-}$;*Bax*$^{-/-}$ animals appropriately respond to the detection of visual stimuli by the outer retina, the ability of these RGCs to form postsynaptic connections in the brain is compromised. We observed a substantially reduced pupillary light response (PLR) in *Atoh7*$^{-/-}$;*Bax*$^{-/-}$ animals compared to controls (Figure 3B,C). To determine the cause of behavioral deficits, we assessed the distribution of RGC axons. Immunostaining for Smi32 (non-phosphorylated Nfh) (Figure 3A,D, Supplemental Figure 4C), Nfh, and Nfm (Supplemental Figure 4A,B) was used to evaluate RGC axonal integrity, and showed normal architecture in wildtype and *Bax*$^{-/-}$ mice. We were surprised to find that the <1% of RGCs that survive in the *Atoh7*$^{-/-}$ showed severe guidance defects, in that they fasciculate, come in close proximity to where the optic disc should be, seem to overshoot the optic disc, and then continue to extend within the retina. The great majority of *Atoh7*$^{-/-}$ RGC axons fail to correctly target the optic disc, with only a few axons exiting and forming a rudimentary optic nerve, leading to a severely reduced PLR (Figure 3B,C, Supplemental Figure 5A-C). The gross misguidance of axons was also observed in *Atoh7*$^{-/-}$;*Bax*$^{-/-}$ mice (Figure 3A,D). As in *Atoh7*$^{-/-}$ mice, RGC axons in *Atoh7*$^{-/-}$;*Bax*$^{-/-}$ mice fasciculate, fail to correctly target the optic disk, and form tracts that extend around the retina, with only rudimentary optic nerves observed. This guidance defect did not result from the defective formation of the optic disc, as Pax2-positive glial cells that mark this structure are present in the *Atoh7*$^{-/-}$;*Bax*$^{-/-}$ at E12.5 (Supplemental Figure 6A,B). This demonstrates that the optic disk is present, but the axons are unable to find their way out of the retina in large numbers. These findings are reminiscent of previous reports in

zebrafish, in which morpholino-mediated disruption of *atoh7* expression in early-stage RPCs disrupted the correct targeting of axons of later-born, *atoh7*-positive RGCs to the optic tectum (Pittman et al., 2008).

Previous studies have observed a lack or massive reduction in physical or functional connection to the brain in *Atoh7*$^{-/-}$ mice (Brown et al., 2001; Brzezinski et al., 2005; Triplett et al., 2011; Wee et al., 2002). Consistent with the failure of mutant RGCs to correctly target the optic nerve, we observe severe disruptions in behavioral responses to light in *Atoh7*$^{-/-}$*;Bax*$^{-/-}$ mice that are essentially indistinguishable from those seen in *Atoh7*$^{-/-}$ mice. *Atoh7*$^{-/-}$*;Bax*$^{-/-}$ mice show no detectable optokinetic response (Supplemental Figure 7A), and show no visual cue-dependent reduction in escape time during successive trials of the Morris water maze (Supplemental Figure 7B). *Opn4:Tau-lacZ* knock-in mice, which visualize the axonal projections of M1 ipRGCs, show no detectable signal in the brain (Supplemental Figure 7C) (Hattar et al., 2002). Intraocular injection of fluorescently-labeled cholera toxin beta, which visualizes RGC axonal terminals (Bedont et al., 2014), likewise shows no brain labeling in both *Atoh7*$^{-/-}$*;Bax*$^{-/-}$ and *Atoh7*$^{-/-}$ *mice* (Supplemental Figure 7D). However, while the contralateral PLR is significantly reduced compared to wildtype in both the Atoh7$^{-/-}$ and *Atoh7*$^{-/-}$*;Bax*$^{-/-}$ mice, it is nonetheless detectable, indicating that a small number of RGC axons target the olivary pretectal nucleus in *Atoh7*$^{-/-}$*;Bax*$^{-/-}$ mice, although we are unable to detect these using standard techniques (Figure 3B,C, Supplemental Figure 5 A-C).

2.3.4. Retinal vasculature development is disrupted in the absence of *Atoh7*

In both mice and humans, loss of *Atoh7* expression results in persistence of the hyaloid vasculature (Edwards et al., 2012; Ghiasvand et al., 2011; Kondo et al., 2016; Prasov et al., 2012). The persistence of the hyaloid vasculature in *Atoh7*$^{-/-}$ retinas until P14 was previously observed. We likewise observe persistence of the hyaloid vasculature into adulthood in *Atoh7*$^{-/-}$ retinas (Figure 3E), which is observed even in one year old mice (data not shown). Surprisingly, even with the rescue of a majority of Brn3a RGCs in *Atoh7*$^{-/-}$*;Bax*$^{-/-}$ animals, the hyaloid vasculature still fails to regress (Figure 3E). Likewise, *Crx>Atoh7;Atoh7*$^{-/-}$ mice, in which *Atoh7* is misexpressed in photoreceptor precursors, also fail to induce hyaloid regression (Figure 3E). This is in sharp contrast to the rescued vascular phenotype observed in *Atoh7*$^{tTA/tTA}$*;B&I-EE* mice, when *Brn3b* & *Isl1* are ectopically expressed from the endogenous *Atoh7* locus in a *Atoh7*-deficient mouse using the tet-off system (Wu et al., 2015)(Figure 3E), and implies that *Brn3b* and *Isl1* may activate expression of secreted factors that drive vascular regression in a narrow time window during development.

2.3.5 ScRNA-seq analysis of RGCs generated in the absence of *Atoh7*

In order to examine potential differences in RGC development within *Atoh7*$^{-/-}$ and *Atoh7*$^{-/-}$*;Bax*$^{-/-}$ compared to wildtype and *Bax*$^{-/-}$ control animals, we next performed single-cell RNA-sequencing (scRNA-Seq) on *Bax*$^{-/-}$, *Atoh7*$^{-/-}$, and *Atoh7*$^{-/-}$*;Bax*$^{-/-}$ retinas to more comprehensively profile changes in cell type specification and global transcriptional

differences across the genotypes. We profiled 67,050 E14.5 retinal cells from *Bax*$^{-/-}$, *Atoh7*$^{-/-}$ and *Atoh7*$^{-/-}$;*Bax*$^{-/-}$ mice, and aggregated the datasets with 26,078 age-matched wildtype retinal cells from previous studies (Clark et al., 2019) (Figure 4A,B, Supplemental Figure 8). Consistent with the previous single-cell studies of E14 mouse retinal development (Clark et al., 2019; Giudice et al., 2019), we observed a continuous manifold of cells, from primary RPCs to neurogenic RPCs, leading to three separate differentiation trajectories that give rise to RGCs, cones, and amacrine/horizontal cells, respectively (Figure 4A-B; Supplemental Figure 9A). Analysis of the cell type proportions across the genotypes revealed a depletion of RGCs in both *Atoh7* mutant samples (*Atoh7*$^{-/-}$ and *Atoh7*$^{-/-}$;*Bax*$^{-/-}$) compared to both wildtype and *Bax*$^{-/-}$ controls (Figure 4C-D, Supplemental Figure 8E-F). This reduction in the number of RGCs included a compensatory increase in cone photoreceptors and neurogenic RPCs, consistent with previous findings (Figure 4C-D, Supplemental Figure 8E-F) (Brown et al., 2001; Brzezinski et al., 2005; Hufnagel et al., 2010; Wang et al., 2001).

Using the scRNA-seq data, we next assessed the differential gene expression within neurogenic RPCs and RGCs across control -- WT and *Bax*$^{-/-}$ -- and *Atoh7*-deficient -- *Atoh7*$^{-/-}$ and *Atoh7*$^{-/-}$;*Bax*$^{-/-}$ -- samples. Using strict differential expression cutoffs (q-value < 1e-300), we identified 230 *Atoh7*-dependent differentially expressed transcripts within neurogenic RPCs and RGCs (Table 1). Genes enriched within control samples (Figure 4E) highlighted many known factors in the specification and differentiation of RGCs, including *Pou4f2* (*Brn3b*), *Isl1*, *Pou6f2* (*Rpf-1*), *Elavl4*, *Gap43*, and *Irx2* (Choy et al., 2010; Ekström and Johansson, 2003; Kruger et al., 1998; Zhou et al., 1996)

(Supplemental Figure 9B). Conversely, differentially expressed transcripts enriched in the *Atoh7* knockout samples (Figure 4E) were enriched for genes involved in the Notch-signaling pathway -- *Rbpj, Dll3, Notch1,* and *Hes6* -- and for transcripts enriched in neurogenic cells and photoreceptor precursors during retinal development -- *Btg2, Neurog2, Bhlhe22, Insm1, Neurod1, Mybl1, Sstr2, 3110035E14Rik* (Clark et al., 2019; Supplemental Figure 9B).

Atoh7-deficient RGCs also show dramatically reduced expression of genes known to regulate axon guidance including *Islr2*, which has been found to control RGC axon fasciculation, as well as axon guidance at the optic chiasm (Panza et al., 2015). Of particular interest are the observed increases in *Rbpj* and *3110035E14Rik* expressions in $Atoh7^{-/-}$ and $Atoh7^{-/-};Bax^{-/-}$ samples. *Rpbj* is an upstream regulator of *Atoh7* expression (Miesfeld et al., 2018b), and *3110035E14Rik* (*Vxn*), which functions similarly to Atoh7 by promoting retinal neurogenesis and early retinal cell fate specification (Moore et al., 2018). The increased expression of transcripts that show enriched expression in neurogenic cells and photoreceptor precursors is consistent with the increase in generation of cone photoreceptor precursors seen in *Atoh7*-deficient retinas (Fig. 4D) (Brown et al., 2001). Combined with a recovery in the specification of RGC numbers in adult $Atoh7^{-/-};Bax^{-/-}$ animals, these data suggest that loss of *Atoh7* expression leads to an increase in expression of genes specific to neurogenic RPCs at the expense of RGC-enriched transcripts, results consistent with a developmental delay.

2.3.6 Pseudotemporal analyses identify changes in *Atoh7*-dependent gene expression during RGC specification.

In order to further assess the degree of an RGC-specific developmental delay, we performed pseudotemporal analyses using Scanpy (Wolf et al., 2018)(Figure 4F). We observed bias of the *Atoh7*-deficient cells within early pseudotime stages during RGC differentiation. Both wildtype and *Bax*$^{-/-}$ control cells had a broader distribution of cells across pseudotime, results consistent with a failure of maturation or developmental delay of RGC specification in *Atoh7*-deficient RGCs (Figure 4G). Differential expression analysis assessing the changes in gene expression across the interaction of pseudotime and genotypes revealed significant genotypic differences across RGC development (Figure 4H).

In both *Atoh7*$^{-/-}$ and *Atoh7*$^{-/-}$;*Bax*$^{-/-}$ samples, we observed a reduction of expression in many genes enriched within mature RGCs -- *Pou4f2, Gap43, Sncg, and Isl1*. We likewise observed reduced expression of a subset of genes in neurogenic RPCs, including *Gal*. Increased expression of other genes predominantly expressed in neurogenic RPCs including *Neurod1, Insm1, Neurod4, Hes6, Onecut1, Onecut2,* and *Sox4* -- is observed in both *Atoh7*-deficient neurogenic RPCs and RGCs compared to controls (Figure 4H). This implies that loss of function of *Atoh7* may delay the differentiation of RGCs from neurogenic RPCs. The temporal expression patterns of genes involved in RGC specification mimic those observed within additional E14 scRNA-seq datasets (Giudice et al., 2019), and analyses of transcriptomic changes

resulting from loss of *Atoh7* expression closely match those obtained from scRNA-Seq-based analysis of *Atoh7*$^{-/-}$ retina conducted at E13.5 (Wu et al., 2020).

We next performed *in situ* hybridization to examine changes in global transcript expression within the developing retina. RNA transcript expression was detected at E14.5, at which point most RGCs are specified (Sidman, 1960; Young, 1985), and we observed decreased expression of *Pou4f2 (Brn3b), Isl1* and *Gal*, in both *Atoh7*$^{-/-}$ and *Atoh7*$^{-/-}$*;Bax*$^{-/-}$ mice, as determined by chromogenic *in situ* hybridization (Figure 4I). Immunostaining of E14 retinas confirms a reduction in the number of cells immunopositive for Brn3a (Pou4f1) and Brn3b (Pou4f2) (Figure 4J), as well as the pan-RGC markers RBPMS and Isl1 (Figure 4K), in the developing ganglion cell layer of *Atoh7*-deficient retinas. At E12.5 we observed a marked decrease in both overall RGC density and RGC number (Supplemental Figure 3). Together these results suggest that loss of function of *Atoh7* delays RGC differentiation and leads to an accumulation of neurogenic RPCs.

To further identify patterns of temporal changes in gene expression across RGC genesis between *Atoh7* mutant and control retinas, we performed the non-negative matrix factorization technique scCoGAPS (Stein-O'Brien et al., 2019). Implementation of scCoGAPS parses the gene expression into groups ('patterns') based on gene expression profiles and without *a priori*, literature-based knowledge of gene interactions. Using 5235 highly variable genes across the 29,182 neurogenic RPCs and differentiating RGCs, we identified 31 patterns of gene expression (Supplemental Figure 10). These patterns correlated with both neurogenic RPCs Patterns 6, 25, 5, 24, 11, 13, 18, 7, 21, 1, and 4

and RGC Patterns 8, 27, 28, 9, 26, 20, 22, 17, 31 cell type annotations and highlighted temporal changes in gene expression as assessed through pseudotime analyses. Individual patterns - patterns 4, 5, and 29 - were highly correlated with neurogenic cell annotations and *Atoh7*$^{-/-}$ and *Atoh7*$^{-/-}$;*Bax*$^{-/-}$ genotypes, consistent with a temporal delay in RGC specification, increased number of neurogenic cells, or failure of cell-type specification of neurogenic RPCs as a consequence of lost *Atoh7* expression. Genes driving pattern 5 include genes enriched in early-stage neurogenic RPCs, *Gadd45a* and *Sox11* (Clark et al., 2019).

Conversely, patterns highly correlated with RGC cell type annotations and pseudotime Patterns 9, 26, and 28 had a high correlation with control samples. The most highly weighted genes in Patterns 9 and 26 are *Gap43* and *Igfbpl1*, respectively, which have been implicated in RGC axonal growth (Guo et al., 2018; Zhang et al., 2000). Pattern 28 highlights cells towards the end of the RGC trajectory and is largely driven by Sncg; a transcript enriched in most RGCs in the adult mouse retina (Soto et al., 2008). The association of neurogenic patterns with *Atoh7*$^{-/-}$ mutant retinas versus those that highlight RGC differentiation and maturation patterns with control retinas further support a developmental delay in mutant RGCs. Analysis of pattern marker expression across the genotypes (Supplemental Figure 10) highlights both the temporal delay and global changes in gene expression across the *Atoh7*$^{-/-}$ mutant retinas compared to controls.

Recent studies have comprehensively profiled RGC subtype diversity in the mouse retina (Rheaume et al., 2018; Tran et al., 2019). However, these studies did not characterize either the birthdates of individual RGC subtypes, or the transcriptional

networks controlling RGC subtype specification. Our combined data supports evidence of both *Atoh7*-dependent and independent populations of RGCs. The delay in RGC maturation and the failure of optic nerve formation seen in *Atoh7*-deficient retinas suggest that the earliest pathfinding RGCs are *Atoh7*-dependent. We examined expression of markers of mature RGC subtypes (Tran et al., 2019) within the developing retina and correlated expression of the transcripts with RGC pseudotime (Supplemental Figure 11) as many of the mature RGC subtype markers are not specific to RGCs. We detected expression of selective markers for a fraction of mature RGC subtypes within the E14.5 scRNA-Seq dataset. Of transcripts in which readily detectable expression was observed, many including *Igfbp4, Foxp1, Stxbp6, Bhlhe22, Penk* also display enriched expression in primary or neurogenic RPCs. Expression of some markers of RGC development and maturation *Ebf3, Pou4f1, Pou4f2, Prdm8* and *Slc17a6* correlated well with pseudotemporal ordering and were depleted in *Atoh7*-deficient RGCs. However, a limited number of RGC subtype markers, including *Irx3, Calb2,* and *Tac1* were largely absent from *Atoh7* mutant RGCs.

2.3.7 Atoh7 binds to loci associated with both RGC and photoreceptor transcripts

In order to gain insight into the function of Atoh7 during RGC specification, we performed Cut&Run experiments (Skene and Henikoff, 2017) on E14 mouse retinas using the established Atoh7 antibody (Miesfeld et al., 2018a) and IgG as a control. Peak calling was performed using the MACS2 pipeline (Zhang et al., 2008). High concordance of called peaks is observed between Atoh7 Cut&Run replicates (Supplemental Figure

12A), with >3,000 shared peaks, and little enrichment of peak sequences within the IgG sample. Comparisons of Atoh7 peaks to developmental chromatin accessibility (Aldiri et al., 2017) determined that peaks proximal to gene transcription start sites, corresponding to proximal promoters, exhibited high accessibility throughout retinal development (Supplemental figure 12B). Distal peaks, corresponding to enhancer sequences (>3kb from the transcription start sites), however, displayed the greatest accessibility during early periods of retinal development when RGCs are being generated, and when Atoh7 expression is maximal ((Miesfeld et al., 2018a); Supplemental Figure 12B). We next determined the enrichment of DNA sequence motifs underneath called peaks using HOMER (Heinz et al., 2010). We observed a highly enriched motif (CAGCTG; p = 1e-763) that was present within >55% of called peaks (13.75% of background peaks; Figure 6A). Analysis of motif similarity to known transcription factor motifs indicated a high similarity of the called Atoh7 motif to the Atoh1 motif (CAGCTG; p = 1e-784; Figure 6A) and other E-Box transcription factors.

We next assigned peaks to genes using ChiPSeeker (Yu et al., 2015). Many strong peaks were located within genetic loci of transcripts with known functions during early retinal development, including *Neurod1*, *Elavl4, Neurog2, Pou6f2, Otx2, Meis2,* and *Lhx4* (Figure 6B-E; SupplementalTable 3). We also observed strong enrichment of Atoh7 binding within the *Atoh7* proximal promoter and distal enhancer sequences (Miesfeld et al., 2020), suggestive of auto-regulation of *Atoh7* expression (Figure 6D).

In order to better understand the mechanism by which Atoh7 regulates transcription of nearby genes, we next examined the consequence of *Atoh7* loss-of-

function on bound loci gene expression as determined by our scRNA-seq experiments in Control (WT and *Bax*$^{-/-}$) versus *Atoh7* Null (*Atoh7*$^{-/-}$ and *Atoh7*$^{-/-}$;*Bax*$^{-/-}$) neurogenic cells and RGCs. Our analyses indicated that many Atoh7-bound genes display decreased expression within *Atoh7* mutant retinas, including the RGC-enriched genes *Pou6f2, Elavl4, Isl1* and *Tubb2b* (Figure 6E). Conversely, roughly similar numbers of genes displayed increased expression in *Atoh7* mutant retinas, including neurogenic RPC-enriched transcripts *Hes6, Btg2, Neurod1, Neurog2, Sstr2, Pkib, and Bhlhe22* (Clark et al., 2019; Figure 6E). To gain further insight into the biological relevance of Atoh7-bound and differentially expressed transcripts, we first binned transcripts into 5 categories: 1) Atoh7-bound and down-regulated in *Atoh7* mutants; 2) Atoh7-bound and up-regulated in *Atoh7* mutants; 3) no binding, down-regulated in *Atoh7* mutants; 4) no binding and up-regulated in *Atoh7* mutants; and 5) Atoh7-bound but no change in expression. Following binning, we calculated z-scores of gene expression on an individual cell basis using the mouse retinal development single-cell dataset (Clark et al., 2019), and examined the enrichment of expression of binned genes within annotated cell types. Our analysis determined that Atoh7-bound genes that displayed decreased expression in *Atoh7* mutant retinas show enriched expression in RGCs, suggesting an active role of Atoh7 in promoting RGC fate (Figure 6F-H). Conversely, Atoh7-bound genes that are upregulated in *Atoh7* mutant retinas display high expression within neurogenic cells or photoreceptor precursors, and include *Neurod1, Neurog2,* and *Hes6* (Figure 6F; I). We also observe Atoh7-binding within additional cone photoreceptor gene loci, including *Lhx4, Otx2,* and *Thrb* (Table 2), although these genes did not display

robust differences in gene expression between control and Atoh7 mutant retinas. The upregulation of Atoh7-bound neurogenic and photoreceptor-enriched genes in *Atoh7* mutant retinas suggest that Atoh7 actively represses photoreceptor fate during early retinogenesis, an interpretation that is supported by the observed modest increase in cone photoreceptor proportions within *Atoh7* mutant scRNA-Seq samples (Figure 4D).

2.3.8 *Galanin* is not the Atoh7-dependent secreted factor that promotes RGC survival and pathfinding

Our data suggest the existence of *Atoh7*-dependent factors that promote both RGC survival and pathfinding, as well as hyaloid vascular regression, in a non cell-autonomous manner. These are likely derived from *Atoh7*-expressing neurogenic RPCs and/or RGCs. Factors mediating hyaloid regression are likely to be secreted, while those regulating RGC survival could also potentially act through contact-mediated signaling. Few annotated secreted proteins show clear *Atoh7*-dependent expression in our scRNA-Seq dataset. The neuropeptide galanin *(Gal*), which is strongly expressed in both neurogenic RPCs and RGCs and is a direct target of Atoh7 (Figure 6E) was by far the most differentially expressed secreted factor in *Atoh7*-deficient mice (Figure 4E,I, Figure 6E; Table 1). Galanin has been implicated in promoting the survival of neural precursors (Cordero-Llana et al., 2014; Holmes et al., 2000), and to be enriched in ipsilaterally projecting retinal ganglion cells (Giudice et al., 2019). However, *Gal*-deficient animals showed no differences in either the hyaloid vasculature regression or RGC density, as compared to the control animals (Supplemental Figure 13).

2.4 Discussion

It is broadly accepted that *Atoh7* acts in RPCs as a competence factor that is essential for RGC specification (Brzezinski et al., 2012; Mu et al., 2005; Yang et al., 2003; Baker and Brown, 2018). In this study, though, we show that the specification of the great majority of RGCs occurs even in the absence of *Atoh7*. While RGC specification can occur independent of *Atoh7*, *Atoh7* function is required to maintain RGC survival and proper targeting of RGC axons to the optic nerve head. Following disruption of both *Atoh7* and *Bax*, we observe only a 20% reduction in the number of RGCs relative to *Bax*-deficient controls. This compares to a greater than 95% reduction in RGC numbers in *Atoh7* mutants relative to wildtype controls. Although RGCs in *Atoh7*$^{-/-}$;*Bax*$^{-/-}$ retinas show severe defects in targeting the optic nerve head, they respond robustly to photoreceptor stimulation. The presence of specified RGCs in the absence of Atoh7 helps explain long-standing, puzzling observations: 1) 45% of RGCs are not derived from *Atoh7*-expressing progenitors; 2) molecular markers of RGCs are observed at considerably higher levels during early stages of retinal development than in adults in Atoh7-deficient retinas; and 3) the marked increase in apoptosis in the ganglion cell layer that occurs in the absence of Atoh7 (Brzezinski et al., 2012; Feng et al., 2010; Prasov and Glaser, 2012). Previous studies have implicated Atoh7 as a direct upstream regulator of the essential RGC transcription factors *Brn3a*, *Brn3b*, and *Isl1*. Supporting this, an *Atoh7* hierarchy of RGC determinants, studies in which Brn3b and Islet1 were inserted in place of the Atoh7 coding sequence observed a complete rescue of normal RGC development (Wu et al., 2015). Our studies, however, indicate that when apoptosis is inhibited, Brn3a, Brn3b,

Islet1, and Rbpms expression is induced at near normal levels within RGCs in both E14 and adult retinas, regardless of Atoh7 expression. Indeed, we observe that Atoh7 binds to sites in the *Isl1* and *Pou4f1* (Brn3a) loci, suggesting active regulation of *Isl1* and *Brn3a* transcription by Atoh7. While no Atoh7 Cut&Run peak was assigned to *Pou4f2* (*Brn3b*), two Atoh7-binding sites were identified in the terminal intron of *Pou4f2*-neighboring gene *Ttc29*. While further evidence is required to clearly demonstrate that Atoh7 regulates *Pou4f2* expression via these binding sites, we observed reduced expression of *Isl1, Pou4f1,* and *Pou4f2* within Atoh7-deficient retinal cells. Therefore, we conclude that other factor(s) in addition to Atoh7 activate expression of these genes.

The molecular mechanisms by which *Atoh7* controls axonal guidance and cell survival remain unclear. One hypothesis is that RGC axonal guidance and cell survival are linked and that loss of *Atoh7* expression fails to initiate expression of target-derived trophic cues. Because other studies have failed to detect substantial numbers of RGCs in $Atoh7^{-/-}$ mice at P0 (Brown et al., 2001; Feng et al., 2010; Prasov and Glaser, 2012; Wang et al., 2001) and target derived neurotrophic factors regulate apoptosis of RGCs between P0 and P12, we suspect that Atoh7-induced cell survival is functioning at earlier time points than target-derived trophic signals. Additionally, as we did not observe RGC rescue within $Atoh7^{Cre/Cre};Bax^{fl/fl}$ mice, we suggest that immature RGCs rapidly degenerate as the result of the lack of an *Atoh7*-dependent survival factor. This wave of developmental apoptosis has been observed previously, but the underlying molecular mechanisms are unknown (Farah and Easter, 2005; Frade et al., 1997; Ogilvie et al., 1998; Péquignot et al., 2003; Rodríguez-Gallardo et al., 2005; Strom and Williams, 1998;

Valenciano et al., 2009). We hypothesize that this unknown factor or factors must be produced by either *Atoh7*-expressing neurogenic RPCs or RGCs derived from these cells.

Our data also reveal a marked delay in the formation of RGCs from neurogenic RPCs in the absence of *Atoh7*. This is consistent with previous results in *Atoh7*$^{-/-}$ retinas, where RGC formation is delayed by at least a day (Le et al., 2006; Prasov and Glaser, 2012). When *Atoh7*-dependent RGCs are rescued later in development, as seen in targeted mutants in which *Atoh7* is expressed from the endogenous *Crx* locus, the hyaloid vasculature regression was not rescued, even though a modest rescue of RGC formation is observed (Prasov and Glaser, 2012). In zebrafish retina, consistent with this result, loss of function of *atoh7* in early-stage RPCs disrupts the correct targeting of axons in later-born RGCs to the optic nerve (Pittman et al., 2008). Taken together with the fact that 45% of RGCs arising from a non-Atoh7-dependent lineage in mice, we hypothesize that early, pathfinding RGCs are Atoh7-dependent and provide both survival and guidance cues for later-born RGCs.

Since *Atoh7* was previously thought to be a master transcriptional regulator of RGC specification, strategies aimed at targeted differentiation of RGCs for therapeutic purposes have focused on using the forced expression of *Atoh7*. We, however, now appreciate RGC specification to be a far more complicated process. Although ectopic expression of *Atoh7* activates expression of RGC-specific genes in cultured retinal progenitor cells (Yao et al., 2007), induced pluripotent stem cells (Chen et al., 2010), and Müller glia-derived retinal stem cells (Song et al., 2015, 2014), it is nonetheless typically

not sufficient to drive these cells to become RGCs. This study sheds light on why this may be the case.

These findings demonstrate that additional factors act in parallel to *Atoh7* to control RGC specification. While multiple other transcription factors have been reported to regulate RGC specification -- including *Neurod1*, *Sox4*, and *Onecut2* (Jiang et al., 2013; Mao et al., 2013; Sapkota et al., 2014) -- these factors are unable to individually activate expression of *Brn3b* and *Isl1*. In *Atoh7*$^{-/-}$*;Bax*$^{-/-}$ RGCs, however, we observe substantially increased expression of each of these transcription factors (Figure 4E; Supplemental Figure 10), suggesting the possibility that these factors, among others, may compensate for the loss of *Atoh7*. The observations that Atoh7 binds to target sites in the genomic loci of multiple genes that are upregulated in *Atoh7* mutant retinas -- including *Neurod1, Neurog2, Otx2, and Onecut2* -- suggest that Atoh7 directly inhibit alternate mechanisms of RGC genesis. However, the identity of the non-cell-autonomous cues by which *Atoh7* regulates RGC survival, axon guidance, and hyaloid vasculature regression remain unknown. Further identification of the mechanisms regulating the interplay of intrinsic and extrinsic signals on RGC specification, survival, and maturation will help guide the future design of therapies aimed at maintaining and replacing RGCs lost due to degenerative disease.

2.5 Material and Methods

2.5.1 Mice

Animals were housed and treated in accordance with NIH and IACUC guidelines, and used protocols approved by the Johns Hopkins University Animal Care and Use Committee (Protocol numbers MO16A212). *Atoh7*$^{Cre/Cre}$ mice are a knock-in line where Cre recombinase replaced the entire *Atoh7* gene and was a gift from Dr. Lin Gan (referred to as Atoh7$^{-/-}$) (Yang et al., 2003) (RRID:MGI:3717726). The Bax$^{tm1Sjk/tm1Sjk}$ (*Bax*$^{-/-}$) mice containing a neomycin cassette that replaces critical exons 2-5, were purchased from The Jackson Laboratory (Knudson et al., 1995)(JAX:002994, RRID:IMSR_JAX:002994). The *Bax*$^{-/-}$ mice are unpigmented since the *Bax* gene is linked to the *Tyrosinase* (Tyr) and *Pink-eyed dilution* (*p*) gene by 21cM and 5cM respectively. The conditional Bax$^{tm2Sjk/tm2Sjk}$ (Bax$^{fl/fl}$) mice containing LoxP sites flanking exons 2-4, were purchased from The Jackson Laboratory (JAX:006329, RRID:IMSR_JAX:006329)(Takeuchi et al., 2005). *Atoh7*$^{tTA/tTA}$;B&I-EE mice are a combination of two genetic strains. In the first strain (*Atoh7*$^{tTA/tTA}$), the tetracycline-responsive artificial transcription factor tTA replaces the *Atoh7* gene. In the absence of tetracycline, the tTA activates the tetracycline responsive element which is driving the expression of *Brn3b* and *Isl1* in the second strain (B&I-EE). Therefore, in effect the Atoh7 promoter will drive the expression of *Brn3b* and *Isl1*. This mouse line has been previously reported to rescue all reported effects of *Atoh7* loss of function, and was a gift from Dr. Xiuqian Mu (Wu et al., 2015)(MGI:5749708 and MGI:5749713). The *Crx>Atoh7* mice, a transgene that expresses the full-length *Atoh7* coding sequence under

the control of the *Crx* promoter, was previously published (Prasov and Glaser, 2012)(MGI:5433215). A tdTomato Cre recombinase reporter mouse*Rosa26*^{tdTomAi14} (JAX:007914, RRID:IMSR_JAX:007914)(Madisen et al., 2010) was used to label cells in a Cre recombinase-dependent manner. The *Chx10-Cre* mouse line is a transgenic line purchased from The Jackson Laboratory, originally developed by Constance Cepko's laboratory (JAX:005105, RRID:IMSR_JAX:005105)(Rowan and Cepko, 2004), expresses Cre recombinase broadly in all retinal progenitor cells from E10-E15.5. The *Opn4*^{taulacZ} mice were used to trace the ipRGC projections to the brain (Hattar et al., 2002). Throughout the manuscript, controls are heterozygous for both *Atoh7* and *Bax* (*Atoh7*$^{+/-}$;*Bax*$^{+/-}$), whereas *Atoh7*$^{-/-}$ mice were also are heterozygous for *Bax* (*Atoh7*$^{-/-}$;*Bax*$^{+/-}$).

2.5.2 Statistics

All statistical tests, apart from analysis of the scRNA-seq data, were performed in Graphpad Prism 6 (RRID:SCR_002798). The statistical tests used are listed in figure captions.

2.5.3 Immunohistochemistry

Adult retinas from P40-P200 mice were obtained by enucleating whole eyes, fixing for 30 minutes in 4% paraformaldehyde (PFA) diluted in PBS, dissecting to remove the cornea and lens, dissecting the retina from the RPE, and antibody staining proceeded in a 24-Multiwell Cell Culture Plate (Corning #353047). Retinas were blocked in 500 µl of

PBS containing 0.3% Triton X100 and 6% goat serum for 2 hours at room temperature. Several antibodies were used in this study (dilutions are between brackets): Mouse IgG1 anti-Brn3a (Millipore Cat# MAB1585 RRID:AB_94166) (1:250), Rabbit anti-RBPMS (GeneTex Cat# GTX118619 RRID:AB_10720427) (1:250), Rabbit anti Brn3b (Badea et al., 2009) (1:100), Mouse anti-Smi32 (non-phosphorylated anti-Neurofilament H (NF-H)) (BioLegend Cat# 801701 RRID:AB_2564642) (1:500), Mouse anti Neurofilament Medium (Thermo Fisher Scientific Cat# 13-0700, RRID:AB_2532998) (1:500), Chicken anti Neurofilament Heavy (Millipore Cat# AB5539, RRID:AB_11212161) (1:250), Mouse anti-GFAP (Sigma-Aldrich Cat# C9205 RRID:AB_476889) (1:1000), GS-IB4 (Molecular Probes Cat# I21411 also I21411 RRID:AB_2314662) (1:250), Rabbit anti-Pax2 (BioLegend Cat# 901001 RRID:AB_2565001) (1:100), Mouse anti-Tuj1 (R and D Systems Cat# MAB1195 RRID:AB_357520) (1:200), Rabbit anti DsRed Takara Bio (Cat# 632496, RRID:AB_10013483) (1:250), Mouse anti-Islet1 (DSHB Cat# 40.2D6 RRID:AB_528315) (1:200), and Rabbit anti-Opn4 (Advanced Targeting Systems Cat# UF006, RRID:AB_2314781) (1:500). The appropriate antibodies were diluted in blocking solution and incubated for two days at 4ºC. Retinas were then washed in three changes of PBS, 15 minutes each, then placed in the appropriate Alexa Fluor secondary antibody (Invitrogen) (1:500) overnight at 4ºC. Retinas were washed in 200 µl of PBS containing 1xDAPI, then washed three times in PBS for 15 minutes each, and mounted flat on slides in VectaShield (Vector Labs, RRID:AB_2336789). Regionalized dissections were done as follows; before enucleation, the most nasal part of the sclera was marked with a cauterizer. This mark was used during the dissection to make a

marking incision into the retina, following the above staining protocol. Retinas were imaged on a Zeiss LSM 700 or 800 Confocal at the Johns Hopkins University Integrated Imaging Center Core Facility (RRID:SCR_016187).

For embryonic studies, developing embryos harvested at E12.5 and E14.5 were washed in a Petri dish with sterile PBS three times for 10 minutes. Tail was used for genotyping. The heads were fixed in 4% PFA for 30 minutes and then cryoprotected in 30% sucrose at 4ºC overnight, frozen in OCT, and sectioned at 18 µm thickness using a cryostat. Sections were dried at 30ºC for 15 minutes and then washed 10 minutes in three changes of PBS. Sections were then blocked and stained as above in a humidified chamber overnight. Sections were then mounted and imaged as described.

2.5.4 Cell density analysis

All cell counting was done manually. To confirm the reproducibility of the cell counts, randomly selected selections from each sample were counted twice, and counts were consistently found to be essentially identical. Density was calculated as the number of cells per area. All measurements and cell number analysis were done manually in ImageJ (Fiji, RRID:SCR_002285) and Adobe Photoshop CS6 (RRID:SCR_014199).

In adult flat-mounted retinas, the density of RGCs was calculated by obtaining at least 4 representative images at 40x of 600 µm x 600 µm with 1 µm optical sections. Optical sections were projected together with maximum intensity, including cells only in the retinal layers of interest. Representative images were taken similarly across all genotypes without *a priori* knowledge of the genotype. However, some genotypes

contain marked phenotypic differences, which include a pigment mutation linked to the *Bax* locus, drastic RGC number reduction as in the *Atoh7*$^{-/-}$, and/or misguided axons. Three representative areas of each retina were averaged for the density analysis

In E12.5 embryonic retinal sections, a representative confocal image was taken at 40x of 600 μm x 600 μm with optical sections of 1 μm projected together with maximum intensity. The sections chosen for analysis were all positive for Pax2+ optic nerve head cells, as the central retina contains the earliest-born RGCs. At least two sections with matching criteria were analyzed for each E12.5 embryo. Density was calculated by dividing the number of Brn3a+ RGCs and dividing by the area of the retina. To limit the analysis to the RGC neurogenic zone, we limited the quantification to the leading edge of RGC genesis. The percentage of mature Brn3a+ RGCs at E12.5 were determined by counting their number within the ganglion cell layer (GCL). The number of mature Brn3a+ RGCs was then divided by the number of total Brn3a+ RGCs in a section, and then averaged across all sections. This ratio represents the number of Brn3a+ RGCs already in the nascent ganglion cell layer versus RGCs migrating through the neuroblast layer to the ganglion cell layer.

2.5.5 Multielectrode array recordings

Mice were dark-adapted for 1-2 hours before being sacrificed and dissected under dim red light. Retinas were isolated in Ames' medium (Sigma) bubbled with 95% O_2/5% CO_2 (carbogen) at room temperature, trimmed into small rectangles, and then placed on a 6x10 perforated multielectrode array (Multichannel Systems, Tübingen, Germany),

ganglion-cell-side down. Tissue was perfused with Ames' bubbled with carbogen and kept at 32°C throughout the experiment. Data acquisition was performed using the MC_Rack software (ALA Scientific Instruments, Inc.), at a 50-kHz sampling rate. An offline spike sorter (Plexon Inc) was used for spike sorting.

UV stimuli ($I_{mean} \approx 5$ x 103 photons/cm2/s, 398 nm) were generated through a modified DLP projector (HP Notebook Projection Companion Projector, Model: HSTNN-FP01) (frame rate = 60 Hz) and were delivered through an inverted microscope objective. All stimuli were programmed using the *Psychophysics Toolbox* in Matlab (The Mathworks, Natick, MA). Stimuli include: (1) 120-s, 1-Hz full-field square-wave flash (100% Michelson contrast); (2) 10-min Gaussian white noise (GWN) flickering checkerboard (pixel size = 44.77 μm); (3) 10-min spatially correlated "cloud" stimulus that was generated by low-pass filtering the GWN. The cloud stimulus introduced dark and bright areas of a range of scales within each frame, with the purpose of driving large spatial receptive fields.

The analysis was first performed using custom-written Matlab (MATLAB R2014b) codes, the results later were exported and edited in Adobe Illustrator CS6. For each cell, the peristimulus time histogram (PSTH) of responses to square-wave flash was calculated using 10-ms bins. Spatial and temporal receptive fields were identified based on noise data using a nonlinear model previously described in detail (McFarland et al., 2013; Shi et al., 2019).

Fewer cells were recorded from $Atoh7^{Cre/Cre};Bax^{-/-}$ mice compared to the wildtype and $Bax^{-/-}$, as the nerve fiber layer (NFL) and retinal vasculature are improperly

developed and thus provide an insulating layer that needs to be removed in order to obtain high quality recordings. No cells were recorded from *Atoh7*$^{Cre/Cre}$ mice, due to the >99% reduction in RGC numbers.

2.5.6 Pupillary light response (PLR)

PLR experiments were performed on mice that were dark adapted for at least 1 hour prior to any experiment. PLR was measured by gently restraining the mice by hand (without anesthesia) and exposing them to a cool white light LED bulb (6500K, light intensity: 15 W/m^2, MR16, SuperBrightLEDs.com) that was directed at one eye using a gooseneck arm of a dissecting microscope light source. Constriction of the pupil was recorded using a Sony Handycam camcorder (FDRAX33) from either the contralateral or ipsilateral eye to the light source. The baseline pupil size of each mouse was first recorded for at least 5 seconds using an infrared light source, following which the white LED bulb was turned on for at least 30 seconds. Video recordings were analyzed by creating screenshot images in Joint Photographic Experts Group format (jpg) of the pupil prior to and during light stimulation using VLC media player (https://www.videolan.org/vlc/). Pupil area was then quantified in ImageJ (Fiji, RRID:SCR_002285). To determine the relative pupil area, pupil size during the light stimulation was divided by pupil size prior to light stimulation.

2.5.7 Tissue dissociation for generation of single-cell suspensions

Eyes were enucleated from E14 time-pregnant animals and placed directly into ice-cold 1X PBS. Retinas were dissected in cold 1X PBS, and then placed into 200 µl of cold

HBSS per 2-3 retinas. Tissue dissociation was induced through the addition of an equivalent volume of Papain solution (1 ml - 700 µl reagent grade water, 100 μl fresh 50 mM L-Cysteine (Sigma), 100 µl 10 mM EDTA, 10 µl 60 mM 2-mercaptoethanol (Sigma), with Papain added to 1 mg/ml (1:10 dilution of 10 mg/ml Papain solution; Worthington)). Papain-retina mixture was placed at 37°C for 10 minutes with slight trituration every 2-3 minutes. Enzymatic dissociation was halted through the addition of 600 µl of Neurobasal Media + 10% FBS for every 400ul of dissociation solution. DNA from lysed cells was removed using 5 µl RNAse-free DNAse I (Roche) for every 1 ml dissociate and incubated at 37°C for 5 minutes, followed by slight trituration using a 1 ml pipette. Cells were pelleted after centrifugation (300 RCF for 5 minutes at 4°C), followed by resuspension in 2-3 ml of Neurobasal media supplemented with 1% FBS. The final solution was passed through a 50 µm filter to remove cellular aggregates and undissociated debris.

2.5.8 10x Genomics Sequencing and Analysis

Single-cell RNA sequencing of dissociated retinal cells from E14 *Atoh7*$^{-/+}$*;Bax*$^{-/-}$ and *Atoh7*$^{-/-}$*;Bax*$^{-/-}$ was performed using 10x Genomics Chromium 3' v2 platform (PN-120223) (Pleasanton, CA), followed by sequencing using the NextSeq500 platform with default 10x sequencing parameters (R1 - 26bp; R2 - 98bp; i7 - 8bp). Single-cell analysis of the wildtype (WT) E14 developing mouse retina was obtained from previously reported samples obtained from GEO (GSE118614); data obtained using similar isolation protocols are described previously (Clark et al., 2019).

2.5.9 Gene Set Usage Pattern Discovery with scCoGAPS

CoGAPS v.3.5.6 (Sherman et al., 2019; Stein-O'Brien et al., 2019) was used to find patterns of gene set usage by Neurogenic and Retinal Ganglion Cells. The expression matrix used as input was normalized to 10,000 counts per cell, subsetted down to 5235 most highly variable genes and log2 transformed. The CoGAPS parameters used are: singleCell=TRUE, nPatterns = 30, nIterations = 50000, distributed = single-cell, sparseOptimization = True, seed = 803L, and nSets = 10. The final number of patterns stabilized at 31.

2.5.10 Identification of *Atoh7*-Dependent Genes

Data was subsetted down to neurogenic RPCs and RGCs. Monocle's differential gene test was conducted between control (WT and *Bax*$^{-/-}$) and Atoh7 mutants (Atoh7$^{-/-}$ Atoh7$^{-/-}$;Bax$^{-/-}$) using the following parameters:

differentialGeneTest(dat[genes expressed in >=10 cells], fullModelFormulaStr = '~(Atoh7 genotype) + Total_mRNAs', reducedModelFormulaStr = '~Total_mRNAs',cores=4).

2.5.11 Pseudotime Analysis between Genotypes

Scanpy v1.4 (Wolf et al., 2018) was first used to assign diffusion pseudotime values (Haghverdi et al., 2016) to cells in the retinal ganglion cell trajectory. Cell types included in this final dataset were restricted to retinal ganglion cells, primary RPCs, and

neurogenic RPCs. To preprocess the dataset, genes <10 counts were removed, and the expression matrix was normalized to 10,000 counts/cell and log-transformed. Highly variable genes used for ordering were identified using Scanpy's `highly_variable_genes` function with default parameters except flavor='cell_ranger' and n_top_genes=3000. 50 principal components were calculated using default PCA parameters with random_state=123456. To compute the neighborhood graph with the batch effect of genotype removed, we used BBKNN with batch_key = "Genotype" and neighbors_within batch=3 (Polański et al., 2019). 10 diffusion components were then computed and used for input to assign diffusion pseudotime values with an RPC cell as root. To find genes differentially expressed between the developmental trajectories of the WT and *Atoh7*$^{Cre/Cre}$*;Bax*$^{-/-}$ genotypes, Monocle's differential gene test (Qiu et al., 2017; Trapnell et al., 2014) was performed in R, on neurogenic RPCs and RGCs of WT and *Atoh7*$^{Cre/Cre}$*;Bax*$^{-/-}$ null genotypes:

> differentialGeneTest(dat[genes expressed in >=10 cells], fullModelFormulaStr = '~sm.ns(Pseudotime,df=3)*Genotype+Total_mRNAs', reducedModelFormulaStr = '~sm.ns(Pseudotime,df=3)+Genotype+Total_mRNAs',cores=3)

2.5.12 *In situ* Hybridization

Developing embryos harvested at E14.5 were washed in Petri dishes filled with sterile DEPC-treated PBS at least three times. The head of the embryo was plunged into OCT and then immediately frozen and stored at -80ºC until needed, and the tail was used for genotyping. 20 µm sections were taken using a cryostat. Sections were allowed to dry to

slides for a few hours and then were stored at -80ºC until needed. *In situ* hybridization was performed as previously described (Shimogori et al., 2010)**.**

2.5.13 Cut&Run

5 retinas from E14 C57BL6/J embryos were dissected and pooled per biological replicate and processed for Cut&Run as described in (Skene and Henikoff, 2017) with a few modifications. All steps were carried out in 0.2ml PCR tube strips and 22 µl of BioMag Concanavalin A beads (Polysciences: Cat# 86057-3) suspended in an additional 100 µl/sample of Binding Buffer (20 mM HEPES pH 7.9, 10 mM KCl, 1 mM CaCl2, 1 mM MnCl2). After two washes, beads were resuspended in 10 µl/sample of Binding buffer using a magnetic rack. Retinas were dissociated by pipetting and centrifuged for 3 mins at 300g in PBS at RT. Cells were then resuspended in 100 µl Buffer 1 (20mM HEPES pH 7.5, 150 mM NaCl, 0.5 mM Spermidine, 1X Millipore Protease Inhibitor Cocktail Set III: Cat# 539134) at RT. After two washes, cells were resuspended in 100 ul/sample Buffer 1 and incubated with beads for 10 min at RT. Supernatant was discarded and 50 µl cold Buffer 2 (Buffer 1, 2 mM EDTA, 0.01% Digitonin) was used to resuspend the cell/bead mix. 2 ug of Rabbit anti-Atoh7 (Novus Biologicals NBP1-88639) and 2 ug of rabbit isotype control IgG (Thermofisher cat# 02-6102) antibodies were added to the samples and incubated at 4ºC overnight. Supernatant was cleared the next day and the cell/bead mix was gently resuspended in 200 µl cold Buffer 3 (Buffer 1, 0.01% Digitonin). After two washes, cell/bead mix was gently resuspended in 50 µl cold Buffer 3. 1 ul of 50X pAG-MNase was added to the cell/bead mix and incubated at RT for 10 mins. 200 µl

cold Buffer 3 was added to wash the cell/bead mix twice. Supernatant was discarded and the cell/bead mix was resuspended in 50 µl cold Buffer 3. 100 mM CaCl2 was added and the samples were incubated on ice for 30 mins. 33 ul of Stop buffer (340 mM NaCl, 20 mM EDTA, 4 mM EGTA, 50 µg/ml RNase A, 50 ug/ml Glycogen) was added to the cell/bead mix and the samples were incubated for 10 mins at 37ºC. Beads were discarded and the supernatant was used to extract DNA using Qiagen Nucleotide Removal kit as per manufacturer's specifications. DNA was eluted in 20 ul of elution buffer and sent for library preparation. Libraries were prepared per manufacturer's instructions using the KAPA HyperPrep Kit (Roche), and sequenced using the Illumina Hiseq 4000^{TM} Sequencing system with 2x50bp sequencing parameters.

2.5.14 Cut&Run Data Processing

Pair-ended reads were aligned to mm10 with Bowtie2 v2.3.5 under parameters `--local --very-sensitive-local --no-unal --no-mixed--no-discordant --phred33 -I 10 -X 700` as described previously (Langmead and Salzberg, 2012; Meers et al., 2019). Samtools filtered out alignments with less than a 30 MAPQ score (Li et al., 2009). Picard v2.0.1 MarkDuplicates removed duplicate reads. MACS2 v2.2.7.1 called peaks with the following parameters `-t Atoh7_bed -c IgG_bed -f BED -g mm --keep-dup all -p 1e-5 -n output_file` (Zhang et al., 2008). bedtools found an overlap between the two replicates' peaks with `intersect -u -a Rep1.narrowPeak -b Rep2.narrowPeak` (Quinlan and Hall, 2010). Overlapping peaks aligning to mitochondrial or random chromosomes were removed. Homer v4.11 was used for motif discovery by using `findMotifsGenome.pl`

under default parameters (Heinz et al., 2010). In ChIPseeker v1.22.1, `annotatePeak` was used to annotate the overlapping peaks with genomic features (Yu et al., 2015). DeepTools v3.1.0 was used to generate bigwig files for visualization (default parameters and bin size of 5bp) and for coverage heatmaps (Ramírez et al., 2016).

2.5.15 Data Availability

Single-cell RNA-sequencing processed (expression, gene (featureData), and cell (phenoData) matrices) and raw sequence information (.bam files) are available for direct download through GEO GSE148814. Atoh7 Cut&Run data is available through GEO GSE156756. The mouse developmental scRNA-seq (Clark et al., 2019) and ATAC-seq datasets were downloaded from GSE118614 and GSE102092, respectively. ATAC-seq samples were re-aligned to mm10, to conform with scRNA-seq and Cut&Run datasets using the same pipeline as described for Cut&Run samples.

2.5.16 Morris water maze

Vision was tested using a cued Morris water maze (Morris, 1984). A 150cm diameter pool was filled with water made opaque by mixing in non-toxic white tempera paint. A platform ("island", not visible from the surface of the water) was placed in one quadrant with a black and white striped 50 mL conical tube on top as a "flag". Each of six animals in a group (either *Atoh7*$^{-/+}$, *Atoh7*$^{-/-}$, or *Atoh7*$^{-/-}$;*Bax*$^{-/-}$) was allowed a 90 second trial in which to swim and visually locate the island. If the animal found the island, it was allowed to remain on the island for 60 seconds before being removed from the pool. If

the animal did not locate the island, it was placed at the edge of the island, allowed to climb on, and remain on the island for 60 seconds to reinforce the island as a safe spot. Following the first trial, the island was moved to a different quadrant and animals were tested again. In total, four trials were completed with the island in four different locations.

2.5.17 Visual tracking

Visual acuity was assessed using OptoMotry (Cerebral Mechanics). Animals were placed on a platform in the viewing chamber and allowed to adapt for 10 minutes prior to testing. Testing was done for five minutes, during which the position of the animal's head was monitored to assess visual tracking. Following each tracking event, the direction and width of the grating was changed, eventually narrowing down to smaller ranges of acuity.

2.5.18 X-Gal Staining

To examine ipRGCs and projections in animals with one allele of $Opn4^{tauLacZ/+}$, adult animals were transcardially perfused with 10 mL PBS followed by 15 mL of 4% PFA. Brains were dissected and cryoprotected in 30% sucrose in PBS until the tissue had sunk in the solution (kept at 4°C) and then frozen in OCT. Cryosections (50 μm) were mounted on slides and allowed to dry up to 8 hours at room temperature. All X-Gal staining solutions were prepared according to (Mombaerts et al., 1996). Slides were rehydrated in Buffer B for 10 minutes, then immersed in Buffer C (with potassium ferricyanide, potassium ferrocyanide and 100 mg/mL X-Gal in N-N' dimethyl formamide

(DMF)) for 2 days in a dark container. On the third day, fresh Buffer C was added to the slides which were allowed to sit overnight. Following staining, slides were washed 3 times for 5 minutes in PBS, counterstained in Nuclear FastRed (diluted 1:5 in water) for 10 minutes, washed in 70% ethanol, and mounted in glycerol. Retinas were dissected in phosphate buffer and placed in X-Gal Buffer B for 10 minutes, then Buffer C for 2 days at room temperature in a dark container. On the third day, fresh Buffer C was added, and retinas were stained for an additional day. Following staining, retinas were washed 3 times for 5 minutes in PBS, washed in 70% ethanol, and flat mounted in glycerol.

2.5.19 CtB sectioning and visualization

Pulled glass needles were filled via capillary action with roughly 5 μL of Alexa 488 conjugated Cholera toxin b subunit (CTb; Invitrogen) diluted to 5mg/mL in dH20. Filled needles were affixed to a Harvard Apparatus FIL-190 picospritzer. For injection, adult animals were anesthetized with 25ul/g body weight Avertin (1.25% tri-bromo-ethanol and 2.5% tertiary-amyl alcohol in dH20) and tested for alertness via toe pinch. Gentle pressure was applied behind the eye to raise it, the needles were aimed just above the skin margin, and CTb was injected in the intraocular space. Animals were allowed to recover and maintained for three days post-injection to allow the tracer to reach the distal axons tips. Following the three-day survival period, animals were transcardially perfused with 15 mL of PBS, followed by 25 mL of cold 4% PFA. Brains were dissected after perfusion and post-fixed in 4% PFA for 1 hour, then cryoprotected in 30% sucrose. Brains were frozen in OCT and sectioned at 50 μm in a cryostat. Sections were dried overnight, fixed

in 4% PFA for 10 min, mounted in VectaShield (Vector Labs)+1.5 mg/mL DAPI and imaged on a Zeiss Imager Ml upright epifluorescence microscope (AxioVision software).

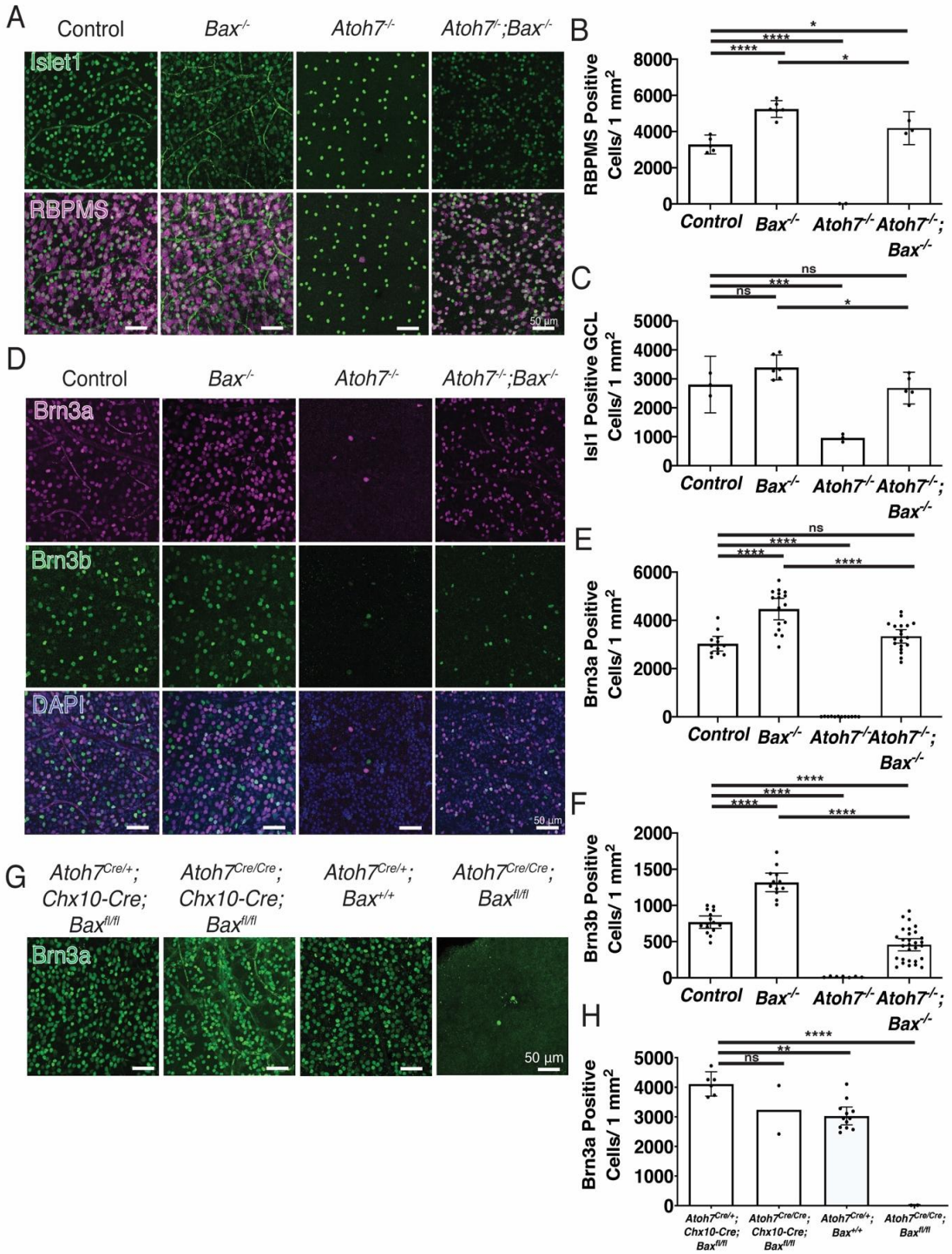

Figure 1. Brodie-Kommit et al. 2020

Figure 1. *Atoh7*-independent development of RGCs. (A-C) We observed a 25.2±0.9% and 21±3% reduction in RBPMS+ RGC density or Isl1+ ganglion cell layer (GCL) cells when comparing *Atoh7*$^{-/-}$*;Bax*$^{-/-}$ to *Bax*$^{-/-}$ mice. (D,E,F,G,H) Brn3a and Brn3b positive RGC density are only moderately reduced when apoptosis is blocked in *Atoh7*$^{-/-}$*;Bax*$^{-/-}$ mice. (G,H) Brn3a positive RGC numbers are rescued when apoptosis is blocked in all neural retinal progenitor cells, when *Bax*$^{lox/lox}$ is crossed to the *Chx10-Cre* transgene, which is expressed in all RPCs. However, when *Bax* is specifically removed in *Atoh7-Cre* knock-in mice, Brn3a RGCs are not rescued. Mean ± 95% confidence intervals. Statistical significance tested by one-way ANOVA with Tukey's post test for multiple comparisons **** $p < 0.0001$.

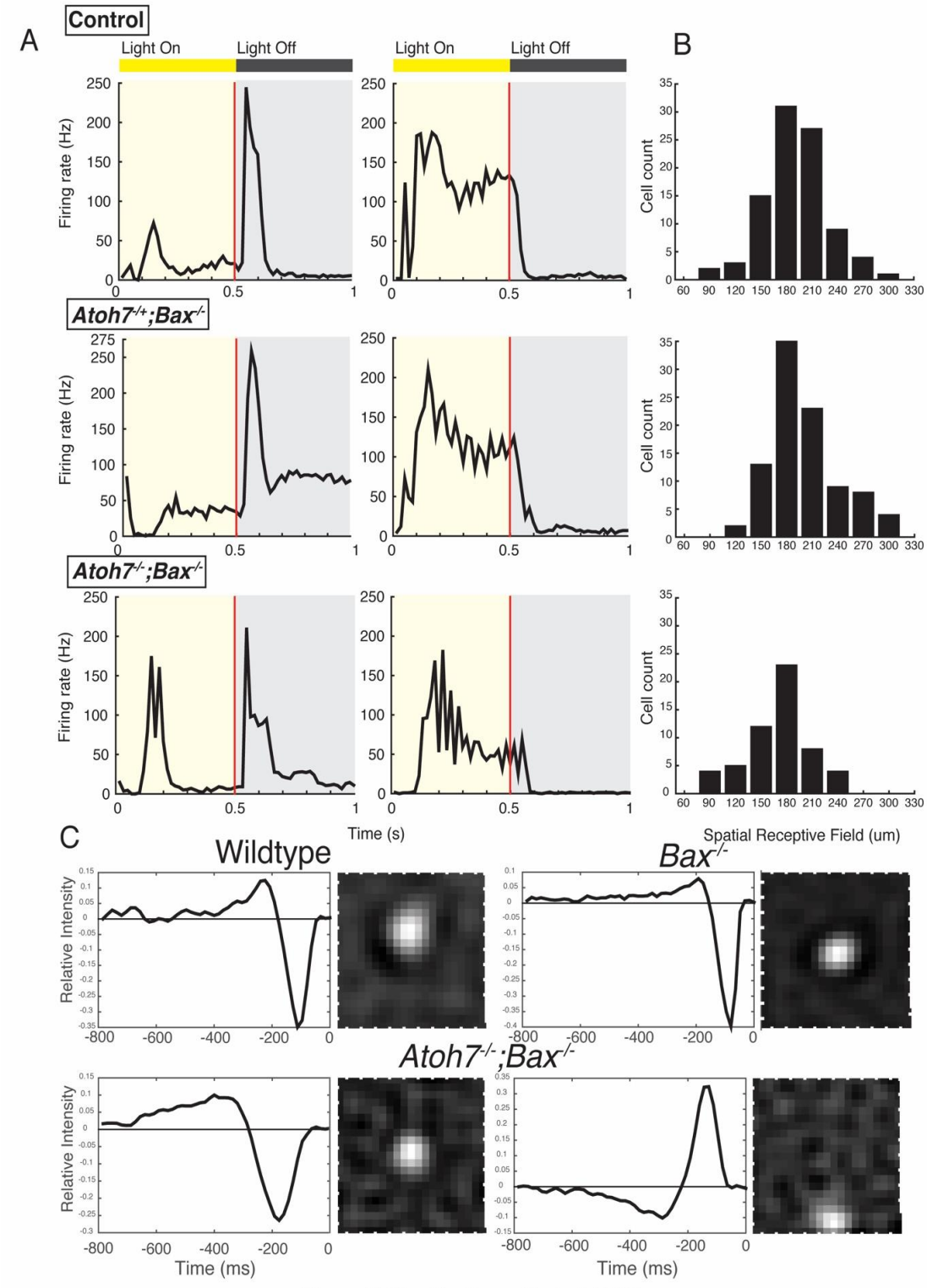

Figure 2. Brodie-Kommit et al. 2020

Figure 2. *Atoh7* is not required for normal retinal wiring and electrophysiological function. Cells from *Atoh7*$^{+/-}$*;Bax*$^{-/-}$, and *Atoh7*$^{-/-}$*;Bax*$^{-/-}$ mice responded to light similarly as those from wild type. (A) Two different examples, corresponding to two different sets of RGCs, per genotype of peristimulus time histogram averaged from 120 repetition of 1-Hz square wave flash: WT (upper panel), *Atoh7*$^{+/-}$*;Bax*$^{-/-}$ (middle), and Atoh7$^{-/-}$;Bax$^{-/-}$ (lower panel). (B) Distribution of the spatial receptive field measured using white noise flickering checkerboard: WT (upper, cell count = 92), *Atoh7*$^{+/-}$*;Bax*$^{-/-}$ (middle, cell count = 94), and *Atoh7*$^{-/-}$*;Bax*$^{-/-}$ (lower, cell count = 56). (C) the peristimulus time histogram (PSTH) of responses to square-wave flash was calculated using 10-ms bins. Mice assayed at P30. one-way ANOVA, followed by Dunnett's test, $p < 0.05$, between *Atoh7*$^{-/-}$*;Bax*$^{-/-}$ and wildtype.

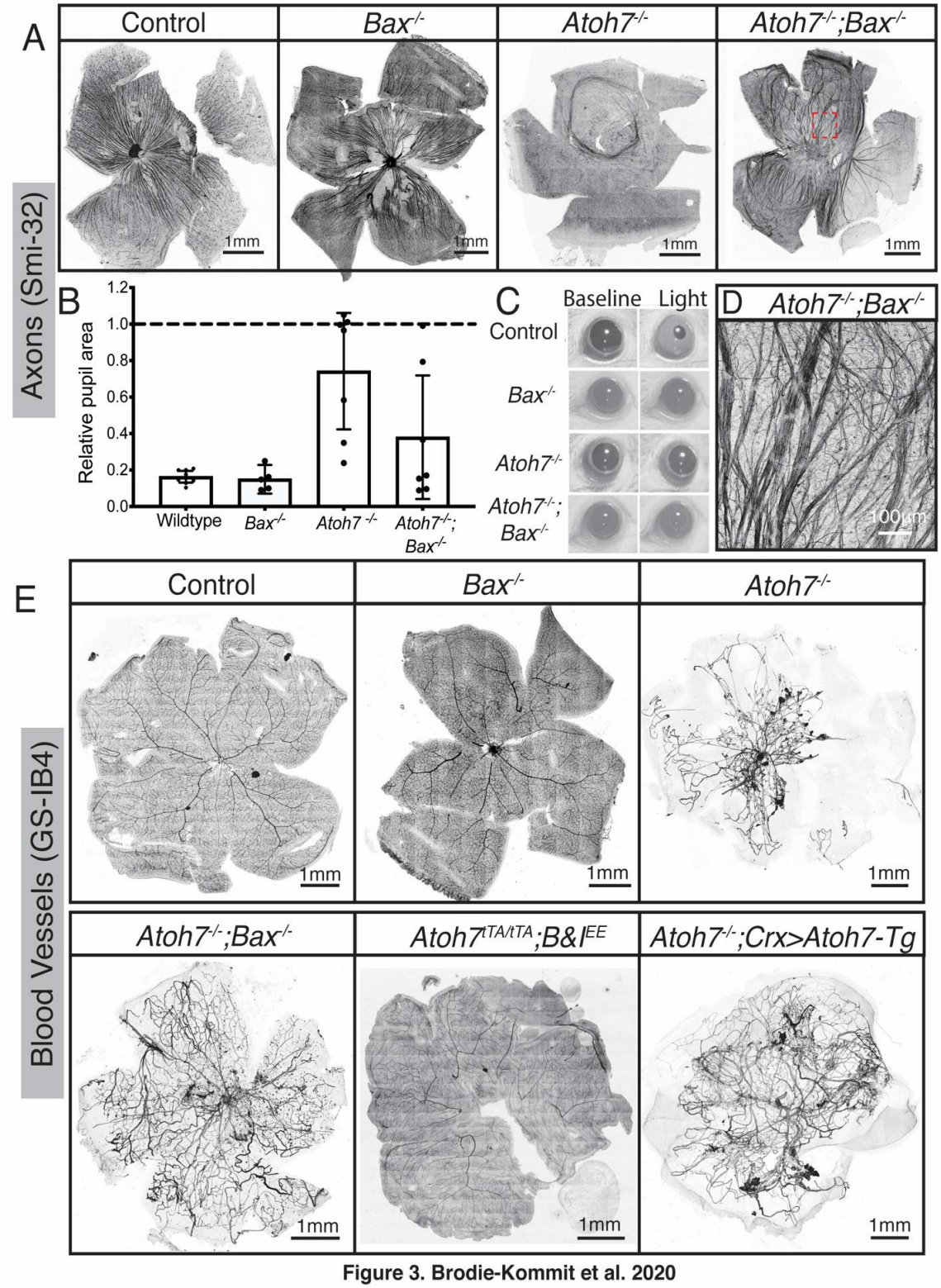

Figure 3. Brodie-Kommit et al. 2020

Figure 3. RGC axon guidance and retinal vasculature development require *Atoh7*-dependent RGCs. (A,D) Smi-32 labels a subset of RGCs and their axons in an adult wildtype retina. In *Atoh7*$^{-/-}$ mice, the Smi-32 positive RGCs have axon guidance deficits. In *Atoh7*$^{-/-}$*;Bax*$^{-/-}$ mice, RGCs have severe axon guidance deficits. Highlighted region (A - *Atoh7*$^{-/-}$*;Bax*$^{-/-}$) is magnified in (D). (B,C) Using the contralateral pupillary light response as a readout of retina to brain connection allows the appreciation that the severe axon guidance deficits allow for some connection to the brain of the RGCs in the *Atoh7*$^{-/-}$ or *Atoh7*$^{-/-}$*;Bax*$^{-/-}$ retinas. (E) It has been previously reported that the hyaloid vasculature fails to regress in *Atoh7*$^{-/-}$ mice, thought to be due to lack of RGCs, however when the RGC numbers are rescued, in *Atoh7*$^{-/-}$*;Bax*$^{-/-}$mice, the hyaloid vasculature fails to regress. However, *Atoh7* is not necessary for the hyaloid regression and retinal vasculature development, seen using *Atoh7*$^{tTA/tTA}$*;B&I*^{EE} mice, which was previously seen to rescue all of the *Atoh7* null phenotypes. When *Atoh7* is rescued using the *Crx>Atoh7* transgene on the *Atoh7* null background, the optic nerve and 12% of RGCS are rescued (Prasov and Glaser, 2012), but the hyaloid vasculature does not regress.

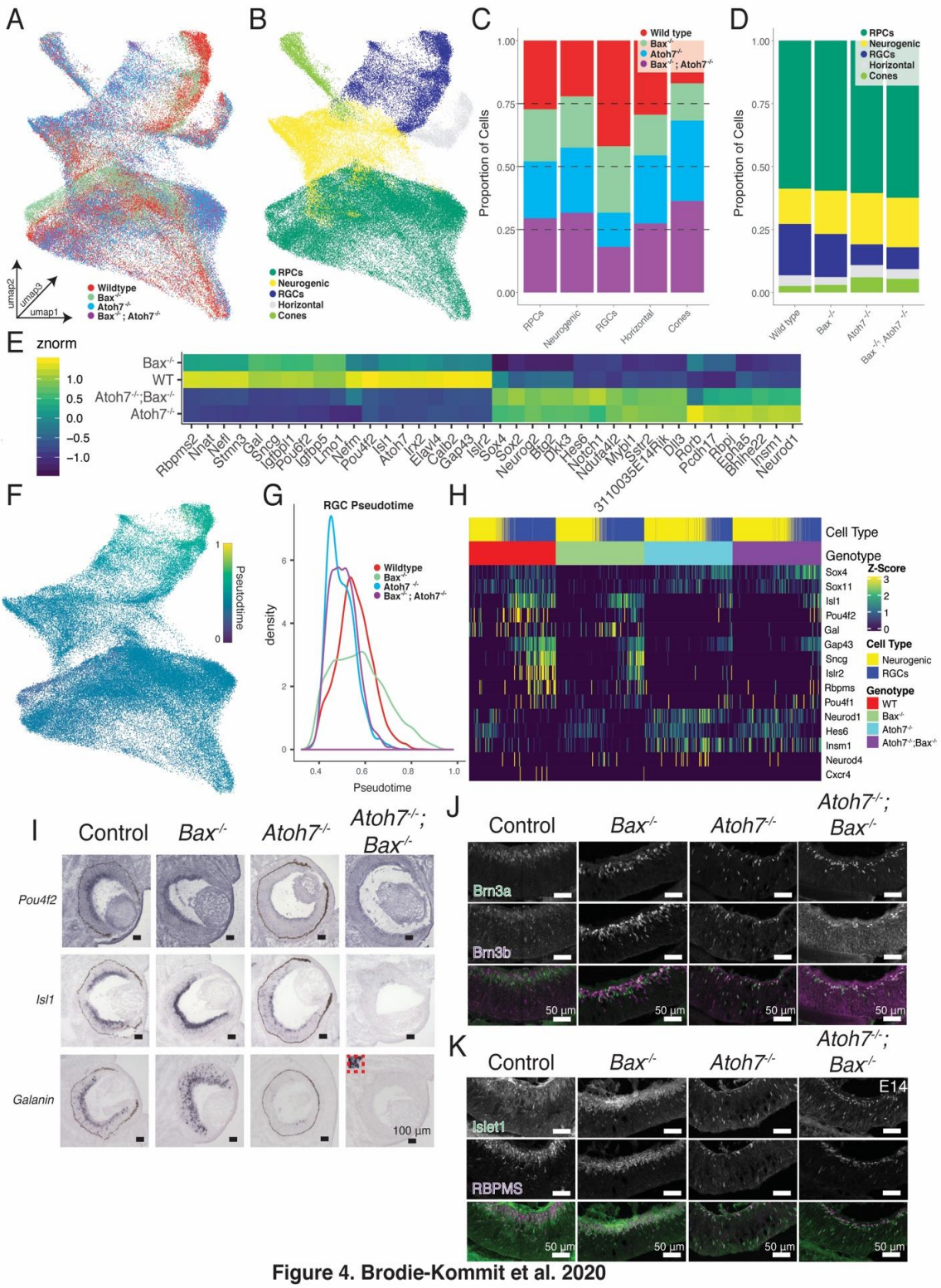

Figure 4. Brodie-Kommit et al. 2020

Figure 4. Single-cell analysis of E14.5 mutant retinas and gene detection in E14 retinas. (A,B) UMAP dimension reduction of aggregated E14.5 single-cell dataset colored by (A) genotype and (B) annotated cell-type. (C) Proportions of cell types derived from each genotype. (D) Proportions of annotated cell types within each genotype. (E) Heatmap of differentially expressed transcripts across control and Atoh7 knockout (*Atoh7*$^{-/-}$ or *Atoh7*$^{-/-}$*;Bax*$^{-/-}$) neurogenic and RGCs. (F) UMAP dimension reduction of cells colored by Scanpy pseudotime values. (G) Density of retinal ganglion cells along pseudotime by genotype. (H) Heatmap displaying differentially expressed transcripts across the interaction of pseudotime and genotype. Cells are ordered by pseudotime within each genotype. (I) Chromogenic *in situ* hybridization detecting RNA transcripts of genes from (H). Insert, depicted by a red dotted line, *Atoh7*$^{-/-}$*;Bax*$^{-/-}$ mice in (H) show robust galanin signal in a region outside the retina, but minimal signal in the retina (J-K). Immunohistochemistry detecting (J) RGC-specific markers: BRN3A and BRN3B and (K) pan-RGC markers: ISL1 and RBPMS in E14 retina from each genotype. Scale bar, 50 μm. Abbreviations: RPCs, retinal progenitor cells; RGCs, retinal ganglion cells.

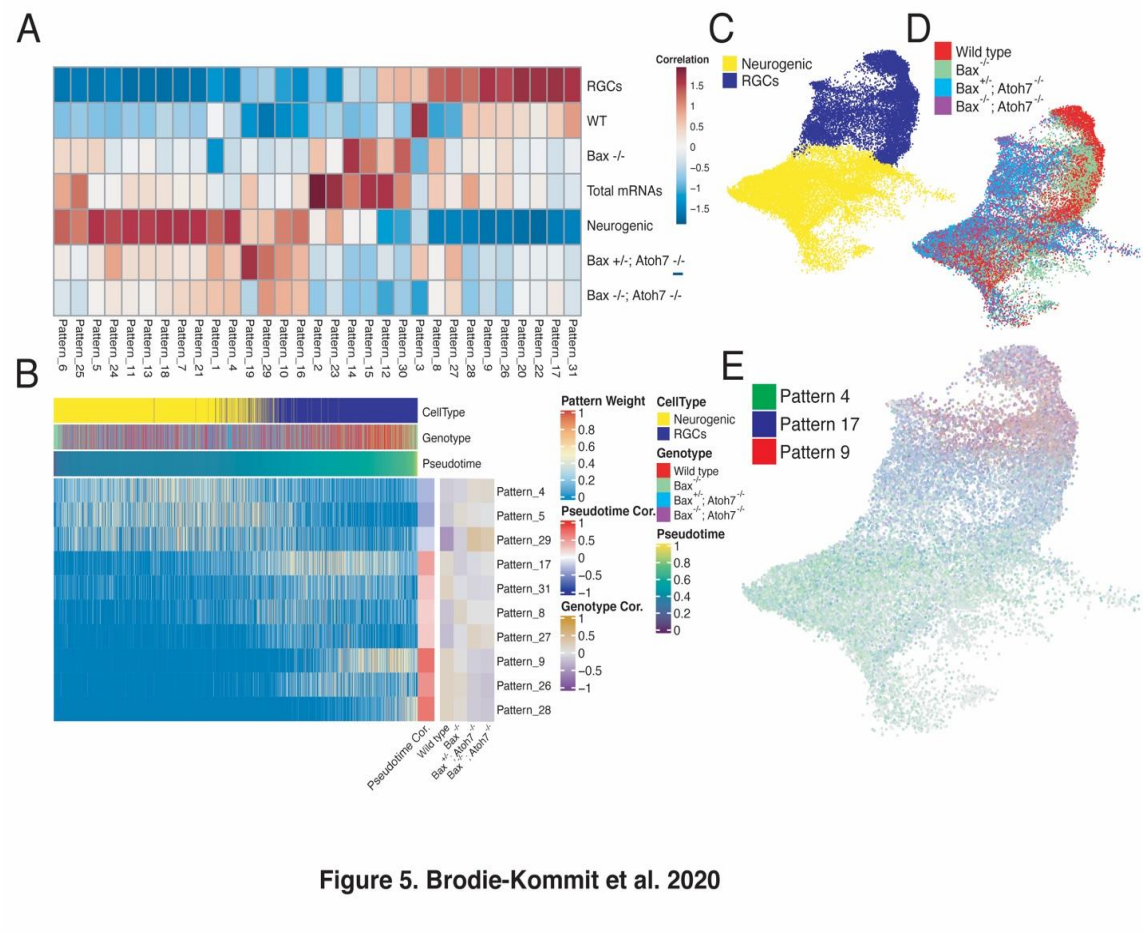

Figure 5. Brodie-Kommit et al. 2020

Figure 5. scCoGAPs analysis of single-cell dataset and RGC population changes in E12.5 retinas show a developmental delay in *Atoh7*$^{-/-}$;*Bax*$^{-/-}$. mutants. (A) Heatmap showing the correlation between scCoGAPS pattern and cellular features. (B) Heatmap of pattern weights within individual cells ordered by pseudotime. Pattern correlations with both pseudotime and each genotype are displayed at the right. (C-E) UMAP embedding of single-cell dataset used for scCoGAPS and colored by (C) celltype or (D) genotype. (E) UMAP embedding of dataset and colored by pattern weights of scCOGAPS patterns 4, 17 and 9, displaying progressive pattern usage across RGC development.

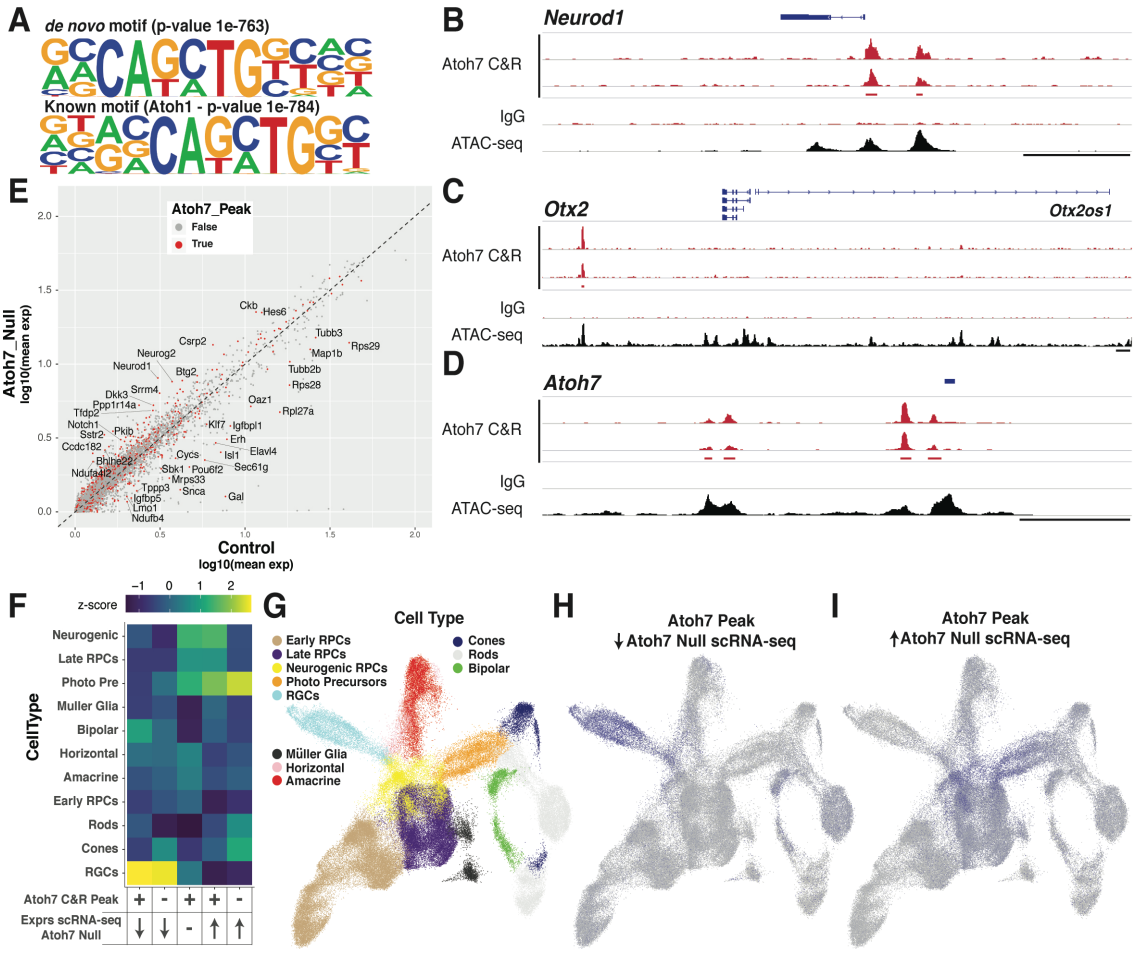

Figure 6. Brodie-Kommit et al. 2020

Figure 6. Cut&Run analysis of Atoh7 genomic binding identifies transcriptional targets of Atoh7. (A) HOMER motif analysis of most significant *de novo* (top) enriched motifs within peaks, and similarity of enriched motifs to established transcription factor motifs (bottom). (B-D) Atoh7 and IgG Cut&Run sequencing tracks within the (B) *Neurod1,* (C) *Otx2*, and (D) Atoh7 genomic loci. Additional E14 ATAC-Seq tracks (Aldiri et al., 2017) show the alignment of Atoh7 Cut&Run peaks with open chromatin. (E) Average expression of transcripts within the control (WT and $Bax^{-/-}$) and Atoh7 Null ($Atoh7^{-/-}$ or $Atoh7^{-/-};Bax^{-/-}$) neurogenic RPCs and RGCs. Transcripts with Atoh7 Cut&Run peaks are indicated in red. Gene names are displayed for transcripts that display both Atoh7 Cut&Run peaks and high residual to the mean expression (no change in expression). (F) Cellular enrichment of transcript expression within the developmental scRNA-Seq dataset (Clark et al., 2019) of genes with the presence/absence of Atoh7 binding and increased, decreased, or no change in expression within *Atoh7* mutant neurogenic RPCs and RGCs compared to control cells. (G-I) UMAP-dimension reductions of the developmental scRNA-Seq dataset (Clark et al., 2019) displaying the annotated (G) cell types or (H-I) normalized cellular z-scores of (H) Atoh7-bound transcripts with decreased or (I) increased expression in *Atoh7* mutants.

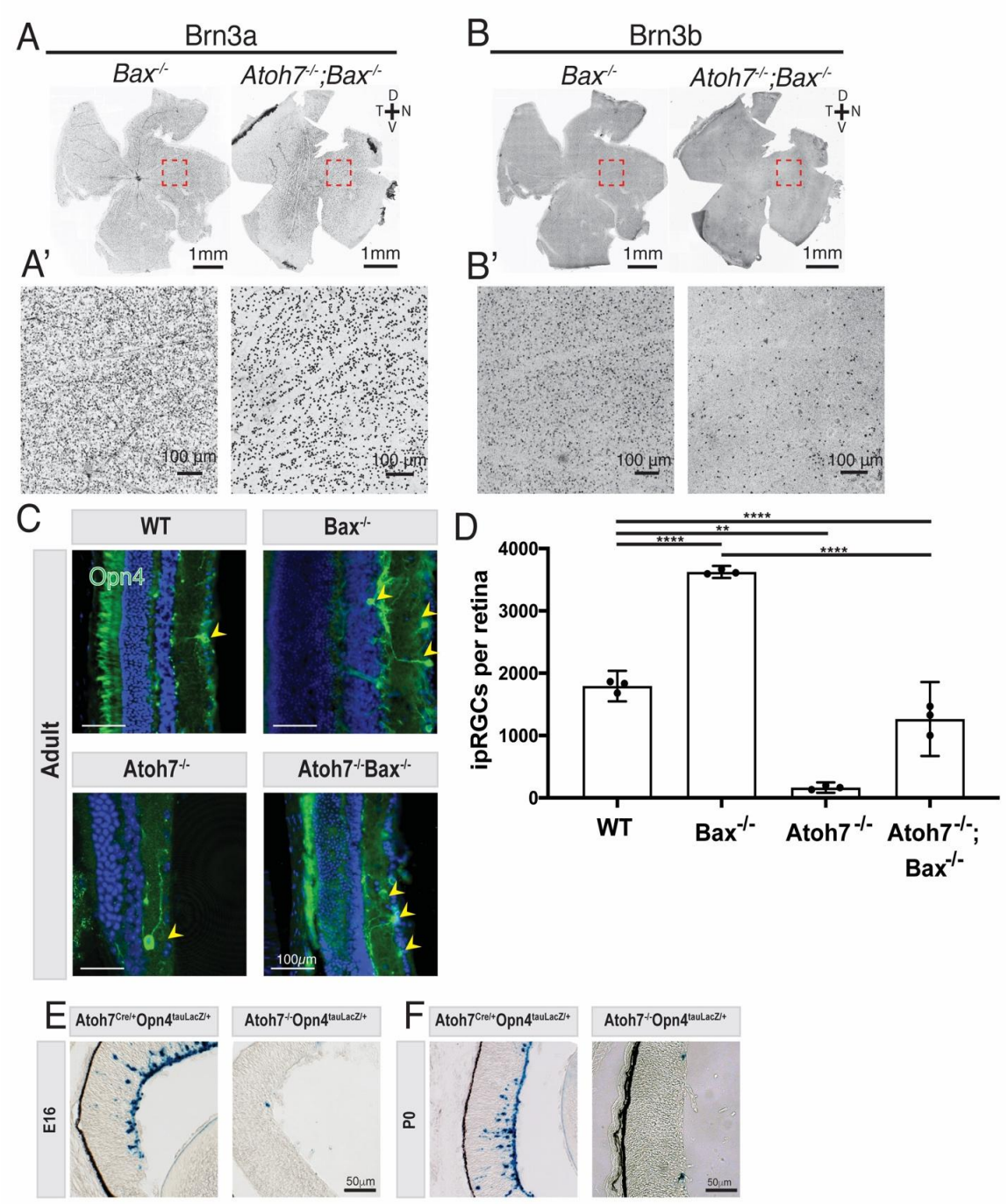

Supplemental Figure 1. Brodie-Kommit et al. 2020

Supplemental Figure 1. *Atoh7*-independent development of RGCs. (A,B) Whole retinal dissection showing the presence of Brn3a and Brn3b positive RGCs respectively. Notice the orientation of the retinas as marked by the orientation rose. Highlighted regions (A,B) are magnified in (A',B'). (C,D,E,F) IpRGCs are partially rescued by preventing apoptosis. (C,D) To determine if ipRGCs were undergoing apoptosis in the Atoh7$^{-/-}$, ipRGC numbers were examined in Atoh7$^{-/-}$ and *Atoh7*$^{-/-}$*;Bax*$^{-/-}$. ipRGCs in the *Atoh7*$^{-/-}$*;Bax*$^{-/-}$ were rescued to 60% of wild type levels. *Bax*$^{-/-}$ showed a 202±9% increase in ipRGCs compared to controls, similar to what has been reported for other RGCs in the *Bax*$^{-/-}$ knockout. (E,F) To determine if ipRGCs were generated in development in Atoh7$^{-/-}$ mice, I examined E16 and P0 timepoints using the Opn4^{tauLacZ} marker. At both E16 and P0, a 90% deficit of ipRGCs was observed. Mean ± 95% confidence intervals. Statistical significance tested by one-way ANOVA with Tukey's post test for multiple comparisons ** p=0.0052, **** p < 0.0001.

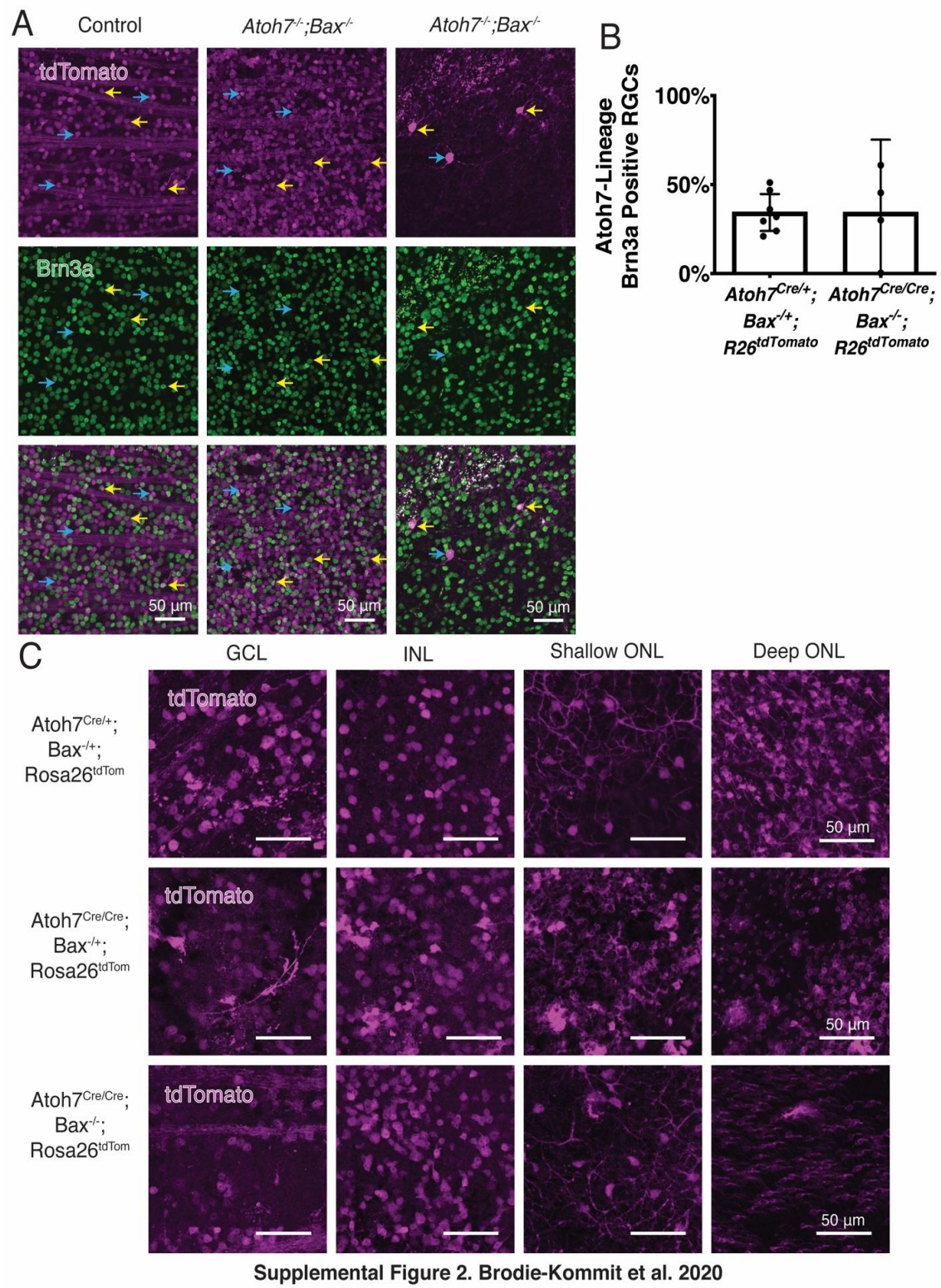

Supplemental Figure 2. Brodie-Kommit et al. 2020

Supplemental Figure 2. Atoh7^{Cre};R26^{tdTomato} lineage labeling. (A,B) A similar percent of RGCs are of the Atoh7 lineage in both wildtype and *Atoh7*$^{-/-}$;*Bax*$^{-/-}$ mice. Yellow arrows highlight Brn3a+ and Atoh7-expressing RPC-derived RGCs while blue arrows highlight non-Brn3a+ cells in the GCL (ganglion cell layer). (C) Atoh7^{Cre};R26^{tdTomato} labels cells of most cell types in the retina in all genotypes examined. Abbreviations: GCL, INL (inner nuclear layer), ONL (outer nuclear layer).

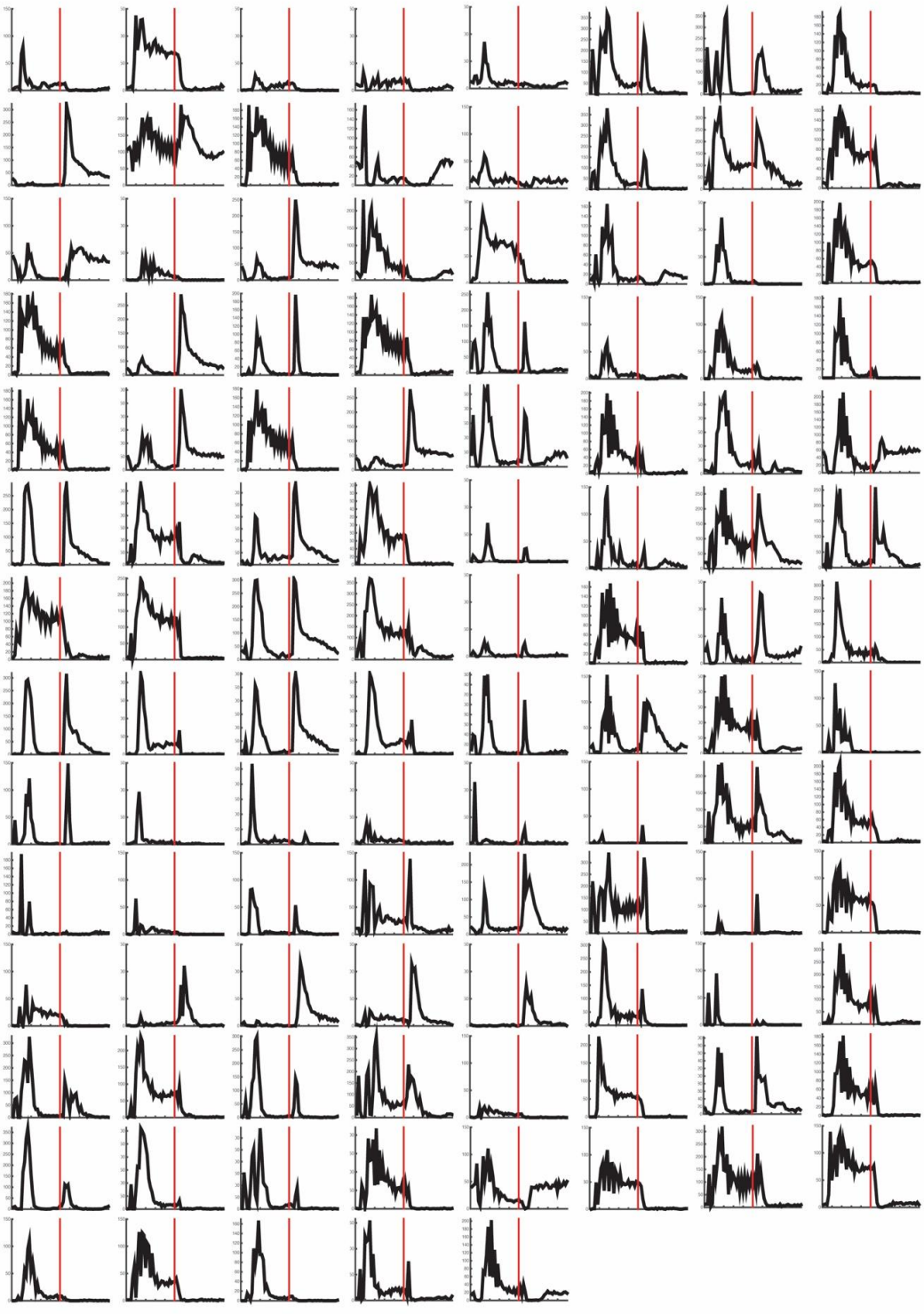

Supplemental Figure 3. Brodie-Kommit et al. 2020

Supplemental Figure 3. Detailed response to light of individual RGCs in *Atoh7*$^{-/-}$;*Bax*$^{-/-}$ mice. Peristimulus time histogram averaged from 120 repetition of 1-Hz square wave flash of every RGC recorded from in *Atoh7*$^{-/-}$;*Bax*$^{-/-}$ mice. The red line represents the transition from Light on to Light off in the square wave light flash.

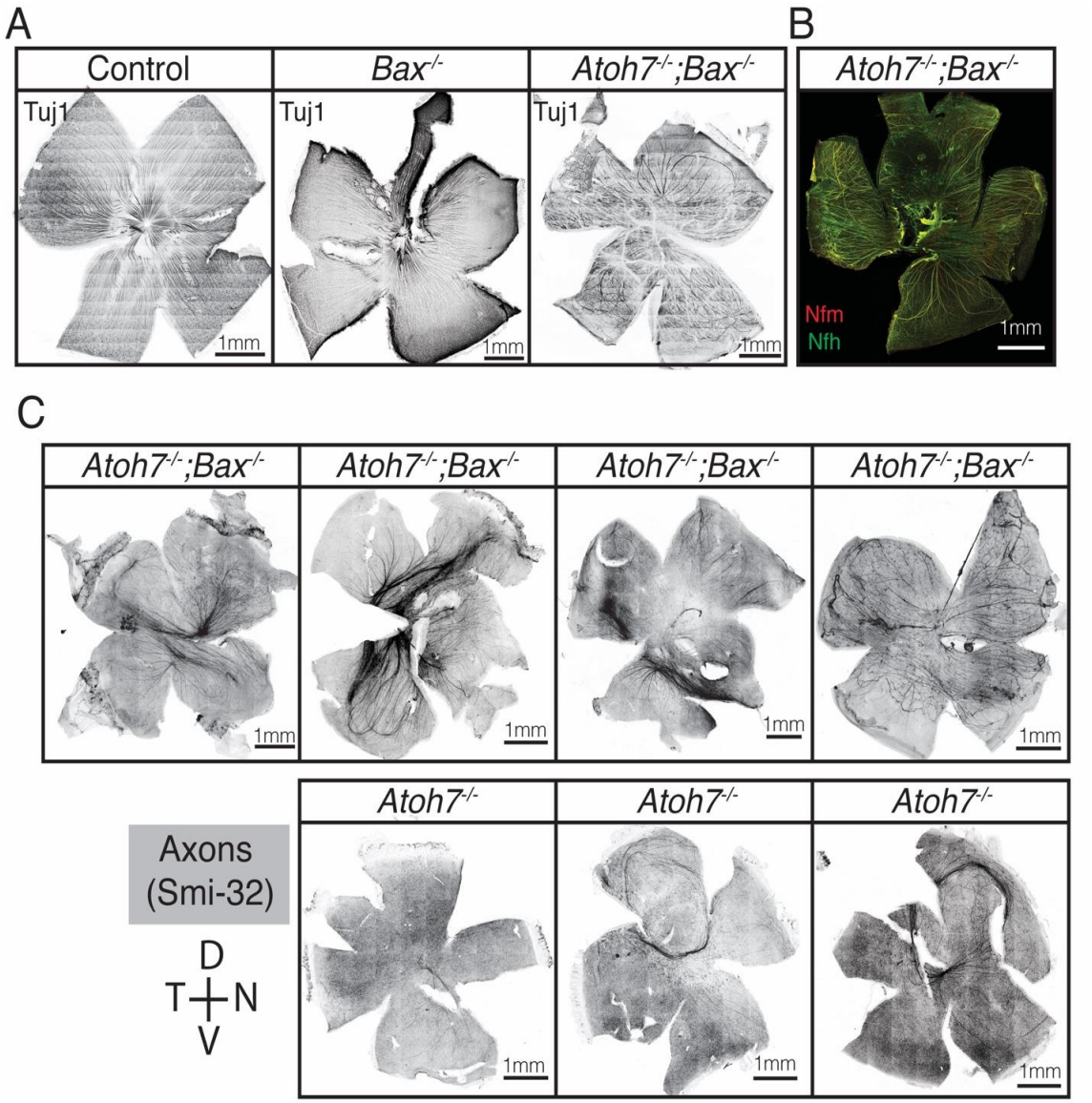

Supplemental Figure 4. Brodie-Kommit et al. 2020

Supplemental Figure 4. RGC axon guidance requires *Atoh7*-dependent RGCs. Similar results seen with Tuj1 (A), NFM, and NFH (B) immunostaining as seen with Smi-32 staining. (C) More examples of orientation preserved dissection of whole retinas of all four genotypes and stained with an antibody to Smi-32, notice the orientation of the retinas as marked by the orientation rose.

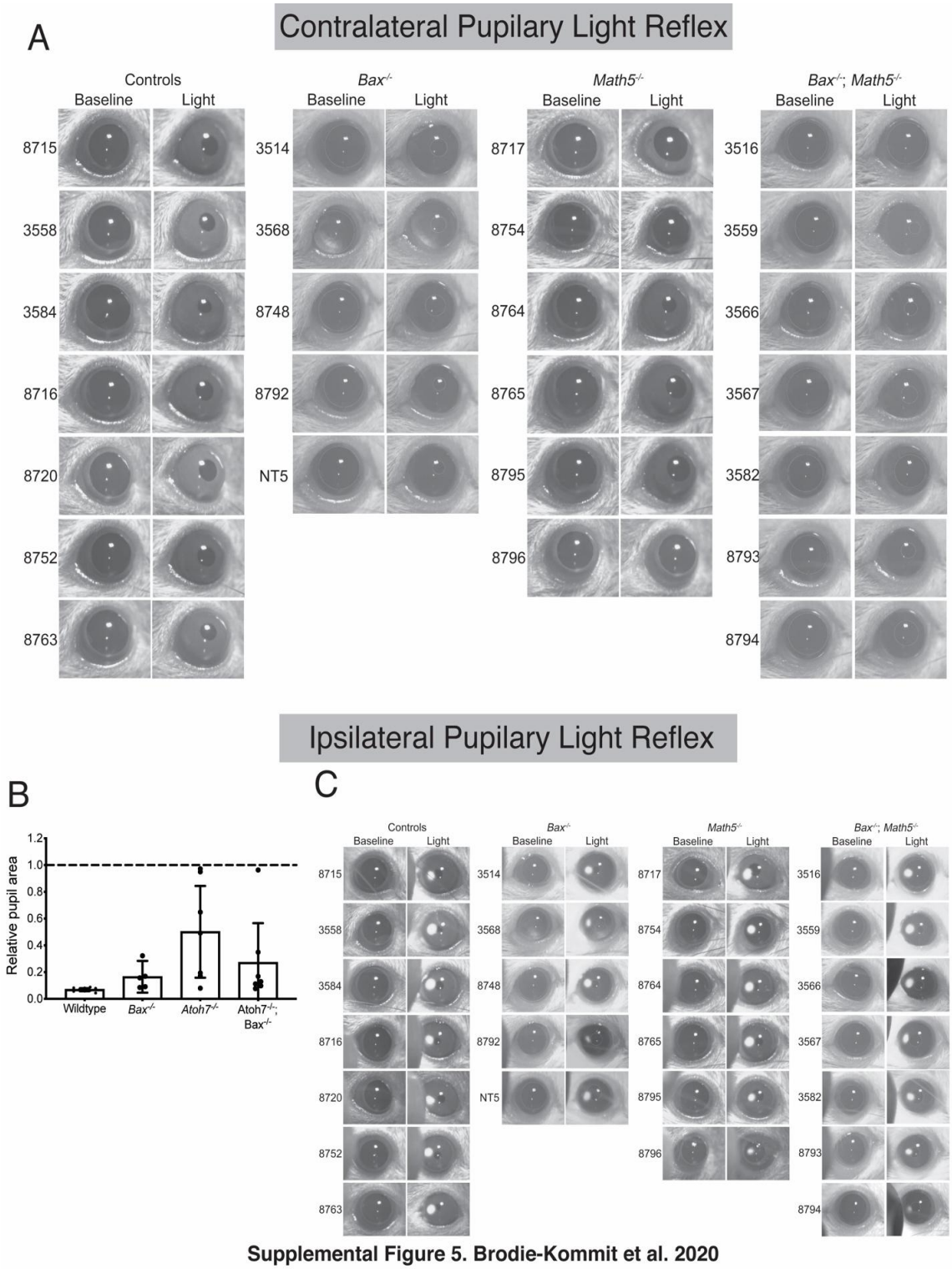

Supplemental Figure 5. Brodie-Kommit et al. 2020

Supplemental Figure 7. Traces of Pupillary light reflex (PLR) of individual mice before and after light stimulus for contralateral (A) and ipsilateral (D) recordings. *Bax*$^{-/-}$ and *Atoh7*$^{-/-}$*;Bax*$^{-/-}$ mice lack retinal pigmentation therefore their pupils are outlined for clarity. Analysis of the relative pupil area of all of the PLR responses between genotypes for contralateral (B) and ipsilateral (C). Mean ± 95% confidence intervals.

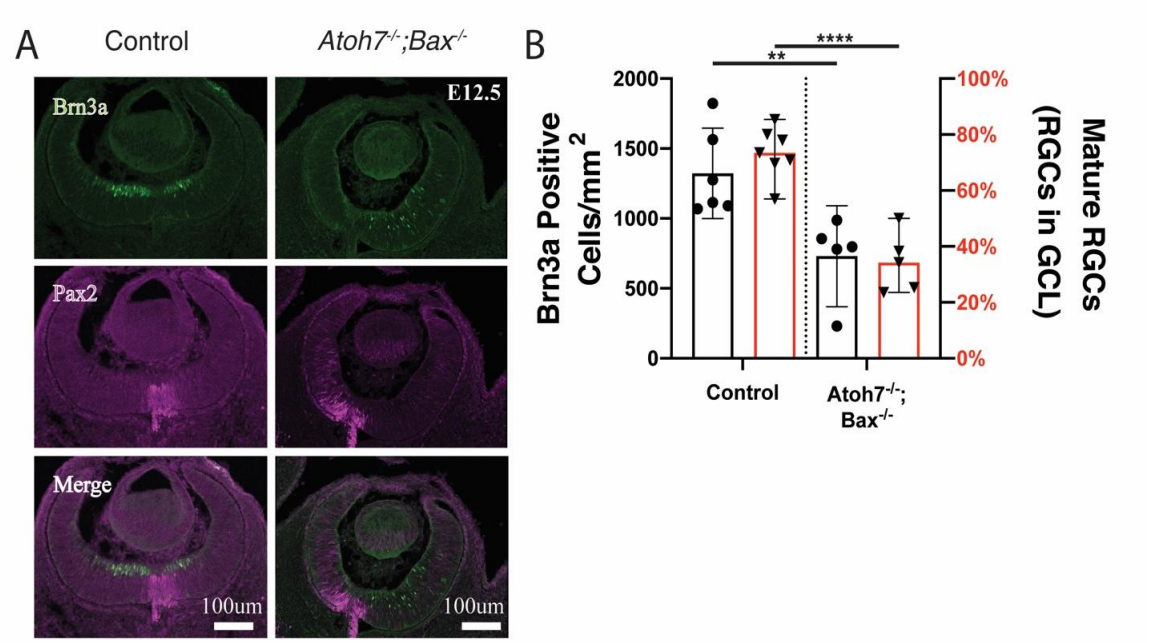

Supplemental Figure 6. Brodie-Kommit et al. 2020

Supplemental Figure 6. During early development, E12.5, *Atoh7*$^{-/-}$*;Bax*$^{-/-}$ mice have both fewer Brn3a positive RGCs and mature RGCs. (A) Pax2 antibody staining was used to help find the central retina to make sure the earliest born RGCs in the central retina were fully sampled. (B) Quantification of the retinal images with the black bars representing density and the red bar plotted on the right side representing the percent of mature RGCs. Mean ± 95% confidence intervals. Statistical Significance tested by unpaired t test ** $p = 0.0099$ **** $p < 0.0001$. Abbreviations: RGCs, retinal ganglion cells; GCL, ganglion cell layer.

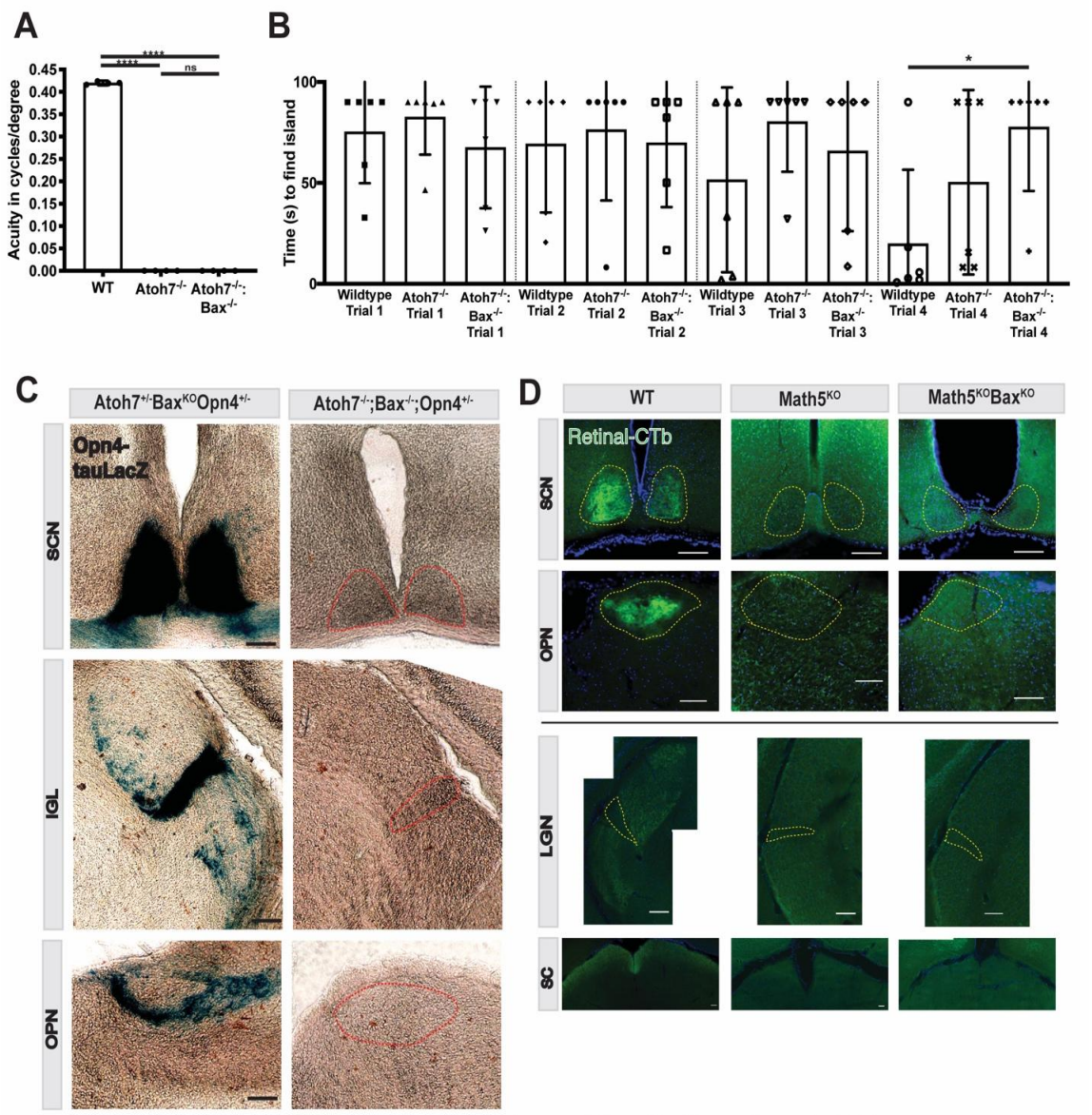

Supplemental Figure 7. Brodie-Kommit et al. 2020

Supplemental Figure 7. RGCs in *Atoh7*$^{-/-}$;*Bax*$^{-/-}$ mice do not sustain visual tasks. In the virtual optometer, animals visually track a moving grating of varied widths. (A) Only wild type animals were able to track gratings with an acuity of 0.4 cycles/degree. In the cued Morris Water Maze (B) animals locate a marked platform to escape the water. In four successive trials, most wild type animals learned to locate the platform relatively quickly. (C) ipRGC projections do not reach the brain in *Atoh7*$^{-/-}$;*Bax*$^{-/-}$ mice. The projections of ipRGCs were genetically labeled with the tauLacZ marker (depicted here as Opn4+/-) in the *Atoh7*$^{-/-}$;*Bax*$^{-/-}$ background. Robust innervation is revealed by X-Gal staining in the control while the *Atoh7*$^{-/-}$;*Bax*$^{-/-}$ mice do not show innervation (target nuclei outlined in red). (n=3, scale bars = 100mm). (D) Fluorescently conjugated Cholera toxin b labels RGC projections . Non-image forming (SCN, OPN) and image-forming targets (LGN, SC) do not receive retinal innervation in *Atoh7*$^{-/-}$ or *Atoh7*$^{-/-}$;*Bax*$^{-/-}$ mice. Yellow outlines depict targets; All scale bars 100mm, n=3 per genotype. Mean ± 95% confidence intervals. Statistical significance tested by one-way ANOVA with Tukey's post test for multiple comparisons * p=0.0386, **** $p < 0.0001$. Abbreviations: SCN: Suprachiasmatic nucleus, OPN: Olivary Pretectal Nucleus, LGN: Lateral geniculate nucleus, SC: Superior colliculus.

A

Sample	# Cells	Mean UMI	Mean Genes	Age	Genotype	Source
WT_rep1	15582	1392	871	E14	CD1 Wild-type	(Clark *et al*., 2019; *Neuron*)
WT_rep2	10496	2789	1491	E14	CD1 Wild-type	(Clark *et al*., 2019; *Neuron*)
Bax_Het_Atoh7_Null_rep1	9622	3029	1465	E14	Bax +/-; Atoh7 -/-	This Study
Bax_Het_Atoh7_Null_rep1	11345	2547	1299	E14	Bax +/-; Atoh7 -/-	This Study
Bax_Null_rep1	10268	6144	1951	E14	Bax -/-; Atoh7 +/+	This Study
Bax_Null_rep2	9269	7185	2130	E14	Bax -/-; Atoh7 +/+	This Study
Bax_Null_Atoh7_Null_rep1	14730	2269	1193	E14	Bax -/-; Atoh7 -/-	This Study
Bax_Null_Atoh7_Null_rep2	11816	1901	1098	E14	Bax -/-; Atoh7 -/-	This Study

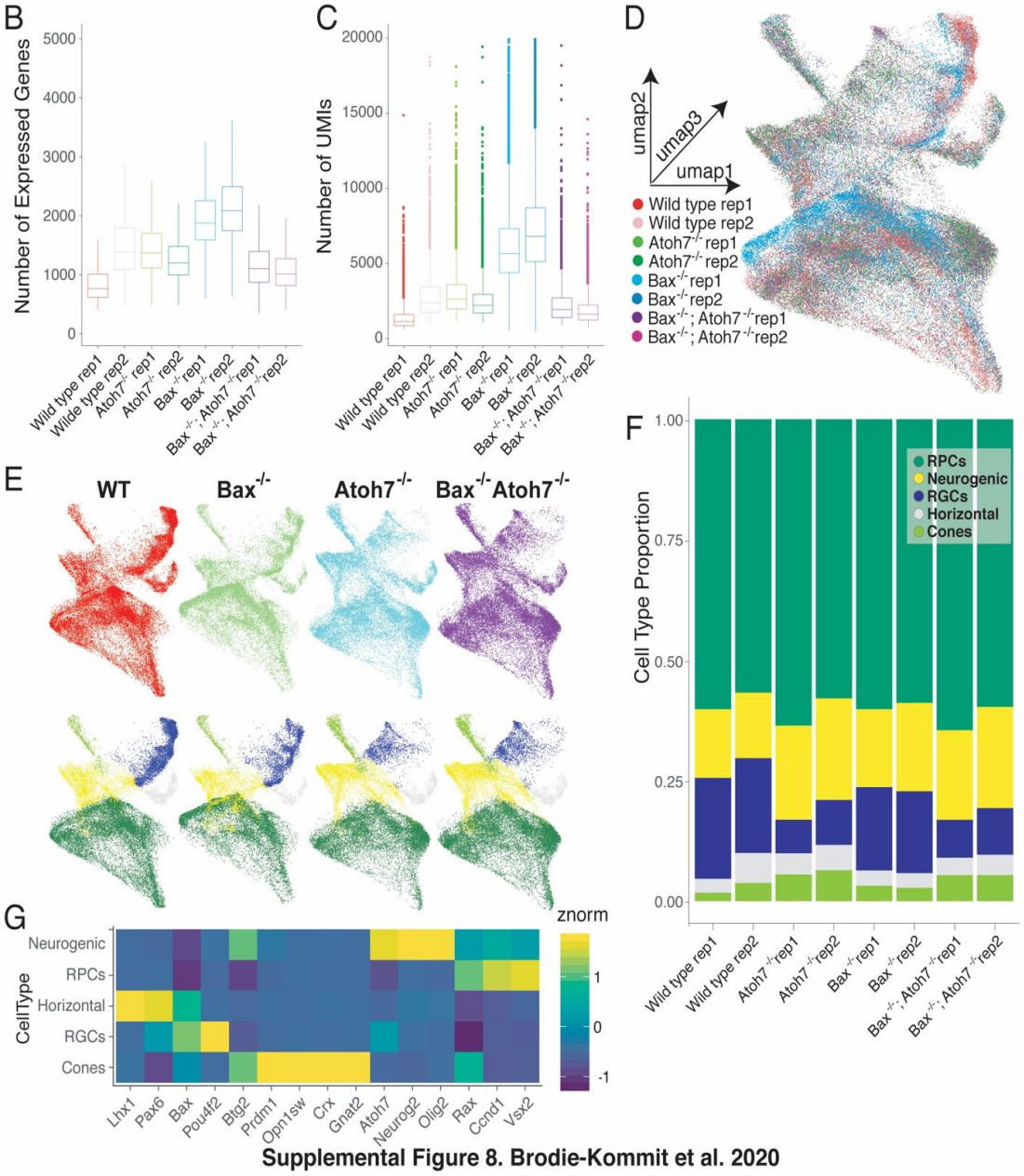

Supplemental Figure 8. Brodie-Kommit et al. 2020

Supplemental Figure 8. (A) Table of scRNA-Seq statistics for each sample. (B-C) Boxplots of the number of (B) Expressed Genes and (C) Unique molecular identifier (UMI) or transcript counts within each cell. (D) UMAP dimension reduction of the aggregate single cell datasets with individual cells colored by originating sample identity. (E) UMAP dimension reductions displaying the subset of cells corresponding to each genotype (top) and the cell type annotations (bottom) of the corresponding cells. (F) Cell type annotations of cells within each scRNA-Seq sample. (G) Heatmap of known cell type markers within annotated cell types.

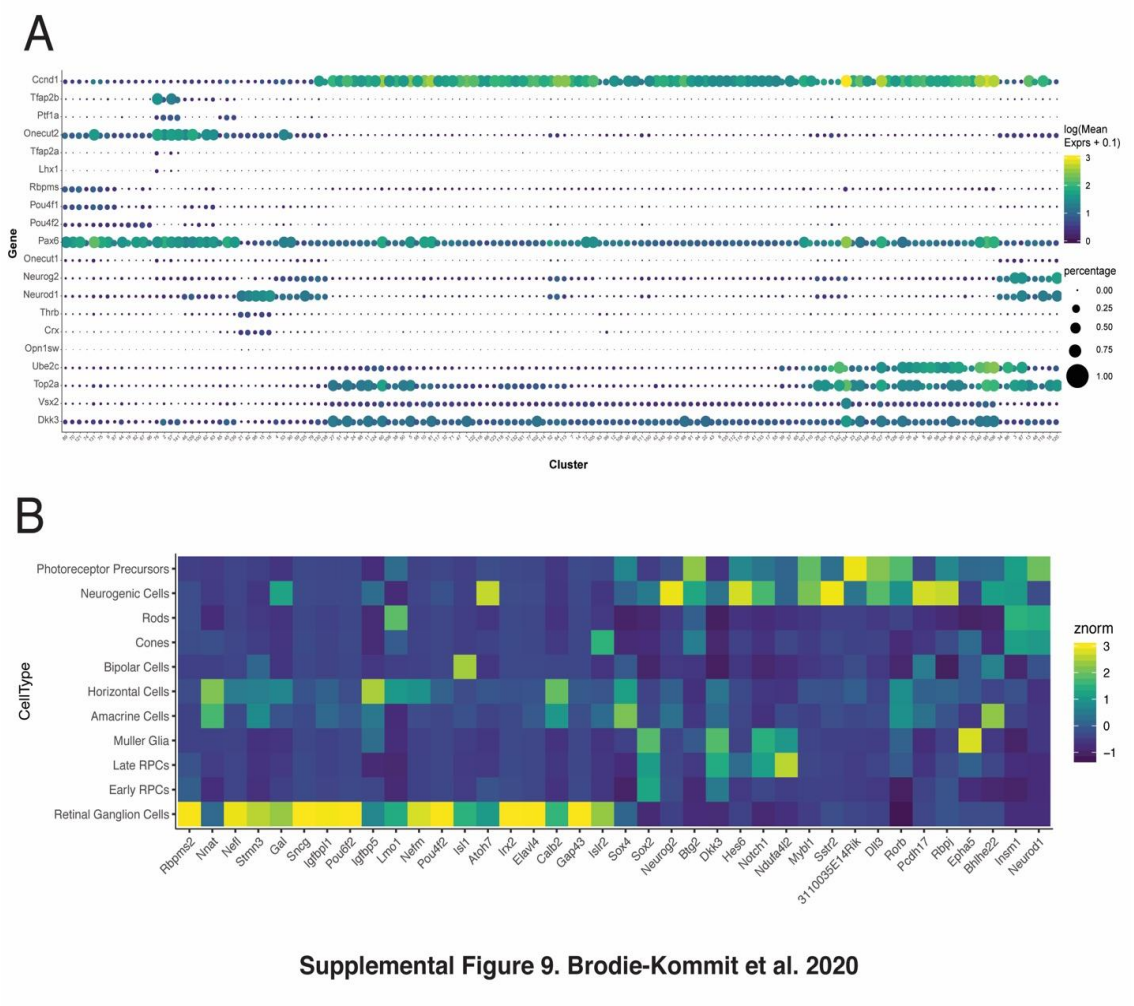

Supplemental Figure 9. Brodie-Kommit et al. 2020

Supplemental Figure 9. (A) Dotplot of a subset of marker genes used to determine cell type annotations of clusters within UMAP dimension reduction space. Color of the circle corresponds to the log() of the mean expression of individual transcripts within cells of each cluster. Size of the circles corresponds to the percentage of cells within the cluster that had at least one transcript detected. (B) Heatmap of the cell type enrichment of *Atoh7*-dependent, differentially expressed transcripts across wildtype mouse retinal development (E11-P14) as assayed by Clark et al., 2019.

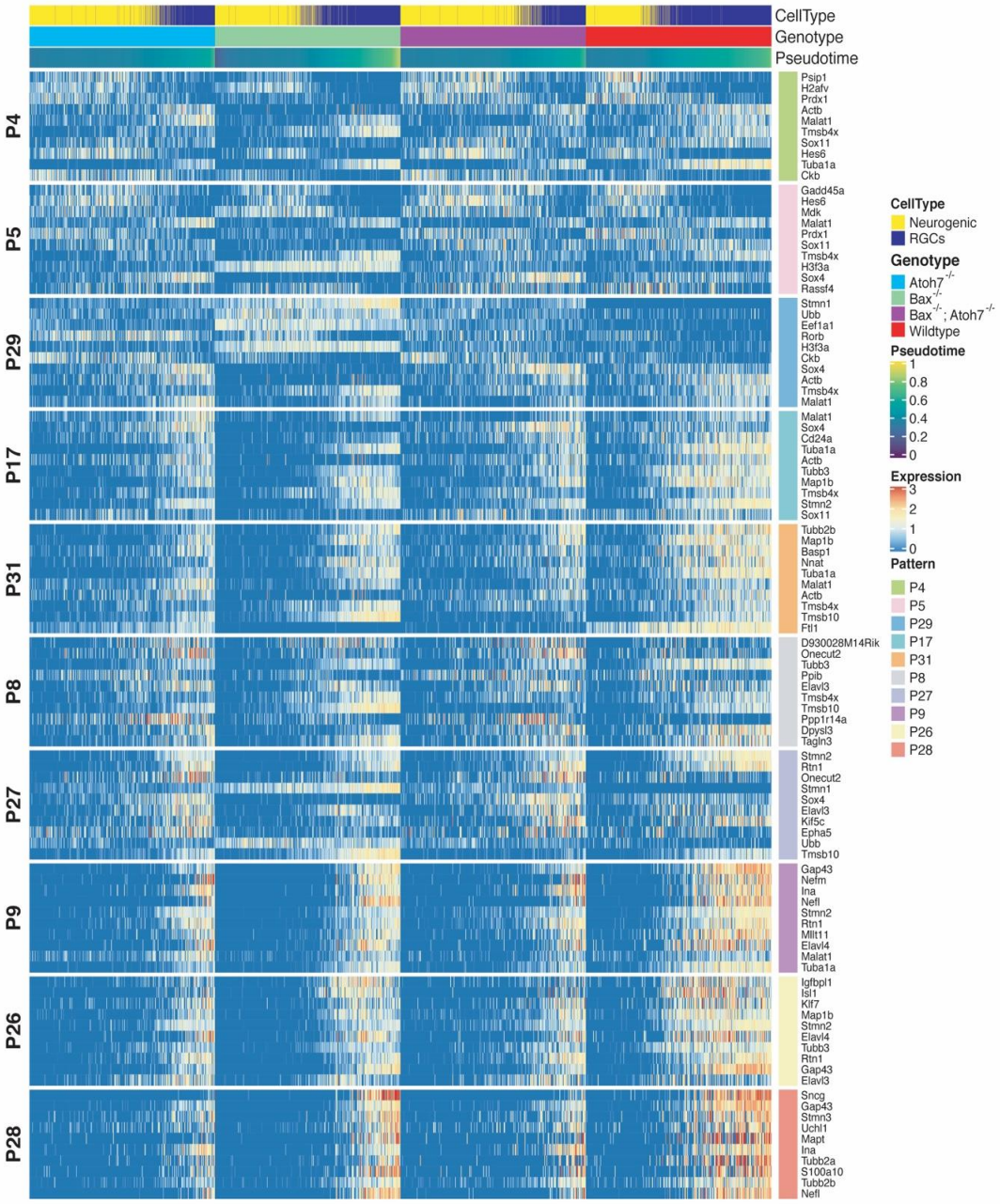

Supplemental Figure 10. Brodie-Kommit et al. 2020

Supplemental Figure 10. Pseudotime heatmap of top 10 weighted genes of scCoGAPS Patterns. Cells are ordered by pseudotime.

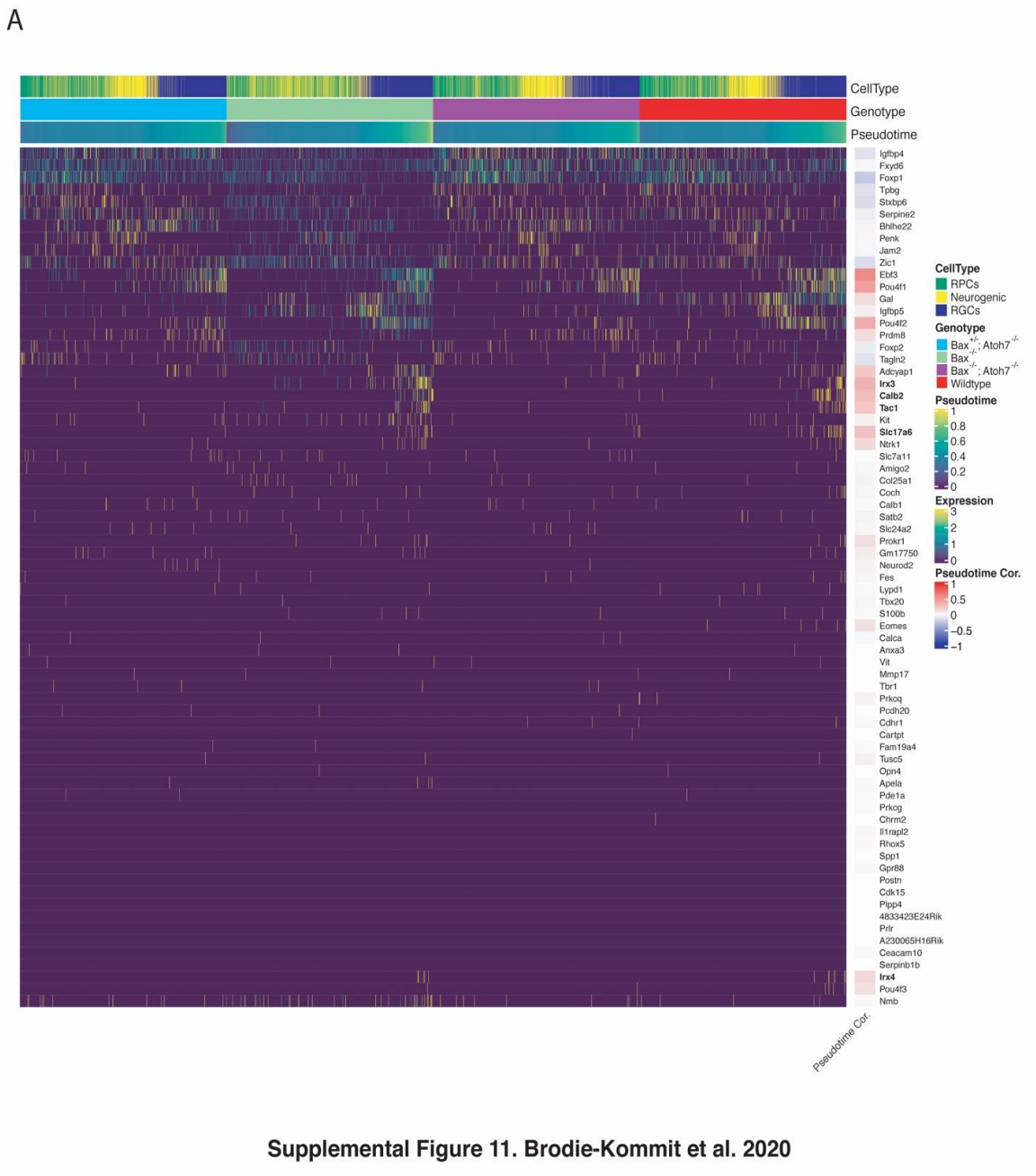

Supplemental Figure 11. Brodie-Kommit et al. 2020

Supplemental Figure 11. Pseudotime heatmap of previously published RGC subtype markers and their correlation to pseudotime

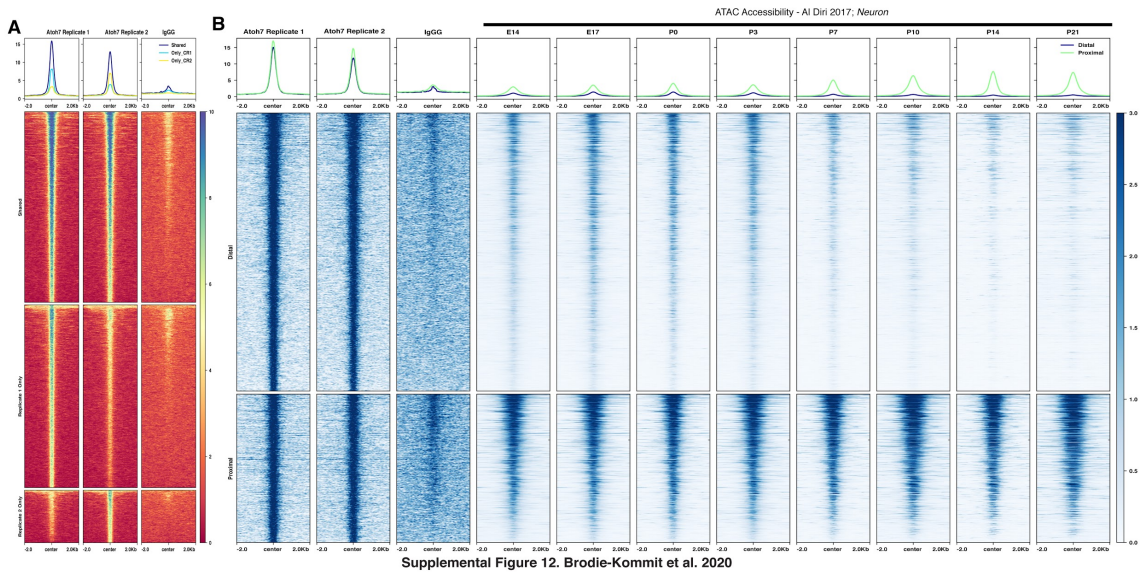

Supplemental Figure 12. Read density heatmaps of Atoh7 Cut&Run indicating (A) reproducibility between replicates and IgG control samples, and (B) accessibility within the whole retina developmental ATAC-Seq series (Aldiri et al., 2017) of proximal (bottom) or distal (top) sites to the transcription start of assigned genes.

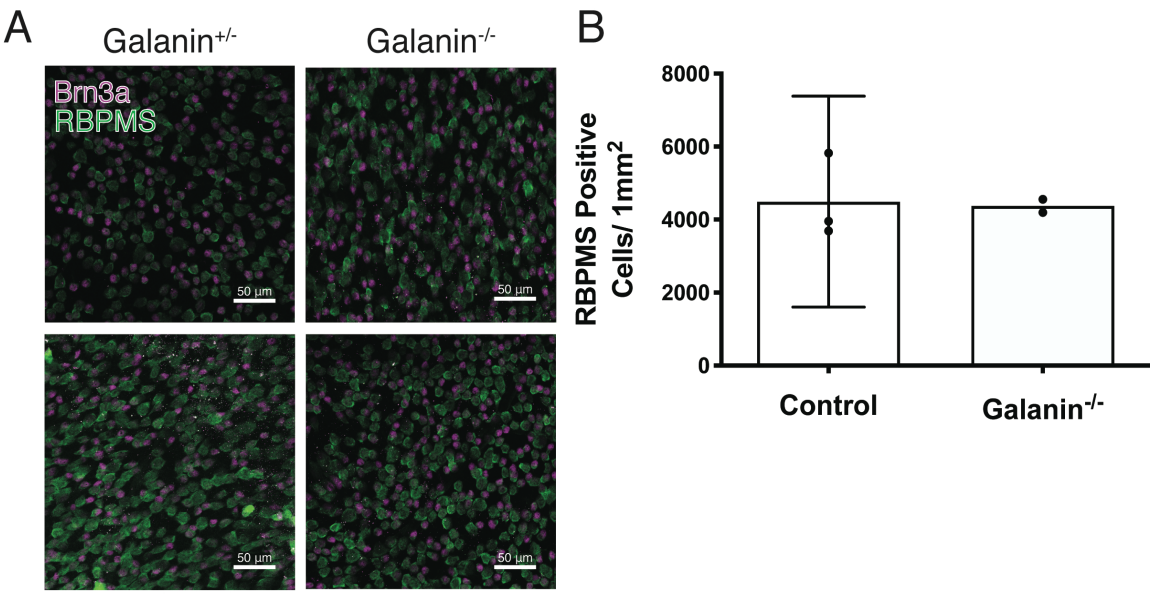

Supplemental Figure 13. Brodie-Kommit et al. 2020

Supplemental Figure 13. (A) Immunohistochemistry images of the RGC layer stained for Brn3a and RBPMS in Galanin heterozygous and knockout retinas. (B) Cell counts of RGCs indicate no difference in RGC number in P8 galanin-deficient retinas.

Table 1. 230 differentially expressed transcripts (q-value < 1e-300) between control (control and *Bax*$^{-/-}$) versus *Atoh7*-deficient *(Atoh7*$^{-/-}$, or *Atoh7*$^{-/-}$*;Bax*$^{-/-}$) neurogenic and retinal ganglion cells.

id	gene_short_name	WT_avg	Bax_Null_avg	Atoh7_Null_avg	Atoh7_Null_Bax_Null_avg
ENSMUSG00000067879	3110035E14Rik	0.055976806	0.134953773	0.29036024	0.219249201
ENSMUSG00000025912	Mybl1	0.1323595	0.286907247	0.475483656	0.327742279
ENSMUSG00000025959	Klf7	1.396186441	2.064121682	0.730653769	0.645367412
ENSMUSG00000026185	Igfbp5	0.203501338	0.641664181	0.055537025	0.050053248
ENSMUSG00000026234	Ncl	1.447368421	4.512078735	2.725316878	2.215255591
ENSMUSG00000026238	Ptma	6.870205174	45.48926335	10.31487658	6.470979766
ENSMUSG00000067071	Hes6	2.238626227	7.10975246	5.207638426	4.388178914
ENSMUSG00000026434	Nucks1	0.948260482	2.552490307	1.697798532	1.432507987
ENSMUSG00000020423	Btg2	0.729594112	1.313898002	1.613742495	1.356096912
ENSMUSG00000026688	Mgst3	0.386485281	0.711899791	0.101400934	0.075212993
ENSMUSG00000060743	H3f3a	1.971677074	22.87623024	3.191460974	2.573482428
ENSMUSG00000026923	Notch1	0.166369313	0.55487623	0.476484323	0.443290735
ENSMUSG00000062647	Rpl7a	1.912132025	7.827169699	3.098065377	2.860356763
ENSMUSG00000038900	Rpl12	1.752453167	13.16537429	3.606237492	3.685170394
ENSMUSG00000062997	Rpl35	3.038470116	16.00864897	4.969479653	2.004392971
ENSMUSG00000017144	Rnd3	0.376338091	0.396659708	0.095230153	0.068290735
ENSMUSG00000034701	Neurod1	0.387042819	1.176110945	1.994496331	1.15228967
ENSMUSG00000023236	Scg5	0.719446922	0.580077542	0.256504336	0.218982961
ENSMUSG00000074884	Serf2	0.414362177	6.902475395	0.555703803	0.346379127
ENSMUSG00000068154	Insm1	0.170495094	0.446465851	1.018178786	0.58213525
ENSMUSG00000067786	Nnat	3.052074041	5.767223382	1.139593062	0.953541001
ENSMUSG00000027581	Stmn3	1.733496878	3.363704146	0.60406938	0.532215122
ENSMUSG00000039278	Pcsk1n	0.532560214	0.88264241	0.074049366	0.076544196
ENSMUSG00000031167	Rbm3	0.042484389	3.946316731	0.059873249	0.049121406
ENSMUSG00000079641	Rpl39	1.723015165	31.95779899	4.37191461	1.400825346
ENSMUSG00000008682	Rpl10	5.219892953	19.30614375	7.45730487	7.133919063
ENSMUSG00000031320	Rps4x	6.917149866	30.69460185	10.54686458	10.28647497
ENSMUSG00000031284	Pak3	0.371431757	0.424843424	0.172281521	0.112486688
ENSMUSG00000041133	Smc1a	0.511596789	1.085296749	0.967978652	0.843184239
ENSMUSG00000049775	Tmsb4x	15.48394291	50.81807337	14.30887258	11.65069223
ENSMUSG00000027500	Stmn2	7.740856378	11.38115121	4.230320213	3.638844515
ENSMUSG00000027533	Fabp5	2.066347012	10.55934984	2.092561708	1.729233227
ENSMUSG00000025128	Bhlhe22	0.10102587	0.229048613	0.437291528	0.267838126
ENSMUSG00000039221	Rpl22l1	1.907783229	8.222189084	1.958805871	1.149627263
ENSMUSG00000074637	Sox2	0.305196253	0.730838055	0.671947965	0.596246006
ENSMUSG00000037161	Mgarp	0.264719001	1.352669251	0.825883923	0.645234292
ENSMUSG00000027996	Sfrp2	0.927854594	3.126155681	1.396430954	1.244142705
ENSMUSG00000028081	Rps3a1	5.434879572	23.18282135	9.019179453	8.236687966
ENSMUSG00000059743	Fdps	0.564339875	0.880703847	0.256170781	0.188365282
ENSMUSG00000041959	S100a10	1.091436218	2.712794512	0.410106738	0.371671991
ENSMUSG00000053192	Mllt11	1.881690455	2.790038771	0.689626418	0.600905218
ENSMUSG00000027967	Neurog2	0.665365745	0.96853564	1.659439626	1.241214058
ENSMUSG00000037894	H2afz	0.737845674	29.06024456	1.618745831	1.35529819
ENSMUSG00000068523	Gng5	0.586195361	7.354309574	0.865243496	0.451810437
ENSMUSG00000041235	Chd7	0.70896521	1.854011333	1.399933289	1.205005325
ENSMUSG00000028410	Dnaja1	0.891168599	4.387712496	0.787525017	0.531682641
ENSMUSG00000035551	Igfbpl1	1.710080285	3.995079034	0.729319546	0.574813632
ENSMUSG00000028333	Anp32b	0.813782337	4.618401432	1.858572382	1.674787007
ENSMUSG00000028495	Rps6	1.920049063	24.77855652	2.555036691	2.112220447
ENSMUSG00000028546	Elavl4	1.491413916	2.477781092	0.598398933	0.381522897
ENSMUSG00000028693	Nasp	0.861730598	2.703549061	1.76551034	1.251730564
ENSMUSG00000047675	Rps8	6.893510259	37.52072771	12.68845897	9.534211928
ENSMUSG00000028645	Slc2a1	0.295718109	0.423799582	0.785023349	0.729233227
ENSMUSG00000028648	Ndufs5	0.170606601	2.777661795	0.068879253	0.032082002
ENSMUSG00000054428	Atpif1	3.123104371	8.705040262	3.221981321	1.889643237
ENSMUSG00000039191	Rbpj	0.150089206	0.840441396	0.637925284	0.379259851
ENSMUSG00000029207	Apbb2	0.392729706	0.314643603	0.061874583	0.050186368
ENSMUSG00000029223	Uchl1	1.333184657	2.502236803	0.546531021	0.54299787

id	gene_short_name	WT_avg	Bax_Null_avg	Atoh7_Null_avg	Atoh7_Null_Bax_Null_avg
ENSMUSG00000058558	Rpl5	0.925066905	9.172830301	2.799366244	2.496538871
ENSMUSG00000063919	Srrm4	0.490633363	0.842678199	1.236991328	1.010915868
ENSMUSG00000032959	Pebp1	0.327609277	6.056367432	0.46664443	0.396166134
ENSMUSG00000029442	Wdr66	0.09823818	0.371458395	0.431287525	0.337726305
ENSMUSG00000029394	Cdk2ap1	0.281222123	1.004771846	0.726817879	0.601970181
ENSMUSG00000041453	Rpl21	2.954950937	25.34476588	6.837224817	5.400425985
ENSMUSG00000029762	Akr1b8	0.019290812	0.087980913	0.197798532	0.153354633
ENSMUSG00000029761	Cald1	0.255798394	0.618252311	0.753002001	0.63658147
ENSMUSG00000029838	Ptn	0.613849242	1.221443483	0.370913943	0.288338658
ENSMUSG00000029918	Mrps33	0.12221231	3.327020579	0.191294196	0.126597444
ENSMUSG00000025889	Snca	0.819246209	1.498061438	0.12108072	0.082667732
ENSMUSG00000079523	Tmsb10	9.44190455	42.33298539	8.882421614	4.051517572
ENSMUSG00000044927	H1fx	0.726360393	1.533999404	1.429953302	1.031815761
ENSMUSG00000057841	Rpl32	7.865744871	35.25201312	13.74132755	9.262912673
ENSMUSG00000006333	Rps9	5.507024978	20.92514166	8.639593062	7.732161874
ENSMUSG00000060860	Ube2s	0.017283675	7.014166418	0.040026684	0.037939297
ENSMUSG00000012848	Rps5	7.698929527	29.4830003	11.73398933	11.07414803
ENSMUSG00000003436	Dll3	0.099130241	0.218013719	0.348732488	0.257587859
ENSMUSG00000037166	Ppp1r14a	0.150535236	1.188040561	1.177618412	0.718184239
ENSMUSG00000050708	Ftl1	8.663470116	0.977930212	4.667778519	0.710197018
ENSMUSG00000063229	Ldha	1.660570919	4.298985983	3.178619079	2.591320554
ENSMUSG00000061787	Rps17	4.086195361	23.89636147	8.481154103	5.217385517
ENSMUSG00000030744	Rps3	5.4926405	21.70369818	8.814376251	8.07827476
ENSMUSG00000070426	Rnf121	0.366636931	1.525350432	0.2251501	0.1564164
ENSMUSG00000052187	Hbb-y	0.082850134	3.648971071	0.0248499	0.049920128
ENSMUSG00000094685	Gm5900	0.175178412	0.001342082	0.000667111	0.000266241
ENSMUSG00000036111	Lmo1	0.204393399	0.576946018	0.05353569	0.069755059
ENSMUSG00000046364	Rpl27a	0.65912132	21.61198926	1.07838559	0.746938232
ENSMUSG00000030772	Dkk3	0.551851026	0.948553534	1.08072048	0.883120341
ENSMUSG00000025508	Rplp2	4.185660125	29.07381449	10.16744496	5.525425985
ENSMUSG00000061983	Rps12	2.485950045	18.15165523	6.3742495	5.022763578
ENSMUSG00000019876	Pkib	0.125669045	0.306740233	0.65993996	0.430111821
ENSMUSG00000019874	Fabp7	0.037020517	0.139576499	0.467478319	0.385250266
ENSMUSG00000036816	Atoh7	0.069580731	0.110796302	0	0
ENSMUSG00000063457	Rps15	4.25278769	21.78422308	8.822548366	5.999068158
ENSMUSG00000035242	Oaz1	0.583296164	12.67342678	1.082054703	0.821485623
ENSMUSG00000034994	Eef2	3.050847458	2.657023561	3.49066044	3.128328009
ENSMUSG00000074781	Ube2n	0.20205174	2.430360871	0.188792528	0.132055378
ENSMUSG00000020186	Csrp2	1.194134701	3.646286907	2.837391594	2.837460064
ENSMUSG00000058799	Nap1l1	1.077720785	4.71846108	2.096230821	1.716719915
ENSMUSG00000040280	Ndufa4l2	0.052631579	0.231583656	0.307705137	0.256656017
ENSMUSG00000090841	Myl6	0.586306869	2.725767969	0.415610407	0.306709265
ENSMUSG00000031633	Slc25a4	2.726248885	4.876677602	1.861074049	1.553514377
ENSMUSG00000031688	Pou4f2	0.299843889	0.281837161	0.044029353	0.035676251
ENSMUSG00000063696	Gm8730	0.183764496	13.46152699	0.392928619	0.413471778
ENSMUSG00000014846	Tppp3	0.40867529	0.822099612	0.10640427	0.08612886
ENSMUSG00000003657	Calb2	0.194357716	0.146286907	0.003335557	0.002928647
ENSMUSG00000062380	Tubb3	7.379683318	10.79555622	3.534022682	2.916932907
ENSMUSG00000093904	Tomm20	0.174955397	3.613331345	0.21664443	0.176118211
ENSMUSG00000025290	Rps24	1.717105263	29.86579183	6.956637759	5.173722045
ENSMUSG00000078126	Rpl23a-ps3	0.014272971	1.669698777	0.010340227	0.006656017
ENSMUSG00000023064	Sncg	3.314339875	7.223083806	0.124583055	0.144834931
ENSMUSG00000022048	Dpysl2	1.236061552	2.137339696	0.859573049	0.482561235
ENSMUSG00000022054	Nefm	2.152319358	3.77333731	1.044863242	1.151490948
ENSMUSG00000022055	Nefl	2.658563782	4.651506114	0.57838559	0.549520767
ENSMUSG00000035566	Pcdh17	0.100022302	0.529973158	0.526350901	0.278620873
ENSMUSG00000058126	Tpm3-rs7	0.248550401	0.011482255	0.007171448	0.006522897
ENSMUSG00000015656	Hspa8	2.685214095	7.274828512	2.470813876	1.664536741

id	gene_short_name	WT_avg	Bax_Null_avg	Atoh7_Null_avg	Atoh7_Null_Bax_Null_avg
ENSMUSG00000049932	H2afx	0.769402319	3.095138682	1.550200133	1.329872204
ENSMUSG00000038717	Atp5l	0.05118198	5.98434238	0.152101401	0.087992545
ENSMUSG00000032076	Cadm1	0.806422837	1.344169401	0.605236825	0.449547391
ENSMUSG00000032291	Crabp1	1.489629795	8.28109156	0.722314877	0.737486688
ENSMUSG00000051243	Islr2	0.668710972	0.528183716	0.030353569	0.032614483
ENSMUSG00000007892	Rplp1	3.302297056	27.09439308	7.289859907	5.303647497
ENSMUSG00000040204	2810417H13Rik	0.762711864	2.822994333	1.835557038	1.374201278
ENSMUSG00000032221	Mns1	0.06411686	0.296003579	0.316877919	0.240947817
ENSMUSG00000062270	Morf4l1	0.275646744	6.035937966	0.449633089	0.231363152
ENSMUSG00000032411	Tfdp2	0.327386262	1.307038473	0.957971981	0.755591054
ENSMUSG00000048758	Rpl29	0.01338091	14.21011035	1.82221481	2.288471778
ENSMUSG00000032562	Gnai2	1.165477252	2.019534745	1.842561708	1.611155485
ENSMUSG00000091537	Tma7	0.403768956	5.966895318	0.585723816	0.293530351
ENSMUSG00000032518	Rpsa	3.123773417	17.50477185	5.281354236	5.179179979
ENSMUSG00000071866	Ppia	1.901204282	24.26960931	2.044196131	1.345580405
ENSMUSG00000041126	H2afv	2.457181088	10.43692216	4.625083389	3.871405751
ENSMUSG00000078974	Sec61g	0.144959857	6.901729794	0.492494997	0.147896699
ENSMUSG00000069919	Hba-a1	0.172725245	1.134804653	0.026350901	0.050319489
ENSMUSG00000020415	Pttg1	0.403322926	0.710408589	0.136591061	0.105963791
ENSMUSG00000057098	Ebf1	1.172167707	6.066805846	0.72981988	0.458067093
ENSMUSG00000020372	Gnb2l1	2.000780553	9.283477483	3.482488326	3.807374867
ENSMUSG00000042436	Mfap4	0.108050847	0.459290188	0.494162775	0.420127796
ENSMUSG00000060938	Rpl26	1.332404103	27.32254697	9.255336891	6.467119276
ENSMUSG00000018293	Pfn1	0.911685995	5.16373397	0.944296197	0.54672524
ENSMUSG00000040158	Tax1bp3	0.00691347	1.280047718	0.003168779	0.002129925
ENSMUSG00000058546	Rpl23a	3.290923283	18.36773039	6.498165444	4.208732694
ENSMUSG00000034031	Ccdc182	0.033898305	0.255890248	0.275850567	0.314297125
ENSMUSG00000018666	Cbx1	1.241302409	3.766626901	2.426617745	1.77329606
ENSMUSG00000071415	Rpl23	4.12455397	31.02594691	8.817044696	6.315628328
ENSMUSG00000020914	Top2a	0.608719893	2.438860722	1.387925284	1.10157082
ENSMUSG00000018411	Mapt	1.107158787	1.240679988	0.147431621	0.15628328
ENSMUSG00000047904	Sstr2	0.102809991	0.243364152	0.600733823	0.437034079
ENSMUSG00000020737	Hn1	2.444692239	6.123769758	1.920613742	1.704206603
ENSMUSG00000020738	Sumo2	0.007582516	10.67551446	0.007505003	0.00399361
ENSMUSG00000034120	Srsf2	1.048394291	2.847300925	2.153602402	1.625532481
ENSMUSG00000062825	Actg1	0.086418376	13.52743812	0.040193462	0.036341853
ENSMUSG00000009734	Pou6f2	0.893844781	2.207724426	0.262675117	0.243477103
ENSMUSG00000094777	Hist1h2ap	0.001338091	3.154935878	0.001334223	0.00013312
ENSMUSG00000051627	Hist1h1e	0.145405888	0.482105577	0.464809873	0.354100106
ENSMUSG00000076431	Sox4	3.429638715	3.618848792	5.366744496	4.46099574
ENSMUSG00000058672	Tubb2a	1.227140946	1.162093647	0.221314209	0.216453674
ENSMUSG00000045136	Tubb2b	5.669826048	9.009692812	2.108238826	2.24613951
ENSMUSG00000091383	Hist1h2al	0.136931311	0.007157769	0.021347565	0.008652822
ENSMUSG00000015937	H2afy	1.601806423	3.628094244	2.556537692	2.236954207
ENSMUSG00000021520	Uqcrb	1.494313113	3.438115121	1.064709807	0.637912673
ENSMUSG00000001504	Irx2	0.17250223	0.209364748	0.008672448	0.007454739
ENSMUSG00000062382	Gm10116	0.038470116	35.71875932	0.007338225	0.004659212
ENSMUSG00000069117	Gm10260	1.948037467	0.013420817	0.007671781	0.003194888
ENSMUSG00000021660	Btf3	0.78322926	6.104682374	0.890593729	0.66001065
ENSMUSG00000052727	Map1b	6.035013381	10.82881002	2.771347565	2.598908413
ENSMUSG00000021643	Serf1	1.495762712	6.764688339	1.459973316	0.896166134
ENSMUSG00000041417	Pik3r1	0.138046387	0.216820758	0.356237492	0.319355698
ENSMUSG00000042258	Isl1	1.583296164	2.42215926	0.397931955	0.339589989
ENSMUSG00000093930	Hmgcs1	1.440008921	1.073814494	0.546030687	0.39470181
ENSMUSG00000044573	Acp1	0.08396521	3.099463167	0.170613742	0.132587859
ENSMUSG00000034892	Rps29	1.575825156	59.35773934	5.571547698	1.352502662
ENSMUSG00000021087	Rtn1	3.452163247	5.072025052	2.045363576	1.891506922
ENSMUSG00000021131	Erh	0.474576271	8.290038771	0.555203469	0.418663472

id	gene_short_name	WT_avg	Bax_Null_avg	Atoh7_Null_avg	Atoh7_Null_Bax_Null_avg
ENSMUSG00000021268	Meg3	1.068800178	1.060841038	0.181120747	0.193556976
ENSMUSG00000021270	Hsp90aa1	4.110727029	11.13405905	6.673782522	5.978301384
ENSMUSG00000001270	Ckb	2.400312221	7.577095139	5.547531688	4.3828541
ENSMUSG00000045763	Basp1	3.464317574	5.113629585	2.207638426	1.783546326
ENSMUSG00000045996	Polr2k	0.15176182	2.626155681	0.251667779	0.092119276
ENSMUSG00000022577	Ly6h	0.243644068	0.328660901	0.018012008	0.022896699
ENSMUSG00000003970	Rpl8	5.0308876	22.68252311	8.034689793	7.911474973
ENSMUSG00000033565	Rbfox2	0.852140946	0.742618551	0.390760507	0.321086262
ENSMUSG00000023004	Tuba1b	2.468220339	7.130778407	3.660440294	2.885782748
ENSMUSG00000072235	Tuba1a	25.57337199	46.15523412	12.48915944	10.56669329
ENSMUSG00000062683	Atp5g2	0.018733274	4.886221294	0.032354903	0.03115016
ENSMUSG00000046434	Hnrnpa1	0.210860839	8.91380853	0.265677118	0.206203408
ENSMUSG00000060636	Rpl35a	0.263603925	25.42007158	4.571047365	2.043397231
ENSMUSG00000047261	Gap43	6.400981267	8.416641813	1.453969313	1.216187433
ENSMUSG00000023861	Mpc1	0.004348796	0.97673725	0.00233489	0.002529286
ENSMUSG00000023832	Acat2	0.903880464	0.887861616	0.358905937	0.294462194
ENSMUSG00000044533	Rps2	2.360615522	10.22427677	5.488492328	5.153487753
ENSMUSG00000015120	Ube2i	0.087421945	2.839546675	0.098732488	0.076011715
ENSMUSG00000052146	Rps10	1.756578947	18.12988369	4.370080053	3.424920128
ENSMUSG00000067288	Rps28	0.680419269	25.64017298	2.6754503	0.657614483
ENSMUSG00000008668	Rps18	2.94190455	26.20951387	10.86641094	7.636448349
ENSMUSG00000036185	Sapcd1	0.276092774	0.982403817	0.810707138	0.612486688
ENSMUSG00000001525	Tubb5	14.16347012	19.74694304	11.68695797	9.937167199
ENSMUSG00000092365	BC023719	0.106489741	0	0	0
ENSMUSG00000023944	Hsp90ab1	7.284678858	18.29824038	10.242495	10.57534611
ENSMUSG00000036438	Calm2	6.345115968	14.50581569	5.660273516	3.914936102
ENSMUSG00000024261	Syt4	0.372769848	0.217864599	0.069212809	0.067092652
ENSMUSG00000046668	Cxxc5	0.725579839	1.449150015	1.306871247	1.150692226
ENSMUSG00000024907	Gal	1.368867083	3.491052789	0.073549033	0.069089457
ENSMUSG00000092341	Malat1	80.70060214	249.4685356	100.9726484	58.4986688
ENSMUSG00000071658	Gng3	0.670718109	2.428571429	0.355737158	0.275292865
ENSMUSG00000024725	Ostf1	0.081400535	0.424992544	0.384589726	0.31656017
ENSMUSG00000036192	Rorb	1.282783229	6.865642708	4.445130087	1.882321619
ENSMUSG00000011752	Pgam1	0.003902765	2.932746794	0.003502335	0.003194888
ENSMUSG00000034336	Ina	2.683429973	3.13301521	1.263509006	1.232161874
ENSMUSG00000067038	Rps12-ps3	0	1.160602446	0	0.00013312
ENSMUSG00000064341	mt-Nd1	9.095785013	29.11407695	9.543695797	7.298588924
ENSMUSG00000064345	mt-Nd2	1.793599465	11.73083806	2.053702468	1.537939297
ENSMUSG00000064351	mt-Co1	0.866525424	34.50566657	1.138425617	0.819488818
ENSMUSG00000064354	mt-Co2	0.006244425	31.78422308	0.004336224	0.004126731
ENSMUSG00000064357	mt-Atp6	0.015945584	60.27945124	0.010507005	0.008652822
ENSMUSG00000064358	mt-Co3	0.018733274	49.00999105	0.01551034	0.009052183
ENSMUSG00000064360	mt-Nd3	0.000111508	6.062928721	0.000166778	0
ENSMUSG00000065947	mt-Nd4l	0	1.027288995	0	0
ENSMUSG00000096257	Ccer2	0.178746655	0.16373397	0.044529686	0.03115016
ENSMUSG00000029245	Epha5	0.542038359	1.458693707	1.297198132	0.794728435
ENSMUSG00000003873	Bax	0.576494202	0.151655234	0.399766511	0.086794462
ENSMUSG00000063694	Cycs	0.333073149	2.880852967	0.401767845	0.23056443
ENSMUSG00000031073	Fgf15	0.873215879	2.245302714	1.196964643	0.983626198
ENSMUSG00000028452	Vcp	0.234611954	1.151655234	0.673615744	0.518104366
ENSMUSG00000000740	Rpl13	5.848349688	32.16313749	7.450800534	6.152555911
ENSMUSG00000031231	Cox7b	1.22970562	2.987026543	1.191127418	0.695553781
ENSMUSG00000052565	Hist1h1d	0.020517395	0.024753952	0.165610407	0.137646432
ENSMUSG00000032387	Rbpms2	0.2970562	0.526543394	0.088559039	0.067625133
ENSMUSG00000061393	Acvr2b	0.436775201	0.540113331	0.672781855	0.648029819
ENSMUSG00000039105	Atp6v1g1	1.153991971	4.187891441	0.994329553	0.814297125

Table 2. ChiPSeeker assignment of Atoh7 Cut&Run peaks to genes. Simplified to show only which genes are assigned.

SYMBOL	ENSEMBL
44077	ENSMUSG00000022456
44081	ENSMUSG00000001833
44082	ENSMUSG00000018398
44083	ENSMUSG00000059248
0610038B21Rik	ENSMUSG00000097882
1110015O18Rik	ENSMUSG00000098659
1110028F18Rik	ENSMUSG00000099139
1190005I06Rik	ENSMUSG00000043687
1500009C09Rik	ENSMUSG00000068099
1500009L16Rik	ENSMUSG00000087651
1500015L24Rik	ENSMUSG00000094732
1600012H06Rik	ENSMUSG00000050088
1600014C10Rik	ENSMUSG00000054676
1600027J07Rik	ENSMUSG00000110340
1700003I22Rik	ENSMUSG00000100372
1700007F19Rik	ENSMUSG00000100666
1700008C04Rik	ENSMUSG00000111986
1700008K24Rik	ENSMUSG00000101012
1700008P02Rik	ENSMUSG00000069118
1700010I02Rik	ENSMUSG00000100010
1700012C14Rik	ENSMUSG00000085470
1700012D14Rik	ENSMUSG00000110424
1700012I11Rik	ENSMUSG00000102069
1700020M21Rik	ENSMUSG00000100146
1700021F07Rik	ENSMUSG00000027518
1700021N21Rik	ENSMUSG00000087343
1700023F02Rik	ENSMUSG00000100000
1700025C18Rik	ENSMUSG00000078935
1700025G04Rik	ENSMUSG00000032666
1700027A15Rik	ENSMUSG00000101968
1700028D13Rik	ENSMUSG00000101683
1700028E10Rik	ENSMUSG00000097321
1700034K08Rik	ENSMUSG00000100294
1700052I22Rik	ENSMUSG00000101912
1700057H15Rik	NA
1700061J23Rik	ENSMUSG00000086366
1700064J06Rik	ENSMUSG00000100681
1700065J11Rik	ENSMUSG00000107341
1700066C05Rik	NA
1700072O05Rik	NA
1700084F23Rik	ENSMUSG00000099639
1700092E19Rik	ENSMUSG00000084811
1700096K18Rik	ENSMUSG00000101856
1700101O22Rik	ENSMUSG00000102096
1700110C19Rik	ENSMUSG00000099384
1700123L14Rik	ENSMUSG00000072878
1700128A07Rik	ENSMUSG00000099794
1700129C05Rik	ENSMUSG00000021977
1810007C17Rik	ENSMUSG00000100844
1810013L24Rik	ENSMUSG00000022507
1810026B05Rik	ENSMUSG00000101970
2210417A02Rik	ENSMUSG00000086494
2310043L19Rik	ENSMUSG00000101746
2310069B03Rik	ENSMUSG00000100291
2410004B18Rik	ENSMUSG00000036873
2410004P03Rik	ENSMUSG00000071398
2610203C22Rik	ENSMUSG00000079671
2610307P16Rik	NA
2700046A07Rik	ENSMUSG00000041789
2810013P06Rik	ENSMUSG00000099881
2810049E08Rik	ENSMUSG00000100891
2810433D01Rik	NA
2810471M01Rik	ENSMUSG00000084966
2900026A02Rik	ENSMUSG00000051339
2900079G21Rik	ENSMUSG00000087038
3300005D01Rik	ENSMUSG00000096965
4631405J19Rik	ENSMUSG00000075027
4632428C04Rik	ENSMUSG00000097184
4732490B19Rik	ENSMUSG00000085421
4833411C07Rik	ENSMUSG00000109089
4833428L15Rik	ENSMUSG00000097074
4833439L19Rik	ENSMUSG00000025871
4921511I17Rik	ENSMUSG00000114136
4921525O09Rik	ENSMUSG00000113211
4921529L05Rik	NA
4930405L22Rik	ENSMUSG00000106602
4930413E15Rik	ENSMUSG00000107144
4930417O22Rik	ENSMUSG00000071818
4930429F24Rik	ENSMUSG00000086918
4930431P22Rik	ENSMUSG00000115709
4930433B08Rik	ENSMUSG00000102699
4930440I19Rik	ENSMUSG00000085431
4930447J18Rik	ENSMUSG00000115609
4930448C13Rik	ENSMUSG00000113644
4930459C07Rik	ENSMUSG00000112762
4930459L07Rik	ENSMUSG00000105234
4930463O16Rik	ENSMUSG00000020033

SYMBOL	ENSEMBL
Daam1	ENSMUSG00000034574
Dab1	ENSMUSG00000028519
Dab2ip	ENSMUSG00000026883
Dach1	ENSMUSG00000055639
Dach2	ENSMUSG00000025592
Dad1	ENSMUSG00000022174
Dapk1	ENSMUSG00000021559
Dars	ENSMUSG00000026356
Dbr1	ENSMUSG00000032469
Dcc	ENSMUSG00000060534
Dclk1	ENSMUSG00000027797
Dclk2	ENSMUSG00000028078
Dclk3	ENSMUSG00000032500
Dclre1c	ENSMUSG00000026648
Dcp1b	ENSMUSG00000041477
Dctn1	ENSMUSG00000031865
Dctn2	ENSMUSG00000025410
Dctn6	ENSMUSG00000031516
Dctpp1	ENSMUSG00000042462
Dcun1d4	ENSMUSG00000051674
Ddc	ENSMUSG00000020182
Ddi2	ENSMUSG00000078515
Ddit4	ENSMUSG00000020108
Ddr1	ENSMUSG00000003534
Ddx11	ENSMUSG00000035842
Ddx20	ENSMUSG00000027905
Ddx31	ENSMUSG00000026806
Ddx3x	ENSMUSG00000000787
Def6	ENSMUSG00000002257
Dennd1a	ENSMUSG00000035392
Dennd4a	ENSMUSG00000053641
Denr	ENSMUSG00000023106
Derl1	ENSMUSG00000022365
Det1	ENSMUSG00000030610
Dgki	ENSMUSG00000038665
Dguok	ENSMUSG00000014554
Dhrs3	ENSMUSG00000066026
Dhrsx	ENSMUSG00000063897
Dhx32	ENSMUSG00000030986
Dhx35	ENSMUSG00000027655
Dhx40	ENSMUSG00000018425
Diablo	ENSMUSG00000029433
Diaph1	ENSMUSG00000024456
Diaph2	ENSMUSG00000034480
Diaph3	ENSMUSG00000022021
Dio3	ENSMUSG00000075707
Dipk2a	ENSMUSG00000045414
Diras2	ENSMUSG00000047842
Disp1	ENSMUSG00000030768
Disp3	ENSMUSG00000041544
Dkk3	ENSMUSG00000030772
Dlg2	ENSMUSG00000052572
Dlgap2	ENSMUSG00000047495
Dll1	ENSMUSG00000014773
Dll3	ENSMUSG00000003436
Dlx2	ENSMUSG00000023391
Dlx3	ENSMUSG00000001510
Dmrta1	ENSMUSG00000043753
Dmrta2	ENSMUSG00000047143
Dmxl1	ENSMUSG00000037416
Dnah11	ENSMUSG00000018581
Dnaic1	ENSMUSG00000061322
Dnajc1	ENSMUSG00000026740
Dnajc13	ENSMUSG00000032560
Dnajc24	ENSMUSG00000027166
Dnajc5	ENSMUSG00000000826
Dnlz	ENSMUSG00000075467
Dnmt3a	ENSMUSG00000020661
Dok7	ENSMUSG00000044716
Dolpp1	ENSMUSG00000026856
Dop1b	ENSMUSG00000022946
Dpp10	ENSMUSG00000036815
Dpp6	ENSMUSG00000061576
Dpp9	ENSMUSG00000001229
Dpy19l3	ENSMUSG00000043671
Dpys	ENSMUSG00000022304
Draxin	ENSMUSG00000029005
Drd1	ENSMUSG00000021478
Dreh	ENSMUSG00000117105
Drg1	ENSMUSG00000020457
Dsc3	ENSMUSG00000059898
Dscam	ENSMUSG00000050272
Dst	ENSMUSG00000026131
Dstyk	ENSMUSG00000042046
Dtd1	ENSMUSG00000027430
Dusp10	ENSMUSG00000039384
Dusp14	ENSMUSG00000018648

SYMBOL	ENSEMBL
Lrfn3	ENSMUSG00000036957
Lrp12	ENSMUSG00000022305
Lrp1b	ENSMUSG00000049252
Lrp5	ENSMUSG00000024913
Lrrc10b	ENSMUSG00000090291
Lrrc18	ENSMUSG00000041673
Lrrc27	ENSMUSG00000015980
Lrrc28	ENSMUSG00000030556
Lrrc47	ENSMUSG00000029028
Lrrc4c	ENSMUSG00000050587
Lrrc8d	ENSMUSG00000046079
Lrrc9	ENSMUSG00000021090
Lrrk1	ENSMUSG00000015133
Lrrn1	ENSMUSG00000034648
Lrrtm2	ENSMUSG00000071862
Lrsam1	ENSMUSG00000026792
Lrtm2	ENSMUSG00000055003
Lsamp	ENSMUSG00000061080
Lsm14a	ENSMUSG00000066568
Lsm8	ENSMUSG00000044155
Ltbp2	ENSMUSG00000002020
Luc7l2	ENSMUSG00000029823
Ly86	ENSMUSG00000021423
Lypd6	ENSMUSG00000050447
Lyrm4	ENSMUSG00000046573
Lyrm9	ENSMUSG00000072640
Lyst	ENSMUSG00000019726
Lzts2	ENSMUSG00000035342
Lzts3	ENSMUSG00000037703
Macf1	ENSMUSG00000028649
Macrod2	ENSMUSG00000068205
Madl1l1	ENSMUSG00000029554
Mad2l2	ENSMUSG00000029003
Mafa	ENSMUSG00000047591
Maged1	ENSMUSG00000025151
Magi1	ENSMUSG00000045095
Magi3	ENSMUSG00000052539
Maml3	ENSMUSG00000061143
Man1c1	ENSMUSG00000037306
Map10	ENSMUSG00000050930
Map1b	ENSMUSG00000052727
Map2	ENSMUSG00000015222
Map2k2	ENSMUSG00000035027
Map3k12	ENSMUSG00000023050
Map3k13	ENSMUSG00000033618
Map3k4	ENSMUSG00000014426
Map3k9	ENSMUSG00000042724
Map4k3	ENSMUSG00000024242
Map4k4	ENSMUSG00000026074
Map6	ENSMUSG00000055407
Map7d1	ENSMUSG00000028849
Mapk1	ENSMUSG00000063358
Mapk10	ENSMUSG00000046709
Mapk14	ENSMUSG00000053436
Mapk8ip1	ENSMUSG00000027223
Mapkapk3	ENSMUSG00000032577
Mapre2	ENSMUSG00000024277
Marcks	ENSMUSG00000069662
Mast1	ENSMUSG00000053693
Mat2b	ENSMUSG00000042032
Max	ENSMUSG00000059436
Maz	ENSMUSG00000030678
Mb21d2	ENSMUSG00000051065
Mbd3	ENSMUSG00000035478
Mbd5	ENSMUSG00000036792
Mbd6	ENSMUSG00000025409
Mbnl2	ENSMUSG00000022139
Mbp	ENSMUSG00000041607
Mbtps1	ENSMUSG00000031835
Mcf2l	ENSMUSG00000031442
Mcoln2	ENSMUSG00000011008
Mcph1	ENSMUSG00000039842
Mcts2	ENSMUSG00000042814
Mcur1	ENSMUSG00000021371
Mdc1	ENSMUSG00000061607
Mdga1	ENSMUSG00000043557
Mdga2	ENSMUSG00000034912
Mdh2	ENSMUSG00000019179
Meak7	ENSMUSG00000034105
Med1	ENSMUSG00000018160
Med13	ENSMUSG00000034297
Med27	ENSMUSG00000026799
Med4	ENSMUSG00000022109
Mef2c	ENSMUSG00000005583
Mef2d	ENSMUSG00000001419
Megf11	ENSMUSG00000036466
Megf6	ENSMUSG00000057751

SYMBOL	ENSEMBL
Reep2	ENSMUSG00000038555
Reep6	ENSMUSG00000035504
Relch	ENSMUSG00000026319
Reln	ENSMUSG00000042453
Resp18	ENSMUSG00000033061
Rfc5	ENSMUSG00000029363
Rflnb	ENSMUSG00000020846
Rfx2	ENSMUSG00000024206
Rfx8	ENSMUSG00000057173
Rfxap	ENSMUSG00000036615
Rgl1	ENSMUSG00000026482
Rgs2	ENSMUSG00000026360
Rgs3	ENSMUSG00000059810
Rgs8	ENSMUSG00000042671
Rhcg	ENSMUSG00000030549
Rhoq	ENSMUSG00000024143
Ric3	ENSMUSG00000048330
Rimbp3	ENSMUSG00000071636
Rimklb	ENSMUSG00000040649
Riok3	ENSMUSG00000024404
Ripor2	ENSMUSG00000036006
Rmdn2	ENSMUSG00000036368
Rnaseh2b	ENSMUSG00000021932
Rnd2	ENSMUSG00000001313
Rnf11	ENSMUSG00000028557
Rnf144b	ENSMUSG00000038068
Rnf165	ENSMUSG00000025427
Rnf220	ENSMUSG00000028677
Rnf38	ENSMUSG00000035696
Rnf4	ENSMUSG00000029110
Rnpc3	ENSMUSG00000027981
Rnu11	NA
Rnu12	ENSMUSG00000065176
Robo1	ENSMUSG00000022883
Robo2	ENSMUSG00000052516
Rogdi	ENSMUSG00000022540
Rora	ENSMUSG00000032238
Rorb	ENSMUSG00000036192
Rpap3	ENSMUSG00000022466
Rpl10a	ENSMUSG00000037805
Rpl19	ENSMUSG00000017404
Rpl23a	ENSMUSG00000058546
Rpl27a	ENSMUSG00000046364
Rpl29	ENSMUSG00000048758
Rpl4	ENSMUSG00000032399
Rplp1	ENSMUSG00000007892
Rpp38	ENSMUSG00000049950
Rprl2	NA
Rps10	ENSMUSG00000052146
Rps11	ENSMUSG00000003429
Rps19	ENSMUSG00000040952
Rps24	ENSMUSG00000025290
Rps28	ENSMUSG00000067288
Rps29	ENSMUSG00000034892
Rps3a1	ENSMUSG00000028081
Rps6ka2	ENSMUSG00000023809
Rps6ka5	ENSMUSG00000021180
Rps6kc1	ENSMUSG00000089872
Rraga	ENSMUSG00000070934
Rrbp1	ENSMUSG00000027422
Rrp9	ENSMUSG00000041506
Rsph3a	ENSMUSG00000073471
Rtkn	ENSMUSG00000034930
Rtl6	ENSMUSG00000055745
Rtn4r	ENSMUSG00000043811
Rtn4rl1	ENSMUSG00000045287
Runx1t1	ENSMUSG00000006586
Runx3	ENSMUSG00000070691
Rwdd1	ENSMUSG00000019782
Rxra	ENSMUSG00000015846
Rybp	ENSMUSG00000072872
S1pr3	ENSMUSG00000067586
Safb	ENSMUSG00000071054
Sall3	ENSMUSG00000024565
Samd4b	ENSMUSG00000109336
Sapcd2	ENSMUSG00000026955
Sash1	ENSMUSG00000015305
Satb2	ENSMUSG00000038331
Sbk1	ENSMUSG00000042978
Sbno1	ENSMUSG00000038095
Scamp1	ENSMUSG00000021687
Scamp2	ENSMUSG00000040188
Scaper	ENSMUSG00000034007
Scarb1	ENSMUSG00000037936
Scgb1a1	ENSMUSG00000024653
Schip1	ENSMUSG00000027777
Scmh1	ENSMUSG00000000085

SYMBOL	ENSEMBL
4930474H20Rik	ENSMUSG00000115001
4930474N09Rik	ENSMUSG00000113210
4930486I03Rik	ENSMUSG00000089914
4930503E24Rik	ENSMUSG00000112364
4930503L19Rik	ENSMUSG00000044906
4930503O07Rik	ENSMUSG00000103692
4930504C09Rik	ENSMUSG00000116167
4930505K13Rik	ENSMUSG00000109414
4930511E03Rik	ENSMUSG00000108187
4930512J16Rik	ENSMUSG00000107622
4930519H02Rik	ENSMUSG00000105185
4930527G23Rik	ENSMUSG00000117554
4930534H03Rik	ENSMUSG00000111544
4930539C22Rik	ENSMUSG00000105765
4930539J05Rik	ENSMUSG00000097032
4930539M17Rik	ENSMUSG00000103116
4930548K13Rik	ENSMUSG00000086257
4930550L24Rik	ENSMUSG00000046180
4930556N09Rik	ENSMUSG00000111924
4930559C10Rik	ENSMUSG00000113164
4930563F08Rik	ENSMUSG00000105773
4930572O13Rik	ENSMUSG00000114916
4930578M01Rik	ENSMUSG00000097587
4930578N18Rik	ENSMUSG00000116695
4930583P06Rik	ENSMUSG00000086954
4930590L20Rik	ENSMUSG00000102368
4930591A17Rik	ENSMUSG00000039138
4931406C07Rik	ENSMUSG00000031938
4931429L15Rik	ENSMUSG00000056617
4932412D23Rik	ENSMUSG00000075070
4932435O22Rik	ENSMUSG00000062391
4932438H23Rik	ENSMUSG00000039851
4933402C06Rik	ENSMUSG00000102004
4933402J10Rik	ENSMUSG00000106013
4933406G16Rik	ENSMUSG00000086025
4933409F18Rik	ENSMUSG00000113218
4933411E08Rik	ENSMUSG00000112500
4933416M06Rik	ENSMUSG00000100733
4933417G07Rik	ENSMUSG00000106572
4933427D06Rik	ENSMUSG00000055403
4933427I22Rik	ENSMUSG00000085928
4933428G20Rik	ENSMUSG00000047988
4933430M04Rik	ENSMUSG00000086892
4933432K03Rik	NA
4933433F19Rik	ENSMUSG00000097044
4933433G08Rik	ENSMUSG00000111807
4933440J02Rik	ENSMUSG00000097082
4933440M02Rik	ENSMUSG00000045928
5031425E22Rik	ENSMUSG00000073147
5031425F14Rik	NA
5033428I22Rik	ENSMUSG00000097910
5330411J11Rik	ENSMUSG00000087455
5330416C01Rik	ENSMUSG00000054944
5430416N02Rik	ENSMUSG00000097772
5430434I15Rik	ENSMUSG00000106002
5830454E08Rik	ENSMUSG00000052658
6030407O03Rik	ENSMUSG00000100301
6030471H07Rik	ENSMUSG00000085217
6330415B21Rik	ENSMUSG00000108077
6430562O15Rik	NA
6430710C18Rik	ENSMUSG00000085427
8030451O07Rik	ENSMUSG00000116769
8430422H06Rik	ENSMUSG00000117633
9130015G15Rik	NA
9230020A06Rik	ENSMUSG00000072753
9330104G04Rik	ENSMUSG00000097842
9330117O12Rik	ENSMUSG00000118154
9330159F19Rik	ENSMUSG00000004360
9430078K24Rik	ENSMUSG00000112765
9530026F06Rik	ENSMUSG00000085447
9530068E07Rik	ENSMUSG00000036275
9630013A20Rik	ENSMUSG00000115529
9630013K17Rik	ENSMUSG00000086359
a	ENSMUSG00000027596
A230056J06Rik	ENSMUSG00000021557
A330048O09Rik	ENSMUSG00000097326
A330074K22Rik	ENSMUSG00000097960
A430035B10Rik	ENSMUSG00000087305
A430088P11Rik	ENSMUSG00000116220
A430090L17Rik	ENSMUSG00000114213
A530016L24Rik	ENSMUSG00000043122
A530021J07Rik	ENSMUSG00000053528
A530072M11Rik	ENSMUSG00000085112
A630001G21Rik	ENSMUSG00000052760
A630023P12Rik	ENSMUSG00000048215
A730013G03Rik	ENSMUSG00000047384
A730018C14Rik	ENSMUSG00000047828

SYMBOL	ENSEMBL
Dync1i2	ENSMUSG00000027012
Dyrk1b	ENSMUSG00000002409
Dytn	ENSMUSG00000069085
Dzip3	ENSMUSG00000064061
E130006D01Rik	ENSMUSG00000085271
E130008D07Rik	ENSMUSG00000117011
E130114P18Rik	NA
E230016M11Rik	ENSMUSG00000087231
E2f1	ENSMUSG00000027490
Ebf2	ENSMUSG00000022053
Ebf3	ENSMUSG00000010476
Ebpl	ENSMUSG00000021928
Edaradd	ENSMUSG00000095105
Edil3	ENSMUSG00000034488
Edrf1	ENSMUSG00000039990
Eef1a1	ENSMUSG00000037742
Eef2kmt	ENSMUSG00000022544
Eepd1	ENSMUSG00000036611
Efcab1	ENSMUSG00000068617
Efna5	ENSMUSG00000048915
Efnb2	ENSMUSG00000001300
Egfem1	ENSMUSG00000063600
Egln3	ENSMUSG00000035105
Ehd1	ENSMUSG00000024772
Ehmt1	ENSMUSG00000036893
Ehmt2	ENSMUSG00000013787
Eif2ak3	ENSMUSG00000031668
Eif4a3	ENSMUSG00000025580
Eif4e3	ENSMUSG00000093661
Eif4g2	ENSMUSG00000005610
Eif5	ENSMUSG00000021282
Eipr1	ENSMUSG00000036613
Elac2	ENSMUSG00000020549
Elavl2	ENSMUSG00000008489
Elavl3	ENSMUSG00000003410
Elavl4	ENSMUSG00000028546
Elfn1	ENSMUSG00000048988
Elk3	ENSMUSG00000008398
Ell	ENSMUSG00000070002
Elp4	ENSMUSG00000027167
Emb	ENSMUSG00000021728
Emc10	ENSMUSG00000008140
Emid1	ENSMUSG00000034164
Eml4	ENSMUSG00000032624
Eml6	ENSMUSG00000044072
Enc1	ENSMUSG00000041773
Endov	ENSMUSG00000039850
Engase	ENSMUSG00000033857
Eno4	ENSMUSG00000048029
Enox1	ENSMUSG00000022012
Enpp7	ENSMUSG00000046697
Entpd5	ENSMUSG00000021236
Entpd6	ENSMUSG00000033068
Eny2	ENSMUSG00000022338
Epb41	ENSMUSG00000028906
Epb41l2	ENSMUSG00000019978
Epb41l3	ENSMUSG00000024044
Epb41l4a	ENSMUSG00000024376
Epcam	ENSMUSG00000045394
Epha2	ENSMUSG00000006445
Epha3	ENSMUSG00000052504
Epha5	ENSMUSG00000029245
Epha6	ENSMUSG00000055540
Ephb3	ENSMUSG00000005958
Epm2a	ENSMUSG00000055493
Epn2	ENSMUSG00000001036
Erbb4	ENSMUSG00000062209
Ercc2	ENSMUSG00000030400
Ercc6l2	ENSMUSG00000021470
Ergic1	ENSMUSG00000001576
Ergic2	ENSMUSG00000030304
Erh	ENSMUSG00000021131
Eri3	ENSMUSG00000033423
Erich3	ENSMUSG00000078161
Ermard	ENSMUSG00000036552
Esco1	ENSMUSG00000024293
Esrp2	ENSMUSG00000084128
Esrra	ENSMUSG00000024955
Esrrg	ENSMUSG00000026610
Esyt1	ENSMUSG00000025366
Etfa	ENSMUSG00000032314
Etfdh	ENSMUSG00000027809
Ets1	ENSMUSG00000032035
Etv1	ENSMUSG00000004151
Exo5	ENSMUSG00000028629
Exoc2	ENSMUSG00000021357
Exoc4	ENSMUSG00000029763

SYMBOL	ENSEMBL
Megf8	ENSMUSG00000045039
Meis1	ENSMUSG00000020160
Meis2	ENSMUSG00000027210
Meis3	ENSMUSG00000041420
Metap1d	ENSMUSG00000041921
Mettl14	ENSMUSG00000028114
Mettl16	ENSMUSG00000010554
Mex3c	ENSMUSG00000037253
Mfap3	ENSMUSG00000020522
Mfng	ENSMUSG00000018169
Mfsd5	ENSMUSG00000045665
Mfsd8	ENSMUSG00000025759
Mgarp	ENSMUSG00000037161
Mgat3	ENSMUSG00000042428
Mgat4c	ENSMUSG00000019888
Mgat5b	ENSMUSG00000043857
Mgst2	ENSMUSG00000074604
Miat	ENSMUSG00000097767
Mical2	ENSMUSG00000038244
Micos10	ENSMUSG00000050608
Micu2	ENSMUSG00000021973
Mief2	ENSMUSG00000018599
Miga2	ENSMUSG00000026858
Minar2	ENSMUSG00000050875
Mindy4	ENSMUSG00000038022
Mipol1	ENSMUSG00000047022
Mir1187	ENSMUSG00000080586
Mir124-2hg	ENSMUSG00000100252
Mir124a-1hg	ENSMUSG00000097545
Mir128-2	ENSMUSG00000065441
Mir130a	ENSMUSG00000065484
Mir135a-2	ENSMUSG00000065524
Mir137	ENSMUSG00000065569
Mir148a	ENSMUSG00000065505
Mir1945	ENSMUSG00000088544
Mir1953	ENSMUSG00000088491
Mir195b	ENSMUSG00000098437
Mir216b	ENSMUSG00000076318
Mir22hg	ENSMUSG00000085148
Mir3059	ENSMUSG00000092952
Mir3068	ENSMUSG00000105428
Mir3075	ENSMUSG00000093081
Mir3080	ENSMUSG00000092751
Mir3092	ENSMUSG00000092695
Mir346	ENSMUSG00000065481
Mir3475	ENSMUSG00000093102
Mir365-2	ENSMUSG00000065489
Mir3964	ENSMUSG00000092639
Mir3970	ENSMUSG00000106278
Mir467h	ENSMUSG00000080409
Mir496b	ENSMUSG00000098718
Mir5133	ENSMUSG00000092696
Mir5623	ENSMUSG00000093757
Mir5624	ENSMUSG00000093480
Mir598	ENSMUSG00000076049
Mir6237	ENSMUSG00000098408
Mir6346	ENSMUSG00000098273
Mir6354	ENSMUSG00000098829
Mir6356	ENSMUSG00000099300
Mir6358	ENSMUSG00000098276
Mir6363	ENSMUSG00000098482
Mir6368	ENSMUSG00000099158
Mir6379	ENSMUSG00000098417
Mir6395	ENSMUSG00000098785
Mir6401	ENSMUSG00000098619
Mir6403	ENSMUSG00000099289
Mir6413	ENSMUSG00000098887
Mir6540	ENSMUSG00000098300
Mir680-3	ENSMUSG00000076253
Mir682	ENSMUSG00000076236
Mir6899	ENSMUSG00000098487
Mir691	ENSMUSG00000104758
Mir692-2	ENSMUSG00000094403
Mir6923	ENSMUSG00000098855
Mir6931	ENSMUSG00000098613
Mir6941	ENSMUSG00000098338
Mir6951	ENSMUSG00000099110
Mir6976	ENSMUSG00000106514
Mir6995	ENSMUSG00000098786
Mir7000	ENSMUSG00000099093
Mir7008	ENSMUSG00000098890
Mir7021	ENSMUSG00000106597
Mir7078	ENSMUSG00000098483
Mir721	ENSMUSG00000106479
Mir7218	ENSMUSG00000106215
Mir7243	ENSMUSG00000098521
Mir7687	ENSMUSG00000098280

SYMBOL	ENSEMBL
Scn11a	ENSMUSG00000034115
Scn8a	ENSMUSG00000023033
Scnn1b	ENSMUSG00000030873
Scrn1	ENSMUSG00000019124
Sdc3	ENSMUSG00000025743
Sdccag8	ENSMUSG00000026504
Sdf2l1	ENSMUSG00000022769
Sdk1	ENSMUSG00000039683
Sdk2	ENSMUSG00000041592
Sec13	ENSMUSG00000030298
Sec16b	ENSMUSG00000026589
Sec22a	ENSMUSG00000034473
Sec23ip	ENSMUSG00000055319
Sec61a1	ENSMUSG00000030082
Sec61g	ENSMUSG00000078974
Sec62	ENSMUSG00000027706
Sec63	ENSMUSG00000019802
Sel1l	ENSMUSG00000020964
Sel1l3	ENSMUSG00000029189
Sema6a	ENSMUSG00000019647
Serinc1	ENSMUSG00000019877
Serinc5	ENSMUSG00000021703
Serping1	ENSMUSG00000023224
Serpinh1	ENSMUSG00000070436
Serpini1	ENSMUSG00000027834
Sertad2	ENSMUSG00000049800
Sertad3	ENSMUSG00000055200
Sesn3	ENSMUSG00000032009
Setbp1	ENSMUSG00000024548
Setd7	ENSMUSG00000037111
Setx	ENSMUSG00000043535
Sez6l	ENSMUSG00000058153
Sfmbt2	ENSMUSG00000061186
Sfr1	ENSMUSG00000025066
Sfswap	ENSMUSG00000029439
Sfta3-ps	ENSMUSG00000112343
Sfxn3	ENSMUSG00000025212
Sfxn5	ENSMUSG00000033720
Sgip1	ENSMUSG00000028524
Sgo1	ENSMUSG00000023940
Sgpp2	ENSMUSG00000032908
Sgsm1	ENSMUSG00000042216
Sh3bgrl	ENSMUSG00000031246
Sh3bp4	ENSMUSG00000036206
Sh3gl1	ENSMUSG00000003200
Sh3glb1	ENSMUSG00000037062
Sh3glb2	ENSMUSG00000026860
Sh3pxd2a	ENSMUSG00000053617
Sh3rf1	ENSMUSG00000031642
Sh3rf3	ENSMUSG00000037990
Shb	ENSMUSG00000044813
Shc4	ENSMUSG00000035109
Shf	ENSMUSG00000033256
Shisa2	ENSMUSG00000044461
Shisa6	ENSMUSG00000053930
Shisa9	ENSMUSG00000022494
Shisal1	ENSMUSG00000062760
Shld1	ENSMUSG00000044991
Shmt2	ENSMUSG00000025403
Shox2	ENSMUSG00000027833
Shprh	ENSMUSG00000090112
Shroom3	ENSMUSG00000029381
Siah2	ENSMUSG00000036432
Sik1	ENSMUSG00000024042
Sipa1l1	ENSMUSG00000042700
Sipa1l2	ENSMUSG00000001995
Sipa1l3	ENSMUSG00000030583
Sirt4	ENSMUSG00000029524
Siva1	ENSMUSG00000064326
Six2	ENSMUSG00000024134
Six3	ENSMUSG00000038805
Six5	ENSMUSG00000040841
Ska2	ENSMUSG00000020492
Skap2	ENSMUSG00000059182
Ski	ENSMUSG00000029050
Skil	ENSMUSG00000027660
Skor2	ENSMUSG00000091519
Slc10a2	ENSMUSG00000023073
Slc12a6	ENSMUSG00000027130
Slc12a9	ENSMUSG00000037344
Slc13a1	ENSMUSG00000029700
Slc15a4	ENSMUSG00000029416
Slc16a2	ENSMUSG00000033965
Slc16a7	ENSMUSG00000020102
Slc18a2	ENSMUSG00000025094
Slc19a1	ENSMUSG00000001436
Slc1a2	ENSMUSG00000005089

SYMBOL	ENSEMBL
A830009L08Rik	ENSMUSG00000097182
A830010M20Rik	ENSMUSG00000111375
A830082K12Rik	ENSMUSG00000087143
A930001A20Rik	ENSMUSG00000098008
A930003A15Rik	ENSMUSG00000075330
A930009A15Rik	ENSMUSG00000092210
A930031H19Rik	ENSMUSG00000086262
AA414768	ENSMUSG00000083307
Aacs	ENSMUSG00000029482
Aard	ENSMUSG00000068522
Aatk	ENSMUSG00000025375
Abat	ENSMUSG00000057880
Abca12	ENSMUSG00000050296
Abcb8	ENSMUSG00000028973
Abcc3	ENSMUSG00000020865
Abcc4	ENSMUSG00000032849
Abcd2	ENSMUSG00000055782
Abcd4	ENSMUSG00000021240
Abhd2	ENSMUSG00000039202
Abhd8	ENSMUSG00000007950
Abi1	ENSMUSG00000058835
Ablim1	ENSMUSG00000025085
Abr	ENSMUSG00000017631
Abra	ENSMUSG00000042895
Abracl	ENSMUSG00000078453
Acadsb	ENSMUSG00000030861
Acbd3	ENSMUSG00000026499
Acbd6	ENSMUSG00000033701
Aco2	ENSMUSG00000022477
Acot10	ENSMUSG00000047565
Acot11	ENSMUSG00000034853
Acsl1	ENSMUSG00000018796
Acsl6	ENSMUSG00000020333
Actn1	ENSMUSG00000015143
Actn3	ENSMUSG00000006457
Actr1b	ENSMUSG00000037351
Actr3	ENSMUSG00000026341
Actr5	ENSMUSG00000037761
Actrt3	ENSMUSG00000037737
Acvr1	ENSMUSG00000026836
Acvr1c	ENSMUSG00000026834
Adam11	ENSMUSG00000020926
Adam12	ENSMUSG00000054555
Adam7	ENSMUSG00000022056
Adamts1	ENSMUSG00000022893
Adamts5	ENSMUSG00000022894
Adamtsl2	ENSMUSG00000036040
Adarb2	ENSMUSG00000052551
Adcyap1	ENSMUSG00000024256
Adgrb1	ENSMUSG00000034730
Adgre5	ENSMUSG00000002885
Adgrg1	ENSMUSG00000031785
Adgrl3	ENSMUSG00000037605
Adk	ENSMUSG00000039197
Adnp	ENSMUSG00000051149
Ado	ENSMUSG00000057134
Adora1	ENSMUSG00000042429
Adra1a	ENSMUSG00000045875
Adra1b	ENSMUSG00000050541
Afap1	ENSMUSG00000029094
Aff1	ENSMUSG00000029313
Aff3	ENSMUSG00000037138
Afg1l	ENSMUSG00000038302
Afmid	ENSMUSG00000017718
Aga	ENSMUSG00000031521
Agap1	ENSMUSG00000055013
Agap3	ENSMUSG00000023353
Agbl3	ENSMUSG00000038836
Agl	ENSMUSG00000033400
Agtrap	ENSMUSG00000029007
Ahctf1	ENSMUSG00000026491
Ahdc1	ENSMUSG00000037692
Ahsa2	ENSMUSG00000020288
AI467606	ENSMUSG00000045165
AI837181	ENSMUSG00000047423
Aida	ENSMUSG00000042901
Aip	ENSMUSG00000024847
Ajap1	ENSMUSG00000039546
Akap1	ENSMUSG00000018428
Akap11	ENSMUSG00000022016
Akap13	ENSMUSG00000066406
Akap6	ENSMUSG00000061603
Akna	ENSMUSG00000039158
Akt1	ENSMUSG00000001729
Akt3	ENSMUSG00000019699
Aldh1l1	ENSMUSG00000030088
Aldh4a1	ENSMUSG00000028737

SYMBOL	ENSEMBL
Exoc7	ENSMUSG00000020792
Exosc10	ENSMUSG00000017264
Exosc9	ENSMUSG00000027714
Eya2	ENSMUSG00000017897
Eyelinc18	ENSMUSG00000097346
Ezh1	ENSMUSG00000006920
F13a1	ENSMUSG00000039109
F630206G17Rik	NA
F8	ENSMUSG00000031196
Fabp5	ENSMUSG00000027533
Fadd	ENSMUSG00000031077
Faf1	ENSMUSG00000010517
Fam110a	ENSMUSG00000027459
Fam110b	ENSMUSG00000049119
Fam120b	ENSMUSG00000014763
Fam122a	ENSMUSG00000074922
Fam131a	ENSMUSG00000050821
Fam135a	ENSMUSG00000026153
Fam135b	ENSMUSG00000036800
Fam160a1	ENSMUSG00000051000
Fam163a	ENSMUSG00000015484
Fam171a2	ENSMUSG00000034685
Fam174b	ENSMUSG00000078670
Fam178b	ENSMUSG00000046337
Fam183b	ENSMUSG00000049154
Fam184a	ENSMUSG00000019856
Fam189a1	ENSMUSG00000030518
Fam192a	ENSMUSG00000031774
Fam20c	ENSMUSG00000025854
Fam210b	ENSMUSG00000027495
Fam222a	ENSMUSG00000041930
Fam49b	ENSMUSG00000022378
Fam72a	ENSMUSG00000055184
Fam76a	ENSMUSG00000028878
Fam76b	ENSMUSG00000037808
Fam78a	ENSMUSG00000050592
Fam78b	ENSMUSG00000060568
Fam92b	ENSMUSG00000042269
Fam98a	ENSMUSG00000002017
Fanca	ENSMUSG00000032815
Fancc	ENSMUSG00000021461
Fap	ENSMUSG00000000392
Fars2	ENSMUSG00000021420
Fasn	ENSMUSG00000025153
Fat4	ENSMUSG00000046743
Fbn1	ENSMUSG00000027204
Fbrsl1	ENSMUSG00000043323
Fbxl12	ENSMUSG00000066892
Fbxl16	ENSMUSG00000025738
Fbxl18	ENSMUSG00000066640
Fbxl19	ENSMUSG00000030811
Fbxo16	ENSMUSG00000034532
Fbxo8	ENSMUSG00000038206
Fbxw4	ENSMUSG00000040913
Fbxw7	ENSMUSG00000028086
Fcho1	ENSMUSG00000070000
Fchsd2	ENSMUSG00000030691
Fcnb	ENSMUSG00000026835
Fem1b	ENSMUSG00000032244
Fem1c	ENSMUSG00000033319
Fermt2	ENSMUSG00000037712
Fgd2	ENSMUSG00000024013
Fgd4	ENSMUSG00000022788
Fgd6	ENSMUSG00000020021
Fgf11	ENSMUSG00000042826
Fgf9	ENSMUSG00000021974
Fgfr1	ENSMUSG00000031565
Fgfr1op2	ENSMUSG00000040242
Fgfr4	ENSMUSG00000005320
Fgr	ENSMUSG00000028874
Fhad1	ENSMUSG00000051435
Fhit	ENSMUSG00000060579
Fhl2	ENSMUSG00000008136
Fkbpl	ENSMUSG00000033739
Flrt1	ENSMUSG00000047787
Fmn2	ENSMUSG00000028354
Fmo4	ENSMUSG00000026692
Fndc7	ENSMUSG00000045326
Fnip2	ENSMUSG00000061175
Fntb	ENSMUSG00000033373
Fos	ENSMUSG00000021250
Foxi3	ENSMUSG00000055874
Foxk1	ENSMUSG00000056493
Foxn3	ENSMUSG00000033713
Foxn4	ENSMUSG00000042002
Foxo6	ENSMUSG00000052135
Foxp1	ENSMUSG00000030067

SYMBOL	ENSEMBL
Mir7688	ENSMUSG00000098679
Mir8099-1	ENSMUSG00000098498
Mir8118	ENSMUSG00000098310
Mir96	ENSMUSG00000065586
Mir99ahg	ENSMUSG00000090386
Mirlet7i	ENSMUSG00000065406
Mllt3	ENSMUSG00000028496
Mlycd	ENSMUSG00000074064
Mmd2	ENSMUSG00000039533
Mmp2	ENSMUSG00000031740
Mmp25	ENSMUSG00000023903
Mmrn1	ENSMUSG00000054641
Mms22l	ENSMUSG00000045751
Mnd1-ps	ENSMUSG00000089686
Mnt	ENSMUSG00000000282
Mob1b	ENSMUSG00000006262
Mog	ENSMUSG00000076439
Mon1b	ENSMUSG00000078908
Morc1	ENSMUSG00000022652
Morrbid	NA
Mpc2	ENSMUSG00000026568
Mphosph6	ENSMUSG00000031843
Mpp3	ENSMUSG00000052373
Mre11a	ENSMUSG00000031928
Mreg	ENSMUSG00000039395
Mrgprd	ENSMUSG00000051207
Mrgpre	ENSMUSG00000048965
Mrm3	ENSMUSG00000038046
Mrpl34	ENSMUSG00000034880
Mrpl38	ENSMUSG00000020775
Mrpl41	ENSMUSG00000036850
Mrpl45	ENSMUSG00000018882
Mrps14	ENSMUSG00000058267
Mrps23	ENSMUSG00000023723
Mrps27	ENSMUSG00000041632
Mrps33	ENSMUSG00000029918
Mrtfb	ENSMUSG00000009569
Msh2	ENSMUSG00000024151
Msi1	ENSMUSG00000054256
Msi2	ENSMUSG00000069769
Msln	ENSMUSG00000063011
Msr1	ENSMUSG00000025044
Msra	ENSMUSG00000054733
Msx1	ENSMUSG00000048450
Mtcl1	ENSMUSG00000052105
Mtf1	ENSMUSG00000028890
Mtfr1	ENSMUSG00000027601
Mthfd2	ENSMUSG00000005667
Mthfs	ENSMUSG00000066442
Mtmr4	ENSMUSG00000018401
Mtmr6	ENSMUSG00000021987
Mtss1	ENSMUSG00000022353
Mturn	ENSMUSG00000038065
Mtus2	ENSMUSG00000029651
Mtx2	ENSMUSG00000027099
Mus81	ENSMUSG00000024906
Mvd	ENSMUSG00000006517
Mvk	ENSMUSG00000041939
Mvp	ENSMUSG00000030681
Mxd4	ENSMUSG00000037235
Mxi1	ENSMUSG00000025025
Mxra7	ENSMUSG00000020814
Myadm	ENSMUSG00000068566
Mybl2	ENSMUSG00000017861
Mycbp2	ENSMUSG00000033004
Mycbpap	ENSMUSG00000039110
Mycl	ENSMUSG00000028654
Mycn	ENSMUSG00000037169
Myh14	ENSMUSG00000030739
Myh3	ENSMUSG00000020908
Myh9	ENSMUSG00000022443
Myl3	ENSMUSG00000059741
Myo10	ENSMUSG00000022272
Myo16	ENSMUSG00000039057
Myo18a	ENSMUSG00000000631
Myo18b	ENSMUSG00000072720
Myo1h	ENSMUSG00000066952
Myo3a	ENSMUSG00000025716
Myom1	ENSMUSG00000024049
Mypop	ENSMUSG00000048481
Myt1	ENSMUSG00000010505
NA	NA
Naa11	ENSMUSG00000046000
Naaladl2	ENSMUSG00000102758
Nab1	ENSMUSG00000002881
Naca	ENSMUSG00000061315
Nanp	ENSMUSG00000053916

SYMBOL	ENSEMBL
Slc1a5	ENSMUSG00000001918
Slc22a15	ENSMUSG00000033147
Slc22a2	ENSMUSG00000040966
Slc22a8	ENSMUSG00000063796
Slc23a3	ENSMUSG00000026205
Slc23a4	ENSMUSG00000029847
Slc24a2	ENSMUSG00000037996
Slc24a4	ENSMUSG00000041771
Slc25a11	ENSMUSG00000014606
Slc25a13	ENSMUSG00000015112
Slc25a23	ENSMUSG00000046329
Slc25a26	ENSMUSG00000045100
Slc25a36	ENSMUSG00000032449
Slc25a42	ENSMUSG00000002346
Slc25a51	ENSMUSG00000045973
Slc35a2	ENSMUSG00000031156
Slc35b1	ENSMUSG00000020873
Slc35f1	ENSMUSG00000038602
Slc35g1	ENSMUSG00000044026
Slc37a1	ENSMUSG00000024036
Slc39a10	ENSMUSG00000025986
Slc39a11	ENSMUSG00000041654
Slc39a3	ENSMUSG00000046822
Slc39a7	ENSMUSG00000024327
Slc44a3	ENSMUSG00000039865
Slc4a2	ENSMUSG00000028962
Slc52a3	ENSMUSG00000027463
Slc5a6	ENSMUSG00000006641
Slc6a11	ENSMUSG00000030307
Slc6a6	ENSMUSG00000030096
Slc6a9	ENSMUSG00000028542
Slc7a1	ENSMUSG00000041313
Slc7a11	ENSMUSG00000027737
Slc7a5	ENSMUSG00000040010
Slc8a3	ENSMUSG00000079055
Slc9a1	ENSMUSG00000028854
Slc9a9	ENSMUSG00000031129
Slco3a1	ENSMUSG00000025790
Slco6d1	ENSMUSG00000026336
Slit1	ENSMUSG00000025020
Slitrk5	ENSMUSG00000033214
Smad2	ENSMUSG00000024563
Smad3	ENSMUSG00000032402
Smad5	ENSMUSG00000021540
Smad7	ENSMUSG00000025880
Smarcc1	ENSMUSG00000032481
Smarcd2	ENSMUSG00000078619
Smdt1	ENSMUSG00000022452
Smg5	ENSMUSG00000001415
Smg7	ENSMUSG00000042772
Smg9	ENSMUSG00000002210
Smim12	ENSMUSG00000042380
Smim13	ENSMUSG00000091264
Smim38	ENSMUSG00000109305
Smndc1	ENSMUSG00000025024
Smoc1	ENSMUSG00000021136
Smpd3	ENSMUSG00000031906
Smtn	ENSMUSG00000020439
Snai1	ENSMUSG00000042821
Snai2	ENSMUSG00000022676
Snca	ENSMUSG00000025889
Snd1	ENSMUSG00000001424
Snhg17	NA
Snhg8	ENSMUSG00000104960
Snn	ENSMUSG00000037972
Snora33	ENSMUSG00000070063
Snord104	ENSMUSG00000065126
Snord65	NA
Snord85	ENSMUSG00000065196
Snta1	ENSMUSG00000027488
Sntn	ENSMUSG00000044772
Snx32	ENSMUSG00000056185
Snx8	ENSMUSG00000029560
Socs3	ENSMUSG00000053113
Socs6	ENSMUSG00000056153
Soga1	ENSMUSG00000055485
Sorbs2	ENSMUSG00000031626
Sorcs1	ENSMUSG00000043531
Sorcs2	ENSMUSG00000029093
Sorcs3	ENSMUSG00000063434
Sorl1	ENSMUSG00000049313
Sox11	ENSMUSG00000063632
Sox14	ENSMUSG00000053747
Sox1ot	ENSMUSG00000047935
Sox2ot	ENSMUSG00000105265
Sox5os3	ENSMUSG00000085785
Sox6	ENSMUSG00000051910

SYMBOL	ENSEMBL
Aldoart1	ENSMUSG00000059343
Aldoart2	ENSMUSG00000063129
Alg12	ENSMUSG00000035845
Alg2	ENSMUSG00000039740
Alox5ap	ENSMUSG00000060063
Alyref2	ENSMUSG00000060244
Amer2	ENSMUSG00000021986
Amotl2	ENSMUSG00000032531
Angel1	ENSMUSG00000021257
Angpt1	ENSMUSG00000022309
Angptl6	ENSMUSG00000038742
Ank2	ENSMUSG00000032826
Ank3	ENSMUSG00000069601
Ankdd1a	ENSMUSG00000066510
Ankfn1	ENSMUSG00000047773
Ankfy1	ENSMUSG00000020790
Ankrd13a	ENSMUSG00000041870
Ankrd13c	ENSMUSG00000039988
Ankrd33b	ENSMUSG00000022237
Ankrd44	ENSMUSG00000052331
Ankrd54	ENSMUSG00000033055
Ankrd55	ENSMUSG00000049985
Anks1	ENSMUSG00000024219
Ano10	ENSMUSG00000037949
Antxr2	ENSMUSG00000029338
Anxa2	ENSMUSG00000032231
Aopep	ENSMUSG00000021458
Ap2a1	ENSMUSG00000060279
Ap3m2	ENSMUSG00000031539
Apba2	ENSMUSG00000030519
Aph1b	ENSMUSG00000032375
App	ENSMUSG00000022892
Aqp4	ENSMUSG00000024411
Aqp6	ENSMUSG00000043144
Aqp9	ENSMUSG00000032204
Arf1	ENSMUSG00000048076
Arf3	ENSMUSG00000051853
Arfip1	ENSMUSG00000074513
Arhgap12	ENSMUSG00000041225
Arhgap15	ENSMUSG00000049744
Arhgap17	ENSMUSG00000030766
Arhgap18	ENSMUSG00000039031
Arhgap23	ENSMUSG00000049807
Arhgap24	ENSMUSG00000057315
Arhgap29	ENSMUSG00000039831
Arhgap35	ENSMUSG00000058230
Arhgef10	ENSMUSG00000071176
Arhgef10l	ENSMUSG00000040964
Arhgef19	ENSMUSG00000028919
Arhgef37	ENSMUSG00000045094
Arid1a	ENSMUSG00000007880
Arid3a	ENSMUSG00000019564
Arid3b	ENSMUSG00000004661
Arid5b	ENSMUSG00000019947
Arl14ep	ENSMUSG00000027122
Arl4a	ENSMUSG00000047446
Arl4d	ENSMUSG00000034936
Armh3	ENSMUSG00000039901
Arntl	ENSMUSG00000055116
Arpp21	ENSMUSG00000032503
Arrb2	ENSMUSG00000060216
Arsb	ENSMUSG00000042082
Art3	ENSMUSG00000034842
Asb14	ENSMUSG00000021898
Asb2	ENSMUSG00000021200
Asb4	ENSMUSG00000042607
Asgr1	ENSMUSG00000020884
Ash2l	ENSMUSG00000031575
Asic4	ENSMUSG00000033007
Asph	ENSMUSG00000028207
Atf2	ENSMUSG00000027104
Atf7	ENSMUSG00000099083
Atf7ip	ENSMUSG00000030213
Atg16l2	ENSMUSG00000047767
Atg3	ENSMUSG00000022663
Atg9b	ENSMUSG00000038295
Atoh7	ENSMUSG00000036816
Atoh8	ENSMUSG00000037621
Atp5g1	ENSMUSG00000006057
Atp5mpl	ENSMUSG00000021290
Atp5pb	ENSMUSG00000000563
Atp6ap1l	ENSMUSG00000078958
Atp6v1b1	ENSMUSG00000006269
Atp6v1b2	ENSMUSG00000006273
Atp6v1e2	ENSMUSG00000053375
Atp6v1g3	ENSMUSG00000026394
Atp9a	ENSMUSG00000027546

SYMBOL	ENSEMBL
Foxp4	ENSMUSG00000023991
Fpgs	ENSMUSG00000009566
Fras1	ENSMUSG00000034687
Frat1	ENSMUSG00000067199
Frem1	ENSMUSG00000059049
Frk	ENSMUSG00000019779
Frmd4a	ENSMUSG00000026657
Frmd4b	ENSMUSG00000030064
Frmd5	ENSMUSG00000027238
Frmpd1	ENSMUSG00000035615
Frrs1	ENSMUSG00000033386
Frrs1l	ENSMUSG00000045589
Fry	ENSMUSG00000056602
Fscb	ENSMUSG00000043060
Fsd2	ENSMUSG00000038663
Fsip1	ENSMUSG00000027344
Fstl1	ENSMUSG00000022816
Fstl5	ENSMUSG00000034098
Fth1	ENSMUSG00000024661
Fthl17a	ENSMUSG00000035491
Fto	ENSMUSG00000055932
Fubp1	ENSMUSG00000028034
Fuca1	ENSMUSG00000028673
Fut8	ENSMUSG00000021065
Fyn	ENSMUSG00000019843
Fzd1	ENSMUSG00000044674
Fzr1	ENSMUSG00000020235
G3bp1	ENSMUSG00000018583
Gabbr2	ENSMUSG00000039809
Gadd45a	ENSMUSG00000036390
Gadd45g	ENSMUSG00000021453
Gadl1	ENSMUSG00000056880
Gal	ENSMUSG00000024907
Galc	ENSMUSG00000021003
Galk1	ENSMUSG00000020766
Galk2	ENSMUSG00000027207
Galns	ENSMUSG00000015027
Galnt13	ENSMUSG00000060988
Galnt14	ENSMUSG00000024064
Galnt17	ENSMUSG00000034040
Galnt18	ENSMUSG00000038296
Galnt3	ENSMUSG00000026994
Galnt9	ENSMUSG00000033316
Galntl6	ENSMUSG00000096914
Galr3	ENSMUSG00000114755
Gas7	ENSMUSG00000033066
Gas8	ENSMUSG00000040220
Gask1b	ENSMUSG00000027955
Gata2	ENSMUSG00000015053
Gatb	ENSMUSG00000028085
Gbe1	ENSMUSG00000022707
Gdpd5	ENSMUSG00000035314
Get4	ENSMUSG00000025858
Gfm2	ENSMUSG00000021666
Gfra2	ENSMUSG00000022103
Gga1	ENSMUSG00000033128
Gga3	ENSMUSG00000020740
Ghsr	ENSMUSG00000051136
Gid8	ENSMUSG00000027573
Gins1	ENSMUSG00000027454
Gja10	ENSMUSG00000051056
Glce	ENSMUSG00000032252
Gldc	ENSMUSG00000024827
Gli2	ENSMUSG00000048402
Glis1	ENSMUSG00000034762
Glis3	ENSMUSG00000052942
Glt1d1	ENSMUSG00000049971
Gm10046	ENSMUSG00000109143
Gm10318	ENSMUSG00000071195
Gm10400	ENSMUSG00000107456
Gm10421	ENSMUSG00000099907
Gm10516	ENSMUSG00000097316
Gm10637	ENSMUSG00000099207
Gm10638	NA
Gm10845	ENSMUSG00000095959
Gm11468	ENSMUSG00000084840
Gm11487	ENSMUSG00000066137
Gm11681	ENSMUSG00000075437
Gm12130	NA
Gm12295	ENSMUSG00000085162
Gm12296	ENSMUSG00000084967
Gm12866	ENSMUSG00000066060
Gm13029	NA
Gm13031	ENSMUSG00000087698
Gm13497	ENSMUSG00000086349
Gm13498	ENSMUSG00000083270
Gm13830	NA

SYMBOL	ENSEMBL
Nap1l1	ENSMUSG00000058799
Napa	ENSMUSG00000006024
Nav2	ENSMUSG00000052512
Nav3	ENSMUSG00000020181
Nbas	ENSMUSG00000020576
Nbea	ENSMUSG00000027799
Nbeal1	ENSMUSG00000073664
Nbr1	ENSMUSG00000017119
Ncam1	ENSMUSG00000039542
Ncam2	ENSMUSG00000022762
Ncapg	ENSMUSG00000015880
Ncf2	ENSMUSG00000026480
Nckap5	ENSMUSG00000049690
Nckap5l	ENSMUSG00000023009
Ncl	ENSMUSG00000026234
Ncoa1	ENSMUSG00000020647
Ncoa4	ENSMUSG00000056234
Ncor2	ENSMUSG00000029478
Ncstn	ENSMUSG00000003458
Ndrg3	ENSMUSG00000027634
Ndst3	ENSMUSG00000027977
Ndst4	ENSMUSG00000027971
Ndufa4l2	ENSMUSG00000040280
Ndufaf3	ENSMUSG00000070283
Ndufaf8	ENSMUSG00000078572
Ndufb4	ENSMUSG00000022820
Ndufs5-ps	NA
Ndufs8	ENSMUSG00000059734
Neat1	ENSMUSG00000092274
Nectin1	ENSMUSG00000032012
Nedd1	ENSMUSG00000019988
Nedd4l	ENSMUSG00000024589
Nedd9	ENSMUSG00000021365
Negr1	ENSMUSG00000040037
Neil1	ENSMUSG00000032298
Nek10	ENSMUSG00000042567
Nek11	ENSMUSG00000035032
Nek6	ENSMUSG00000026749
Nek7	ENSMUSG00000026393
Nell1	ENSMUSG00000055409
Neurl1a	ENSMUSG00000006435
Neurod1	ENSMUSG00000034701
Neurod4	ENSMUSG00000048015
Neurod6	ENSMUSG00000037984
Neurog2	ENSMUSG00000027967
Nfasc	ENSMUSG00000026442
Nfe2l1	ENSMUSG00000038615
Nfia	ENSMUSG00000028565
Nfkbia	ENSMUSG00000021025
Nfya	ENSMUSG00000023994
Nfyc	ENSMUSG00000032897
Ngly1	ENSMUSG00000021785
Nhlh1	ENSMUSG00000051251
Nhlh2	ENSMUSG00000048540
Nhlrc3	ENSMUSG00000042997
Nhp2	ENSMUSG00000001056
Nhs	ENSMUSG00000059493
Nhsl1	ENSMUSG00000039835
Nim1k	ENSMUSG00000095930
Nkain1	ENSMUSG00000078532
Nkain4	ENSMUSG00000027574
Nkd1	ENSMUSG00000031661
Nkrf	ENSMUSG00000044149
Nktr	ENSMUSG00000032525
Nkx1-1	ENSMUSG00000029112
Nkx6-1	ENSMUSG00000035187
Nlgn1	ENSMUSG00000063887
Nlk	ENSMUSG00000017376
Nlrp1c-ps	ENSMUSG00000092528
Nmd3	ENSMUSG00000027787
Nme5	ENSMUSG00000035984
Nme7	ENSMUSG00000026575
Nmnat2	ENSMUSG00000042751
Nmt2	ENSMUSG00000026643
Nnmt	ENSMUSG00000032271
Nnt	ENSMUSG00000116207
Nol11	ENSMUSG00000018433
Nol4	ENSMUSG00000041923
Nol4l	ENSMUSG00000061411
Nop58	ENSMUSG00000026020
Nos1	ENSMUSG00000029361
Nostrin	ENSMUSG00000034738
Notch1	ENSMUSG00000026923
Notch2	ENSMUSG00000027878
Notum	ENSMUSG00000042988
Nova1	ENSMUSG00000021047
Npffr2	ENSMUSG00000035528

SYMBOL	ENSEMBL
Sp2	ENSMUSG00000018678
Sp8	ENSMUSG00000048562
Spag9	ENSMUSG00000020859
Spdl1	ENSMUSG00000069910
Specc1l	ENSMUSG00000033444
Speer2	ENSMUSG00000063163
Spen	ENSMUSG00000040761
Spertl	ENSMUSG00000034689
Spg11	ENSMUSG00000033396
Spg20	ENSMUSG00000036580
Sphkap	ENSMUSG00000026163
Spns2	ENSMUSG00000040447
Spock1	ENSMUSG00000056222
Spock2	ENSMUSG00000058297
Spop	ENSMUSG00000057522
Spred1	ENSMUSG00000027351
Spred2	ENSMUSG00000045671
Spry1	ENSMUSG00000037211
Spsb1	ENSMUSG00000039911
Spsb3	ENSMUSG00000024160
Spsb4	ENSMUSG00000046997
Sptb	ENSMUSG00000021061
Sptlc2	ENSMUSG00000021036
Sqor	ENSMUSG00000005803
Srcap	ENSMUSG00000053877
Srebf1	ENSMUSG00000020538
Srf	ENSMUSG00000015605
Srgap2	ENSMUSG00000026425
Srgap3	ENSMUSG00000030257
Srl	ENSMUSG00000022519
Srp19	ENSMUSG00000014504
Srpk2	ENSMUSG00000062604
Srprb	ENSMUSG00000032553
Srrm3	ENSMUSG00000039860
Srrm4	ENSMUSG00000063919
Srrt	ENSMUSG00000037364
Srsf10	ENSMUSG00000028676
Srsf4	ENSMUSG00000028911
Srsf9	ENSMUSG00000029538
Ssbp2	ENSMUSG00000003992
Ssbp3	ENSMUSG00000061887
Ssc5d	ENSMUSG00000035279
Sstr2	ENSMUSG00000047904
St18	ENSMUSG00000033740
St6gal1	ENSMUSG00000022885
St6galnac5	ENSMUSG00000039037
St7	ENSMUSG00000029534
St8sia2	ENSMUSG00000025789
St8sia3os	ENSMUSG00000086128
Stac	ENSMUSG00000032502
Stam	ENSMUSG00000026718
Stard13	ENSMUSG00000016128
Stard4	ENSMUSG00000024378
Stat1	ENSMUSG00000026104
Stau2	ENSMUSG00000025920
Stip1	ENSMUSG00000024966
Stk10	ENSMUSG00000020272
Stk32a	ENSMUSG00000039954
Stk33	ENSMUSG00000031027
Stk36	ENSMUSG00000033276
Stk38l	ENSMUSG00000001630
Stk39	ENSMUSG00000027030
Stmn4	ENSMUSG00000022044
Stn1	ENSMUSG00000042694
Ston2	ENSMUSG00000020961
Stpg1	ENSMUSG00000028801
Strip1	ENSMUSG00000014601
Stx16	ENSMUSG00000027522
Stxbp1	ENSMUSG00000026797
Stxbp4	ENSMUSG00000020546
Suds3	ENSMUSG00000066900
Sufu	ENSMUSG00000025231
Sugp1	ENSMUSG00000011306
Suif2	ENSMUSG00000006800
Supt5	ENSMUSG00000003435
Surf4	ENSMUSG00000014867
Susd6	ENSMUSG00000021133
Sv2b	ENSMUSG00000053025
Svil	ENSMUSG00000024236
Sybu	ENSMUSG00000022340
Syf2	ENSMUSG00000028821
Syne3	ENSMUSG00000054150
Synpo	ENSMUSG00000043079
Synrg	ENSMUSG00000034940
Sypl	ENSMUSG00000020570
Syt13	ENSMUSG00000027220
Syt2	ENSMUSG00000026452

SYMBOL	ENSEMBL
Atp9b	ENSMUSG00000024566
Atpsckmt	ENSMUSG00000039065
Atxn2	ENSMUSG00000042605
Atxn2l	ENSMUSG00000032637
Atxn7l2	ENSMUSG00000048997
AU021063	ENSMUSG00000115944
AU023762	ENSMUSG00000109890
AU041133	ENSMUSG00000078435
Auts2	ENSMUSG00000029673
Avpr1a	ENSMUSG00000020123
AW549542	ENSMUSG00000087516
AY512915	ENSMUSG00000068180
AY702102	ENSMUSG00000103935
AY702103	ENSMUSG00000067103
B130024G19Rik	ENSMUSG00000100005
B230118H07Rik	ENSMUSG00000027165
B230219D22Rik	ENSMUSG00000045767
B230354K17Rik	ENSMUSG00000097119
B3galt2	ENSMUSG00000033849
B3galt4	ENSMUSG00000067370
B3gat1	ENSMUSG00000045994
B4galt1	ENSMUSG00000028413
B4galt5	ENSMUSG00000017929
B930059L03Rik	NA
B930092H01Rik	ENSMUSG00000111658
B9d2	ENSMUSG00000063439
Bach2	ENSMUSG00000040270
Banp	ENSMUSG00000025316
Bard1	ENSMUSG00000026196
Barhl1	ENSMUSG00000026805
Barhl2	ENSMUSG00000034384
Barx2	ENSMUSG00000032033
Baz1b	ENSMUSG00000002748
Baz2b	ENSMUSG00000026987
Bbc3	ENSMUSG00000002083
Bbs2	ENSMUSG00000031755
Bbx	ENSMUSG00000022641
BC004004	ENSMUSG00000052712
BC034090	ENSMUSG00000033722
BC037704	ENSMUSG00000117698
Bcar1	ENSMUSG00000031955
Bcas3	ENSMUSG00000059439
Bcat2	ENSMUSG00000030826
Bche	ENSMUSG00000027792
Bcl2	ENSMUSG00000057329
Bcl2l1	ENSMUSG00000007659
Bcl2l11	ENSMUSG00000027381
Bcl2l13	ENSMUSG00000009112
Bcl7a	ENSMUSG00000029438
Bcl9	ENSMUSG00000038256
Bclaf1	ENSMUSG00000037608
Bcor	ENSMUSG00000040363
Bcr	ENSMUSG00000009681
Bdkrb2	ENSMUSG00000021070
Begain	ENSMUSG00000040867
Bend5	ENSMUSG00000028545
Bfsp1	ENSMUSG00000027420
Bhlhe22	ENSMUSG00000025128
Bicd1	ENSMUSG00000003452
Bicd2	ENSMUSG00000037933
Bicdl1	ENSMUSG00000041609
Birc5	ENSMUSG00000017716
Blcap	ENSMUSG00000067787
Bloc1s4	ENSMUSG00000060708
Bmp1	ENSMUSG00000022098
Borcs6	ENSMUSG00000045176
Brinp2	ENSMUSG00000004031
Brinp3	ENSMUSG00000035131
Brip1	ENSMUSG00000034329
Brms1l	ENSMUSG00000012076
Brpf1	ENSMUSG00000001632
Brsk2	ENSMUSG00000053046
Btbd10	ENSMUSG00000038187
Btbd11	ENSMUSG00000020042
Btbd17	ENSMUSG00000000202
Btbd3	ENSMUSG00000062098
Btbd9	ENSMUSG00000062202
Btg1	ENSMUSG00000036478
Btg2	ENSMUSG00000020423
Bves	ENSMUSG00000071317
C030013C21Rik	ENSMUSG00000085078
C030029H02Rik	ENSMUSG00000110027
C130026L21Rik	ENSMUSG00000052848
C1galt1	ENSMUSG00000042460
C1galt1c1	ENSMUSG00000048970
C230024C17Rik	ENSMUSG00000100334
C330004P14Rik	ENSMUSG00000112227

SYMBOL	ENSEMBL
Gm13944	ENSMUSG00000085845
Gm14015	ENSMUSG00000087226
Gm14204	ENSMUSG00000086496
Gm14207	ENSMUSG00000074912
Gm14486	NA
Gm15501	ENSMUSG00000047675
Gm15509	ENSMUSG00000089947
Gm15559	ENSMUSG00000086401
Gm15638	ENSMUSG00000085826
Gm15663	ENSMUSG00000085282
Gm15679	ENSMUSG00000089819
Gm15723	ENSMUSG00000084865
Gm15772	ENSMUSG00000062353
Gm15881	NA
Gm15915	ENSMUSG00000085723
Gm15997	ENSMUSG00000107132
Gm16551	ENSMUSG00000066477
Gm16596	NA
Gm16701	ENSMUSG00000102548
Gm1720	ENSMUSG00000086860
Gm17597	ENSMUSG00000097613
Gm17746	NA
Gm17767	ENSMUSG00000099413
Gm19668	ENSMUSG00000096380
Gm19689	ENSMUSG00000117399
Gm2011	ENSMUSG00000107741
Gm20187	ENSMUSG00000094002
Gm20268	ENSMUSG00000100684
Gm20740	ENSMUSG00000115520
Gm20755	ENSMUSG00000106461
Gm20757	ENSMUSG00000098040
Gm2093	ENSMUSG00000097662
Gm2109	ENSMUSG00000100155
Gm21992	ENSMUSG00000096370
Gm2516	ENSMUSG00000110281
Gm266	ENSMUSG00000010529
Gm28590	ENSMUSG00000099960
Gm29461	ENSMUSG00000100711
Gm29678	ENSMUSG00000103644
Gm29687	ENSMUSG00000113550
Gm2a	ENSMUSG00000000594
Gm30539	ENSMUSG00000112035
Gm30731	ENSMUSG00000107859
Gm31333	ENSMUSG00000113986
Gm32693	ENSMUSG00000106505
Gm32921	ENSMUSG00000105508
Gm33035	ENSMUSG00000112331
Gm33337	ENSMUSG00000112029
Gm34284	ENSMUSG00000116371
Gm35725	ENSMUSG00000113666
Gm36480	ENSMUSG00000116204
Gm36669	ENSMUSG00000107022
Gm36742	ENSMUSG00000116965
Gm3716	ENSMUSG00000105402
Gm38409	ENSMUSG00000114744
Gm3942	NA
Gm4265	ENSMUSG00000108504
Gm4532	ENSMUSG00000000486
Gm4791	ENSMUSG00000094893
Gm48908	NA
Gm5069	NA
Gm5089	ENSMUSG00000064052
Gm5091	ENSMUSG00000097624
Gm5424	ENSMUSG00000046687
Gm5570	ENSMUSG00000073045
Gm572	ENSMUSG00000070577
Gm597	ENSMUSG00000048411
Gm6249	ENSMUSG00000110101
Gm6402	NA
Gm6578	ENSMUSG00000057223
Gm6602	ENSMUSG00000104543
Gm6878	ENSMUSG00000075549
Gm8013	ENSMUSG00000106357
Gm805	ENSMUSG00000097543
Gm815	ENSMUSG00000074913
Gm833	NA
Gm960	ENSMUSG00000071691
Gm973	ENSMUSG00000047361
Gm9736	ENSMUSG00000112380
Gm9866	ENSMUSG00000094002
Gmpr	ENSMUSG00000000253
Gna14	ENSMUSG00000024697
Gnai2	ENSMUSG00000032562
Gnaq	ENSMUSG00000024639
Gnat1	ENSMUSG00000034837
Gnaz	ENSMUSG00000040009
Gng2	ENSMUSG00000043004

SYMBOL	ENSEMBL
Nphp4	ENSMUSG00000039577
Npm1	ENSMUSG00000057113
Nprl3	ENSMUSG00000020289
Nptn	ENSMUSG00000032336
Npy	ENSMUSG00000029819
Npy1r	ENSMUSG00000036437
Nr1h4	ENSMUSG00000047638
Nr2f1	ENSMUSG00000069171
Nr2f6	ENSMUSG00000002393
Nr5a2	ENSMUSG00000026398
Nrep	ENSMUSG00000042834
Nrg1	ENSMUSG00000062991
Nrip1	ENSMUSG00000048490
Nrl	ENSMUSG00000040632
Nrxn1	ENSMUSG00000024109
Nrxn2	ENSMUSG00000033768
Nrxn3	ENSMUSG00000066392
Nsd1	ENSMUSG00000021488
Nsd3	ENSMUSG00000054823
Nsf	ENSMUSG00000034187
Nsun3	ENSMUSG00000050312
Nt5c2	ENSMUSG00000025041
Nt5dc1	ENSMUSG00000039480
Ntan1	ENSMUSG00000022681
Ntm	ENSMUSG00000059974
Ntng1	ENSMUSG00000059857
Ntrk3	ENSMUSG00000059146
Nuak1	ENSMUSG00000020032
Nuak2	ENSMUSG00000009772
Nudt7	ENSMUSG00000031767
Nudt8	ENSMUSG00000110949
Nudt9	ENSMUSG00000029310
Nufip2	ENSMUSG00000037857
Numbl	ENSMUSG00000063160
Nup35	ENSMUSG00000026999
Nup62	ENSMUSG00000109511
Nupl1	ENSMUSG00000114797
Nutf2	ENSMUSG00000008450
Nwd2	ENSMUSG00000090061
Nxpe4	ENSMUSG00000044229
Nxph1	ENSMUSG00000046178
Nxph3	ENSMUSG00000046719
Oaz1	ENSMUSG00000035242
Ocstamp	ENSMUSG00000027670
Ofcc1	ENSMUSG00000047094
Ofd1	ENSMUSG00000040586
Ogdh	ENSMUSG00000020456
Ogfod2	ENSMUSG00000023707
Olfm1	ENSMUSG00000026833
Olfm2	ENSMUSG00000032172
Olfm4	ENSMUSG00000022026
Olfml2b	ENSMUSG00000038463
Olfr1505	ENSMUSG00000062314
Olfr223	ENSMUSG00000048919
Olfr827	ENSMUSG00000045559
Olig2	ENSMUSG00000039830
Olig3	ENSMUSG00000045591
Onecut1	ENSMUSG00000043013
Onecut2	ENSMUSG00000045991
Opa1	ENSMUSG00000038084
Opn3	ENSMUSG00000026525
Opn4	ENSMUSG00000021799
Optc	ENSMUSG00000010311
Orc6	ENSMUSG00000031697
Ormdl3	ENSMUSG00000038150
Osbpl2	ENSMUSG00000039050
Osbpl3	ENSMUSG00000029822
Osbpl9	ENSMUSG00000028559
Ostm1	ENSMUSG00000038280
Otub1	ENSMUSG00000024767
Otx2	ENSMUSG00000021848
Oxsm	ENSMUSG00000021786
Oxsr1	ENSMUSG00000036737
P2ry2	ENSMUSG00000032860
P3h4	ENSMUSG00000006931
P4ha2	ENSMUSG00000018906
P4htm	ENSMUSG00000006675
Pa2g4	ENSMUSG00000025364
Pacrg	ENSMUSG00000037196
Pacs1	ENSMUSG00000024855
Pacs2	ENSMUSG00000021143
Pag1	ENSMUSG00000027508
Pak3	ENSMUSG00000031284
Pak4	ENSMUSG00000030602
Palld	ENSMUSG00000058056
Pam	ENSMUSG00000026335
Papolb	ENSMUSG00000074817

SYMBOL	ENSEMBL
Syvn1	ENSMUSG00000024807
T2	ENSMUSG00000058159
Tab2	ENSMUSG00000015755
Tac1	ENSMUSG00000061762
Tac4	ENSMUSG00000020872
Tacc2	ENSMUSG00000030852
Tacc3	ENSMUSG00000037313
Tacr3	ENSMUSG00000028172
Tafa4	ENSMUSG00000046500
Tafa5	ENSMUSG00000054863
Tagln3	ENSMUSG00000022658
Tanc2	ENSMUSG00000053580
Tango2	ENSMUSG00000013539
Tango6	ENSMUSG00000041949
Tank	ENSMUSG00000064289
Taok1	ENSMUSG00000017291
Tardbp	ENSMUSG00000041459
Tas2r119	ENSMUSG00000045267
Tasor2	ENSMUSG00000033799
Tbc1d14	ENSMUSG00000029192
Tbc1d17	ENSMUSG00000038520
Tbc1d22a	ENSMUSG00000051864
Tbc1d5	ENSMUSG00000023923
Tbc1d9b	ENSMUSG00000036644
Tbcc	ENSMUSG00000036430
Tbcel	ENSMUSG00000037287
Tbl1xr1	ENSMUSG00000027630
Tbl2	ENSMUSG00000005374
Tbx4	ENSMUSG00000000094
Tceanc2	ENSMUSG00000028619
Tcerg1	ENSMUSG00000024498
Tcerg1l	ENSMUSG00000091002
Tcf12	ENSMUSG00000032228
Tcf20	ENSMUSG00000041852
Tcf25	ENSMUSG00000001472
Tcf3	ENSMUSG00000020167
Tcf4	ENSMUSG00000053477
Tcf7l2	ENSMUSG00000024985
Tcim	ENSMUSG00000056313
Tcp11	ENSMUSG00000062859
Tdrkh	ENSMUSG00000041912
Tead1	ENSMUSG00000055320
Tead2	ENSMUSG00000030796
Tecrl	ENSMUSG00000049537
Tedc2	ENSMUSG00000024118
Tef	ENSMUSG00000022389
Tekt1	ENSMUSG00000020799
Tenm2	ENSMUSG00000049336
Tenm3	ENSMUSG00000031561
Tenm4	ENSMUSG00000048078
Tent5b	ENSMUSG00000046694
Terc	ENSMUSG00000118406
Tesc	ENSMUSG00000029359
Tex14	ENSMUSG00000010342
Tex26	ENSMUSG00000029660
Tex35	ENSMUSG00000026592
Tex44	ENSMUSG00000036574
Tfap2c	ENSMUSG00000028640
Tfap2d	ENSMUSG00000042596
Tfap4	ENSMUSG00000005718
Tfb1m	ENSMUSG00000036983
Tfdp2	ENSMUSG00000032411
Tff3	ENSMUSG00000024029
Tgfbi	ENSMUSG00000035493
Tgfbr2	ENSMUSG00000032440
Tgfbrap1	ENSMUSG00000070939
Tgm2	ENSMUSG00000037820
Thada	ENSMUSG00000024251
Thap1	ENSMUSG00000037214
Thap7	ENSMUSG00000022760
Thbs2	ENSMUSG00000023885
Them7	ENSMUSG00000055312
Thrb	ENSMUSG00000021779
Thsd7a	ENSMUSG00000032625
Thsd7b	ENSMUSG00000042581
Thy1	ENSMUSG00000032011
Tiam1	ENSMUSG00000002489
Tifab	ENSMUSG00000049625
Tipin	ENSMUSG00000032397
Tjap1	ENSMUSG00000012296
Tle1	ENSMUSG00000008305
Tle3	ENSMUSG00000032280
Tle4	ENSMUSG00000024642
Tlk2	ENSMUSG00000020694
Tm2d2	ENSMUSG00000031556
Tm9sf3	ENSMUSG00000025016
Tmbim1	ENSMUSG00000006301

SYMBOL	ENSEMBL
C530008M17Rik	ENSMUSG00000036377
C530044C16Rik	ENSMUSG00000107667
C730036E19Rik	NA
C9orf72	ENSMUSG00000028300
Cabp1	ENSMUSG00000029544
Cachd1	ENSMUSG00000028532
Cacna1a	ENSMUSG00000034656
Cacna1b	ENSMUSG00000004113
Cacna1c	ENSMUSG00000051331
Cacna1d	ENSMUSG00000015968
Cacna1g	ENSMUSG00000020866
Cacna1i	ENSMUSG00000022416
Cacna1s	ENSMUSG00000026407
Cacna2d1	ENSMUSG00000040118
Cacna2d2	ENSMUSG00000010066
Cacna2d3	ENSMUSG00000021991
Cacng4	ENSMUSG00000020723
Cacng7	ENSMUSG00000069806
Cadm1	ENSMUSG00000032076
Cadps	ENSMUSG00000054423
Calr	ENSMUSG00000003814
Camk1g	ENSMUSG00000016179
Camk2d	ENSMUSG00000053819
Camk2n1	ENSMUSG00000046447
Camkk1	ENSMUSG00000020785
Camsap1	ENSMUSG00000026933
Camta1	ENSMUSG00000014592
Cand1	ENSMUSG00000020114
Capn9	ENSMUSG00000031981
Capzb	ENSMUSG00000028745
Card11	ENSMUSG00000036526
Carhsp1	ENSMUSG00000008393
Carm1	ENSMUSG00000032185
Carns1	ENSMUSG00000075289
Casc1	ENSMUSG00000043541
Casc4	ENSMUSG00000060227
Cass4	ENSMUSG00000074570
Castor2	ENSMUSG00000015944
Casz1	ENSMUSG00000028977
Cbfa2t2	ENSMUSG00000038533
Cbfa2t3	ENSMUSG00000006362
Cbwd1	ENSMUSG00000024878
Cbx4	ENSMUSG00000039989
Cbx5	ENSMUSG00000009575
Cbx8	ENSMUSG00000025578
Ccdc126	ENSMUSG00000050786
Ccdc134	ENSMUSG00000068114
Ccdc141	ENSMUSG00000044033
Ccdc171	ENSMUSG00000052407
Ccdc182	ENSMUSG00000034031
Ccdc187	ENSMUSG00000048038
Ccdc189	ENSMUSG00000057176
Ccdc190	ENSMUSG00000070532
Ccdc32	ENSMUSG00000039983
Ccdc33	ENSMUSG00000037716
Ccdc40	ENSMUSG00000039963
Ccdc60	ENSMUSG00000043913
Ccdc62	ENSMUSG00000061882
Ccdc71l	ENSMUSG00000090946
Ccdc85c	ENSMUSG00000084883
Ccdc96	ENSMUSG00000050677
Ccdc9b	ENSMUSG00000045838
Ccl1	ENSMUSG00000020702
Ccl26	ENSMUSG00000070464
Ccm2l	ENSMUSG00000027474
Ccnd3	ENSMUSG00000034165
Ccnl1	ENSMUSG00000027829
Ccnq	ENSMUSG00000049489
Ccser1	ENSMUSG00000039578
Cct5	ENSMUSG00000022234
Cct7	ENSMUSG00000030007
Ccz1	ENSMUSG00000029617
Cd180	ENSMUSG00000021624
Cd2ap	ENSMUSG00000061665
Cd2bp2	ENSMUSG00000042502
Cd55b	ENSMUSG00000026401
Cd83	ENSMUSG00000015396
Cd9	ENSMUSG00000030342
Cda	ENSMUSG00000028755
Cdc20	ENSMUSG00000006398
Cdc25b	ENSMUSG00000027330
Cdc34	ENSMUSG00000020307
Cdc37	ENSMUSG00000019471
Cdc42bpa	ENSMUSG00000026490
Cdca3	ENSMUSG00000023505
Cdca7	ENSMUSG00000055612
Cdca7l	ENSMUSG00000021175

SYMBOL	ENSEMBL
Golph3l	ENSMUSG00000046519
Gpam	ENSMUSG00000024978
Gpat4	ENSMUSG00000031545
Gpatch3	ENSMUSG00000028850
Gpbp1	ENSMUSG00000032745
Gpd1l	ENSMUSG00000050627
Gpd2	ENSMUSG00000026827
Gpm6a	ENSMUSG00000031517
Gpm6b	ENSMUSG00000031342
Gpr108	ENSMUSG00000005823
Gpr162	ENSMUSG00000038390
Gpr19	ENSMUSG00000032641
Gpr20	ENSMUSG00000045281
Gpr61	ENSMUSG00000046793
Gpr89	ENSMUSG00000028096
Gprc5c	ENSMUSG00000051043
Gpt2	ENSMUSG00000031700
Gramd1b	ENSMUSG00000040111
Gramd3	ENSMUSG00000001700
Grb10	ENSMUSG00000020176
Grb2	ENSMUSG00000059923
Grifin	ENSMUSG00000036586
Grik2	ENSMUSG00000056073
Grik4	ENSMUSG00000032017
Grin2c	ENSMUSG00000020734
Grk3	ENSMUSG00000042249
Grk4	ENSMUSG00000052783
Grm3	ENSMUSG00000003974
Grm4	ENSMUSG00000063239
Grpel1	ENSMUSG00000029198
Grxcr1	ENSMUSG00000068082
Gse1	ENSMUSG00000031822
Gsg1l	ENSMUSG00000046182
Gtdc1	ENSMUSG00000036890
Gtf2a1	ENSMUSG00000020962
Gtf2f2	ENSMUSG00000067995
Gtf2i	ENSMUSG00000060261
Guca2a	ENSMUSG00000023247
Gxylt1	ENSMUSG00000036197
H13	ENSMUSG00000019188
H2al1j	ENSMUSG00000069038
H2al2a	ENSMUSG00000062651
H3c14	ENSMUSG00000093769
H6pd	ENSMUSG00000028980
Hacl1	ENSMUSG00000021884
Hand2os1	NA
Has2	ENSMUSG00000022367
Hcfc2	ENSMUSG00000020246
Hcn4	ENSMUSG00000032338
Hdac11	ENSMUSG00000034245
Hdac4	ENSMUSG00000026313
Hdhd5	ENSMUSG00000058979
Hectd4	ENSMUSG00000042744
Hecw2	ENSMUSG00000042807
Heg1	ENSMUSG00000075254
Hells	ENSMUSG00000025001
Helq	ENSMUSG00000035266
Herc1	ENSMUSG00000038664
Herpud2	ENSMUSG00000008429
Hes5	ENSMUSG00000048001
Hes6	ENSMUSG00000067071
Hexdc	ENSMUSG00000039307
Hexim1	ENSMUSG00000048878
Hey1	ENSMUSG00000040289
Heyl	ENSMUSG00000032744
Hgd	ENSMUSG00000022821
Hibadh	ENSMUSG00000029776
Hif1a	ENSMUSG00000021109
Hint2	ENSMUSG00000028470
Hip1	ENSMUSG00000039959
Hipk2	ENSMUSG00000061436
Hivep1	ENSMUSG00000021366
Hivep3	ENSMUSG00000028634
Hlcs	ENSMUSG00000040820
Hmcn2	ENSMUSG00000055632
Hmgb1	ENSMUSG00000066551
Hmgcr	ENSMUSG00000021670
Hmgn3	ENSMUSG00000066456
Hmx1	ENSMUSG00000067438
Hnrnph3	ENSMUSG00000020069
Hnrnpk	ENSMUSG00000021546
Hnrnpl	ENSMUSG00000015165
Homer3	ENSMUSG00000003573
Hook1	ENSMUSG00000028572
Hpca	ENSMUSG00000028785
Hps1	ENSMUSG00000025188
Hpse	ENSMUSG00000035273

SYMBOL	ENSEMBL
Paqr3	ENSMUSG00000055725
Pard3	ENSMUSG00000025812
Pard3b	ENSMUSG00000052062
Parp8	ENSMUSG00000021725
Parva	ENSMUSG00000030770
Paupar	ENSMUSG00000102424
Pax3	ENSMUSG00000004872
Pax7	ENSMUSG00000028736
Pbx1	ENSMUSG00000052534
Pbx3	ENSMUSG00000038718
Pbx4	ENSMUSG00000031860
Pcbp3	ENSMUSG00000001120
Pcbp4	ENSMUSG00000023495
Pcca	ENSMUSG00000041650
Pcdh15	ENSMUSG00000052613
Pcdh18	ENSMUSG00000037892
Pcdh20	ENSMUSG00000050505
Pcdh9	ENSMUSG00000055421
Pcid2	ENSMUSG00000038542
Pcif1	ENSMUSG00000039849
Pclo	ENSMUSG00000061601
Pcm1	ENSMUSG00000031592
Pcmtd1	ENSMUSG00000051285
Pcnt	ENSMUSG00000001151
Pcsk2os2	ENSMUSG00000087115
Pcsk5	ENSMUSG00000024713
Pcsk6	ENSMUSG00000030513
Pcx	ENSMUSG00000024892
Pde10a	ENSMUSG00000023868
Pde1c	ENSMUSG00000004347
Pde4b	ENSMUSG00000028525
Pde4d	ENSMUSG00000021699
Pdha2	ENSMUSG00000047674
Pdia3	ENSMUSG00000027248
Pdp1	ENSMUSG00000049225
Pdxp	ENSMUSG00000116165
Pdzrn3	ENSMUSG00000035357
Pdzrn4	ENSMUSG00000036218
Pea15a	ENSMUSG00000013698
Peak1	ENSMUSG00000074305
Pecr	ENSMUSG00000026189
Peg13	ENSMUSG00000106847
Peg3	ENSMUSG00000002265
Per1	ENSMUSG00000020893
Pex2	ENSMUSG00000040374
Pex5l	ENSMUSG00000027674
Pfdn4	ENSMUSG00000052033
Pfkfb2	ENSMUSG00000026409
Pfkp	ENSMUSG00000021196
Pgbd5	ENSMUSG00000050751
Pgm2l1	ENSMUSG00000030729
Pgrmc2	ENSMUSG00000049940
Pgs1	ENSMUSG00000017715
Phax	ENSMUSG00000008301
Phc2	ENSMUSG00000028796
Phf19	ENSMUSG00000026873
Pianp	ENSMUSG00000030329
Pias1	ENSMUSG00000032405
Pigk	ENSMUSG00000039047
Pigz	ENSMUSG00000045625
Pik3c2b	ENSMUSG00000026447
Pik3c2g	ENSMUSG00000030228
Pim1	ENSMUSG00000024014
Pin1	ENSMUSG00000032171
Pip4k2a	ENSMUSG00000026737
Pip5k1b	ENSMUSG00000024867
Pirt	ENSMUSG00000048070
Pitpnm2	ENSMUSG00000029406
Pja1	ENSMUSG00000034403
Pkd1	ENSMUSG00000032855
Pkia	ENSMUSG00000027499
Pkib	ENSMUSG00000019876
Pkm	ENSMUSG00000032294
Pknox1	ENSMUSG00000006705
Pknox2	ENSMUSG00000035934
Pla2g15	ENSMUSG00000031903
Pla2g2c	ENSMUSG00000028750
Pla2g4a	ENSMUSG00000056220
Platr14	ENSMUSG00000086454
Plcb3	ENSMUSG00000024960
Plcg1	ENSMUSG00000016933
Plec	ENSMUSG00000022565
Plekha1	ENSMUSG00000040268
Plekha2	ENSMUSG00000031557
Plekha6	ENSMUSG00000041757
Plekha7	ENSMUSG00000045659
Plekhg5	ENSMUSG00000039713

SYMBOL	ENSEMBL
Tmc3	ENSMUSG00000038540
Tmcc1	ENSMUSG00000030126
Tmco1	ENSMUSG00000052428
Tmed3	ENSMUSG00000032353
Tmeff2	ENSMUSG00000026109
Tmem104	ENSMUSG00000045980
Tmem107	ENSMUSG00000020895
Tmem108	ENSMUSG00000042757
Tmem120b	ENSMUSG00000054434
Tmem131l	ENSMUSG00000033767
Tmem132b	ENSMUSG00000070498
Tmem132cos	ENSMUSG00000087104
Tmem132d	ENSMUSG00000034310
Tmem132e	ENSMUSG00000020701
Tmem143	ENSMUSG00000002781
Tmem156	ENSMUSG00000037913
Tmem161b	ENSMUSG00000035762
Tmem163	ENSMUSG00000026347
Tmem170	ENSMUSG00000031953
Tmem176b	ENSMUSG00000029810
Tmem178	ENSMUSG00000024245
Tmem18	ENSMUSG00000043061
Tmem185a	ENSMUSG00000073139
Tmem209	ENSMUSG00000029782
Tmem222	ENSMUSG00000028857
Tmem240	ENSMUSG00000084845
Tmem250-ps	ENSMUSG00000087679
Tmem256	ENSMUSG00000070394
Tmem260	ENSMUSG00000036339
Tmem268	ENSMUSG00000045917
Tmem273	ENSMUSG00000041707
Tmem64	ENSMUSG00000043252
Tmem87b	ENSMUSG00000014353
Tmem88b	ENSMUSG00000073680
Tmprss15	ENSMUSG00000022857
Tmprss5	ENSMUSG00000032268
Tmtc1	ENSMUSG00000030306
Tmtc2	ENSMUSG00000036019
Tmub1	ENSMUSG00000028958
Tmx1	ENSMUSG00000021072
Tnfaip8	ENSMUSG00000062210
Tnfsf11	ENSMUSG00000022015
Tnik	ENSMUSG00000027692
Tnip1	ENSMUSG00000020400
Tnni3	ENSMUSG00000035458
Tnnt1	ENSMUSG00000064179
Tns1	ENSMUSG00000055322
Tomm40	ENSMUSG00000002984
Tonsl	ENSMUSG00000059323
Top1	ENSMUSG00000070544
Tor1aip2	ENSMUSG00000050565
Tor2a	ENSMUSG00000009563
Tox3	ENSMUSG00000043668
Tpcn1	ENSMUSG00000032741
Tpd52	ENSMUSG00000027506
Tph2	ENSMUSG00000006764
Tpm4	ENSMUSG00000031799
Tppp3	ENSMUSG00000014846
Tpra1	ENSMUSG00000002871
Traf3	ENSMUSG00000021277
Trak1	ENSMUSG00000032536
Trank1	ENSMUSG00000062296
Trdmt1	ENSMUSG00000026723
Trhde	ENSMUSG00000050663
Trib1	ENSMUSG00000032501
Trib2	ENSMUSG00000020601
Tril	ENSMUSG00000043496
Trim2	ENSMUSG00000027993
Trim26	ENSMUSG00000024457
Trim42	ENSMUSG00000032451
Trim62	ENSMUSG00000041000
Trim8	ENSMUSG00000025034
Trio	ENSMUSG00000022263
Trmt61a	ENSMUSG00000060950
Trp53bp1	ENSMUSG00000043909
Trp53i11	ENSMUSG00000068735
Trp53inp2	ENSMUSG00000038375
Trpc4	ENSMUSG00000027748
Trpc7	ENSMUSG00000021541
Trpm3	ENSMUSG00000052387
Trpm6	ENSMUSG00000024727
Tsc22d1	ENSMUSG00000022010
Tshr	ENSMUSG00000020963
Tshz1	ENSMUSG00000046982
Tshz2	ENSMUSG00000047907
Tsku	ENSMUSG00000049580
Tspan11	ENSMUSG00000030351

SYMBOL	ENSEMBL
Cdcp2	ENSMUSG00000047636
Cdh11	ENSMUSG00000031673
Cdh13	ENSMUSG00000031841
Cdh20	ENSMUSG00000050840
Cdh22	ENSMUSG00000053166
Cdh26	ENSMUSG00000039155
Cdh4	ENSMUSG00000000305
Cdk12	ENSMUSG00000003119
Cdk15	ENSMUSG00000026023
Cdk20	ENSMUSG00000021483
Cdk2ap1	ENSMUSG00000029394
Cdk2ap2	ENSMUSG00000024856
Cdk5rap2	ENSMUSG00000039298
Cdk5rap3	ENSMUSG00000018669
Cdk6	ENSMUSG00000040274
Cdkal1	ENSMUSG00000006191
Cdkn1c	ENSMUSG00000037664
Cdkn2aipnl	ENSMUSG00000020392
Cdkn2d	ENSMUSG00000096472
Cdrt4os1	ENSMUSG00000087604
Cecr2	ENSMUSG00000071226
Celf2	ENSMUSG00000002107
Celf4	ENSMUSG00000024268
Cemip2	ENSMUSG00000024754
Cenpj	ENSMUSG00000064128
Cenpt	ENSMUSG00000036672
Cenpu	ENSMUSG00000031629
Cep128	ENSMUSG00000061533
Cep162	ENSMUSG00000056919
Cep170	ENSMUSG00000057335
Cep295	ENSMUSG00000046111
Cep350	ENSMUSG00000033671
Cep41	ENSMUSG00000029790
Cep68	ENSMUSG00000044066
Cep70	ENSMUSG00000056267
Cerk	ENSMUSG00000035891
Cerkl	ENSMUSG00000075256
Cetn3	ENSMUSG00000021537
Cfap58	ENSMUSG00000046585
Cfap61	ENSMUSG00000037143
Cfap73	ENSMUSG00000094282
Cfap77	ENSMUSG00000079502
Cfap97d2	ENSMUSG00000090336
Cggbp1	ENSMUSG00000054604
Chaf1a	ENSMUSG00000002835
Chat	ENSMUSG00000021919
Chchd6	ENSMUSG00000030086
Chchd7	ENSMUSG00000042198
Chd1	ENSMUSG00000023852
Chd6	ENSMUSG00000057133
Chd7	ENSMUSG00000041235
Chd9	ENSMUSG00000056608
Chgb	ENSMUSG00000027350
Chkb	ENSMUSG00000022617
Chmp1a	ENSMUSG00000000743
Chn2	ENSMUSG00000004633
Chrm3	ENSMUSG00000046159
Chrna4	ENSMUSG00000027577
Chrnb4	ENSMUSG00000035200
Chst10	ENSMUSG00000026080
Chst11	ENSMUSG00000034612
Chst12	ENSMUSG00000036599
Chst15	ENSMUSG00000030930
Chst8	ENSMUSG00000060402
Chst9	ENSMUSG00000047161
Chsy1	ENSMUSG00000032640
Chuk	ENSMUSG00000025199
Ciao3	ENSMUSG00000002280
Ciapin1	ENSMUSG00000031781
Cic	ENSMUSG00000005442
Cirbp	ENSMUSG00000045193
Ckap4	ENSMUSG00000046841
Ckb	ENSMUSG00000001270
Cklf	ENSMUSG00000054400
Clasp2	ENSMUSG00000033392
Clcn4	ENSMUSG00000000605
Cldn34d	ENSMUSG00000079525
Clec11a	ENSMUSG00000004473
Clic4	ENSMUSG00000037242
Clip4	ENSMUSG00000024059
Clmn	ENSMUSG00000021097
Clmp	ENSMUSG00000032024
Clnk	ENSMUSG00000039315
Clptm1l	ENSMUSG00000021610
Cluap1	ENSMUSG00000014232
Clvs1	ENSMUSG00000041216
Cmip	ENSMUSG00000034390

SYMBOL	ENSEMBL
Hrg	ENSMUSG00000022877
Hrh4	ENSMUSG00000037346
Hs2st1	ENSMUSG00000040151
Hs3st3a1	ENSMUSG00000047759
Hs3st3b1	ENSMUSG00000070407
Hs3st5	ENSMUSG00000044499
Hsbp1	ENSMUSG00000031839
Hsd17b3	ENSMUSG00000033122
Hsp90b1	ENSMUSG00000020048
Hspa12a	ENSMUSG00000025092
Hspa2	ENSMUSG00000059970
Hspa4	ENSMUSG00000020361
Hspg2	ENSMUSG00000028763
Hsph1	ENSMUSG00000029657
Huwe1	ENSMUSG00000025261
Hyou1	ENSMUSG00000032115
Ibtk	ENSMUSG00000035941
Icmt	ENSMUSG00000039662
Id1	ENSMUSG00000042745
Id3	ENSMUSG00000007872
Id4	ENSMUSG00000021379
Idh2	ENSMUSG00000030541
Idh3g	ENSMUSG00000002010
Ido2	ENSMUSG00000031549
Ier2	ENSMUSG00000053560
Iffo1	ENSMUSG00000038271
Ift22	ENSMUSG00000007987
Ift74	ENSMUSG00000028576
Ift80	ENSMUSG00000027778
Igdcc3	ENSMUSG00000032394
Igdcc4	ENSMUSG00000032816
Igfbp5	ENSMUSG00000026185
Igfbpl1	ENSMUSG00000035551
Il17ra	ENSMUSG00000002897
Immp1l	ENSMUSG00000042670
Inava	ENSMUSG00000041605
Inhbb	ENSMUSG00000037035
Inka2	ENSMUSG00000048458
Ino80	ENSMUSG00000034154
Inpp4b	ENSMUSG00000037940
Inpp5a	ENSMUSG00000025477
Insig1	ENSMUSG00000045294
Insyn2a	ENSMUSG00000073805
Insyn2b	ENSMUSG00000069911
Ints9	ENSMUSG00000021975
Invs	ENSMUSG00000028344
Ip6k3	ENSMUSG00000024210
Iqca	ENSMUSG00000026301
Iqcg	ENSMUSG00000035578
Iqck	ENSMUSG00000073856
Iqgap1	ENSMUSG00000030536
Iqgap2	ENSMUSG00000021676
Iqsec1	ENSMUSG00000034312
Ireb2	ENSMUSG00000032293
Irx3	ENSMUSG00000031734
Irx4	ENSMUSG00000021604
Irx6	ENSMUSG00000031738
Isl1	ENSMUSG00000042258
Isoc1	ENSMUSG00000024601
Itga1	ENSMUSG00000042284
Itga4	ENSMUSG00000027009
Itgav	ENSMUSG00000027087
Itgb1	ENSMUSG00000025809
Itgb5	ENSMUSG00000022817
Itsn2	ENSMUSG00000020640
Ivns1abp	ENSMUSG00000023150
Jag1	ENSMUSG00000027276
Jak1	ENSMUSG00000028530
Jakmip3	ENSMUSG00000056856
Jam2	ENSMUSG00000053062
Jam3	ENSMUSG00000031990
Jarid2	ENSMUSG00000038518
Jazf1	ENSMUSG00000063568
Josd2	ENSMUSG00000038695
Jph3	ENSMUSG00000025318
Jtb	ENSMUSG00000027937
Kalrn	ENSMUSG00000061751
Kank3	ENSMUSG00000042099
Kat2b	ENSMUSG00000000708
Kat8	ENSMUSG00000030801
Kazald1	ENSMUSG00000025213
Kcnab2	ENSMUSG00000028931
Kcnd3	ENSMUSG00000040896
Kcnd3os	ENSMUSG00000074346
Kcng4	ENSMUSG00000045246
Kcnh1	ENSMUSG00000058248
Kcnh2	ENSMUSG00000038319

SYMBOL	ENSEMBL
Plekhh2	ENSMUSG00000040852
Plekho1	ENSMUSG00000015745
Plet1	ENSMUSG00000032068
Plk3	ENSMUSG00000028680
Plpp7	ENSMUSG00000051373
Plppr4	ENSMUSG00000044667
Plxdc1	ENSMUSG00000017417
Plxdc2	ENSMUSG00000026748
Plxna1	ENSMUSG00000030084
Plxna2	ENSMUSG00000026640
Plxna4os1	ENSMUSG00000086763
Pmaip1	ENSMUSG00000024521
Pnkd	ENSMUSG00000026179
Pnmal1	ENSMUSG00000041141
Pnmal2	ENSMUSG00000070802
Pnp	ENSMUSG00000115338
Poc5	ENSMUSG00000021671
Pole	ENSMUSG00000007080
Poll	ENSMUSG00000025218
Polr1c	ENSMUSG00000067148
Polr2b	ENSMUSG00000029250
Polr2e	ENSMUSG00000004667
Pop7	ENSMUSG00000029715
Popdc2	ENSMUSG00000022803
Por	ENSMUSG00000005514
Pou2af1	ENSMUSG00000032053
Pou2f1	ENSMUSG00000026565
Pou3f1	ENSMUSG00000090125
Pou3f2	ENSMUSG00000095139
Pou4f1	ENSMUSG00000048349
Pou5f1-rs5	NA
Pou6f2	ENSMUSG00000009734
Pparg	ENSMUSG00000000440
Ppcdc	ENSMUSG00000063849
Ppfia4	ENSMUSG00000026458
Ppfibp2	ENSMUSG00000036528
Ppib	ENSMUSG00000032383
Ppm1a	ENSMUSG00000021096
Ppm1h	ENSMUSG00000034613
Ppp1cb	ENSMUSG00000014956
Ppp1r12b	ENSMUSG00000073557
Ppp1r14a	ENSMUSG00000037166
Ppp1r2	ENSMUSG00000047714
Ppp1r26	ENSMUSG00000035829
Ppp1r3e	ENSMUSG00000072494
Ppp1r9a	ENSMUSG00000032827
Ppp1r9b	ENSMUSG00000038976
Ppp3ca	ENSMUSG00000028161
Ppp4r3b	ENSMUSG00000020463
Ppp6r2	ENSMUSG00000036561
Ppp6r3	ENSMUSG00000024908
Prdm13	ENSMUSG00000040478
Prdm8	ENSMUSG00000035456
Prdx1	ENSMUSG00000028691
Prelid3a	ENSMUSG00000024530
Prex1	ENSMUSG00000039621
Prex2	ENSMUSG00000048960
Prickle2	ENSMUSG00000030020
Prkar1a	ENSMUSG00000020612
Prkar2a	ENSMUSG00000032601
Prkcb	ENSMUSG00000052889
Prkcz	ENSMUSG00000029053
Prkg1	ENSMUSG00000052920
Prkg2	ENSMUSG00000029334
Prkn	ENSMUSG00000023826
Prok2	ENSMUSG00000030069
Prokr1	ENSMUSG00000049409
Prom1	ENSMUSG00000029086
Pros1	ENSMUSG00000022912
Prpsap1	ENSMUSG00000015869
Prr30	ENSMUSG00000042888
Prr5	ENSMUSG00000036106
Prrc2b	ENSMUSG00000039262
Prrxl1	ENSMUSG00000041730
Prss36	ENSMUSG00000070371
Prss52	ENSMUSG00000021966
Psapl1	ENSMUSG00000043430
Psat1	ENSMUSG00000024640
Psd2	ENSMUSG00000024347
Psen2	ENSMUSG00000010609
Psg16	ENSMUSG00000066760
Psmc2	ENSMUSG00000028932
Psmd3	ENSMUSG00000017221
Psmd4	ENSMUSG00000005625
Psmd5	ENSMUSG00000026869
Psph	ENSMUSG00000029446
Ptbp1	ENSMUSG00000006498

SYMBOL	ENSEMBL
Tspan12	ENSMUSG00000029669
Tspan14	ENSMUSG00000037824
Tspan15	ENSMUSG00000037031
Tspan18	ENSMUSG00000027217
Tspan2os	ENSMUSG00000086745
Tspan3	ENSMUSG00000032324
Tspan9	ENSMUSG00000030352
Tspyl1	ENSMUSG00000047514
Ttbk1	ENSMUSG00000015599
Ttc14	ENSMUSG00000027677
Ttc27	ENSMUSG00000024078
Ttc28	ENSMUSG00000033209
Ttc29	ENSMUSG00000037101
Ttc30a2	ENSMUSG00000075272
Ttc32	ENSMUSG00000066637
Ttc34	ENSMUSG00000046637
Ttc41	ENSMUSG00000044937
Ttc7	ENSMUSG00000036918
Ttc7b	ENSMUSG00000033530
Ttc8	ENSMUSG00000021013
Ttll7	ENSMUSG00000036745
Ttll9	ENSMUSG00000074673
Tubb2b	ENSMUSG00000045136
Tubb3	ENSMUSG00000062380
Tubg1	ENSMUSG00000035198
Tubgcp5	ENSMUSG00000033790
Txlng	ENSMUSG00000038344
Txn1	ENSMUSG00000028367
Txndc9	ENSMUSG00000058407
Txnrd2	ENSMUSG00000075704
Ubald1	ENSMUSG00000039568
Ubc	ENSMUSG00000008348
Ube2cbp	ENSMUSG00000032415
Ube2e2	ENSMUSG00000058317
Ubfd1	ENSMUSG00000030870
Ubl3	ENSMUSG00000001687
Ubr3	ENSMUSG00000044308
Uck2	ENSMUSG00000026558
Uhrf2	ENSMUSG00000024817
Ulk3	ENSMUSG00000032308
Unc13a	ENSMUSG00000034799
Unc13c	ENSMUSG00000062151
Unc5c	ENSMUSG00000059921
Unc5d	ENSMUSG00000063626
Uncx	ENSMUSG00000029546
Upf3a	ENSMUSG00000038398
Upf3b	ENSMUSG00000036572
Urgcp	ENSMUSG00000049680
Uri1	ENSMUSG00000030421
Usf1	ENSMUSG00000026641
Ush2a	ENSMUSG00000026609
Usp28	ENSMUSG00000032267
Usp29	ENSMUSG00000051527
Usp33	ENSMUSG00000025437
Usp35	ENSMUSG00000035713
Usp36	ENSMUSG00000033909
Usp44	ENSMUSG00000020020
Usp46	ENSMUSG00000054814
Usp47	ENSMUSG00000059263
Usp53	ENSMUSG00000039701
Usp54	ENSMUSG00000034235
Utp25	ENSMUSG00000016181
Uvrag	ENSMUSG00000035354
Vamp1	ENSMUSG00000030337
Vash1	ENSMUSG00000021256
Vav3	ENSMUSG00000033721
Vdac3	ENSMUSG00000008892
Veph1	ENSMUSG00000027831
Vgll3	ENSMUSG00000091243
Vkorc1l1	ENSMUSG00000066735
Vma21	ENSMUSG00000073131
Vmac	ENSMUSG00000054723
Vps13a	ENSMUSG00000046230
Vps37b	ENSMUSG00000066278
Vps41	ENSMUSG00000041236
Vps45	ENSMUSG00000015747
Vps4b	ENSMUSG00000009907
Vps53	ENSMUSG00000017288
Vps8	ENSMUSG00000033653
Vrk1	ENSMUSG00000021115
Vsir	ENSMUSG00000020101
Vsx2	ENSMUSG00000021239
Vwa3b	ENSMUSG00000050122
Vxn	ENSMUSG00000067879
Wdfy3	ENSMUSG00000043940
Wdr44	ENSMUSG00000036769
Wdr6	ENSMUSG00000066357

SYMBOL	ENSEMBL
Cdcp2	ENSMUSG00000047636
Cdh11	ENSMUSG00000031673
Cdh13	ENSMUSG00000031841
Cdh20	ENSMUSG00000050840
Cdh22	ENSMUSG00000053166
Cdh26	ENSMUSG00000039155
Cdh4	ENSMUSG00000000305
Cdk12	ENSMUSG00000003119
Cdk15	ENSMUSG00000026023
Cdk20	ENSMUSG00000021483
Cdk2ap1	ENSMUSG00000029394
Cdk2ap2	ENSMUSG00000024856
Cdk5rap2	ENSMUSG00000039298
Cdk5rap3	ENSMUSG00000018669
Cdk6	ENSMUSG00000040274
Cdkal1	ENSMUSG00000006191
Cdkn1c	ENSMUSG00000037664
Cdkn2aipnl	ENSMUSG00000020392
Cdkn2d	ENSMUSG00000096472
Cdrt4os1	ENSMUSG00000087604
Cecr2	ENSMUSG00000071226
Celf2	ENSMUSG00000002107
Celf4	ENSMUSG00000024268
Cemip2	ENSMUSG00000024754
Cenpj	ENSMUSG00000064128
Cenpt	ENSMUSG00000036672
Cenpu	ENSMUSG00000031629
Cep128	ENSMUSG00000061533
Cep162	ENSMUSG00000056919
Cep170	ENSMUSG00000057335
Cep295	ENSMUSG00000046111
Cep350	ENSMUSG00000033671
Cep41	ENSMUSG00000029790
Cep68	ENSMUSG00000044066
Cep70	ENSMUSG00000056267
Cerk	ENSMUSG00000035891
Cerkl	ENSMUSG00000075256
Cetn3	ENSMUSG00000021537
Cfap58	ENSMUSG00000046585
Cfap61	ENSMUSG00000037143
Cfap73	ENSMUSG00000094282
Cfap77	ENSMUSG00000079502
Cfap97d2	ENSMUSG00000090336
Cggbp1	ENSMUSG00000054604
Chaf1a	ENSMUSG00000002835
Chat	ENSMUSG00000021919
Chchd6	ENSMUSG00000030086
Chchd7	ENSMUSG00000042198
Chd1	ENSMUSG00000023852
Chd6	ENSMUSG00000057133
Chd7	ENSMUSG00000041235
Chd9	ENSMUSG00000056608
Chgb	ENSMUSG00000027350
Chkb	ENSMUSG00000022617
Chmp1a	ENSMUSG00000000743
Chn2	ENSMUSG00000004633
Chrm3	ENSMUSG00000046159
Chrna4	ENSMUSG00000027577
Chrnb4	ENSMUSG00000035200
Chst10	ENSMUSG00000026080
Chst11	ENSMUSG00000034612
Chst12	ENSMUSG00000036599
Chst15	ENSMUSG00000030930
Chst8	ENSMUSG00000060402
Chst9	ENSMUSG00000047161
Chsy1	ENSMUSG00000032640
Chuk	ENSMUSG00000025199
Ciao3	ENSMUSG00000002280
Ciapin1	ENSMUSG00000031781
Cic	ENSMUSG00000005442
Cirbp	ENSMUSG00000045193
Ckap4	ENSMUSG00000046841
Ckb	ENSMUSG00000001270
Cklf	ENSMUSG00000054400
Clasp2	ENSMUSG00000033392
Clcn4	ENSMUSG00000000605
Cldn34d	ENSMUSG00000079525
Clec11a	ENSMUSG00000004473
Clic4	ENSMUSG00000037242
Clip4	ENSMUSG00000024059
Clmn	ENSMUSG00000021097
Clmp	ENSMUSG00000032024
Clnk	ENSMUSG00000039315
Clptm1l	ENSMUSG00000021610
Cluap1	ENSMUSG00000014232
Clvs1	ENSMUSG00000041216
Cmip	ENSMUSG00000034390

SYMBOL	ENSEMBL
Hrg	ENSMUSG00000022877
Hrh4	ENSMUSG00000037346
Hs2st1	ENSMUSG00000040151
Hs3st3a1	ENSMUSG00000047759
Hs3st3b1	ENSMUSG00000070407
Hs3st5	ENSMUSG00000044499
Hsbp1	ENSMUSG00000031839
Hsd17b3	ENSMUSG00000033122
Hsp90b1	ENSMUSG00000020048
Hspa12a	ENSMUSG00000025092
Hspa2	ENSMUSG00000059970
Hspa4	ENSMUSG00000020361
Hspg2	ENSMUSG00000028763
Hsph1	ENSMUSG00000029657
Huwe1	ENSMUSG00000025261
Hyou1	ENSMUSG00000032115
Ibtk	ENSMUSG00000035941
Icmt	ENSMUSG00000039662
Id1	ENSMUSG00000042745
Id3	ENSMUSG00000007872
Id4	ENSMUSG00000021379
Idh2	ENSMUSG00000030541
Idh3g	ENSMUSG00000002010
Ido2	ENSMUSG00000031549
Ier2	ENSMUSG00000053560
Iffo1	ENSMUSG00000038271
Ift22	ENSMUSG00000007987
Ift74	ENSMUSG00000028576
Ift80	ENSMUSG00000027778
Igdcc3	ENSMUSG00000032394
Igdcc4	ENSMUSG00000032816
Igfbp5	ENSMUSG00000026185
Igfbpl1	ENSMUSG00000035551
Il17ra	ENSMUSG00000002897
Immp1l	ENSMUSG00000042670
Inava	ENSMUSG00000041605
Inhbb	ENSMUSG00000037035
Inka2	ENSMUSG00000048458
Ino80	ENSMUSG00000034154
Inpp4b	ENSMUSG00000037940
Inpp5a	ENSMUSG00000025477
Insig1	ENSMUSG00000045294
Insyn2a	ENSMUSG00000073805
Insyn2b	ENSMUSG00000069911
Ints9	ENSMUSG00000021975
Invs	ENSMUSG00000028344
Ip6k3	ENSMUSG00000024210
Iqca	ENSMUSG00000026301
Iqcg	ENSMUSG00000035578
Iqck	ENSMUSG00000073856
Iqgap1	ENSMUSG00000030536
Iqgap2	ENSMUSG00000021676
Iqsec1	ENSMUSG00000034312
Ireb2	ENSMUSG00000032293
Irx3	ENSMUSG00000031734
Irx4	ENSMUSG00000021604
Irx6	ENSMUSG00000031738
Isl1	ENSMUSG00000042258
Isoc1	ENSMUSG00000024601
Itga1	ENSMUSG00000042284
Itga4	ENSMUSG00000027009
Itgav	ENSMUSG00000027087
Itgb1	ENSMUSG00000025809
Itgb5	ENSMUSG00000022817
Itsn2	ENSMUSG00000020640
Ivns1abp	ENSMUSG00000023150
Jag1	ENSMUSG00000027276
Jak1	ENSMUSG00000028530
Jakmip3	ENSMUSG00000056856
Jam2	ENSMUSG00000053062
Jam3	ENSMUSG00000031990
Jarid2	ENSMUSG00000038518
Jazf1	ENSMUSG00000063568
Josd2	ENSMUSG00000038695
Jph3	ENSMUSG00000025318
Jtb	ENSMUSG00000027937
Kalrn	ENSMUSG00000061751
Kank3	ENSMUSG00000042099
Kat2b	ENSMUSG00000000708
Kat8	ENSMUSG00000030801
Kazald1	ENSMUSG00000025213
Kcnab2	ENSMUSG00000028931
Kcnd3	ENSMUSG00000040896
Kcnd3os	ENSMUSG00000074346
Kcng4	ENSMUSG00000045246
Kcnh1	ENSMUSG00000058248
Kcnh2	ENSMUSG00000038319

SYMBOL	ENSEMBL
Plekhh2	ENSMUSG00000040852
Plekho1	ENSMUSG00000015745
Plet1	ENSMUSG00000032068
Plk3	ENSMUSG00000028680
Plpp7	ENSMUSG00000051373
Plppr4	ENSMUSG00000044667
Plxdc1	ENSMUSG00000017417
Plxdc2	ENSMUSG00000026748
Plxna1	ENSMUSG00000030084
Plxna2	ENSMUSG00000026640
Plxna4os1	ENSMUSG00000086763
Pmaip1	ENSMUSG00000024521
Pnkd	ENSMUSG00000026179
Pnmal1	ENSMUSG00000041141
Pnmal2	ENSMUSG00000070802
Pnp	ENSMUSG00000115338
Poc5	ENSMUSG00000021671
Pole	ENSMUSG00000007080
Poll	ENSMUSG00000025218
Polr1c	ENSMUSG00000067148
Polr2b	ENSMUSG00000029250
Polr2e	ENSMUSG00000004667
Pop7	ENSMUSG00000029715
Popdc2	ENSMUSG00000022803
Por	ENSMUSG00000005514
Pou2af1	ENSMUSG00000032053
Pou2f1	ENSMUSG00000026565
Pou3f1	ENSMUSG00000090125
Pou3f2	ENSMUSG00000095139
Pou4f1	ENSMUSG00000048349
Pou5f1-rs5	NA
Pou6f2	ENSMUSG00000009734
Pparg	ENSMUSG00000000440
Ppcdc	ENSMUSG00000063849
Ppfia4	ENSMUSG00000026458
Ppfibp2	ENSMUSG00000036528
Ppib	ENSMUSG00000032383
Ppm1a	ENSMUSG00000021096
Ppm1h	ENSMUSG00000034613
Ppp1cb	ENSMUSG00000014956
Ppp1r12b	ENSMUSG00000073557
Ppp1r14a	ENSMUSG00000037166
Ppp1r2	ENSMUSG00000047714
Ppp1r26	ENSMUSG00000035829
Ppp1r3e	ENSMUSG00000072494
Ppp1r9a	ENSMUSG00000032827
Ppp1r9b	ENSMUSG00000038976
Ppp3ca	ENSMUSG00000028161
Ppp4r3b	ENSMUSG00000020463
Ppp6r2	ENSMUSG00000036561
Ppp6r3	ENSMUSG00000024908
Prdm13	ENSMUSG00000040478
Prdm8	ENSMUSG00000035456
Prdx1	ENSMUSG00000028691
Prelid3a	ENSMUSG00000024530
Prex1	ENSMUSG00000039621
Prex2	ENSMUSG00000048960
Prickle2	ENSMUSG00000030020
Prkar1a	ENSMUSG00000020612
Prkar2a	ENSMUSG00000032601
Prkcb	ENSMUSG00000052889
Prkcz	ENSMUSG00000029053
Prkg1	ENSMUSG00000052920
Prkg2	ENSMUSG00000029334
Prkn	ENSMUSG00000023826
Prok2	ENSMUSG00000030069
Prokr1	ENSMUSG00000049409
Prom1	ENSMUSG00000029086
Pros1	ENSMUSG00000022912
Prpsap1	ENSMUSG00000015869
Prr30	ENSMUSG00000042888
Prr5	ENSMUSG00000036106
Prrc2b	ENSMUSG00000039262
Prrxl1	ENSMUSG00000041730
Prss36	ENSMUSG00000070371
Prss52	ENSMUSG00000021966
Psapl1	ENSMUSG00000043430
Psat1	ENSMUSG00000024640
Psd2	ENSMUSG00000024347
Psen2	ENSMUSG00000010609
Psg16	ENSMUSG00000066760
Psmc2	ENSMUSG00000028932
Psmd3	ENSMUSG00000017221
Psmd4	ENSMUSG00000005625
Psmd5	ENSMUSG00000026869
Psph	ENSMUSG00000029446
Ptbp1	ENSMUSG00000006498

SYMBOL	ENSEMBL
Tspan12	ENSMUSG00000029669
Tspan14	ENSMUSG00000037824
Tspan15	ENSMUSG00000037031
Tspan18	ENSMUSG00000027217
Tspan2os	ENSMUSG00000086745
Tspan3	ENSMUSG00000032324
Tspan9	ENSMUSG00000030352
Tspyl1	ENSMUSG00000047514
Ttbk1	ENSMUSG00000015599
Ttc14	ENSMUSG00000027677
Ttc27	ENSMUSG00000024078
Ttc28	ENSMUSG00000033209
Ttc29	ENSMUSG00000037101
Ttc30a2	ENSMUSG00000075272
Ttc32	ENSMUSG00000066637
Ttc34	ENSMUSG00000046637
Ttc41	ENSMUSG00000044937
Ttc7	ENSMUSG00000036918
Ttc7b	ENSMUSG00000033530
Ttc8	ENSMUSG00000021013
Ttll7	ENSMUSG00000036745
Ttll9	ENSMUSG00000074673
Tubb2b	ENSMUSG00000045136
Tubb3	ENSMUSG00000062380
Tubg1	ENSMUSG00000035198
Tubgcp5	ENSMUSG00000033790
Txlng	ENSMUSG00000038344
Txn1	ENSMUSG00000028367
Txndc9	ENSMUSG00000058407
Txnrd2	ENSMUSG00000075704
Ubald1	ENSMUSG00000039568
Ubc	ENSMUSG00000008348
Ube2cbp	ENSMUSG00000032415
Ube2e2	ENSMUSG00000058317
Ubfd1	ENSMUSG00000030870
Ubl3	ENSMUSG00000001687
Ubr3	ENSMUSG00000044308
Uck2	ENSMUSG00000026558
Uhrf2	ENSMUSG00000024817
Ulk3	ENSMUSG00000032308
Unc13a	ENSMUSG00000034799
Unc13c	ENSMUSG00000062151
Unc5c	ENSMUSG00000059921
Unc5d	ENSMUSG00000063626
Uncx	ENSMUSG00000029546
Upf3a	ENSMUSG00000038398
Upf3b	ENSMUSG00000036572
Urgcp	ENSMUSG00000049680
Uri1	ENSMUSG00000030421
Usf1	ENSMUSG00000026641
Ush2a	ENSMUSG00000026609
Usp28	ENSMUSG00000032267
Usp29	ENSMUSG00000051527
Usp33	ENSMUSG00000025437
Usp35	ENSMUSG00000035713
Usp36	ENSMUSG00000033909
Usp44	ENSMUSG00000020020
Usp46	ENSMUSG00000054814
Usp47	ENSMUSG00000059263
Usp53	ENSMUSG00000039701
Usp54	ENSMUSG00000034235
Utp25	ENSMUSG00000016181
Uvrag	ENSMUSG00000035354
Vamp1	ENSMUSG00000030337
Vash1	ENSMUSG00000021256
Vav3	ENSMUSG00000033721
Vdac3	ENSMUSG00000008892
Veph1	ENSMUSG00000027831
Vgll3	ENSMUSG00000091243
Vkorc1l1	ENSMUSG00000066735
Vma21	ENSMUSG00000073131
Vmac	ENSMUSG00000054723
Vps13a	ENSMUSG00000046230
Vps37b	ENSMUSG00000066278
Vps41	ENSMUSG00000041236
Vps45	ENSMUSG00000015747
Vps4b	ENSMUSG00000009907
Vps53	ENSMUSG00000017288
Vps8	ENSMUSG00000033653
Vrk1	ENSMUSG00000021115
Vsir	ENSMUSG00000020101
Vsx2	ENSMUSG00000021239
Vwa3b	ENSMUSG00000050122
Vxn	ENSMUSG00000067879
Wdfy3	ENSMUSG00000043940
Wdr44	ENSMUSG00000036769
Wdr6	ENSMUSG00000066357

SYMBOL	ENSEMBL
Cmpk1	ENSMUSG00000028719
Cmpk2	ENSMUSG00000020638
Cmtm6	ENSMUSG00000032434
Cmtm7	ENSMUSG00000032436
Cnih3	ENSMUSG00000026514
Cnot6l	ENSMUSG00000034724
Cnpy1	ENSMUSG00000044681
Cnpy2	ENSMUSG00000025381
Cnr2	ENSMUSG00000062585
Cntfr	ENSMUSG00000028444
Cntln	ENSMUSG00000038070
Cntn1	ENSMUSG00000055022
Cntn2	ENSMUSG00000053024
Cntn4	ENSMUSG00000064293
Cntn6	ENSMUSG00000030092
Cntnap2	ENSMUSG00000039419
Cntnap5a	ENSMUSG00000070695
Col18a1	ENSMUSG00000001435
Col1a1	ENSMUSG00000001506
Col1a2	ENSMUSG00000029661
Col26a1	ENSMUSG00000004415
Col9a1	ENSMUSG00000026147
Copa	ENSMUSG00000026553
Copz1	ENSMUSG00000060992
Copz2	ENSMUSG00000018672
Coro1c	ENSMUSG00000004530
Coro2b	ENSMUSG00000041729
Cox4i1	ENSMUSG00000031818
Cox6a1	ENSMUSG00000041697
Cox7a2l	ENSMUSG00000024248
Cpeb2	ENSMUSG00000039782
Cplx2	ENSMUSG00000025867
Cplx3	ENSMUSG00000039714
Cplx4	ENSMUSG00000024519
Cpvl	ENSMUSG00000052955
Cracr2a	ENSMUSG00000061414
Creb1	ENSMUSG00000025958
Crebzf	ENSMUSG00000051451
Creld1	ENSMUSG00000030284
Crim1	ENSMUSG00000024074
Crip2	ENSMUSG00000006356
Crisp4	ENSMUSG00000025774
Crispld2	ENSMUSG00000031825
Crnde	ENSMUSG00000031736
Crtac1	ENSMUSG00000042401
Crybg3	ENSMUSG00000022723
Cs	ENSMUSG00000005683
Csde1	ENSMUSG00000068823
Csf2	ENSMUSG00000018916
Csmd2	ENSMUSG00000028804
Csnk1g2	ENSMUSG00000003345
Csrp1	ENSMUSG00000026421
Csrp2	ENSMUSG00000020186
Cstf2t	ENSMUSG00000053536
Ctif	ENSMUSG00000052928
Ctnnb1	ENSMUSG00000006932
Ctns	ENSMUSG00000005949
Ctsc	ENSMUSG00000030560
Cul1	ENSMUSG00000029686
Cul3	ENSMUSG00000004364
Cul5	ENSMUSG00000032030
Cul7	ENSMUSG00000038545
Cux2	ENSMUSG00000042589
Cwc22	ENSMUSG00000027014
Cxcl12	ENSMUSG00000061353
Cxcr4	ENSMUSG00000045382
Cxxc4	ENSMUSG00000044365
Cxxc5	ENSMUSG00000046668
Cyb561d1	ENSMUSG00000048796
Cyb5d1	ENSMUSG00000044795
Cycs	ENSMUSG00000063694
Cyld	ENSMUSG00000036712
Cyp11a1	ENSMUSG00000032323
Cyp7b1	ENSMUSG00000039519
Cyth2	ENSMUSG00000003269
D030025E07Rik	ENSMUSG00000105816
D1Pas1	ENSMUSG00000039224
D230030E09Rik	ENSMUSG00000113875
D3Ertd751e	ENSMUSG00000025766
D430020J02Rik	ENSMUSG00000112980
D6Ertd474e	NA
D730050B12Rik	ENSMUSG00000113082
D830032E09Rik	ENSMUSG00000100457

SYMBOL	ENSEMBL
Kcnh7	ENSMUSG00000059742
Kcnip4	ENSMUSG00000029088
Kcnj3	ENSMUSG00000026824
Kcnj6	ENSMUSG00000043301
Kcnmb1	ENSMUSG00000020155
Kcnq1ot1	ENSMUSG00000101609
Kcnv1	ENSMUSG00000022342
Kctd15	ENSMUSG00000030499
Kctd16	ENSMUSG00000051401
Kctd4	ENSMUSG00000046523
Kdm1b	ENSMUSG00000038080
Kdm4a	ENSMUSG00000033326
Kdm4c	ENSMUSG00000028397
Kdm6a	ENSMUSG00000037369
Kdm6b	ENSMUSG00000018476
Khdc1b	ENSMUSG00000085079
Khdrbs1	ENSMUSG00000028790
Khsrp	ENSMUSG00000007670
Kif13b	ENSMUSG00000060012
Kif16b	ENSMUSG00000038844
Kif16bos	ENSMUSG00000086504
Kif21a	ENSMUSG00000022629
Kif26a	ENSMUSG00000021294
Kif6	ENSMUSG00000023999
Kitl	ENSMUSG00000019966
Kiz	ENSMUSG00000074749
Klf10	ENSMUSG00000037465
Klf12	ENSMUSG00000072294
Klf3	ENSMUSG00000029178
Klf7	ENSMUSG00000025959
Klhdc7a	ENSMUSG00000078234
Klhdc7b	ENSMUSG00000091680
Klhl1	ENSMUSG00000022076
Klhl21	ENSMUSG00000073700
Klhl25	ENSMUSG00000055652
Klhl29	ENSMUSG00000020627
Klhl8	ENSMUSG00000029312
Klrb1b	ENSMUSG00000079298
Kmt2a	ENSMUSG00000002028
Kmt2b	ENSMUSG00000006307
Kremen1	ENSMUSG00000020393
Krr1	ENSMUSG00000063334
Krt8	ENSMUSG00000049382
Krt82	ENSMUSG00000049548
Ksr1	ENSMUSG00000018334
Ksr2	ENSMUSG00000061578
Lag3	ENSMUSG00000030124
Lama1	ENSMUSG00000032796
Lama5	ENSMUSG00000015647
Lamc1	ENSMUSG00000026478
Lamtor3	ENSMUSG00000091512
Lancl1	ENSMUSG00000026000
Laptm4a	ENSMUSG00000020585
Laptm5	ENSMUSG00000028581
Lcmt2	ENSMUSG00000074890
Ldhal6b	ENSMUSG00000101959
Ldlrad3	ENSMUSG00000048058
Lef1	ENSMUSG00000027985
Lemd2	ENSMUSG00000044857
Lgr4	ENSMUSG00000050199
Lgr6	ENSMUSG00000042793
Lhpp	ENSMUSG00000030946
Lhx1os	ENSMUSG00000087211
Lhx2	ENSMUSG00000000247
Lhx4	ENSMUSG00000026468
Lilrb4a	ENSMUSG00000062593
Limk1	ENSMUSG00000029674
Lin52	ENSMUSG00000085793
Lin7a	ENSMUSG00000019906
Lingo1	ENSMUSG00000049556
Lingo3	ENSMUSG00000051067
Lins1	ENSMUSG00000053091
Lipi	ENSMUSG00000032948
Lix1	ENSMUSG00000047786
Lmna	ENSMUSG00000028063
Lmo1	ENSMUSG00000036111
Lmo2	ENSMUSG00000032698
Lmx1b	ENSMUSG00000038765
Lnpk	ENSMUSG00000009207
Lpar5	ENSMUSG00000067714
Lpgat1	ENSMUSG00000026623
Lpo	ENSMUSG00000009356
Lrba	ENSMUSG00000028080
Lrch1	ENSMUSG00000068015

SYMBOL	ENSEMBL
Ptch1	ENSMUSG00000021466
Pter	ENSMUSG00000026730
Ptgds	ENSMUSG00000015090
Ptger3	ENSMUSG00000040016
Ptgr2	ENSMUSG00000072946
Ptk2	ENSMUSG00000022607
Ptk7	ENSMUSG00000023972
Ptma	ENSMUSG00000026238
Ptp4a3	ENSMUSG00000059895
Ptpn13	ENSMUSG00000034573
Ptpn14	ENSMUSG00000026604
Ptpn23	ENSMUSG00000036057
Ptpn4	ENSMUSG00000026384
Ptprd	ENSMUSG00000028399
Ptprg	ENSMUSG00000021745
Ptprs	ENSMUSG00000013236
Ptprt	ENSMUSG00000053141
Ptprtos	ENSMUSG00000084919
Ptprz1	ENSMUSG00000068748
Pudp	ENSMUSG00000048875
Puf60	ENSMUSG00000002524
Pura	ENSMUSG00000043991
Pwwp2a	ENSMUSG00000044950
Pxdn	ENSMUSG00000020674
Pxt1	ENSMUSG00000045378
Qdpr	ENSMUSG00000015806
Qrich1	ENSMUSG00000006673
Qsox1	ENSMUSG00000033684
Rab10os	ENSMUSG00000079179
Rab11b	ENSMUSG00000077450
Rab11fip2	ENSMUSG00000040022
Rab11fip4	ENSMUSG00000017639
Rab15	ENSMUSG00000021062
Rab17	ENSMUSG00000026304
Rab1a	ENSMUSG00000020149
Rab25	ENSMUSG00000008601
Rab2a	ENSMUSG00000047187
Rab31	ENSMUSG00000056515
Rab33b	ENSMUSG00000027739
Rab39	ENSMUSG00000055069
Rab40c	ENSMUSG00000025730
Rab6a	ENSMUSG00000030704
Rabgap1	ENSMUSG00000035437
Rabgap1l	ENSMUSG00000026721
Rabif	ENSMUSG00000042229
Racgap1	ENSMUSG00000023015
Rad23b	ENSMUSG00000028426
Rai1	ENSMUSG00000062115
Ralbp1	ENSMUSG00000024096
Ralgapa1	ENSMUSG00000021027
Ralgapa2	ENSMUSG00000037110
Ralgds	ENSMUSG00000026821
Ralgps1	ENSMUSG00000038831
Ralgps2	ENSMUSG00000026594
Ramac	ENSMUSG00000038646
Rap1gap2	ENSMUSG00000038807
Rap2b	ENSMUSG00000036894
Rapgef2	ENSMUSG00000062232
Rapgef4	ENSMUSG00000049044
Rasgef1b	ENSMUSG00000089809
Rasl10b	ENSMUSG00000020684
Rassf3	ENSMUSG00000025795
Rassf4	ENSMUSG00000042129
Rassf6	ENSMUSG00000029370
Rbfox1	ENSMUSG00000008658
Rbfox3	ENSMUSG00000025576
Rbm15	ENSMUSG00000048109
Rbm19	ENSMUSG00000029594
Rbm26	ENSMUSG00000022119
Rbm39	ENSMUSG00000027620
Rbm4	ENSMUSG00000094936
Rbm5	ENSMUSG00000032580
Rbms1	ENSMUSG00000026970
Rbp7	ENSMUSG00000028996
Rbpj	ENSMUSG00000039191
Rbpms	ENSMUSG00000031586
Rc3h2	ENSMUSG00000075376
Rcan1	ENSMUSG00000022951
Rchy1	ENSMUSG00000029397
Rcn1	ENSMUSG00000005973
Rcor2	ENSMUSG00000024968
Rd3	ENSMUSG00000049353
Rdm1	ENSMUSG00000010362
Redrum	ENSMUSG00000096982

SYMBOL	ENSEMBL
Wdr66	ENSMUSG00000029442
Wdr7	ENSMUSG00000040560
Wdr72	ENSMUSG00000044976
Wdr95	ENSMUSG00000029658
Wfdc11	ENSMUSG00000078940
Wfs1	ENSMUSG00000039474
Whamm	ENSMUSG00000045795
Whrn	ENSMUSG00000039137
Wipi1	ENSMUSG00000041895
Wnk2	ENSMUSG00000037989
Wnt10a	ENSMUSG00000026167
Wrnip1	ENSMUSG00000021400
Wscd2	ENSMUSG00000063430
Wwc1	ENSMUSG00000018849
Xbp1	ENSMUSG00000020484
Xkr7	ENSMUSG00000042631
Xrcc2	ENSMUSG00000028933
Xrra1	ENSMUSG00000035211
Xxylt1	ENSMUSG00000047434
Yme1l1	ENSMUSG00000026775
Yod1	ENSMUSG00000046404
Ypel2	ENSMUSG00000018427
Ypel3	ENSMUSG00000042675
Ypel5	ENSMUSG00000039770
Ythdc2	ENSMUSG00000034653
Yy1	ENSMUSG00000021264
Zbed4	ENSMUSG00000034333
Zbtb10	ENSMUSG00000069114
Zbtb12	ENSMUSG00000049823
Zbtb18	ENSMUSG00000063659
Zbtb38	ENSMUSG00000040433
Zbtb40	ENSMUSG00000060862
Zbtb42	ENSMUSG00000037638
Zc3h12a	ENSMUSG00000042677
Zc3h12c	ENSMUSG00000035164
Zc3h4	ENSMUSG00000059273
Zc3h7a	ENSMUSG00000037965
Zdhhc13	ENSMUSG00000030471
Zdhhc14	ENSMUSG00000034265
Zdhhc17	ENSMUSG00000035798
Zdhhc19	ENSMUSG00000052363
Zdhhc25	ENSMUSG00000054117
Zeb1	ENSMUSG00000024238
Zeb2	ENSMUSG00000026872
Zfand6	ENSMUSG00000030629
Zfat	ENSMUSG00000022335
Zfhx4	ENSMUSG00000025255
Zfp219	ENSMUSG00000049295
Zfp286	ENSMUSG00000047342
Zfp3	ENSMUSG00000043602
Zfp317	ENSMUSG00000057551
Zfp346	ENSMUSG00000021481
Zfp385c	ENSMUSG00000014198
Zfp386	ENSMUSG00000042063
Zfp407	ENSMUSG00000048410
Zfp414	ENSMUSG00000073423
Zfp423	ENSMUSG00000045333
Zfp438	ENSMUSG00000050945
Zfp51	ENSMUSG00000023892
Zfp536	ENSMUSG00000043456
Zfp568	ENSMUSG00000074221
Zfp597	ENSMUSG00000039789
Zfp607b	ENSMUSG00000057093
Zfp608	ENSMUSG00000052713
Zfp619	ENSMUSG00000068959
Zfp622	ENSMUSG00000052253
Zfp644	ENSMUSG00000049606
Zfp647	ENSMUSG00000054967
Zfp687	ENSMUSG00000019338
Zfp706	ENSMUSG00000062397
Zfp82	ENSMUSG00000098022
Zfp839	ENSMUSG00000021271
Zfp869	ENSMUSG00000054648
Zfp873	ENSMUSG00000061371
Zfp958	ENSMUSG00000058748
Zfpm1	ENSMUSG00000049577
Zfpm2	ENSMUSG00000022306
Zkscan2	ENSMUSG00000030757
Zmiz1	ENSMUSG00000007817
Zmym2	ENSMUSG00000021945
Znrf4	ENSMUSG00000044526
Zpld1	ENSMUSG00000064310
Zranb3	ENSMUSG00000036086
Zswim3	ENSMUSG00000045822
Zzz3	ENSMUSG00000039068

Bibliography

Aldiri I, Xu B, Wang L, Chen X, Hiler D, Griffiths L, Valentine M, Shirinifard A, Thiagarajan S, Sablauer A, Barabas M-E, Zhang Jiakun, Johnson D, Frase S, Zhou X, Easton J, Zhang Jinghui, Mardis ER, Wilson RK, Downing JR, Dyer MA, Project SJCRHUPCG. (2017). The Dynamic Epigenetic Landscape of the Retina During Development, Reprogramming, and Tumorigenesis. Neuron 94:550-568.e10. doi:10.1016/j.neuron.2017.04.022

Aparicio, J. G., Hopp, H., Choi, A., Mandayam Comar, J., Liao, V. C., Harutyunyan, N., & Lee, T. C. (2017). Temporal expression of CD184(CXCR4) and CD171(L1CAM) identifies distinct early developmental stages of human retinal ganglion cells in embryonic stem cell derived retina. *Experimental Eye Research*, *154*, 177 189. http://doi.org/10.1016/j.exer.2016.11.013

Azuma, N., Yamaguchi, Y., Handa, H., Tadokoro, K., Asaka, A., Kawase, E., & Yamada, M. (2003). Mutations of the PAX6 gene detected in patients with a variety of optic-nerve malformations. *The American Journal of Human Genetics*, *72*(6), 1565 1570. http://doi.org/10.1086/375555

Badea, T. C., & Nathans, J. (2011). Morphologies of mouse retinal ganglion cells expressing transcription factors Brn3a, Brn3b, and Brn3c: analysis of wild type and mutant cells using genetically-directed sparse labeling. *Vision Research*, *51*(2), 269 279. http://doi.org/10.1016/j.visres.2010.08.039

Badea, T. C., Cahill, H., Ecker, J., Hattar, S., & Nathans, J. (2009). Distinct Roles of Transcription Factors Brn3a and Brn3b in Controlling the Development, Morphology, and Function of Retinal Ganglion Cells. *Neuron*, *61*(6), 852 864. http://doi.org/10.1016/j.neuron.2009.01.020

Baden, T., Berens, P., Franke, K., Rosón, M. R., Bethge, M., & Euler, T. (2016). The functional diversity of retinal ganglion cells in the mouse. *Nature Publishing Group*, *529*(7586), 345 350. http://doi.org/10.1038/nature16468

Baker, N. E., & Brown, N. L. (2018). All in the family: proneural bHLH genes and neuronal diversity. *Development (Cambridge, England)*, *145*(9), dev159426. http://doi.org/10.1242/dev.159426

Barbieri, A. M., Broccoli, V., Bovolenta, P., Alfano, G., Marchitiello, A., Mocchetti, C., et al. (2002). Vax2 inactivation in mouse determines alteration of the eye dorsal-ventral axis, misrouting of the optic fibres and eye coloboma. *Development (Cambridge, England)*, *129*(3), 805 813.

Barbieri, A. M., Lupo, G., Bulfone, A., Andreazzoli, M., Mariani, M., Fougerousse, F., et al. (1999). A homeobox gene, vax2, controls the patterning of the eye dorsoventral axis. *Proceedings of the National Academy of Sciences of the United States of America*, *96*(19), 10729 10734. http://doi.org/10.1073/pnas.96.19.10729

Bedont, J. L., Rohr, K. E., Bathini, A., Hattar, S., Blackshaw, S., Sehgal, A., & Evans, J. A. (2018). Asymmetric vasopressin signaling spatially organizes the master circadian clock. *The Journal of Comparative Neurology*, 1 49. http://doi.org/10.1002/cne.24478

Bernier, G., Vukovich, W., Neidhardt, L., Herrmann, B. G., & Gruss, P. (2001). Isolation and characterization of a downstream target of Pax6 in the mammalian retinal primordium. *Development (Cambridge, England)*, *128*(20), 3987 3994.

Berson DM, Dunn FA, Takao M. (2002). Phototransduction by Retinal Ganglion Cells That Set the Circadian Clock. Science 295:1070 1073. doi:10.1126/science.1067262

Bertuzzi, S., Hindges, R., Mui, S. H., O'Leary, D. D., & Lemke, G. (1999). The homeodomain protein vax1 is required for axon guidance and major tract formation in the developing forebrain. *Genes & Development*, *13*(23), 3092 3105.

Bessa, J., Tavares, M. J., Santos, J., Kikuta, H., Laplante, M., Becker, T. S., et al. (2008). meis1 regulates cyclin D1 and c-myc expression, and controls the proliferation of the multipotent cells in the early developing zebrafish eye. *Development (Cambridge, England)*, *135*(5), 799 803. http://doi.org/10.1242/dev.011932

Braunger, B. M., Pielmeier, S., Demmer, C., Landstorfer, V., Kawall, D., Abramov, N., et al. (2013). TGF- Signaling Protects Retinal Neurons from Programmed Cell Death during the Development of the Mammalian Eye. *The Journal of Neuroscience : the Official Journal of the Society for Neuroscience*, *33*(35), 14246 14258. http://doi.org/10.1523/JNEUROSCI.0991-13.2013

Brown, N. L., Kanekar, S., Vetter, M. L., Tucker, P. K., Gemza, D. L., & Glaser, T. (1998). Math5 encodes a murine basic helix-loop-helix transcription factor

expressed during early stages of retinal neurogenesis. *Development (Cambridge, England)*, *125*(23), 4821 4833.

Brown, N. L., Patel, S., Brzezinski, J., & Glaser, T. (2001). Math5 is required for retinal ganglion cell and optic nerve formation. *Development (Cambridge, England)*, *128*(13), 2497 2508.

Brzezinski, J. A., Brown, N. L., Tanikawa, A., Bush, R. A., Sieving, P. A., Vitaterna, M. H., et al. (2005). Loss of circadian photoentrainment and abnormal retinal electrophysiology in Math5 mutant mice. *Investigative Ophthalmology & Visual Science*, *46*(7), 2540 2551. http://doi.org/10.1167/iovs.04-1123

Brzezinski, J. A., Prasov, L., & Glaser, T. (2012). Math 5 defines the ganglion cell competence state in a subpopulation of retinal progenitor cells exiting the cell cycle. *Developmental Biology*, *365*(2), 395 413. http://doi.org/10.1016/j.ydbio.2012.03.006

Cai, Z., Feng, G.-S., & Zhang, X. (2010). Temporal Requirement of the Protein Tyrosine Phosphatase Shp2 in Establishing the Neuronal Fate in Early Retinal Development. *The Journal of Neuroscience : the Official Journal of the Society for Neuroscience*, *30*(11), 4110 4119. http://doi.org/10.1523/JNEUROSCI.4364-09.2010

Carbe, C., Garg, A., Cai, Z., Li, H., Powers, A., & Zhang, X. (2013). An allelic series at the paired box gene 6 (Pax6) locus reveals the functional specificity of Pax genes. *Journal of Biological Chemistry*, *288*(17), 12130 12141. http://doi.org/10.1074/jbc.M112.436865

Carter-Dawson, L. D., & LaVail, M. M. (1979). Rods and cones in the mouse retina. I. Structural analysis using light and electron microscopy. *The Journal of Comparative Neurology*, *188*(2), 245 262. http://doi.org/10.1002/cne.901880204

Chalasani, S. H., Sabol, A., Xu, H., Gyda, M. A., Rasband, K., Granato, M., et al. (2007). Stromal cell-derived factor-1 antagonizes slit/robo signaling in vivo. *Journal of Neuroscience*, *27*(5), 973 980. http://doi.org/10.1523/JNEUROSCI.4132-06.2007

Chapman, D. L., Garvey, N., Hancock, S., Alexiou, M., Agulnik, S. I., Gibson-Brown, J. J., et al. (1996). Expression of the T-box family genes, Tbx1-Tbx5, during early mouse development. *Developmental Dynamics*, *206*(4), 379 390. http://doi.org/10.1002/(SICI)1097-0177(199608)206:4<379::AID-AJA4>3.0.CO;2-F

Chen, M., Chen, Q., Sun, X., Shen, W., Liu, B., Zhong, X., et al. (2010). Generation of retinal ganglion-like cells from reprogrammed mouse fibroblasts. *Investigative Ophthalmology & Visual Science*, *51*(11), 5970 5978. http://doi.org/10.1167/iovs.09-4504

Chen, S. K., & Hattar, S. (2012). Photoentrainment and pupillary light reflex are mediated by distinct populations of ipRGCs. *Nature*, *476*(7358), 92 95. http://doi.org/10.1038/nature10206

Chen, S.-K., Chew, K. S., McNeill, D. S., Keeley, P. W., Ecker, J. L., Mao, B. Q., et al. (2013). Apoptosis regulates ipRGC spacing necessary for rods and cones to drive circadian photoentrainment. *Neuron*, *77*(3), 503 515. http://doi.org/10.1016/j.neuron.2012.11.028

Choy SW, Cheng CW, Lee ST, Li VWT, Hui MNY, Hui C-C, Liu D, Cheng SH. (2010). A cascade of irx1a and irx2a controls shh expression during retinogenesis. Dev Dyn Official Publ Am Assoc Anatomists 239:3204 14. doi:10.1002/dvdy.22462

Chuang, J. C., & Raymond, P. A. (2001). Zebrafish genes rx1 and rx2 help define the region of forebrain that gives rise to retina. *Developmental Biology*, *231*(1), 13 30. http://doi.org/10.1006/dbio.2000.0125

Clark, B. S., Stein-O'Brien, G. L., Shiau, F., Cannon, G. H., Davis-Marcisak, E., Sherman, T., et al. (2019). Single-Cell RNA-Seq Analysis of Retinal Development Identifies NFI Factors as Regulating Mitotic Exit and Late-Born Cell Specification. *Neuron*, *102*(6), 1 22. http://doi.org/10.1016/j.neuron.2019.04.010

Cordero-Llana, O., Rinaldi, F., Brennan, P. A., Wynick, D., & Caldwell, M. A. (2014). Galanin promotes neuronal differentiation from neural progenitor cells in vitro and contributes to the generation of new olfactory neurons in the adult mouse brain. *Experimental Neurology*, *256*, 93 104. http://doi.org/10.1016/j.expneurol.2014.04.001

Dattani, M. T., Martinez-Barbera, J.-P., Thomas, P. Q., Brickman, J. M., Gupta, R., Mårtensson, I.-L., et al. (1998). Mutations in the homeobox gene HESX1/Hesx1 associated with septo-optic dysplasia in human and mouse. *Nature Genetics*, *19*(2), 125 133. http://doi.org/10.1038/477

de Melo, J., Du, G., Fonseca, M., Gillespie, L.-A., Turk, W. J., Rubenstein, J. L. R., & Eisenstat, D. D. (2005). Dlx1 and Dlx2 function is necessary for terminal

differentiation and survival of late-born retinal ganglion cells in the developing mouse retina. *Development (Cambridge, England)*, *132*(2), 311 322. http://doi.org/10.1242/dev.01560

de Melo, J., Zhou, Q. P., Zhang, Q., Zhang, S., Fonseca, M., Wigle, J. T., & Eisenstat, D. D. (2007). Dlx2 homeobox gene transcriptional regulation of Trkb neurotrophin receptor expression during mouse retinal development. *Nucleic Acids Research*, *36*(3), 872 884. http://doi.org/10.1093/nar/gkm1099

Del Bene, F., Ettwiller, L., Skowronska-Krawczyk, D., Baier, H., Matter, J.-M., Birney, E., & Wittbrodt, J. (2007). In vivo validation of a computationally predicted conserved Ath5 target gene set. *PLoS Genetics*, *3*(9), 1661 1671. http://doi.org/10.1371/journal.pgen.0030159

Ding, Q., Chen, H., Xie, X., Libby, R. T., Tian, N., & Gan, L. (2009). BARHL2 differentially regulates the development of retinal amacrine and ganglion neurons. *The Journal of Neuroscience : the Official Journal of the Society for Neuroscience*, *29*(13), 3992 4003. http://doi.org/10.1523/JNEUROSCI.5237-08.2009

Do MTH. (2019). Melanopsin and the Intrinsically Photosensitive Retinal Ganglion Cells: Biophysics to Behavior. Neuron 104:205 226. doi:10.1016/j.neuron.2019.07.016

Do MTH, Yau K-W. (2010). Intrinsically photosensitive retinal ganglion cells. Physiol Rev 90:1547 81. doi:10.1152/physrev.00013.2010

Dorrell, M. I., Aguilar, E., & Friedlander, M. (2002). Retinal vascular development is mediated by endothelial filopodia, a preexisting astrocytic template and specific R-cadherin adhesion. *Investigative Ophthalmology & Visual Science*, *43*(11), 3500 3510.

Edwards, M. M., McLeod, D. S., Grebe, R., Heng, C., Lefebvre, O., & Lutty, G. A. (2011). Lama1 mutations lead to vitreoretinal blood vessel formation, persistence of fetal vasculature, and epiretinal membrane formation in mice. *Bmc Developmental Biology*, *11*(1), 60. http://doi.org/10.1186/1471-213X-11-60

Edwards, M. M., McLeod, D. S., Li, R., Grebe, R., Bhutto, I., Mu, X., & Lutty, G. A. (2012). The deletion of Math5 disrupts retinal blood vessel and glial development in mice. *Experimental Eye Research*, *96*(1), 147 156. http://doi.org/10.1016/j.exer.2011.12.005

Eisenstat, D. D., Liu, J. K., Mione, M., & Zhong, W. (1999). DLX-1, DLX-2, and DLX-5 expression define distinct stages of basal forebrain differentiation. *Journal of ...*. http://doi.org/10.1002/(SICI)1096-9861(19991115)414:2<217::AID-CNE6>3.0.CO;2-I

Ekström P, Johansson K. (2003). Differentiation of ganglion cells and amacrine cells in the rat retina: correlation with expression of HuC/D and GAP-43 proteins. Dev Brain Res 145:1 8. doi:10.1016/s0165-3806(03)00170-6

Elshatory, Y., Everhart, D., Deng, M., Xie, X., Barlow, R. B., & Gan, L. (2007). Islet-1 Controls the Differentiation of Retinal Bipolar and Cholinergic Amacrine Cells.

Journal of Neuroscience, *27*(46), 12707 12720. http://doi.org/10.1523/JNEUROSCI.3951-07.2007

Erkman, L., McEvilly, R. J., Luo, L., Ryan, A. K., Hooshmand, F., O'Connell, S. M., et al. (1996). Role of transcription factors Brn-3.1 and Brn-3.2 in auditory and visual system development. *Nature*, *381*(6583), 603 606. http://doi.org/10.1038/381603a0

Fan, B. J., Wang, D. Y., Pasquale, L. R., Haines, J. L., & Wiggs, J. L. (2011). Genetic variants associated with optic nerve vertical cup-to-disc ratio are risk factors for primary open angle glaucoma in a US Caucasian population. *Investigative Ophthalmology & Visual Science*, *52*(3), 1788 1792. http://doi.org/10.1167/iovs.10-6339

Farah, M. H., & Easter, S. S. (2005). Cell birth and death in the mouse retinal ganglion cell layer. *The Journal of Comparative Neurology*, *489*(1), 120 134. http://doi.org/10.1002/cne.20615

Feng, L., Eisenstat, D. D., Chiba, S., Ishizaki, Y., Gan, L., & Shibasaki, K. (2011). Brn-3b inhibits generation of amacrine cells by binding to and negatively regulating DLX1/2 in developing retina. *Neuroscience*, *195*(C), 9 20. http://doi.org/10.1016/j.neuroscience.2011.08.015

Feng, L., Xie, Z.-H., Ding, Q., Xie, X., Libby, R. T., & Gan, L. (2010). MATH5 controls the acquisition of multiple retinal cell fates. *Molecular Brain*, *3*(1), 36. http://doi.org/10.1186/1756-6606-3-36

Frade, J. M., Bovolenta, P., MartinezMorales, J. R., Arribas, A., & RodriguezTebar, A. (1997). Control of early cell death by BDNF in the chick retina. *Development (Cambridge, England)*, *124*(17), 3313 3320.

French, C. R., Erickson, T., Callander, D., Berry, K. M., Koss, R., Hagey, D. W., et al. (2007). Pbx homeodomain proteins pattern both the zebrafish retina and tectum. *Bmc Developmental Biology*, *7*(1). http://doi.org/10.1186/1471-213X-7-85

Fuhrmann, S. (2010). Eye Morphogenesis and Patterning of the Optic Vesicle. *Current Topics in Developmental Biology*, *93*, 61 84. http://doi.org/10.1016/B978-0-12-385044-7.00003-5

Furukawa, T., Kozak, C. A., & Cepko, C. L. (1997). rax, a novel paired-type homeobox gene, shows expression in the anterior neural fold and developing retina. *Proceedings of the National Academy of Sciences of the United States of America*, *94*(7), 3088 3093. http://doi.org/10.1073/pnas.94.7.3088

Gan, L., Wang, S. W., Huang, Z., & Klein, W. H. (1999). POU domain factor Brn-3b is essential for retinal ganglion cell differentiation and survival but not for initial cell fate specification. *Developmental Biology*, *210*(2), 469 480. http://doi.org/10.1006/dbio.1999.9280

Gan, L., Xiang, M., Zhou, L., Wagner, D. S., Klein, W. H., & Nathans, J. (1996). POU domain factor Brn-3b is required for the development of a large set of retinal ganglion cells. *Proceedings of the National Academy of Sciences of the United States of America*, *93*(9), 3920 3925. http://doi.org/10.1073/pnas.93.9.3920

Gao, Z., Mao, C.-A., Pan, P., Mu, X., & Klein, W. H. (2014). Transcriptome of Atoh7 retinal progenitor cells identifies new Atoh7-dependent regulatory genes for retinal ganglion cell formation. *Developmental Neurobiology*, *74*(11), 1123 1140. http://doi.org/10.1002/dneu.22188

Giudice QL, Leleu M, Manno GL, Fabre PJ. (2019). Single-cell transcriptional logic of cell-fate specification and axon guidance in early born retinal neurons. Dev Camb Engl 146:dev178103. doi:10.1242/dev.178103

Ghiasvand NM, Rudolph DD, Mashayekhi M, Brzezinski JA, Goldman D, Glaser T. (2011). Deletion of a remote enhancer near ATOH7 disrupts retinal neurogenesis, causing NCRNA disease. Nat Neurosci 14:578 86. doi:10.1038/nn.2798

Grindley, J. C., Davidson, D. R., & Hill, R. E. (1995). The role of Pax-6 in eye and nasal development. *Development (Cambridge, England)*, *121*(5), 1433 1442.

Haghverdi L, Büttner M, Wolf FA, Buettner F, Theis FJ. (2016). Diffusion pseudotime robustly reconstructs lineage branching. Nat Methods 13:845 848. doi:10.1038/nmeth.3971

Halder, G., Callaerts, P., & Gehring, W. J. (1995). Induction of ectopic eyes by targeted expression of the eyeless gene in Drosophila. *Science (New York, N.Y.)*, *267*(5205), 1788 1792. http://doi.org/10.1126/science.7892602

Hallonet, M., Hollemann, T., Wehr, R., Jenkins, N. A., Copeland, N. G., Pieler, T., & Gruss, P. (1998). Vax1 is a novel homeobox-containing gene expressed in the

developing anterior ventral forebrain. *Development (Cambridge, England)*, *125*(14), 2599 2610. http://doi.org/10.1101/gad.13.23.3106

Harada, C., Harada, T., Nakamura, K., Sakai, Y., Tanaka, K., & Parada, L. F. (2006). Effect of p75NTR on the regulation of naturally occurring cell death and retinal ganglion cell number in the mouse eye. *Developmental Biology*, *290*(1), 57 65. http://doi.org/10.1016/j.ydbio.2005.08.051

Hashimoto, T., Zhang, X.-M., Chen, B. Y.-K., & Yang, X.-J. (2006). VEGF activates divergent intracellular signaling components to regulate retinal progenitor cell proliferation and neuronal differentiation. *Development (Cambridge, England)*, *133*(11), 2201 2210. http://doi.org/10.1242/dev.02385

Hattar S, Liao H-W, Takao M, Berson DM, Yau K-W. (2002). Melanopsin-Containing Retinal Ganglion Cells: Architecture, Projections, and Intrinsic Photosensitivity. Science 295:1065 1070. doi:10.1126/science.1069609

Heine, P., Dohle, E., Bumsted-O'Brien, K., Engelkamp, D., & Schulte, D. (2008). Evidence for an evolutionary conserved role of homothorax/Meis1/2 during vertebrate retina development. *Development (Cambridge, England)*, *135*(5), 805 811. http://doi.org/10.1242/dev.012088

Heinz S, Benner C, Spann N, Bertolino E, Lin YC, Laslo P, Cheng JX, Murre C, Singh H, Glass CK. (2010). Simple combinations of lineage-determining transcription factors prime cis-regulatory elements required for macrophage and B cell identities. Mol Cell 38:576 89. doi:10.1016/j.molcel.2010.05.004

Heskamp, A., Leibinger, M., Andreadaki, A., Gobrecht, P., Diekmann, H., & Fischer, D. (2013). CXCL12/SDF-1 facilitates optic nerve regeneration. *Neurobiology of Disease*, *55*, 76 86. http://doi.org/10.1016/j.nbd.2013.04.001

Hinds, J. W., & Hinds, P. L. (1979). Differentiation of photoreceptors and horizontal cells in the embryonic mouse retina: an electron microscopic, serial section analysis. *The Journal of Comparative Neurology*, *187*(3), 495 511. http://doi.org/10.1002/cne.901870303

Hoffmann, E. M., Zangwill, L. M., Crowston, J. G., & Weinreb, R. N. (2007). Optic disk size and glaucoma. *Survey of Ophthalmology*, *52*(1), 32 49. http://doi.org/10.1016/j.survophthal.2006.10.002

Holmes, F. E., Mahoney, S., King, V. R., Bacon, A., Kerr, N. C., Pachnis, V., et al. (2000). Targeted disruption of the galanin gene reduces the number of sensory neurons and their regenerative capacity. *Proceedings of the National Academy of Sciences of the United States of America*, *97*(21), 11563 11568. http://doi.org/10.1073/pnas.210221897

Hufnagel, R. B., Le, T. T., Riesenberg, A. L., & Brown, N. L. (2010). Neurog2 controls the leading edge of neurogenesis in the mammalian retina. *Developmental Biology*, *340*(2), 490 503. http://doi.org/10.1016/j.ydbio.2010.02.002

Hufnagel, R. B., Riesenberg, A. N., Quinn, M., Brzezinski, J. A., Glaser, T., & Brown, N. L. (2013). Heterochronic misexpression of Ascl1 in the Atoh7 retinal cell lineage blocks cell cycle exit. *Molecular and Cellular Neuroscience*, *54*, 108 120. http://doi.org/10.1016/j.mcn.2013.02.004

Hyer, J., Kuhlman, J., Afif, E., & Mikawa, T. (2003). Optic cup morphogenesis requires pre-lens ectoderm but not lens differentiation. *Developmental Biology*, *259*(2), 351 363. http://doi.org/10.1016/S0012-1606(03)00205-7

Jarman, A. P., Grau, Y., Jan, L. Y., & Jan, Y. N. (1995). Role of the proneural gene, atonal, in formation of Drosophila chordotonal organs and photoreceptors. *Cell*, *73*(7), 1 12. http://doi.org/10.1016/0092-8674(93)90358-w

Jarman, A. P., Grell, E. H., Ackerman, L., Jan, L. Y., & Jan, Y. N. (1994). Atonal is the proneural gene for Drosophila photoreceptors. *Nature*, *369*(6479), 398 400. http://doi.org/10.1038/369398a0

Kanekar S, Perron M, Dorsky R, Harris WA, Jan LY, Jan YN, Vetter ML. (1997). Xath5 Participates in a Network of bHLH Genes in the Developing Xenopus Retina. Neuron 19:981 994. doi:10.1016/s0896-6273(00)80391-8

Kay, J. N., Finger-Baier, K. C., Roeser, T., Staub, W., & Baier, H. (2001). Retinal ganglion cell genesis requires lakritz, a Zebrafish atonal Homolog. *Neuron*, *30*(3), 725 736. http://doi.org/10.1016/S0896-6273(01)00312-9

Kelberman, D., & Dattani, M. T. (2007). Genetics of septo-optic dysplasia. *Pituitary*, *10*(4), 393 407. http://doi.org/10.1007/s11102-007-0055-5

Khan, K., Logan, C. V., McKibbin, M., Sheridan, E., Elçioglu, N. H., Yenice, O., et al. (2012). Next generation sequencing identifies mutations in Atonal homolog 7 (ATOH7) in families with global eye developmental defects. *Human Molecular Genetics*, *21*(4), 776 783. http://doi.org/10.1093/hmg/ddr509

Khor, C. C., Ramdas, W. D., Vithana, E. N., Cornes, B. K., Sim, X., Tay, W.-T., et al. (2011). Genome-wide association studies in Asians confirm the involvement of ATOH7 and TGFBR3, and further identify CARD10 as a novel locus influencing optic disc area. *Human Molecular Genetics*, *20*(9), 1864 1872. http://doi.org/10.1093/hmg/ddr060

Kim, J., Wu, H.-H., Lander, A. D., Lyons, K. M., Matzuk, M. M., & Calof, A. L. (2005). GDF11 controls the timing of progenitor cell competence in developing retina. *Science (New York, N.Y.)*, *308*(5730), 1927 1930. http://doi.org/10.1126/science.1110175

Kiyama, T., Mao, C.-A., Cho, J.-H., Fu, X., Pan, P., Mu, X., & Klein, W. H. (2011). Overlapping spatiotemporal patterns of regulatory gene expression are required for neuronal progenitors to specify retinal ganglion cell fate. *Vision Research*, *51*(2), 251 259. http://doi.org/10.1016/j.visres.2010.10.016

Knudson, C. M., Tung, K. S., Tourtellotte, W. G., Brown, G. A., & Korsmeyer, S. J. (1995). Bax-deficient mice with lymphoid hyperplasia and male germ cell death. *Science (New York, N.Y.)*, *270*(5233), 96 99. http://doi.org/10.1126/science.270.5233.96

Koshiba-Takeuchi, K., Takeuchi, J. K., Matsumoto, K., Momose, T., Uno, K., Hoepker, V., et al. (2000). Tbx5 and the retinotectum projection. *Science (New York, N.Y.)*, *287*(5450), 134 137. http://doi.org/10.1126/science.287.5450.134

Kruger K, Tam AS, Lu C, Sretavan DW. (1998). Retinal Ganglion Cell Axon Progression from the Optic Chiasm to Initiate Optic Tract Development Requires Cell

Autonomous Function of GAP-43. J Neurosci 18:5692 5705. doi:10.1523/jneurosci.18-15-05692.1998

Lagutin, O., Zhu, C. C., Furuta, Y., Rowitch, D. H., McMahon, A. P., & Oliver, G. (2001). Six3 promotes the formation of ectopic optic vesicle-like structures in mouse embryos. *Developmental Dynamics*, *221*(3), 342 349. http://doi.org/10.1002/dvdy.1148

Langmead B, Salzberg SL. (2012). Fast gapped-read alignment with Bowtie 2. Nat Methods 9:357 9. doi:10.1038/nmeth.1923

Le, T. T., Wroblewski, E., Patel, S., Riesenberg, A. N., & Brown, N. L. (2006). Math5 is required for both early retinal neuron differentiation and cell cycle progression. *Developmental Biology*, *295*(2), 764 778. http://doi.org/10.1016/j.ydbio.2006.03.055

Li H, Handsaker B, Wysoker A, Fennell T, Ruan J, Homer N, Marth G, Abecasis G, Durbin R, Subgroup 1000 Genome Project Data Processing. (2009). The Sequence Alignment/Map format and SAMtools. Bioinform Oxf Engl 25:2078 9. doi:10.1093/bioinformatics/btp352

Li, Q. (2005). Chemokine Signaling Guides Axons within the Retina in Zebrafish. *The Journal of Neuroscience : the Official Journal of the Society for Neuroscience*, *25*(7), 1711 1717. http://doi.org/10.1523/JNEUROSCI.4393-04.2005

Li, R., Wu, F., Ruonala, R., Sapkota, D., Hu, Z., & Mu, X. (2014). Isl1 and pou4f2 form a complex to regulate target genes in developing retinal ganglion cells. *PLoS ONE*, *9*(3), e92105 e92105. http://doi.org/10.1371/journal.pone.0092105

Li, X., Perissi, V., Liu, F., Rose, D. W., & Rosenfeld, M. G. (2002). Tissue-specific regulation of retinal and pituitary precursor cell proliferation. *Science (New York, N.Y.)*, *297*(5584), 1180 1183.

Linden, R., & PINTO, L. H. (1985). Developmental genetics of the retina: evidence that the pearl mutation in the mouse affects the time course of natural cell death in the ganglion cell layer. *Experimental Brain Research*, *60*(1), 79 86.

LIU, I., CHEN, J. D., Ploder, L., Vidgen, D., VANDERKOOY, D., Kalnins, V. I., & McInnes, R. R. (1994). Developmental Expression of a Novel Murine Homeobox Gene (Chx10) - Evidence for Roles in Determination of the Neuroretina and Inner Nuclear Layer. *Neuron*, *13*(2), 377 393. http://doi.org/10.1016/0896-6273(94)90354-9

Liu, W., Lagutin, O., Swindell, E., Jamrich, M., & Oliver, G. (2010). Neuroretina specification in mouse embryos requires Six3-mediated suppression of Wnt8b in the anterior neural plate. *The Journal of Clinical Investigation*, *120*(120(10)), 3568 3577. http://doi.org/10.1172/JCI43219

Long, J. Z., Svensson, K. J., Tsai, L., Zeng, X., Roh, H. C., Kong, X., et al. (2014). A smooth muscle-like origin for beige adipocytes. *Cell Metabolism*, *19*(5), 810 820. http://doi.org/10.1016/j.cmet.2014.03.025

Lu Y, Shiau F, Yi W, Lu S, Wu Q, Pearson JD, Kallman A, Zhong S, Hoang T, Zuo Z, Zhao F, Zhang M, Tsai N, Zhuo Y, He S, Zhang J, Stein-O'Brien GL, Sherman TD, Duan X, Fertig EJ, Goff LA, Zack DJ, Handa JT, Xue T, Bremner R, Blackshaw S, Wang X, Clark BS. (2020). Single-Cell Analysis of Human Retina

Identifies Evolutionarily Conserved and Species-Specific Mechanisms Controlling Development. Dev Cell. doi:10.1016/j.devcel.2020.04.009

Macgregor, S., Hewitt, A. W., Hysi, P. G., Ruddle, J. B., Medland, S. E., Henders, A. K., et al. (2010). Genome-wide association identifies ATOH7 as a major gene determining human optic disc size. *Human Molecular Genetics*, *19*(13), 2716 2724. http://doi.org/10.1093/hmg/ddq144

Madisen, L., Zwingman, T. A., Sunkin, S. M., Oh, S. W., Zariwala, H. A., Gu, H., et al. (2010). A robust and high-throughput Cre reporting and characterization system for the whole mouse brain. *Nature Neuroscience*, *13*(1), 133 140. http://doi.org/10.1038/nn.2467

Mao, C. A., Cho, J. H., Wang, J., Gao, Z., Pan, P., Tsai, W. W., et al. (2013). Reprogramming amacrine and photoreceptor progenitors into retinal ganglion cells by replaceing Neurod1 with Atoh7. *Development (Cambridge, England)*, *140*(13), 2849 2849. http://doi.org/10.1242/dev.099549

Mao, C.-A. C., Wang, S. W. S., Pan, P. P., & Klein, W. H. W. (2008a). Rewiring the retinal ganglion cell gene regulatory network: Neurod1 promotes retinal ganglion cell fate in the absence of Math5. *Development (Cambridge, England)*, *135*(20), 3379 3388. http://doi.org/10.1242/dev.024612

Mao, C.-A., Kiyama, T., Pan, P., Furuta, Y., Hadjantonakis, A.-K., & Klein, W. H. (2008b). Eomesodermin, a target gene of Pou4f2, is required for retinal ganglion cell and optic nerve development in the mouse. *Development (Cambridge, England)*, *135*(2), 271 280. http://doi.org/10.1242/dev.009688

Mao, C.-A., Li, H., Zhang, Z., Kiyama, T., Panda, S., Hattar, S., et al. (2014). T-box Transcription Regulator Tbr2 Is Essential for the Formation and Maintenance of Opn4/Melanopsin-Expressing Intrinsically Photosensitive Retinal Ganglion Cells. *The Journal of Neuroscience : the Official Journal of the Society for Neuroscience*, *34*(39), 13083 13095. http://doi.org/10.1523/JNEUROSCI.1027-14.2014

Marquardt, T., Ashery-Padan, R., Andrejewski, N., Scardigli, R., Guillemot, F., & Gruss, P. (2001). Pax6 Is Required for the Multipotent State of Retinal Progenitor Cells. *Cell*, *105*(1), 43 55. http://doi.org/10.1016/S0092-8674(01)00295-1

Masland, R. (2001). Neuronal diversity in the retinaRichard H Masland. *Current Opinion in Neurobiology*, *11*(4), 1 6. http://doi.org/10.1016/s0959-4388(00)00230-0

Mathers, P. H., Grinberg, A., Mahon, K. A., & Jamrich, M. (1997). The Rx homeobox gene is essential for vertebrate eye development. *Nature*, *387*(6633), 603 607. http://doi.org/10.1038/42475

McCabe, M. J., Alatzoglou, K. S., & Dattani, M. T. (2011). Septo-optic dysplasia and other midline defects: The role of transcription factors: HESX1 and beyond. *Best Practice & Research Clinical Endocrinology & Metabolism*, *25*(1), 115 124. http://doi.org/10.1016/j.beem.2010.06.008

McFarland, J. M., Cui, Y., & Butts, D. A. (2013). Inferring nonlinear neuronal computation based on physiologically plausible inputs. *PLoS Computational Biology*, *9*(7), e1003143. http://doi.org/10.1371/journal.pcbi.1003143

Miesfeld JB, Ghiasvand NM, Marsh-Armstrong B, Marsh-Armstrong N, Miller EB,

Zhang P, Manna SK, Zawadzki RJ, Brown NL, Glaser T. (2020). The Atoh7 remote enhancer provides transcriptional robustness during retinal ganglion cell development. Proc National Acad Sci 202006888. doi:10.1073/pnas.2006888117

Meers MP, Bryson TD, Henikoff JG, Henikoff S. (2019). Improved CUT&RUN chromatin profiling tools. Elife 8:e46314. doi:10.7554/elife.46314

Miesfeld, J. B., Moon, M.-S., Riesenberg, A. N., Contreras, A. N., Kovall, R. A., & Brown, N. L. (2018). Rbpj direct regulation of Atoh7 transcription in the embryonic mouse retina. *Scientific Reports*, *8*(1), 10195. http://doi.org/10.1038/s41598-018-28420-y

Miesfeld JB, Glaser T, Brown NL. (2018a). The dynamics of native Atoh7 protein expression during mouse retinal histogenesis, revealed with a new antibody. Gene Expr Patterns 27:114 121. doi:10.1016/j.gep.2017.11.006

Mo, Z., Li, S., Yang, X., & Xiang, M. (2004). Role of the Barhl2 homeobox gene in the specification of glycinergic amacrine cells. *Development (Cambridge, England)*, *131*(7), 1607 1618. http://doi.org/10.1242/dev.01071

Mombaerts P, Wang F, Dulac C, Chao SK, Nemes A, Mendelsohn M, Edmondson J, Axel R. (1996). Visualizing an Olfactory Sensory Map. Cell 87:675 686. doi:10.1016/s0092-8674(00)81387-2

Morin, L. P., & Studholme, K. M. (2014). Retinofugal projections in the mouse. *Journal of Comparative Neurology*, *522*(16), 3733 3753. http://doi.org/10.1002/cne.23635

Morris R. (1984). Developments of a water-maze procedure for studying spatial learning in the rat. J Neurosci Meth 11:47 60. doi:10.1016/0165-0270(84)90007-4

Mosinger Ogilvie, J., Deckwerth, T. L., Knudson, C. M., & Korsmeyer, S. J. (1998). Suppression of developmental retinal cell death but not of photoreceptor degeneration in Bax-deficient mice. *Investigative Ophthalmology & Visual Science*, *39*(9), 1713 1720. Retrieved from http://eutils.ncbi.nlm.nih.gov/entrez/eutils/elink.fcgi?dbfrom=pubmed&id=9699561&retmode=ref&cmd=prlinks

Mu, X. X., Fu, X. X., Sun, H. H., Beremand, P. D. P., Thomas, T. L. T., & Klein, W. H. W. (2005a). A gene network downstream of transcription factor Math5 regulates retinal progenitor cell competence and ganglion cell fate. *Developmental Biology*, *280*(2), 15 15. http://doi.org/10.1016/j.ydbio.2005.01.028

Mu, X., Beremand, P. D., Zhao, S., Pershad, R., Sun, H., Scarpa, A., et al. (2004). Discrete gene sets depend on POU domain transcription factor Brn3b/Brn-3.2/POU4f2 for their expression in the mouse embryonic retina. *Development (Cambridge, England)*, *131*(6), 1197 1210. http://doi.org/10.1242/dev.01010

Mu, X., Fu, X., Beremand, P. D., Thomas, T. L., & Klein, W. H. (2008). Gene regulation logic in retinal ganglion cell development: Isl1 defines a critical branch distinct from but overlapping with Pou4f2. *Proceedings of the National Academy of Sciences*, *105*(19), 6942 6947. http://doi.org/10.1073/pnas.0802627105

Mu, X., Fu, X., Sun, H., Liang, S., Maeda, H., Frishman, L. J., & Klein, W. H. (2005b). Ganglion cells are required for normal progenitor- cell proliferation but not cell-

fate determination or patterning in the developing mouse retina. *Current Biology*, *15*(6), 525 530. http://doi.org/10.1016/j.cub.2005.01.043

Nguyen, M., & Arnheiter, H. (2000). Signaling and transcriptional regulation in early mammalian eye development: a link between FGF and MITF. *Development (Cambridge, England)*, *127*(16), 3581 3591.

Nguyen, M.-T. T., Vemaraju, S., Nayak, G., Odaka, Y., Buhr, E. D., Alonzo, N., et al. (2019). An opsin 5-dopamine pathway mediates light-dependent vascular development in the eye. *Nature Cell Biology*, *21*(4), 420 429. http://doi.org/10.1038/s41556-019-0301-x

Nishiguchi, K. M., Nakamura, M., Kaneko, H., Kachi, S., & Terasaki, H. (2007). The role of VEGF and VEGFR2/Flk1 in proliferation of retinal progenitor cells in murine retinal degeneration. *Investigative Ophthalmology & Visual Science*, *48*(9), 4315 4320. http://doi.org/10.1167/iovs.07-0354

NORNES, H. O., DRESSLER, G. R., KNAPIK, E. W., DEUTSCH, U., & Gruss, P. (1990). Spatially and temporally restricted expression of Pax2 during murine neurogenesis. *Development (Cambridge, England)*, *109*(4), 797 809.

Ogilvie JM, Deckwerth TL, Knudson CM, Korsmeyer SJ. (1998). Suppression of developmental retinal cell death but not of photoreceptor degeneration in Bax-deficient mice. Investigative Ophthalmology & Visual Science 39:1713 1720.

Ohnuma, S.-I., Hopper, S., Wang, K. C., Philpott, A., & Harris, W. A. (2002). Co-ordinating retinal histogenesis: early cell cycle exit enhances early cell fate

determination in the Xenopus retina. *Development (Cambridge, England)*, *129*(10), 2435 2446.

Oliver, G., Mailhos, A., Wehr, R., Copeland, N. G., Jenkins, N. A., & Gruss, P. (1995). Six3, a murine homologue of the sine oculis gene, demarcates the most anterior border of the developing neural plate and is expressed during eye development. *Development (Cambridge, England)*, *121*(12), 4045 4055.

Oster, S. F., Deiner, M., Birgbauer, E., & Sretavan, D. W. (2004). Ganglion cell axon pathfinding in the retina and optic nerve. *Seminars in Cell & Developmental Biology*, *15*(1), 125 136. http://doi.org/10.1016/j.semcdb.2003.09.006

Pacal, M., & Bremner, R. (2014). Induction of the ganglion cell differentiation program in human retinal progenitors before cell cycle exit. *Developmental Dynamics*, *243*(5), 712 729. http://doi.org/10.1002/dvdy.24103

Pak, W., Hindges, R., Lim, Y.-S., Pfaff, S. L., & O'Leary, D. D. M. (2004). Magnitude of binocular vision controlled by islet-2 repression of a genetic program that specifies laterality of retinal axon pathfinding. *Cell*, *119*(4), 567 578. http://doi.org/10.1016/j.cell.2004.10.026

Pan, L., Deng, M., Xie, X., & Gan, L. (2008). ISL1 and BRN3B co-regulate the differentiation of murine retinal ganglion cells. *Development (Cambridge, England)*, *135*(11), 1981 1990. http://doi.org/10.1242/dev.010751

Pan, L., Yang, Z., Feng, L., & Gan, L. (2005). Functional equivalence of Brn3 POU-domain transcription factors in mouse retinal neurogenesis. *Development (Cambridge, England)*, *132*(4), 703 712. http://doi.org/10.1242/dev.01646

Panza P, Sitko AA, Maischein H-M, Koch I, Flötenmeyer M, Wright GJ, Mandai K, Mason CA, Söllner C. (2015). The LRR receptor Islr2 is required for retinal axon routing at the vertebrate optic chiasm. Neural Dev 10:23. doi:10.1186/s13064-015-0050-x

Péquignot, M. O., Provost, A. C., Sallé, S., Taupin, P., Sainton, K. M., Marchant, D., et al. (2003). Major role of BAX in apoptosis during retinal development and in establishment of a functional postnatal retina. *Developmental Dynamics*, *228*(2), 231 238. http://doi.org/10.1002/dvdy.10376

Pittman, A. J., Law, M. Y., & Chien, C. B. (2008). Pathfinding in a large vertebrate axon tract: isotypic interactions guide retinotectal axons at multiple choice points. *Development (Cambridge, England)*, *135*(17), 2865 2871. http://doi.org/10.1242/dev.025049

Poggi, L., Vitorino, M., Masai, I., & Harris, W. A. (2005). Influences on neural lineage and mode of division in the zebrafish retina in vivo. *Journal of Cell Biology*, *171*(6), 991 999. http://doi.org/10.1083/jcb.200509098

Polański K, Young MD, Miao Z, Meyer KB, Teichmann SA, Park J-E. (2019). BBKNN: fast batch alignment of single cell transcriptomes. Bioinformatics. doi:10.1093/bioinformatics/btz625

Pollock, G. S., Robichon, R., Boyd, K. A., Kerkel, K. A., Kramer, M., Lyles, J., et al. (2003). TrkB receptor signaling regulates developmental death dynamics, but not final number, of retinal ganglion cells. *The Journal of Neuroscience : the Official Journal of the Society for Neuroscience*, *23*(31), 10137 10145.

Prasov, L. (2012). *The role of Math5 (Atoh7) in retinal and optic nerve development and human disease*. (T. T. Glaser, Ed.). University of Michigan.

Prasov, L., & Glaser, T. (2012a). Dynamic expression of ganglion cell markers in retinal progenitors during the terminal cell cycle. *Molecular and Cellular Neuroscience*, *50*(2), 160 168. http://doi.org/10.1016/j.mcn.2012.05.002

Prasov, L., & Glaser, T. (2012b). Pushing the envelope of retinal ganglion cell genesis: Context dependent function of Math5(Atoh7). *Developmental Biology*, *368*(2), 214 230. http://doi.org/10.1016/j.ydbio.2012.05.005

Prasov, L., Masud, T., Khaliq, S., Mehdi, S. Q., Abid, A., Oliver, E. R., et al. (2012a). ATOH7 mutations cause autosomal recessive persistent hyperplasia of the primary vitreous. *Human Molecular Genetics*, *21*(16), 3681 3694. http://doi.org/10.1093/hmg/dds197

Prasov, L., Nagy, M., Rudolph, D. D., & Glaser, T. (2012b). Math5 (Atoh7) gene dosage limits retinal ganglion cell genesis. *Neuroreport*, *23*(10), 631 634. http://doi.org/10.1097/WNR.0b013e328355f260

Quigley, H. A., & Broman, A. T. (2006). The number of people with glaucoma worldwide in 2010 and 2020. *British Journal of Ophthalmology*, *90*(3), 262 267. http://doi.org/10.1136/bjo.2005.081224

Quinlan AR, Hall IM. (2010). BEDTools: a flexible suite of utilities for comparing genomic features. Bioinform Oxf Engl 26:841 2. doi:10.1093/bioinformatics/btq033

Rachel, R. A., Dolen, G., Hayes, N. L., Lu, A., Erskine, L., Nowakowski, R. S., & Mason, C. A. (2002). Spatiotemporal features of early neuronogenesis differ in wild-type and albino mouse retina. *Journal of Neuroscience*, *22*(11), 4249 4263. Retrieved from http://www.jneurosci.org/content/22/11/4249.full.pdf+html

Ragge, N. K., Brown, A. G., Poloschek, C. M., Lorenz, B., Henderson, R. A., Clarke, M. P., et al. (2005). Heterozygous mutations of OTX2 cause severe ocular malformations. *The American Journal of Human Genetics*, *76*(6), 1008 1022. http://doi.org/10.1086/430721

Ramdas, W. D. W., van Koolwijk, L. M. E. L., Lemij, H. G. H., Pasutto, F. F., Cree, A. J. A., Thorleifsson, G. G., et al. (2011). Common genetic variants associated with open-angle glaucoma. *Human Molecular Genetics*, *20*(12), 2464 2471. http://doi.org/10.1093/hmg/ddr120

Ramírez F, Ryan DP, Grüning B, Bhardwaj V, Kilpert F, Richter AS, Heyne S, Dündar F, Manke T. (2016). deepTools2: a next generation web server for deep-sequencing data analysis. Nucleic Acids Res 44:W160-5. doi:10.1093/nar/gkw257

Rao, S., Chun, C., Fan, J., Kofron, J. M., Yang, M. B., Hegde, R. S., et al. (2013). A direct and melanopsin-dependent fetal light response regulates mouse eye development. *Nature*, *494*(7436), 243 246. http://doi.org/10.1038/nature11823

Rapaport, D. H., Wong, L. L., Wood, E. D., Yasumura, D., & LaVail, M. M. (2004). Timing and topography of cell genesis in the rat retina. *The Journal of Comparative Neurology*, *474*(2), 304 324. http://doi.org/10.1002/cne.20134

Rheaume, B. A., Jereen, A., Bolisetty, M., Sajid, M. S., Yang, Y., Renna, K., et al. (2018). Single cell transcriptome profiling of retinal ganglion cells identifies cellular subtypes. *Nature Communications*, *9*(1), 2759. http://doi.org/10.1038/s41467-018-05134-3

Riesenberg, A. N., Le, T. T., Willardsen, M. I., Blackburn, D. C., Vetter, M. L., & Brown, N. L. (2009a). Pax6 regulation of Math5 during mouse retinal neurogenesis. *Genesis*, *47*(3), 175 187. http://doi.org/10.1002/dvg.20479

Riesenberg, A. N., Liu, Z., Kopan, R., & Brown, N. L. (2009b). Rbpj cell autonomous regulation of retinal ganglion cell and cone photoreceptor fates in the mouse retina. *Journal of Neuroscience*, *29*(41), 12865 12877. http://doi.org/10.1523/JNEUROSCI.3382-09.2009

Rodriguez, A. R., de Sevilla Müller, L. P., & Brecha, N. C. (2014). The RNA binding protein RBPMS is a selective marker of ganglion cells in the mammalian retina. *The Journal of Comparative Neurology*, *522*(6), 1411 1443. http://doi.org/10.1002/cne.23521

Rodríguez-Gallardo, L., Lineros-Domínguez, M. D. C., Francisco-Morcillo, J., & Martín-Partido, G. (2005). Macrophages during retina and optic nerve development in the mouse embryo: relationship to cell death and optic fibres. *Anatomy and Embryology*, *210*(4), 303 316. http://doi.org/10.1007/s00429-005-0051-3

Rowan, S., & Cepko, C. L. (2004). Genetic analysis of the homeodomain transcription factor Chx10 in the retina using a novel multifunctional BAC transgenic mouse

reporter. *Developmental Biology*, *271*(2), 388 402. http://doi.org/10.1016/j.ydbio.2004.03.039

Saint-Geniez, M., & D'amore, P. A. (2004). Development and pathology of the hyaloid, choroidal and retinal vasculature. *International Journal of Developmental Biology*, *48*(8-9), 1045 1058. http://doi.org/10.1387/ijdb.041895ms

Sakagami, K., Gan, L., & Yang, X.-J. (2009). Distinct Effects of Hedgehog Signaling on Neuronal Fate Specification and Cell Cycle Progression in the Embryonic Mouse Retina. *The Journal of Neuroscience : the Official Journal of the Society for Neuroscience*, *29*(21), 6932 6944. http://doi.org/10.1523/JNEUROSCI.0289-09.2009

Sanes, J. R., & Masland, R. H. (2015). The Types of Retinal Ganglion Cells: Current Status and Implications for Neuronal Classification. *Annual Review of Neuroscience*, *38*(1), 221 246. http://doi.org/10.1146/annurev-neuro-071714-034120

Sapieha, P., Sirinyan, M., Hamel, D., Zaniolo, K., Joyal, J.-S., Cho, J.-H., et al. (2008). The succinate receptor GPR91 in neurons has a major role in retinal angiogenesis. *Nature Medicine*, *14*(10), 1067 1076. http://doi.org/10.1038/nm.1873

Sapkota, D., Chintala, H., Wu, F., Fliesler, S. J., Hu, Z., & Mu, X. (2014). Onecut1 and Onecut2 redundantly regulate early retinal cell fates during development. *Proceedings of the National Academy of Sciences*, *111*(39), E4086 95. http://doi.org/10.1073/pnas.1405354111

Saul, S. M., Brzezinski, J. A., Altschuler, R. A., Shore, S. E., Rudolph, D. D., Kabara, L. L., et al. (2008). Math5 expression and function in the central auditory system. *Molecular and Cellular Neuroscience*, *37*(1), 153 169. http://doi.org/10.1016/j.mcn.2007.09.006

Schulte, D., & Bumsted-O'Brien, K. M. (2008). Molecular mechanisms of vertebrate retina development: Implications for ganglion cell and photoreceptor patterning. *Brain Research*, *1192*, 151 164. http://doi.org/10.1016/j.brainres.2007.04.079

Seimiya, M., & Gehring, W. J. (2000). The Drosophila homeobox gene optix is capable of inducing ectopic eyes by an eyeless-independent mechanism. *Development (Cambridge, England)*, *127*(9), 1879 1886.

Sham, C. W., Chan, A. M., Kwong, J. M. K., Caprioli, J., Nusinowitz, S., Chen, B., et al. (2012). Neuronal Programmed Cell Death-1 Ligand Expression Regulates Retinal Ganglion Cell Number in Neonatal and Adult Mice. *Journal of Neuro-Ophthalmology*, *32*(3), 227 237. http://doi.org/10.1097/WNO.0b013e3182589589

Shi, M., Kumar, S. R., Motajo, O., Kretschmer, F., Mu, X., & Badea, T. C. (2013). Genetic interactions between Brn3 transcription factors in retinal ganglion cell type specification. *PLoS ONE*, *8*(10), e76347. http://doi.org/10.1371/journal.pone.0076347

Shi, Q., Gupta, P., Boukhvalova, A. K., Singer, J. H., & Butts, D. A. (2019). Functional characterization of retinal ganglion cells using tailored nonlinear modeling. *Scientific Reports*, *9*(1), 8713. http://doi.org/10.1038/s41598-019-45048-8

Shimogori T, Lee DA, Miranda-Angulo A, Yang Y, Wang H, Jiang L, Yoshida AC, Kataoka A, Mashiko H, Avetisyan M, Qi L, Qian J, Blackshaw S. (2010). A genomic atlas of mouse hypothalamic development. Nat Neurosci 13:767 775. doi:10.1038/nn.2545

Sidman, R. L. (1960). Histogenesis of mouse retina studied with thymidine-H-3. ANATOMICAL RECORD.

Skene PJ, Henikoff S. (2017). An efficient targeted nuclease strategy for high-resolution mapping of DNA binding sites. Elife 6:e21856. doi:10.7554/elife.21856

Skowronska-Krawczyk, D., Ballivet, M., Dynlacht, B. D., & Matter, J.-M. (2004). Highly specific interactions between bHLH transcription factors and chromatin during retina development. *Development (Cambridge, England)*, *131*(18), 4447 4454. http://doi.org/10.1242/dev.01302

Smith, A. N., Miller, L.-A., Radice, G., Ashery-Padan, R., & Lang, R. A. (2009). Stage-dependent modes of Pax6-Sox2 epistasis regulate lens development and eye morphogenesis. *Development (Cambridge, England)*, *136*(17), 2977 2985. http://doi.org/10.1242/dev.037341

Song, W.-T., Zeng, Q., Xia, X.-B., Xia, K., & Pan, Q. (2014). Atoh7 promotes retinal Müller cell differentiation into retinal ganglion cells. *Cytotechnology*, 1 11. http://doi.org/10.1007/s10616-014-9777-1

Song, W.-T., Zhang, X.-Y., & Xia, X.-B. (2015). Atoh7 promotes the differentiation of Müller cells-derived retinal stem cells into retinal ganglion cells in a rat model of

glaucoma. *Experimental Biology and Medicine (Maywood, N.J.)*, *240*(5), 682 690. http://doi.org/10.1177/1535370214560965

Souren, M., Ramon Martinez-Morales, J., Makri, P., Wittbrodt, B., & Wittbrodt, J. (2009). A global survey identifies novel upstream components of the Ath5 neurogenic network. *Genome Biology*, *10*(9). http://doi.org/10.1186/gb-2009-10-9-r92

Sowden, J. C., Holt, J., Meins, A., Smith, H. K., & Bhattacharya, S. S. (2001). Expression of Drosophila omb-related T-box genes in the developing human and mouse neural retina. *Investigative Ophthalmology & Visual Science*, *42*(13), 3095 3102.

Strom, R. C. R., & Williams, R. W. R. (1998). Cell production and cell death in the generation of variation in neuron number. *The Journal of Neuroscience : the Official Journal of the Society for Neuroscience*, *18*(23), 9948 9953.

Stuermer, C. A. O., & Bastmeyer, M. (2000). The retinal axon's pathfinding to the optic disk. *Progress in Neurobiology*, *62*(2), 197 214. http://doi.org/10.1016/S0301-0082(00)00012-5

Takeuchi, O., Fisher, J., Suh, H., Harada, H., Malynn, B. A., & Korsmeyer, S. J. (2005). Essential role of BAX,BAK in B cell homeostasis and prevention of autoimmune disease. *Proceedings of the National Academy of Sciences of the United States of America*, *102*(32), 11272 11277. http://doi.org/10.1073/pnas.0504783102

Tétreault, N., Champagne, M.-P., & Bernier, G. (2009). The LIM homeobox transcription factor Lhx2 is required to specify the retina field and synergistically cooperates

with Pax6 for Six6 trans-activation. *Developmental Biology*, *327*(2), 541 550. http://doi.org/10.1016/j.ydbio.2008.12.022

Torres, M., Gómez-Pardo, E., & Gruss, P. (1996). Pax2 contributes to inner ear patterning and optic nerve trajectory. *Development (Cambridge, England)*, *122*(11), 3381 3391.

Tran NM, Shekhar K, Whitney IE, Jacobi A, Benhar I, Hong G, Yan W, Adiconis X, Arnold ME, Lee JM, Levin JZ, Lin D, Wang C, Lieber CM, Regev A, He Z, Sanes JR. (2019). Single-Cell Profiles of Retinal Ganglion Cells Differing in Resilience to Injury Reveal Neuroprotective Genes. Neuron 104:1039-1055.e12. doi:10.1016/j.neuron.2019.11.006

Triplett, J. W., Pfeiffenberger, C., Yamada, J., Ben K Stafford, Sweeney, N. T., Litke, A. M., et al. (2011). Competition is a driving force in topographic mapping. *Proceedings of the National Academy of Sciences of the United States of America*, *108*(47), 19060 19065. http://doi.org/10.2307/23058648?ref=search-gateway:fbbcb215bfbc109f20fc6b833ad09bbc

Valenciano, A. I., Boya, P., & la Rosa, de, E. J. (2009). Early neural cell death: numbers and cues from the developing neuroretina. *International Journal of Developmental Biology*, *53*(8-10), 1515 1528. http://doi.org/10.1387/ijdb.072446av

Wang, S. W., Kim, B. S., Ding, K., Wang, H., Sun, D., Johnson, R. L., et al. (2001). Requirement for math5 in the development of retinal ganglion cells. *Genes & Development*, *15*(1), 24 29. http://doi.org/10.1101/gad.855301

Wang, S. W., Mu, X., Bowers, W. J., Kim, D.-S., Plas, D. J., Crair, M. C., et al. (2002). Brn3b/Brn3c double knockout mice reveal an unsuspected role for Brn3c in retinal ganglion cell axon outgrowth. *Development (Cambridge, England)*, *129*(2), 467 477. Retrieved from http://eutils.ncbi.nlm.nih.gov/entrez/eutils/elink.fcgi?dbfrom=pubmed&id=11807038&retmode=ref&cmd=prlinks

Wang, V. Y., Rose, M. F., & Zoghbi, H. Y. (2005a). Math1 expression redefines the rhombic lip derivatives and reveals novel lineages within the brainstem and cerebellum. *Neuron*, *48*(1), 31 43. http://doi.org/10.1016/j.neuron.2005.08.024

Wang, Y. P., Dakubo, G. D., Thurig, S., Mazerolle, C. J., & Wallace, V. A. (2005b). Retinal ganglion cell-derived sonic hedgehog locally controls proliferation and the timing of RGC development in the embryonic mouse retina. *Development (Cambridge, England)*, *132*(22), 5103 5113. http://doi.org/10.1242/dev.02096

Wang YV, Weick M, Demb JB. (2011). Spectral and temporal sensitivity of cone-mediated responses in mouse retinal ganglion cells. J Neurosci Official J Soc Neurosci 31:7670 81. doi:10.1523/jneurosci.0629-11.2011

Wee, R., Castrucci, A. M., Provencio, I., Gan, L., & Van Gelder, R. N. (2002). Loss of photic entrainment and altered free-running circadian rhythms in math5-/- mice. *Journal of Neuroscience*, *22*(23), 10427 10433. Retrieved from http://www.jneurosci.org/content/22/23/10427.full

Wernet, M. F., Huberman, A. D., & Desplan, C. (2014). So many pieces, one puzzle: cell type specification and visual circuitry in flies and mice. *Genes & Development*, *28*(23), 2565 2584. http://doi.org/10.1101/gad.248245.114

Willardsen, M. I., Suli, A., Pan, Y., Marsh-Armstrong, N., Chien, C.-B., El-Hodiri, H., et al. (2009). Temporal regulation of Ath5 gene expression during eye development. *Developmental Biology*, *326*(2), 471 481. http://doi.org/10.1016/j.ydbio.2008.10.046

Williams, M. A., Piñon, L. G., Linden, R., & PINTO, L. H. (1990). The pearl mutation accelerates the schedule of natural cell death in the early postnatal retina. *Experimental Brain Research*, *82*(2), 393 400.

Wolf FA, Angerer P, Theis FJ. (2018). SCANPY: large-scale single-cell gene expression data analysis. Genome Biol 19:15. doi:10.1186/s13059-017-1382-0

Wu F, Bard JE, Kann J, Yergeau D, Sapkota D, Ge Y, Hu Z, Wang J, Liu T, Mu X. (2020). RNA-seq and scRNA-seq reveal trajectory progression of the retinal ganglion cell lineage in wild-type and Atoh7-null retinas. Biorxiv 2020.02.26.966093. doi:10.1101/2020.02.26.966093

Wu, F., Kaczynski, T. J., Sethuramanujam, S., Li, R., Jain, V., Slaughter, M., & Mu, X. (2015). Two transcription factors, Pou4f2 and Isl1, are sufficient to specify the retinal ganglion cell fate. *Proceedings of the National Academy of Sciences of the United States of America*, *112*(13), E1559 E1568. http://doi.org/10.1073/pnas.1421535112

Wu, F., Li, R., Umino, Y., Kaczynski, T. J., Sapkota, D., Li, S., et al. (2013). Onecut1 Is Essential for Horizontal Cell Genesis and Retinal Integrity. *The Journal of Neuroscience : the Official Journal of the Society for Neuroscience*, *33*(32), 13053 13065. http://doi.org/10.1523/JNEUROSCI.0116-13.2013

Wu, F., Sapkota, D., Li, R., & Mu, X. (2012). Onecut 1 and Onecut 2 are potential regulators of mouse retinal development. *Journal of Comparative Neurology*, *520*(5), 952 969. http://doi.org/10.1002/cne.22741

Xiang, M., Zhou, L., Macke, J. P., Yoshioka, T., Hendry, S. H., Eddy, R. L., et al. (1995). The Brn-3 family of POU-domain factors: primary structure, binding specificity, and expression in subsets of retinal ganglion cells and somatosensory neurons. *The Journal of Neuroscience : the Official Journal of the Society for Neuroscience*, *15*(7 Pt 1), 4762 4785. Retrieved from http://www.jneurosci.org/content/15/7/4762.short

Yang, Z., Ding, K., Pan, L., Deng, M., & Gan, L. (2003). Math5 determines the competence state of retinal ganglion cell progenitors. *Developmental Biology*, *264*(1), 240 254. http://doi.org/10.1016/j.ydbio.2003.08.005

Yao J, Sun X, Wang Y, Wang L. (2007). Muller glia induce retinal progenitor cells to differentiate into retinal ganglion cells. Neuroreport 17:1263 1267. doi:10.1097/01.wnr.0000227991.23046.b7

Yao, J., Sun, X., Wang, Y., Xu, G., & Qian, J. (2007). Math5 promotes retinal ganglion cell expression patterns in retinal progenitor cells. *Molecular Vision*, *17*(12), 1263 1267. http://doi.org/10.1097/01.wnr.0000227991.23046.b7

Yaron, O., Farhy, C., Marquardt, T., Applebury, M., & Ashery-Padan, R. (2006). Notch1 functions to suppress cone-photoreceptor fate specification in the developing mouse retina. *Development (Cambridge, England)*, *133*(7), 1367 1378. http://doi.org/10.1242/dev.02311

Yoshikawa, Y., Yamada, T., Tai-Nagara, I., Okabe, K., Kitagawa, Y., Ema, M., & Kubota, Y. (2016). Developmental regression of hyaloid vasculature is triggered by neurons. *The Journal of Experimental Medicine*, *213*(7), 1175 1183. http://doi.org/10.1084/jem.20151966

Young, R. W. (1984). Cell-Death During Differentiation of the Retina in the Mouse. *The Journal of Comparative Neurology*, *229*(3), 362 373. http://doi.org/10.1002/cne.902290307

Young, R. W. (1985). Cell differentiation in the retina of the mouse. *The Anatomical Record*, *212*(2), 199 205. http://doi.org/10.1002/ar.1092120215

Yu G, Wang L-G, He Q-Y. (2015). ChIPseeker: an R/Bioconductor package for ChIP peak annotation, comparison and visualization. Bioinform Oxf Engl 31:2382 3. doi:10.1093/bioinformatics/btv145

Yun, S., Saijoh, Y., Hirokawa, K. E., Kopinke, D., Murtaugh, L. C., Monuki, E. S., & Levine, E. M. (2009). Lhx2 links the intrinsic and extrinsic factors that control optic cup formation. *Development (Cambridge, England)*, *136*(23), 3895 3906. http://doi.org/10.1242/dev.041202

Zhang, X. M., & Yang, X. J. (2001). Regulation of retinal ganglion cell production by Sonic hedgehog. *Development (Cambridge, England)*, *128*(6), 943 957.

Zhang, X.-M., Hashimoto, T., Tang, R., & Yang, X.-J. (2018). Elevated expression of human bHLH factor ATOH7 accelerates cell cycle progression of progenitors and enhances production of avian retinal ganglion cells. *Scientific Reports*, *8*(1), 6823. http://doi.org/10.1038/s41598-018-25188-z

Zhang Y, Liu T, Meyer CA, Eeckhoute J, Johnson DS, Bernstein BE, Nusbaum C, Myers RM, Brown M, Li W, Liu XS. (2008). Model-based analysis of ChIP-Seq (MACS). Genome Biol 9:R137. doi:10.1186/gb-2008-9-9-r137

Zhou H, Yoshioka T, Nathans J. (1996). Retina-derived POU-domain factor-1: a complex POU-domain gene implicated in the development of retinal ganglion and amacrine cells. J Neurosci 16:2261 2274. doi:10.1523/jneurosci.16-07-02261.1996

Curriculum vitae

Justin Brodie-Kommit

Born on March 1, 1990 in Boston, Massachusetts, USA

Johns Hopkins University
Biology Department
226 Mudd Hall
Baltimore, MD 21218
Jbrodie3@jh.edu

3714 Hickory Ave
Baltimore, MD 21211
(978)201-9007
Justin@JustinBK.com

Education and Research Experience

Postdoctoral Fellow — 2019-Present
Johns Hopkins University, Baltimore, MD
Laboratory of Samer Hattar, PhD & Haiqing Zhao, PhD

PhD Candidate in Biology — 2012-2019
Graduate program in Cellular, Molecular, Developmental Biology, and Biophysics
Johns Hopkins University, Baltimore, MD
Laboratory of Samer Hattar, PhD
Thesis: "Atoh7-independent specification of retinal ganglion cell identity"

B.S. in Biochemistry/Cell Biology, Minor in Philosophy — 2008-2012
Bucknell University, Lewisburg, PA
Laboratory of Emily Stowe, PhD

Pre-Doctoral Research Intern — Jun-Aug 2011
National Cancer Institute, Frederick, MD
Laboratory of Alan Perantoni, PhD

Teaching Assistantships at Johns Hopkins University

Introduction to the Human Brain	Spring 2018, 2019
Cell Biology Lecture Teaching Assistant	Spring 2016, 2017
Biochemistry Lecture Teaching Assistant	Fall 2016, 2018
Genetics Lecture Teaching Assistant	Fall 2015, 2017, 2018
Developmental Biology Lab Teaching Assistant	Spring 2014
Genetics Lab Teaching Assistant	Fall 2013

Mentoring Experience

Undergraduate mentoring — 2014-2016
Johns Hopkins University, Baltimore, MD
Laboratory of Samer Hattar, PhD

Publications

Justin Brodie-Kommit, Brian S. Clark, Qing Shi, Fion Shiau, Dong Won Kim, Jennifer Langel, Catherine Sheely, Philip A Ruzycki, Michel Fries, Awais Javed, Michel Cayouette, Tiffany Schmidt, Tudor Badea, Thomas Glaser, Haiqing Zhao, Joshua Singer, Seth Blackshaw, Samer Hattar. Atoh7-independent specification of retinal ganglion cell identity. bioRxiv 2020.05.27.116954; doi: https://doi.org/10.1101/2020.05.27.116954

Stowe WC, Brodie-Kommit J, and Stowe-Evans E. Characterization of Complementary Chromatic Adaptation in Gloeotrichia UTEX 583 and Identification of a Transposon-like Insertion in the cpeBAOperon. Plant Cell Physiology (2011) 52(3): 553-562.

Invited Presentation

"Understanding the role of Math5 (Atoh7) in Retinal Ganglion Cell specification." Society for Developmental Biology 76th Annual Meeting, Neuro(R)evolution Satellite Symposium. 2017. Minneapolis, MN.

Poster Presentations

- Brodie-Kommit, J. Shi H., Clark B., Wu F., Schmidt TM, Mu X., Blackshaw S., Singer J, Hattar S. (2018) Understanding the role of Math5 (Atoh7) in Retinal Ganglion Cell specification. Genetics, Genomics, and Evolution of the Eye, Visual System Development, Gordon Research Conference, Barga, Italy
- Brodie-Kommit, J. Shi H., Clark B., Wu F., Schmidt TM, Mu X., Blackshaw S., Singer J, Hattar S. (2018) Understanding the role of Math5 (Atoh7) in Retinal Ganglion Cell specification. Development of the Visual System: Cells, Circuits, and Disease, Visual System Development, Gordon Research Seminar, Barga, Italy.
- Brodie-Kommit, J. Shi H., Clark B., Wu F., Schmidt TM, Mu X., Blackshaw S., Singer J, Hattar S. (2017) Overturning the role of Math5 (Atoh7) in Retinal Ganglion Cell specification. Society for Neuroscience Annual Meeting, Washington DC.
- Brodie-Kommit, J. Shi H., Clark B., Wu F., Schmidt TM, Mu X., Blackshaw S., Singer J, Hattar S. (2017) Overturning the role of Math5 (Atoh7) in Retinal Ganglion Cell specification. Society for Developmental Biology 76th Annual Meeting, Minneapolis, MN.
- Brodie-Kommit, J. Shi H., Wu F., Schmidt TM, Mu X., Singer J, Hattar S. (2017) Overturning the role of Math5 (Atoh7) in Retinal Ganglion Cell specification. Association for Research in Vision and Ophthalmology Annual Meeting, Baltimore, MD.
- Brodie-Kommit, J. Shi H., Wu F., Schmidt TM, Mu X., Singer J, Hattar S. (2016) Math5 (Atoh7) is not necessary for the specification of a subset of retinal ganglion cells. Gordon Research Conference on the Circuits, Evolution and Disease in Visual System Development, West Dover, VT.
- Brodie-Kommit, J. Shi H., Wu F., Schmidt TM, Mu X., Singer J, Hattar S. (2016) Math5 (Atoh7) is not necessary for the specification of a subset of retinal ganglion cells. Gordon Research Seminar on the Fundamental Mechanisms Underlying Health and Disease in Visual System Development, West Dover, VT.
- Brodie-Kommit J, Hattar S, Schmidt TM (2014) The Transcription Factor Math5 is Not Required for Specification of Distinct Subtypes of Retinal Ganglion Cells. Federation of American Societies for Experimental Biology Conference on Retinal Neurobiology and Visual Processing, Saxtons River, VT

- Brodie-Kommit J, Schmidt TM, Hattar S (2014) The Transcription Factor Math5 is Not Required for Specification of A Subset of Retinal Ganglion Cells. Association for Research in Vision and Ophthalmology Annual Meeting, Orlando, FL.
- Brodie-Kommit J, Stowe-Evans E (2011) Characterization of chromatic adaptation of *Gloeotrichia* sp. UTEX 583. Experimental Biology Conference, Washington DC
- Brodie-Kommit J, Stowe WC, Stowe-Evans E (2010) Analysis of Chromatic Adaptation in *Gloeotrichia* sp. UTEX 583. American Society for Microbiology regional meeting in Clearfield, PA

Awards

Society for Developmental Biology Best Graduate Poster Competition, Honorable Mention at 2017 Society for Developmental Biology Annual Meeting in Minneapolis, MN

Society for Developmental Biology Student/Postdoc Travel Award for the 2017 Society for Developmental Biology Annual Meeting in Minneapolis, MN

National Eye Institute Travel Grant for the 2017 annual Association for Research in Vision and Ophthalmology (ARVO) Conference in Baltimore, MD

Association for Research in Vision and Ophthalmology (ARVO) Member in Training 1st Place Poster Award in the Visual Neuroscience section at 2014 annual meeting in Orlando, FL

Victor Corces Teaching Award for excellence while a teaching assistant for Genetics in Fall 2013

American Society for Microbiology 2nd place poster award in the Molecular category during the 2010 regional meeting in Clearfield, PA

Professional Memberships

Society for Neuroscience	2017, 2019, 2020
Association for Research in Vision and Ophthalmology	2014, 2017
Society for Developmental Biology	2017
American Society for Microbiology	2011